OUKA
Osaka University Knowledge Archive

Title	Activation of Chemical Bond by Electron Transfer and the Catalytic Control
Author(s)	Ohkubo, Kei
Citation	大阪大学, 2001, 博士論文
Version Type	VoR
URL	https://doi.org/10.11501/3184275
rights	
Note	

Osaka University Knowledge Archive : OUKA

https://ir.library.osaka-u.ac.jp/

Osaka University

Activation of Chemical Bond by Electron Transfer and the Catalytic Control

2001

Kei Ohkubo

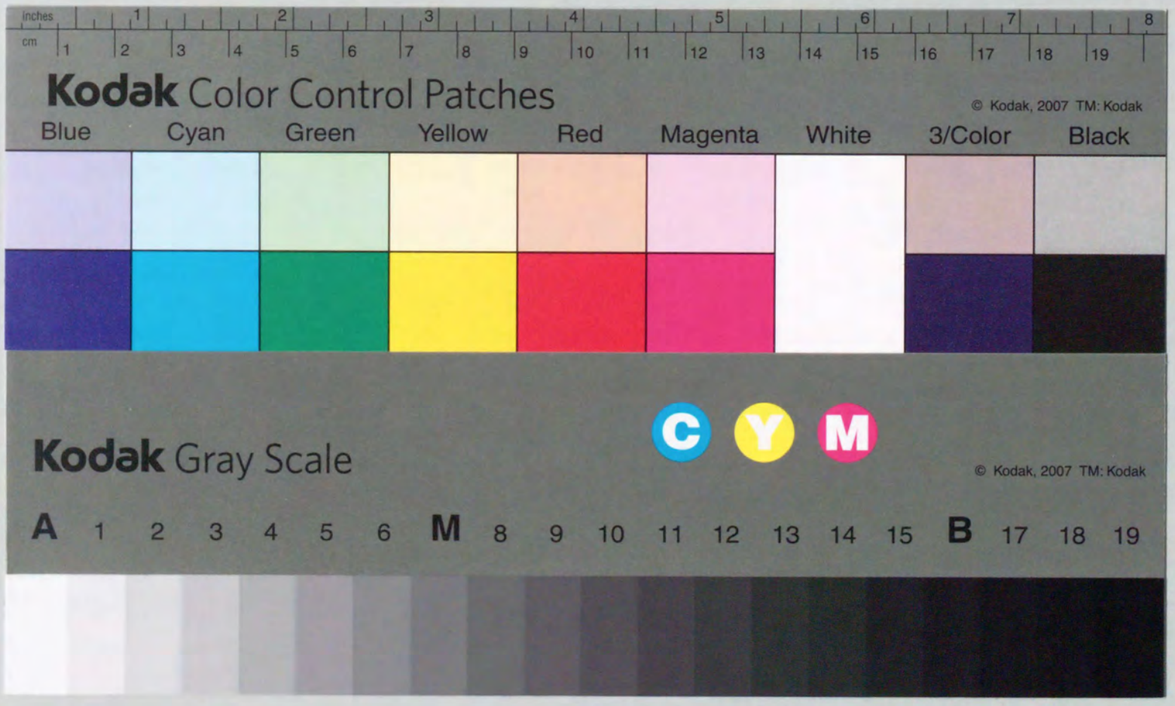

Activation of Chemical Bond by Electron Transfer and the Catalytic Control

2001

Kei Ohkubo

Contents

General Introduction

The importance of electron transfer processes has been recognized in nearly every subdiscipline of chemistry, i.e., not only inorganic chemistry but also organic and organometallic chemistry.[1-10] Numerous chemical reactions, previously formulated by "movements of electron pairs" are now understood as processes in which an initial electron transfer from a nucleophile (reductant) to an electrophile (oxidant) produces a radical ion pair, which leads to the final products via the follow-up steps involving cleavage and formation of chemical bonds.[1-18] Removal of an electron from a bonded orbital results in the weakening of the chemical bond leading to cleavage of the chemical bond.[12] Similarly addition of an electron to an anti-bonding orbital also leads to the bond cleavage.[12] When the highest occupied molecular orbital (HOMO) of an electron donor is a bonded orbital, the electron transfer oxidation of the donor results in the significant weakening of the chemical bond. In particular, metal-carbon and metal-metal bonds are usually electron rich and thereby an electron is likely to be removed from these bonds. However, there have been little cases where the bond energies of different oxidation states have been determined to demonstrate quantitatively the change in the bond energy depending on the oxidation state.

When the lowest unoccupied molecular orbital (LUMO) of an electron acceptor is an antibonding orbital, the one-electron reduction of the acceptor results in the significant weakening of the chemical bond leading to the bond cleavage. Thus, electron transfer from an electron donor having the HOMO bonding orbital to an electron acceptor having the LUMO antibonding orbital gives radical species which recombine to produce new chemical bonds. In such a case, the chemical transformation is preceded by a rapid (diffusion-controlled) association to form an electron donor-acceptor (EDA) complex (eq 1).[19] The presence of an EDA complex as an intermediate has often been suggested for various types of reactions

$$D + A \underset{}{\overset{K_{CT}}{\rightleftharpoons}} (D\,A) \xrightarrow{k_1} \text{products} \qquad (1)$$

between electron donors and acceptors.[2-8] However, the mechanistic involvement of EDA complexes has always been questioned by an alternative mechanism in which the CT complex is merely an innocent bystander in an otherwise dead-end equilibrium, as shown in eq 2.

$$(D\ A) \underset{}{\overset{K_{CT}^{-1}}{\rightleftharpoons}} D + A \xrightarrow{k_2} \text{products} \qquad (2)$$

The difference lies in whether the overall second-order rate constant is a product of the rate constant for the passage of the CT complex to the transition state and the formation constant of the CT complex, $k_{obs} = k_1 K_{CT}$ in eq 1 or a simple bimolecular rate constant, $k_{obs} = k_2$ in eq 2, although the two processes in eqs 1 and 2 are kinetically indistinguishable**.** The heat of formation of CT complex (ΔH_{CT}) of the reactions between electron donors (D) and acceptors (A) generally have a tendency to have large value. The negative activation enthalpy ($\Delta H^{\neq}_{obs} < 0$) could be obtained only if the CT complex is so strong that heat of formation of CT complex ($\Delta H_{CT} < 0$) is of greater magnitude than the activation enthalpy for the passage of the CT complex to the transition state ($\Delta H^{\neq} > 0$), *i.e.*, $\Delta H^{\neq}_{obs} = \Delta H_{CT} + \Delta H^{\neq}$. There has so far been rare cases for observation of such a negative activation enthalpy.[20] Thus, the actual role of the CT complex in reactions between electron donors and acceptors has yet to be clarified.

Since electron donors (D) and electron acceptors (A) which can be employed in electron transfer reactions should be relatively strong reductants and oxidants, respectively, there is a limit to scope of the electron transfer reactions. However, a direct acceleration of the electron transfer processes with use of appropriate catalysts enables us to extend the scope of electron transfer reactions. If a third component as metal ion (M^{n+}) which can stabilize specifically one of the products of electron transfer thermodynamically is introduced into the D–A system, the free energy change of electron transfer is shifted to the negative direction, when the activation barrier of electron transfer is reduced to accelerate the rates of electron transfer, where M^{n+} forms a complex with $A^{\bullet-}$. It should be emphasized that there is no need to have an interaction of M^{n+} with A and that the interaction with the reduced state ($A^{\bullet-}$) is sufficient to accelerate the rate of electron transfer. This contrasts well with the catalysis on conventional ionic or concerted reactions, in which the catalyst needs to interact with a reactant to accelerate the reactions. Since most organic compounds such as π acceptors in particular have small reorganization energies, the change of redox potentials by the interaction of the corresponding radical anions with M^{n+} may be the main factor to accelerate the rates of electron transfer. Thus, any material M^{n+} that can stabilize the radical anions thermodynamically by the complexation may act as an efficient catalyst to accelerate the rates of electron transfer. The stronger the interaction of M^{n+} with the radical anions is, the faster

will the rates of electron transfer be as the free energy change of electron transfer decreases. This means that electron is transferred instantaneously according to the Franck-Condon principle when the reactant pair is activated by the unfavorable interaction with M^{n+} to reach the nuclear configurations where the energy before and after the electron transfer is the same. Once an electron is transferred, the interaction of M^{n+} with the radical anion becomes energetically favorable to give the thermodynamically more stable products as shown in Scheme 1.

Scheme 1.

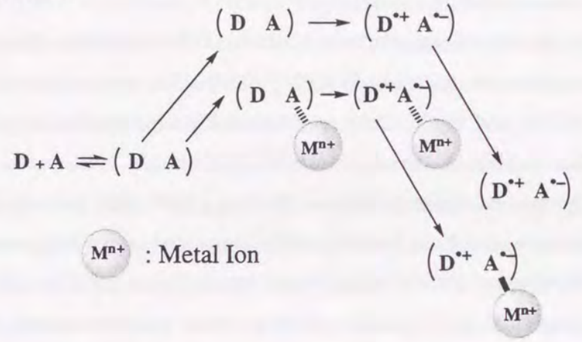

This study is thus intended to investigate the thermal and photoinduced electron transfer reactions involving cleavage of various types of chemical bonds, i.e., carbon–hydrogen, metal–carbon, metal-oxygen and metal–metal bonds. The actual role of the EDA complces in electron transfer reactions between electron donors and acceptors has also been clarified by examining the temperature dependence of the rates of electron transfer. These results are described in Chapters 1-4. The catalysis of metal ions in electron transfer reactions has also been systematically studied in Chapter 5.

In chapter 1, the author has examined the change in the reactivities of 9-substituted 10-methyl-9,10-dihydroacridine (AcrHR) having a variety of substituents R in the reactions with hydride acceptors. The present study provides an excellent opportunity to compare the reactivities of AcrHR in the hydride transfer reactions with those in the deprotonation of the corresponding radical cations. By the proper choice of alkyl (or phenyl) substituents in AcrHR the electron donor property of AcrHR and the acid property of $AcrHR^{\bullet+}$ can be systematically varied and finely tuned to cover wide range of subtle molecular effects. Such fine tuning of the electron donor and acid properties has enabled us to observe negative

activation enthalpies for the hydride transfer reactions of AcrHR, which indicates unequivocally that the CT complex is a true intermediate for the hydride transfer reaction, lying on the reaction pathway.

Chapter 2 describes electron transfer reactions invloving C-H bond cleavage which has synthetic unitary in which the 100 % selective oxygenation of *p*-xylene to *p*-tolualdehyde is initiated by photoinduced electron transfer from *p*-xylene to the singlet excited state of 10-methyl-9-phenylacridinium ion under visible light irradiation. The reason for the high selectivity in the photocatalytic oxygenation of *p*-xylene is discussed based on the photoinduced electron transfer mechanism.

In chapter 3, the activation parameters for the Co(IV)–C bond cleavage of a series of σ–bonded organocobaloximes, $[(DH)_2Co^{IV}(R)(L)]^+$ (DH^- = the anion of dimethylglyoxime, R = Me, Et, Ph, $PhCH_2$ and $PhCH(CH_3)$, and L = substituted pyridines) produced by the electron transfer oxidation of $(DH)_2Co^{III}(R)(L)$ with a one–electron oxidant, $[Fe(bpy)_3](PF_6)_3$ (bpy = 2,2'–bipyridine) or $[Ru(bpy)_3](PF_6)_3$ in acetonitrile (MeCN) are reported in comparison with those for the Co(III)-C bond cleavage. The present data permits an extensive comparison of the activation parameters ($\Delta H^{\neq}$ and $\Delta S^{\neq}$) between the Co(IV)–C and Co(III)–C bond cleavage of a series of organocobalt complexes with a flexible ligand (DH^-) and a rigid ligand (TPP^{2-}). Such an extensive comparison of the activation parameters provides valuable insight into the essential role of the flexible corrin ring in the enzymatic activation of B_{12}, although the one–electron oxidation of coenzyme B_{12} model complexes has no proven biological role at present. In this chapter, the photocleavage of cobalt–carbon bonds of alkylcobalt(III) complexes, $(DH)_2Co^{III}(R)(L)$ in the presence of C_{60} is also reported to give R_2C_{60}. The reaction mechanism is discussed based on detection of the reactive intermediate by ESR as well as the effect of a radical trapping reagent on the photoalkylation of C_{60} by $(DH)_2Co^{III}(R)(L)$.

The photochemical Si–O bond cleavage by the reduction of 10-methylacridinium ion ($AcrH^+$) by allylic silanes and stannanes occurs efficiently and regioselectively to afford the allylated dihydroacridines in which the allylic group is introduced at the α-position but that the thermal reduction by allylic stannanes occurs with the reversed regioselectivities to give the γ-adducts. *Reversed* regioselectivities in the photoreduction of NAD^+ analogs (1-methylquinolinium ions) by hydrostannanes and hydrosilanes are also reported as compared to those in the thermal reduction by hydrostannanes and hydrosilanes. The author could observe the transient absorption spectra in the visible region successfully to clarify the

detailed mechanism of the regioselective photochemical reduction of $AcrH^+$ by organosilanes. Thus, this study provides excellent opportunities to compare directly the regioselectivities in both the thermal and photochemical reduction of NAD^+ analogs by the organometallic compounds and to gain comprehensive and confirmative understanding for their mechanistic difference which leads to the regioreversed addition.

The Si-O bond cleavage in the reactions of β,β-dimethyl-substituted ketene silyl acetal and a much less sterically hindered ketene silyl acetal with a series of *p*-methoxy substituted trityl cations $[(MeOC_6H_4)_x(C_6H_5)_{(3-x)}C^+]$ (x = 0–3) has also been reported and these data are directly compared with those of outer-sphere electron transfer reactions from 10,10'-dimethyl-9,9',10,10'-tetrahydro-9,9'-biacridine $[(AcrH)_2]$ to the same series of trityl cations as well as other electron acceptors. The present study provides valuable insight into the electron transfer vs nucleophilic reactivities of ketene silyl acetals.

The difference in the mechanisms for the regioreversed thermal and photochemical reduction of $AcrH^+$ and QuH^+ has also been revelaed in terms of nucleophilic vs electron transfer pathways. The photochemical reactions proceed via photoinduced electron transfer from organosilanes and organostannanes to the singlet excited states of $AcrH^+$ and QuH^+, followed by the radical coupling of the resulting radical pair in competition with the back electron transfer to the ground state.

In chapter 4, the author report a convenient method for generation of $[CpFe(CO)_2]^-$ by the photochemical reductive cleavage of Fe-Fe bond of $[CpFe(CO)_2]_2$ by a unique organic two-electron donor, that is an NAD (nicotinamide adenine dinucleotide) dimer analogue, 1-benzyl-1,4-dihydronicotinamide dimer $[(BNA)_2]$. Combination of the photochemical and electrochemical results obtained in this study provides confirmative bases to elucidate the reaction mechanism of the photochemical reduction of cyclopentadienyliron dicarbonyl dimer, $[CpFe(CO)_2]_2$ by $(BNA)_2$.

Finally in chapter 5, the first quantitative experimental measure of Lewis acidity of a wide variety of metal ions, which are shown to be directly correlated with the promoting effects in electron transfer reactions has been reported using the g_{zz}-values of ESR spectra of superoxide-metal ion complexes. The binding energies of superoxide-metal ion complexes are readily derived from the g_{zz}-values which are highly sensitive to the Lewis acidity of a variety of metal ions. The biding energies thus determined are shown to be correlated to accelerating effects of metal ions in disproportionation of $C_{60}^{\bullet-}$ in the presence of various metal ions, *i.e.*, Mg^{2+}, Ca^{2+}, Sr^{2+} and Ba^{2+}. This is the first report that the external

coordination of carbon atoms containing π-electrons to metal ions acting as Lewis acids results in an enhanced electron acceptor ability.

References

(1) Eberson, L. *Electron Transfer Reactions in Organic Chemistry; Reactivity and Structure*, Vol. 25, Springler, Heidelberg, 1987.

(2) Kochi, J. K. *Organometallic Mechanisms and Catalysis*, Academic Press, New York, 1978.

(3) J. K. Kochi, *Angew. Chem. Int. Ed. Engl.* **1988**, *27*, 1227.

(4) .Fukuzumi, S. in *Advances in Electron Transfer Chemistry*, Vol. 2 (Ed.: P. S. Mariano), JAI Press, Greenwich, CT, 1992, pp. 67-175.

(5) Patz, M.; Fukuzumi, S. *J. Phys. Org. Chem.* **1997**, *10*, 129.

(6) Rathore, R.; Kochi, J. K. *Adv. Phys. Org. Chem.* **2000**, *35*, 193.

(7) *Electron Transfer in Chemistry*, Vol. 5 (Ed.; V. Balzani), Wiley-VCH, Weinheim, 2001.

(8) Fukuzumi, S.; Kochi, J. K. *Bull. Chem. Soc. Jpn.* **1983**, *56*, 969

(9) Ashby, E. C. *Acc. Chem. Res.* **1988**, *21*, 414.

(10) Fukuzumi, S. *The Porphyrin Handbook*, Vol. 8. Eds. by Kadish, K. M. Smith, K. Guilard, R., Academic Press, San Diego, CA, 2000, pp. 115-152.

(11) Julliard, M.; Chanon, M. *Chem. Rev.* **1983**, *83*, 425.

(12) Chanon, M.; Rajzmann, M.; Chanon, F. *Tetrahedron* **1990**, *46*, 6193.

(13) Shaik, S. S. *Prog. Phys. Org. Chem.* **1985**, *15*, 264.

(14) Pross, A. *Acc. Chem. Res.* **1985**, *18*, 212.

(15) Bauld, N. L. in *Advances in Electron Transfer Chemistry*, Vol. 2, Ed. by Mariano, P. S. , JAI Press, CT, 1992, pp. 1-66.

(16) Bunnett, J. F. *Acc. Chem. Res.* **1992**, *25*, 2.

(17) Jedlinski, Z. *Acc. Chem. Res.* **1998**, *31*, 55.

(18) Hintz, S.; Heidbreder, A.; Mattay, J. *Top. Curr. Chem.* **1996**, *177*, 78.

(19) Mulliken, R. S.; Person W. B. *Molecular Complex, a Lecture and Reprint Volume*, Wiley-Interscience, New York, 1969.

(20) Kiselv. V. D.; Miller, J. G. *J. Am. Chem. Soc.* **1975**, *97*, 4036.

Chapter 1

Activation of Carbon–Hydrogen Bond by Electron Transfer

Hydride Transfer from 9-Substituted 10-Methyl-9,10-dihydroacridines to Hydride Acceptors via Charge-Transfer Complexes and Sequential Electron-Proton-Electron Transfer. A Negative Temperature Dependence of the Rates

Abstract: The reactivity of 9-substituted 10-methyl-9,10-dihydroacridine (AcrHR) in the reactions with hydride acceptors (A) such as *p*-benzoquinone derivatives and tetracyanoethylene (TCNE) in acetonitrile varies significantly spanning a range of 10^7 starting from R = H to Bu^t and CMe_2COOMe. Comparison of the large variation in the reactivity of the hydride transfer reaction with that of the deprotonation of the radical cation ($AcrHR^{\bullet+}$) determined independently indicates that the large variation in the reactivity is attributed mainly to that of proton transfer from $AcrHR^{\bullet+}$ to $A^{\bullet-}$ following the initial electron transfer from AcrHR to A. The overall hydride transfer reaction from AcrHR to A therefore proceeds via sequential electron-proton-electron transfer in which the initial electron transfer to give the radical ion pair ($AcrHR^{\bullet+}$ $A^{\bullet-}$) is in equilibrium and the proton transfer from $AcrHR^{\bullet+}$ to $A^{\bullet-}$ is the rate-determining step. Charge-transfer complexes are shown to be formed in the course of the hydride transfer reactions from AcrHR to *p*-benzoquinone derivatives. A negative temperature dependence was observed for the rates of hydride transfer reactions from AcrHR (R = H, Me, and CH_2Ph) to 2,3-dichloro-5,6-dicyano-*p*-benzoquinone (DDQ) in chloroform (*the lower the temperature, the faster the rate*) to afford the negative activation enthalpy ($\Delta H^{\neq}_{obs}$ = –32, –4 and –13 kJ mol^{-1}, respectively). Such a negative $\Delta H^{\neq}_{obs}$ value indicates clearly that the CT complex lies along the reaction pathway of the hydride transfer reaction via sequential electron-proton-electron transfer and does not enter merely through a side reaction that is indifferent to the hydride transfer reaction. The $\Delta H^{\neq}_{obs}$ value increases with increasing the solvent polarity from a negative value (–13 kJ mol^{-1}) in chloroform to a positive value (13 kJ mol^{-1}) in benzonitrile as the proton transfer rate from $AcrHR^{\bullet+}$ to $DDQ^{\bullet-}$ may be slower.

Introduction

Dihydronicotinamide adenine dinucleotide (NADH) and analogues act as the source of two electrons and a proton, thus formally transferring a hydride ion to a suitable substrate.[1] The mechanism of the hydride transfer has so far been extensively studied by using NADH analogues in the reactions with various substrates.[2-12] In these investigations, the mechanism has been discussed concerning two main possibilities, *i.e.*, concerted hydride transfer or sequential electron-proton-electron (equivalent to a hydride ion) transfer. Since both processes involve the formation of a formal positive charge in the transition state, it has been difficult to differentiate between the mechanisms based on the classical approach of electronic and substitution effects.[13-15] We have previously reported that the distinction between the two mechanisms can be made by comparing the reactivities of different type of NADH analogues which have different donor abilities in the initial and second electron transfer in the electron-proton-electron sequence.[6] Namely, the one-electron donor ability between 1-benzyl-1,4-dihydronicotinamide (BNAH) and 10-methyl-9,10-dihydroacridine ($AcrH_2$) is rather similar to each other, as compared to the large difference in the one-electron donor ability between the corresponding radicals, *i.e.*, $BNA^{\bullet}$ and $AcrH^{\bullet}$.[6] In such a case, the energetics of the initial electron transfer is similar, while the energetics of overall hydride transfer is quite different between the two NADH analogues. We have shown clearly that the activation barrier is mainly determined by the energetics of initial electron transfer rather than the energetics of overall hydride transfer.[6]

The mechanistic discussion is further complicated by formation of charge-transfer (CT) complexes in the course of hydride transfer reactions from NADH analogues to *p*-benzoquinone derivatives and tetracyanoethylene (TCNE).[16,17] The CT complexes have been implicated as intermediates in a variety of reactions between electron donors (D) and acceptors (A), eq 1.[18-20] However, the mechanistic involvement of CT complexes has always

$$D + A \underset{}{\overset{K_{CT}}{\rightleftharpoons}} (D\ A) \xrightarrow{k_1} \text{Products} \qquad (1)$$

been questioned by an alternative mechanism in which the CT complex is merely an innocent bystander in an otherwise dead-end equilibrium, eq 2.[21] The two pathways in eqs 1 and 2

$$(D\ A) \overset{K_{CT}^{-1}}{\rightleftharpoons} D + A \xrightarrow{k_2} \text{Products} \qquad (2)$$

are kinetically indistinguishable.[22] However, Kiselev and Miller[23] have shown that the two pathways in eqs 1 and 2 can be distinguishable by the temperature dependence of the observed second-order rate constant (k_{obs}) if one can observe a negative temperature dependence. A negative activation enthalpy could only arise when the CT complex lies along the reaction pathway (eq 1), since for such a pathway, $k_{obs} = k_1 K_{CT}$ [$\Delta H^{\neq}_{obs} = \Delta H_1^{\neq}$ (>0) + ΔH_{CT} (<0)], whereas for the other pathway (eq 2), $k_{obs} = k$ [$\Delta H^{\neq}_{obs} = \Delta H_2^{\neq}$ (>0)]. Thus, the necessary condition to observe a negative activation enthalpy for reactions involving CT complexes is that the heat of formation of the CT complex ($\Delta H_{CT} < 0$) is of greater magnitude than the activation enthalpy for the passage of the CT complex to the transition state ($\Delta H_1^{\neq} > 0$) in eq 1, *i.e.*, $-\Delta H_{CT} > \Delta H_1^{\neq}$. However, such a system is difficult to examine the kinetics, since formation of strong CT complexes, that is prerequisite to observe negative $\Delta H^{\neq}_{obs}$ values, are usually too fast to follow the reactions. Fine tuning of the strength of the CT complex and the reactivity seems essential to observe the negative $\Delta H^{\neq}_{obs}$ values.[24,25]

We have previously shown that 9-substituted 10-methyl-9,10-dihydroacridines (AcrHR) have similar one-electron donor properties but quite different proton donor abilities in the corresponding radical cations formed by the electron transfer oxidation of AcrHR with Fe^{3+} and that the deprotonation rate varies significantly depending on the substituent R.[26,27]

In this study we have examined the change in the reactivities of AcrHR having a variety of substituents R in the reactions with hydride acceptors. The present study provides an excellent opportunity to compare the reactivities of AcrHR in the hydride transfer reactions with those in the deprotonation of the corresponding radical cations. By the proper choice of alkyl (or phenyl) substituents in AcrHR the electron donor property of AcrHR and the acid property of $AcrHR^{\bullet+}$ can be systematically varied and finely tuned to cover wide range of subtle molecular effects. Such fine tuning of the electron donor and acid properties has enabled us to observe negative activation enthalpies for the hydride transfer reactions of AcrHR, which indicates unequivocally that the CT complex is a true intermediate for the hydride transfer reaction, lying on the reaction pathway.[28]

Experimental Section

Materials. 9,10-Dihydro-10-methylacridine ($AcrH_2$) was prepared from 10-methylacridinium iodide ($AcrH^+I^-$) by the reduction with $NaBH_4$ in methanol, and purified by recrystallization from ethanol.[29] $AcrH^+I^-$ was prepared by the reaction of acridine with methyl iodide in acetone, and was converted to the perchlorate salt ($AcrH^+ClO_4^-$) by the addition of magnesium perchlorate to the iodide salt ($AcrH^+I^-$), and purified by recrystallization from methanol.[6] 9-Alkyl (or phenyl)-9,10-dihydro-10-methylacridine (AcrHR; R = Me, Et, CH_2Ph and Ph) were prepared by the reduction of $AcrH^+I^-$ with the corresponding Grignard reagents (RMgX).[27] AcrHR (R = Pr^i, Bu^t, $CHPh_2$ and 1-$CH_2C_{10}H_7$) was prepared by the photoreduction of $AcrH^+ClO_4^-$ with RCOOH in the presence of NaOH in H_2O-MeCN as described previously.[30] AcrHR (R = CH_2COOEt, CMe(H)COOEt and CMe_2COOMe) was prepared by the reduction of $AcrH^+ClO_4^-$ with the corresponding ketene silyl acetals (CH_2=C(OEt)$OSiEt_3$, CMe(H)=C(OEt)$OSiEt_3$ and Me_2C=C(OMe)$OSiMe_3$, respectively).[31] 9-Substituted 10-methylacridinium perchlorate ($AcrR^+ClO_4^-$: R = Me, Et, Pr^i, Bu^t, $CHPh_2$ and Ph) was prepared by the reaction of 10-methylacridone in dichloromethane with the corresponding Grignard reagents (RMgX), and purified by recrystallization from ethanol-diethylether.[32] *p*-Benzoquinone derivatives (2,3-dichloro-5,6-dicyano-*p*-benzoquinone (DDQ), *p*-chloranil, 2,6-dichloro-*p*-benzoquinone and chloro-*p*-benzoquinone) and tetracyanoethylene (TCNE) were obtained commercially, and purified by the standard methods.[33] Acetonitrile and benzonitrile used as a solvent were purified and dried by the standard procedure.[33] Chloroform and 1,2-dichloroethane (spectral grade) were obtained commercially from Wako Pure Chemicals and used without further purification.

Reaction Procedure. Typically, AcrHR (4.0×10^{-2} M) and DDQ (6.0×10^{-2} M) were added to an NMR tube which contained deaerated CD_3CN solution (0.60 cm^3) under an atmospheric pressure of argon. The oxidized products of AcrHR were identified by the ^1H NMR spectra by comparing with those of authentic samples. The ^1H NMR measurements were performed using a JNM-GSX-400 (400 MHz) NMR spectrometer. ^1H NMR (CD_3CN): $AcrMe^+ClO_4^-$: δ 3.48 (s, 3H), 4.74 (s, 3H), 7.9-8.9 (m, 8H); $AcrEt^+ClO_4^-$: δ 1.52 (t, 3H, J = 7.5 Hz), 3.95 (q, 2H), 4.71 (s, 3H), 7.9-8.9 (m, 8H); $AcrPh^+ClO_4^-$: δ 4.83 (s, 3H), 7.5-8.6 (m, 13H); $AcrCH_2Ph^+ClO_4^-$: δ 4.79 (s, 3H), 5.35 (s, 2H), 7.5–8.9 (m, 13H); $AcrCHPh_2^+ClO_4^-$: δ 4.70 (s, 3H), 5.96 (s, 1H), 7.5–8.9 (m, 18H); $Acr(1\text{-}CH_2C_{10}H_7)^+ClO_4^-$: δ 4.80 (s, 3H), 5.72 (s, 2H), 7.5–8.9 (m, 15H). $AcrCH_2COOEt^+ClO_4^-$ δ 1.09 (t, 3H, J = 8.0 Hz), 2.41 (q, 2H, J = 8.0 Hz), 4.76 (s, 3H), 5.02 (s, 2H), 7.7–8.7 (m, 8H).

Spectral and Kinetic Measurements. The reactions of AcrHR with DDQ and TCNE in deaerated MeCN were monitored with a Shimadzu UV-2200, 160A spectrophotometer or a Hewlett Packard 8453 diode array spectrophotometer when the rates were slow enough to be determined accurately. The rates were determined from appearance of the absorbance due to $AcrR^+$ (λ_{max} = 358 nm, $\varepsilon_{max} = 1.80 \times 10^4$ M^{-1} cm^{-1}) or the radical anion ($DDQ^{\bullet-}$: λ_{max} = 585 nm, $\varepsilon_{max} = 5.6 \times 10^3$ M^{-1} cm^{-1}, $TCNE^{\bullet-}$: λ_{max} = 457 nm, $\varepsilon_{max} = 5.67 \times 10^3$ M^{-1} cm^{-1}).[34,35] The kinetic measurements for faster reactions such as the reaction of $AcrH_2$ or $AcrHCH_2Ph$ with DDQ were carried out with a Union RA-103 stopped-flow spectrophotometer which was thermostated at 298 K under deaerated conditions. The concentration of AcrHR or a hydride acceptor was maintained at more than 15-fold excess of the other reactant to attain pseudo-first-order conditions. Pseudo-first-order rate constants were determined by a least-squares curve fit using an NEC microcomputer. The first-order plots of ln ($A_\infty - A$) vs time (A_∞ and A are the final absorbance and the absorbance at the reaction time, respectively) were linear for three or more half-lives with the correlation coefficient, $\rho > 0.999$. In each case, it was confirmed that the rate constants derived from at least 5 independent measurements agreed within an experimental error of ±5 %.

The transient CT spectra of complexes formed between AcrHR and *p*-benzoquinone derivatives with half-lives < 10 seconds were obtained by plotting the initial rise of the absorbance against the wavelength with a stopped flow spectrophotometer. The CT spectra of stable complexes such as $AcrHCH_2Ph$-chloro-*p*-benzoquinone complex were measured with a Hewlett-Packard 8452 or Hewlett-Packard 8453 diode array spectrophotometer. The formation constant (K_{CT}) of the $AcrHCH_2Ph$-chloro-*p*-benzoquinone complex was determined from the dependence of the initial rise of the absorbance at λ_{max} = 530 nm due to the CT complex on the concentration of chloro-*p*-benzoquinone in MeCN at various temperatures.

The ESR spectra of $DDQ^{\bullet-}$ and $TCNE^{\bullet-}$ formed as final products in the reactions of AcrHR with DDQ and TCNE, respectively, were measured with a JEOL X-band spectrometer (JES-RE1XE). The g values and the hyperfine coupling constants were calibrated with a Mn^{2+} marker.

Cyclic Voltammetry. Cyclic voltammetry measurements were performed at 298 K on

a BAS 100W electrochemical analyzer in deaerated MeCN containing 0.1 M Bu_4NClO_4 (TBAP) as supporting electrolyte. A conventional three-electrode cell was used with a platinum working electrode (surface area of 0.3 mm^2) and a platinum wire as the counter electrode. The Pt working electrode (BAS) was routinely polished with a BAS polishing alumina suspension and rinsed with acetone before use. The measured potentials were recorded with respect to the $Ag/AgNO_3$ (0.01 M) reference electrode. All potentials (vs Ag/Ag^+) were converted to values vs SCE by adding 0.29 V.[36] All electrochemical measurements were carried out under an atmospheric pressure of argon.

Theoretical Calculations. Theoretical calculations were performed using the MOPAC program (Ver. 6) which is incorporated in the MOLMOLIS program (Ver. 2.8) by Daikin Industries, Co. Ltd. The PM3 Hamiltonian was used for the semiempirical MO calculations.[37] Final geometries and energetics were obtained by optimizing the total molecular energy with respect to all structural variables. The heats of formation (ΔH_f) were calculated with the restricted Hartree Fock (RHF) formalism using a key word "PRECISE".

Results and Discussion

Reactions of AcrHR with Hydride Acceptors. It has previously been reported that hydride transfer reactions from 10-methyl-9,10-dihydroacridine ($AcrH_2$) as well as 1-benzyl-1,4-dihydronicotinamide (BNAH) to hydride acceptors (A) such as *p*-benzoquinone derivatives[6,38] and tetracyanoethylene (TCNE)[17,38] occurs efficiently (eq 1) followed by a subsequent fast electron transfer from the reduced product (AH^-) to A (eq 2) and the disproportionation of the resulting radical (eq 3). When $AcrH_2$ is replaced by 9-substituted analogues (AcrHR), essentially the same reactions (eqs 1-3) occur to give the overall stoichiometry as given by eq 4. A typical example

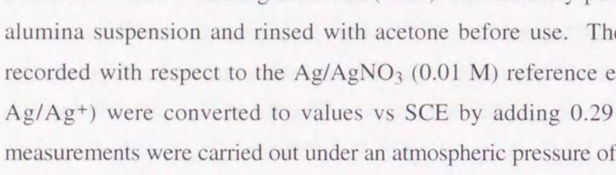

(1)

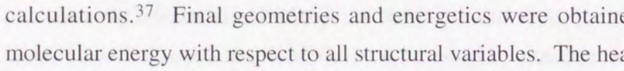

(2)

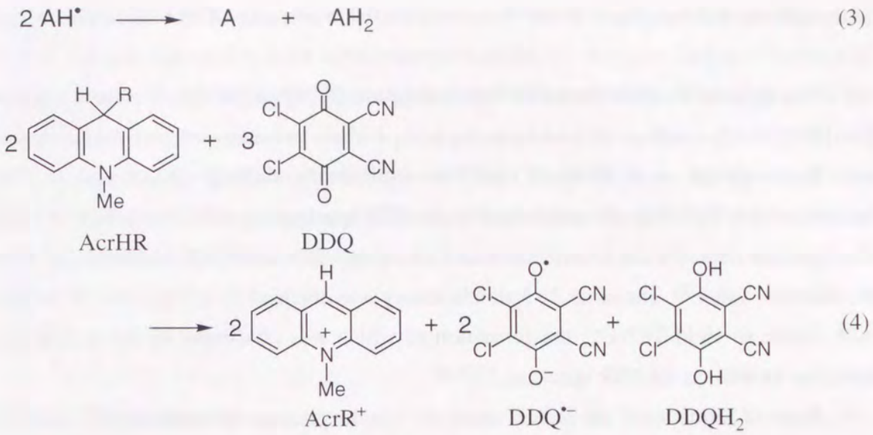

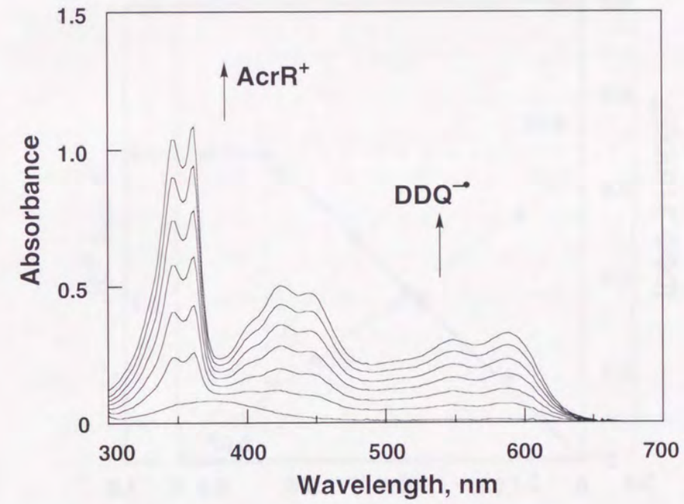

Figure 1. Electronic absorption spectra observed in the reaction of $AcrHCH_2Ph$, (0, 9.3 x 10^{-6}, 2.8 x 10^{-5}, 3.7 x 10^{-5}, 4.7 x 10^{-5}, 5.6 x 10^{-5}, 6.5 x 10^{-5} and 7.5 x 10^{-5} M) with DDQ (8.3 x 10^{-5} M) in deaerated MeCN at 298 K.

of the UV-vis spectral change in the reaction of $AcrHCH_2Ph$ with DDQ is shown in Figure 1.

The spectral titration shown in Figure 2 where $[DDQ^{\bullet-}]/[DDQ]_0$ is plotted against $[AcrHR]/[DDQ]_0$ confirms the stoichiometry in eq 4 where two equivalents of AcrHR reacts with three equivalents of DDQ to yield two equivalents of $DDQ^{\bullet-}$ (67 % yield). The formation of $DDQ^{\bullet-}$ was also confirmed by the ESR spectrum (g = 2.0054) which showed the hyperfine structure due to two equivalent nitrogens (a_N = 0.058 mT) in agreement with the literature value.[39] The same 2 : 3 stoichiometry was obtained for the reaction of AcrHR with TCNE to yield $TCNE^{\bullet-}$, the formation of which was confirmed by the absorption spectrum as well as the ESR spectrum.[17,35,40]

Rates of formation of the radical anion ($A^{\bullet-}$) in the presence of large excess of AcrHR or the hydride acceptor (A) obeyed the pseudo-first-order kinetics.[41] The value of

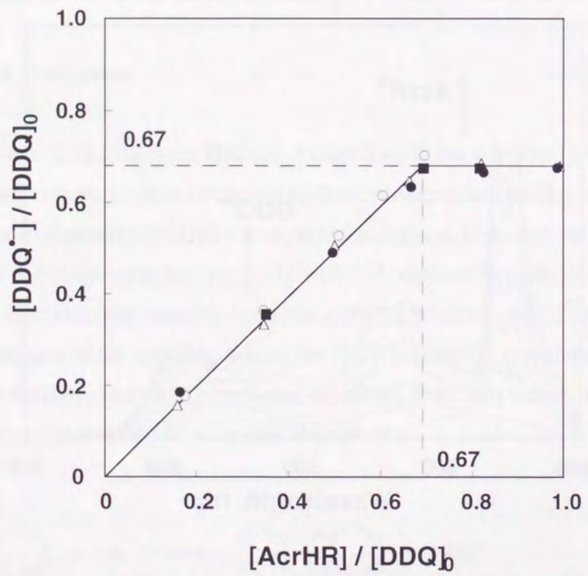

Figure 2. Plot of the ratio of the $DDQ^{\bullet-}$ concentration to the initial concentration of DDQ (1.0 x 10^{-4} M), $[DDQ^{\bullet-}]/[DDQ]_0$ vs the ratio of the initial concentration of AcrHR to DDQ, $[AcrHR]/[DDQ]_0$ for the reaction of AcrHR (R = Me (○), CH_2COOEt (●), 1-$CH_2C_{10}H_7$ (Δ) and CMe(H)COOEt (■)) with DDQ.

the pseudo-first-order rate constant ($k^{(1)}$) in excess of AcrHR (eq 5) is 1.5-fold larger than the $k^{(1)}$ value in excess of A at the same concentration (eq 6). A typical example is shown in Figure 3, where the $k^{(1)}$ values are plotted against [AcrHMe] or [DDQ]. This agrees with the stoichiometry in eq 4.

used in excess for the reaction of AcrHMe with DDQ. Thus, the slope of the plot of $k^{(1)}$ vs [A] gives the rate constant (k_{obs}) of the hydride transfer from AcrHR to A (eq 5), and the slope of $k^{(1)}$ vs [AcrHR] gives $(3/2)k_{obs}$ (eq 6).

$$k^{(1)} = k_{obs}\ [A] \tag{5}$$

$$k^{(1)} = (3/2)\ k_{obs}\ [AcrHR] \tag{6}$$

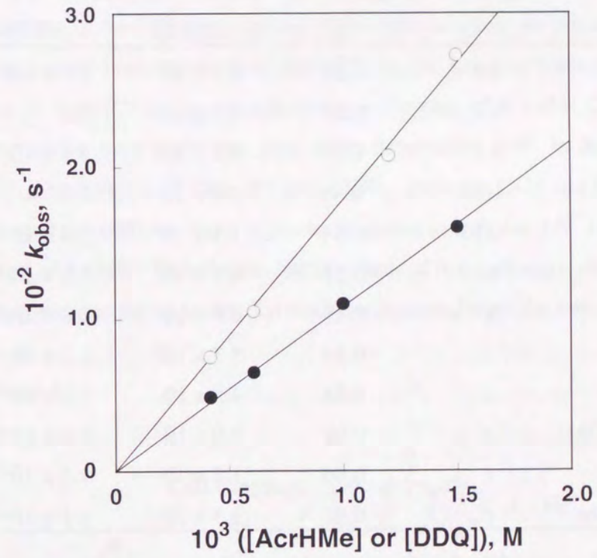

Figure 3. Plots of the pseudo-first-order rate constants ($k^{(1)}$) vs [AcrHMe] (○) or [DDQ] (●) for formation of $DDQ^{\bullet-}$ in the reaction of AcrHMe with DDQ in MeCN at 298 K. Either AcrHMe or DDQ is used in a large excess.

The k_{obs} values for the reactions of a series of AcrHR with hydride acceptors (DDQ and TCNE) are listed in Table 1. The k_{obs} values for the reactions of AcrHR with DDQ vary significantly depending on the substituent R in AcrHR. The magnitude spans a range of 10^7 starting from R = H to Bu^t and CMe_2COOMe. Similar change in the reactivity with R is observed for the reactions of AcrHR with TCNE (Table 1). Such a significant decrease in the reactivity by the introduction of a substituent at C-9 position can hardly be reconciled by a concerted hydride transfer mechanism. The alkyl or phenyl group at C–9 position is known to be in a boat axial conformation, and thereby the hydrogen at C–9 position is

Table 1. Rate Constants (k_d) for Deprotonation of AcrHR$^{\bullet+}$, One-Electron Oxidation Potential (E^0_{ox}) of AcrHR and Rate Constants (k_{obs}) of Hydride Transfer Reactions from AcrHR to DDQ and TCNE in MeCN at 298 K

AcrHR	k_d, s^{-1}	E^0_{ox} (*vs* SCE) [a]	k_{obs}, M^{-1} s^{-1}	
R		V	DDQ	TCNE
H	6.4	0.81	1.5×10^6	1.0×10^2
Me	1.1	0.84	1.1×10^5	7.0
Ph	4.1	0.88	6.5×10^4	7.9×10^{-1}
Et	0.49	0.84	4.0×10^4	3.0
CH_2Ph	0.17[b]	0.84	1.1×10^4	5.4×10^{-1}
$CH_2C_{10}H_7$	*c*	0.85	6.9×10^3	3.3×10^{-1}
CH_2COOEt	*c*	0.89	6.9×10^3	2.3×10^{-1}
$CHPh_2$	*c*	0.84	5.3×10^2	1.5×10^{-2}
Pr^i	*c*	0.84	4.5×10	7.0×10^{-4}
CMe(H)COOMe	*c*	0.92	2.0×10	3.4×10^{-3}
Bu^t	*c*	0.86	1.3×10^{-1}	$< 5 \times 10^{-5}$
CMe_2COOMe	*c*	0.92	1.3×10^{-1}	$< 1 \times 10^{-4}$

[a] Taken from ref 27. [b] The deprotonation rate constant separated from the rate constant for the C–C bond cleavage of AcrHCH$_2$Ph$^{\bullet+}$; see ref 43. [c] Too small to be such as separated from the rate constant for the C–C bond cleavage of AcrHR$^{\bullet+}$ accurately.

located at the equatorial position, where steric hindrance due to the axial substituent is minimized in the hydride transfer reactions. Moreover, the introduction of an electron-donating substituent R = Bu^t would activate the release of a negatively charged hydride ion if the concerted hydride transfer should take place. The remarkable decrease in the reactivity with increasing the electron-donor ability of R (Table 1) rather indicates that the reactivity is determined by the process in which a positive charge is released.

Comparison of the Reactivities in Hydride Transfer Reactions of AcrHR and Deprotonation of AcrHR$^{\bullet+}$. We have previously succeeded in detecting transient absorption and ESR spectra of AcrHR$^{\bullet+}$ produced by the electron transfer oxidation of AcrHR with $[Fe(phen)_3]^{3+}$ (phen = 1,10-phenanthroline).[27] It has been found based on the product analysis that there are two pathways for the decay of AcrHR$^{\bullet+}$: one is the C(9)–H bond cleavage (deprotonation) to give AcrR$^{\bullet}$ and H^+, and the other is the C(9)–C bond cleavage to give AcrH$^+$ and R$^{\bullet}$ as shown in Scheme 1.[27,42] In the case of R = H, Me, Et, Ph and CH_2COOEt, the C(9)–H bond is cleaved exclusively to yield only AcrR$^+$.[27] In such a case the decay rate constant of AcrHR$^{\bullet+}$ corresponds to the deprotonation rate constant (k_d). The k_d values thus determined from the decay of AcrHR$^{\bullet+}$ are also listed in Table 1. In contrast, the C(9)–C bond of AcrHR$^{\bullet+}$ is cleaved selectively in the case of R = Bu^t, CMe_2COOMe when the deprotonation rates were too slow to be determined.[27,42] In the case of R = CH_2Ph, 1-$CH_2C_{10}H_7$, CMe(H)COOEt, Pr^i and $CHPh_2$, both the C–H and C–C bonds of AcrHR$^{\bullet+}$ are cleaved to yield two types of products shown in Scheme 1.[27] In this case the decay rate constant of AcrHR$^{\bullet+}$ includes the rate constants of two pathways. In the case of R = CH_2Ph, the deprotonation rate constant (k_d) could be separated from the rate constant of

Scheme 1

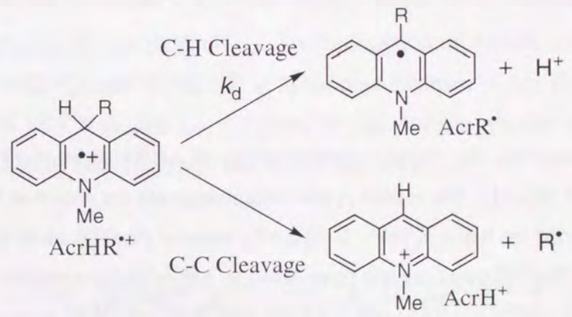

the C–C bond cleavage based on the reaction of $AcrHCH_2Ph^{\bullet+}$ with a base.[43] The k_d value of $AcrHCH_2Ph^{\bullet+}$ is also listed in Table 1.

The log k_{obs} values of the hydride transfer from AcrHR to a hydride acceptor (A: DDQ or TCNE in eq 4) are plotted against the log k_d values of the deprotonation of $AcrHR^{\bullet+}$ in Figure 4a, where a reasonably good linear correlation between them is observed except for R = Ph and CH_2COOEt. Such a linear correlation indicates that the hydride transfer proceeds via electron transfer from AcrHR to A, followed by proton transfer from $AcrHR^{\bullet+}$ to $A^{\bullet-}$ in the radical ion pair and the subsequent electron transfer from $AcrR^{\bullet}$ to $AH^{\bullet}$ and that the proton transfer step may be involved as a rate-determining step.[44] Such a sequential electron-proton-electron transfer leads to the overall hydride transfer to yield $AcrR^+$ and AH^- (Scheme 2).

Since the one-electron reduction potential of DDQ (E^0_{red} *vs* SCE = 0.51 V)[6] or TCNE (E^0_{red} *vs* SCE = 0.22 V)[45] is less positive than the one-electron oxidation potential of examined AcrHR (E^0_{ox} *vs* SCE = 0.81–0.92 V in Table 1),[6,46] the back electron transfer from $A^{\bullet-}$ to $AcrHR^{\bullet+}$ may be much faster than the proton transfer from $AcrHR^{\bullet+}$ to $A^{\bullet-}$ ($k_b >> k_p$ in Scheme 1). In such a case, the observed rate constant (k_{obs}) of the overall hydride transfer is given by eq 9, where $K_{et} = k_{et}/k_b$, provided that an electron transfer from $AcrR^{\bullet}$ to $AH^{\bullet}$ in the final step in Scheme 1 is much faster than the proton transfer from $AcrHR^{\bullet+}$ to $A^{\bullet-}$.

The fast electron transfer from $AcrH^{\bullet}$ to $AH^{\bullet}$ is well supported by the highly negative one-electron oxidation potential of $AcrH^{\bullet}$ ($E^0_{ox} = -0.46$ V)[46] which is much more negative than the one-electron reduction potential of A (E^0_{red} vs SCE = 0.51 V and 0.22 V for DDQ and TCNE, respectively) and these E^0_{red} values are even less positive than the reduction potential of the protonated form of the radical anion ($AH^{\bullet}$).[47] The E^0_{ox} values of 9-substituted 10-methylacridinyl radicals ($AcrR^{\bullet}$: R = Ph, Et, CH_2Ph, Pr^i and Bu^t) are

$$k_{obs} = k_p K_{et} \qquad (9)$$

readily determined from the cyclic voltammograms of $AcrR^+$, since $AcrR^{\bullet}$ is much more stable than $AcrH^{\bullet}$ (R = H). The typical cyclic voltammograms are shown in Figure 5 and the E^0_{ox} values of $AcrR^{\bullet}$ are listed in Table 2. The E^0_{ox} value of $AcrR^{\bullet}$ is more negative than the value of $AcrH^{\bullet}$. Thus, electron transfer from $AcrR^{\bullet}$ to $AH^{\bullet}$ is highly exergonic irrespective of the type of R (*e.g.*, $\Delta G^0_{et} < -97$ kJ mol^{-1} for the $AcrCH_2Ph^{\bullet}$–$DDQH^{\bullet}$ system).

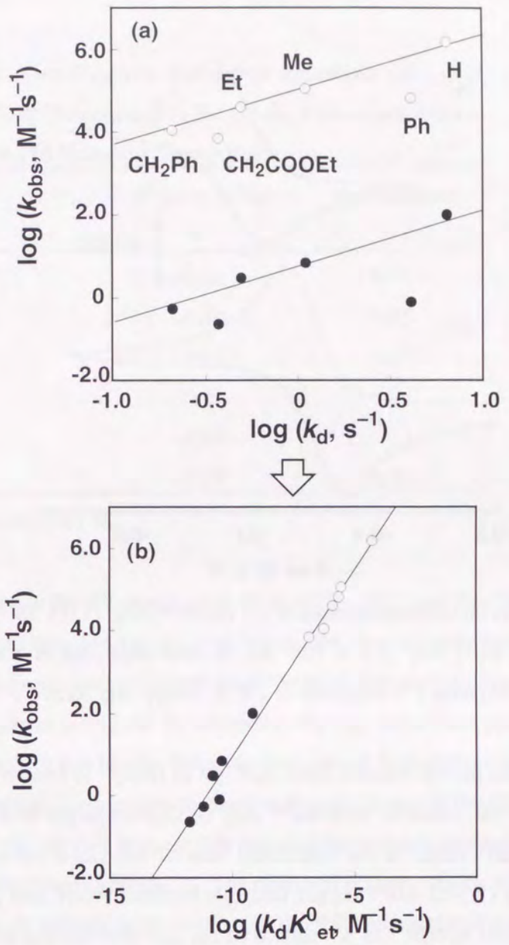

Figure 4. (a) Plots of k_{obs} for the reaction of AcrHR with DDQ (○) and TCNE (●) vs k_d for deprotonation of $AcrHR^{\bullet+}$ in MeCN at 298 K. (b) Plots of k_{obs} for the reaction of AcrHR with DDQ (○) and TCNE (●) vs $k_dK^0_{et}$.

Scheme 2

$$AcrHR + A \underset{k_b}{\overset{k_{et}}{\rightleftharpoons}} (AcrHR^{\bullet+}\ A^{\bullet-}) \xrightarrow{k_p} (AcrR^{\bullet}\ AH^{\bullet}) \xrightarrow{fast} AcrR^+ + AH^-$$

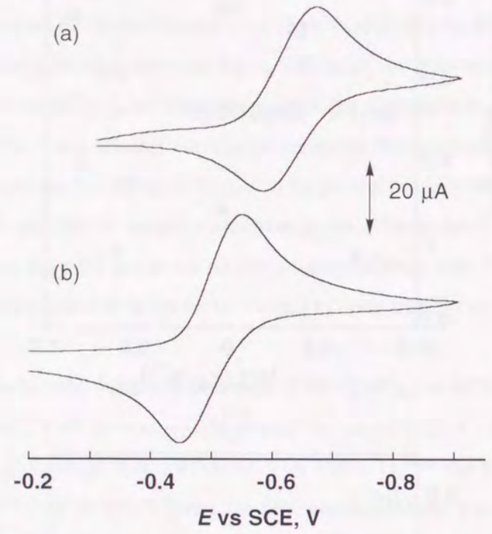

Figure 5. Cyclic voltammograms of (a) $AcrPr^{i+}ClO_4^-$ (1.0×10^{-3} M) and (b) $AcrCH_2\text{-}Ph^+ClO_4^-$ (1.0×10^{-3} M) in deaerated MeCN containing TBAP (0.10 M) with a Pt electrode at 298 K; sweep rate 50 mV s^{-1}.

On the other hand, the proton transfer from $AcrH_2^{\bullet+}$ to $DDQ^{\bullet-}$ is known to be endergonic (27 kJ mol^{-1}).[6] The pK_a value of $AcrHBu^{t\bullet+}$ may be slightly larger than the pK_a value of $AcrH_2^{\bullet+}$, since the difference in the calculated heat of formation between $AcrBu^{t\bullet}$ and $AcrHBu^{t\bullet+}$ is slightly (2.3 kJ mol^{-1}) larger than that between $AcrH^\bullet$ and $AcrH_2^{\bullet+}$.[48] Thus, the proton transfer from $AcrHR^{\bullet+}$ to $A^{\bullet-}$ should be the rate-determining as compared to fast electron transfer from $AcrR^\bullet$ to $AH^\bullet$ as shown in Scheme 2.

According to eq 9, deviation from linear correlations between log k_{obs} and log k_d may be ascribed to the difference in the K_{et} value, since the proton transfer rate constant (k_p) in Scheme 2 may be in parallel with the deprotonation rate constant (k_d) in Scheme 1. The equilibrium constant for electron transfer from AcrHR to A (K^0_{et}) to produce free $AcrHR^{\bullet+}$ and $A^{\bullet-}$ can be obtained from the E^0_{ox} value of AcrHR and E^0_{red} value of A by eq 10.

$$K^0_{et} = \exp[-F(E^0_{ox} - E^0_{red})/RT] \quad (10)$$

Table 2. One-Electron Reduction Potentials (E^0_{red}) of $AcrR^+ClO_4^-$ Determined by the Cyclic Voltammograms in MeCN at 298 K and the Sweep Rates.

$AcrR^+$	E^0_{red}(*vs* SCE)	Sweep Rate
R	V	V s^{-1}
H	–0.46	15000 [a]
$PhCH_2$	–0.50	0.05
Ph	–0.55	0.05
Et	–0.57	1
Bu^t	–0.59	1
Pr^i	–0.63	0.05

[a] Taken from ref 46.

When the difference in the K^0_{et} values for the AcrHR–DDQ and AcrHR–TCNE systems is included in the plots between log k_{obs} and log k_d, the two separate linear correlations and deviation from the linear lines in Figure 4a *are remarkably merged into a single line with a slope of unity* as shown in Figure 4b where the log k_{obs} values are plotted against the log $k_dK^0_{et}$ values.[49] Thus, it can be concluded that the overall hydride transfer from AcrHR to A proceeds via sequential electron-proton-electron transfer in which the initial electron transfer to produce the radical ion pair is in equilibrium and the proton transfer from $AcrHR^{\bullet+}$ to $A^{\bullet-}$ is the rate-determining step (Scheme 2). The observed primary kinetic isotope effects (k_H/k_D) of the overall hydride transfer from $AcrH_2$ and the 9,9'-dideuteriated compound ($AcrD_2$) to *p*-benzoquinone derivatives (Q)[50] can be attributed to those of the proton transfer step from $AcrH_2^{\bullet+}$ and $AcrD_2^{\bullet+}$ to $Q^{\bullet-}$, since the variation of k_H/k_D with *p*-benzoquinone derivatives has been well correlated with the difference in the pK_a values between $AcrH_2^{\bullet+}$ and $QH^\bullet$ (ΔpK_a) and the maximum value ($k_H/k_D = 10.4$) is obtained at $\Delta pK_a = 0$.[50]

It should be noted that $A^{\bullet-}$ is formed as a final product by the subsequent fast reaction of AH^- with A (eq 2) and the disproportionation reaction of $AH^\bullet$ (eq 3) after the overall hydride transfer reaction (eq 1). Such fast reactions following the hydride transfer to produce $A^{\bullet-}$ have precluded the detection of $A^{\bullet-}$ in the course of the hydride transfer reaction. Conversely the detection of radical ions in hydride transfer reactions does not necessarily

mean the involvement of an electron transfer step in the hydride transfer reactions.

CT Complex Formed between AcrHR and *p*-Benzoquinone Derivatives. Although there is an excellent single linear correlation between log k_{obs} and log $k_dK^0_{et}$, the k_{obs} values, which correspond to the k_pK_{et} values in eq 9, are 10^9 times larger than the corresponding $k_dK^0_{et}$ values (Figure 4). The reason for such a huge difference in the absolute values may be two-fold. Firstly the rate constant of proton transfer from $AcrHR^{\bullet+}$ to $A^{\bullet-}$ (k_p) may be much larger than the spontaneous deprotonation rate constant of $AcrHR^{\bullet+}$ (k_d), since $A^{\bullet-}$ acts as a base. This may be the reason why the proton transfer from $AcrHBu^{t\bullet+}$ to $A^{\bullet-}$ preceded the cleavage of the C(9)-C bond of $AcrHBu^{t\bullet+}$ leading to the overall hydride transfer reaction (eq 4). Secondly the K_{et} value for the radical ion pair formation in Scheme 2 may also be larger than the K^0_{et} value for formation of free radical ions ($AcrHR^{\bullet+}$ and $A^{\bullet-}$), since there may be a significant Coulombic interaction between $AcrHR^{\bullet+}$ and $A^{\bullet-}$ in the radical ion pair.[6]

Formation of a radical ion pair is usually preceded by formation of a charge-transfer (CT) complex between an electron donor and acceptor.[18-22,51] The observation of CT complexes is difficult in fast reactions such as hydride transfer from $AcrH_2$ to DDQ because of the instability of the CT complex. When DDQ is replaced by a weaker electron acceptor such as chloro-*p*-benzoquinone, a new broad absorption band, which is characteristic of an intermolecular CT transition, is readily observed upon mixing an MeCN solution of $AcrH_2$ with that of chloro-*p*-benzoquinone as shown in Figure 6a. When $AcrH_2$ is replaced by $AcrHCH_2Ph$, a broad absorption band with the same absorption maximum (λ_{max} = 540 nm) is observed (Figure 6b). The λ_{max} values are shifted to longer wavelengths when chloro-*p*-benzoquinone is replaced by 2,6-dichloro-*p*-benzoquinone and *p*-chloranil which are stronger electron acceptors than chloro-*p*-benzoquinone as shown in Figure 6c and 6d, respectively. A stopped-flow technique was used for the detection of an unstable CT complex formed between $AcrHCH_2Ph$ and *p*-chloranil (see Experimental Section). The CT complex is significantly stabilized when $AcrHBu^t$ is employed as an electron donor which has the least reactivity toward hydride acceptors (Table 1). Thus, the CT spectra of $AcrHBu^t$-*p*-chloranil and $AcrHBu^t$-DDQ complexes are readily observed as shown in Figure 6e and 6f, respectively.[52]

The CT transition energies ($h\nu_{max}$) observed in Figure 6 are compared with those of other known CT complexes formed between a variety of electron donors and *p*-benzoquinone derivatives[16,18,53] in Figure 7 where the $h\nu_{max}$ values are plotted against the difference between the one-electron oxidation potentials of electron donors[16,54,55] and the one-electron

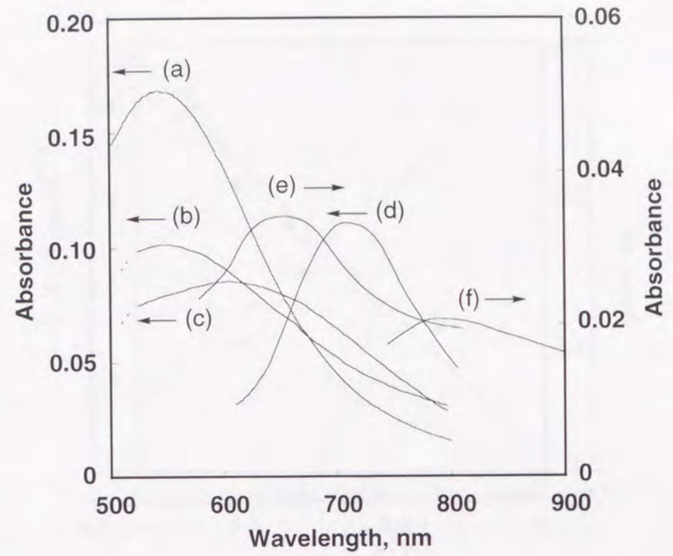

Figure 6. Electronic absorption spectra of CT complexes of (a) $AcrH_2$ (5.9×10^{-2} M) with chloro-*p*-benzoquinone (6.0×10^{-2} M), (b) $AcrHCH_2Ph$ (1.2×10^{-2} M) with chloro-*p*-benzoquinone (6.0×10^{-2} M), (c) $AcrHCH_2Ph$ (1.2×10^{-2} M) with 2,6-dichloro-*p*-benzoquinone (6.0×10^{-2} M), (d) $AcrH_2$ (5.9×10^{-2} M) with *p*-chloranil (1.0×10^{-2} M) (e) $AcrHBu^t$ (6.0×10^{-3} M) with *p*-chloranil (1.0×10^{-2} M) and (f) $AcrHBu^t$ (6.0×10^{-3} M) with DDQ (1.0×10^{-2} M) in MeCN at 298 K.

reduction potential of *p*-benzoquinone derivatives,[6] which is related to the free energy change of electron transfer $\Delta G^0_{et}/F = E^0_{ox} - E^0_{red}$. The $h\nu_{max}$ values of the examined AcrHR–*p*-benzoquinone derivative complexes are consistent with those of other known CT complexes in the correlation with $\Delta G^0_{et}/F$ values (Figure 7). Thus, the observed CT complexes in the course of hydride transfer reactions from AcrHR to *p*-benzoquinone derivatives (Q) are classified as donor-acceptor complexes of a quite general kind as shown in eq 11.

$$AcrHR + Q \overset{K_{CT}}{\rightleftharpoons} (AcrHR\ Q) \xrightarrow{h\nu_{max}} (AcrHR^{\bullet+}\ Q^{\bullet-}) \qquad (11)$$

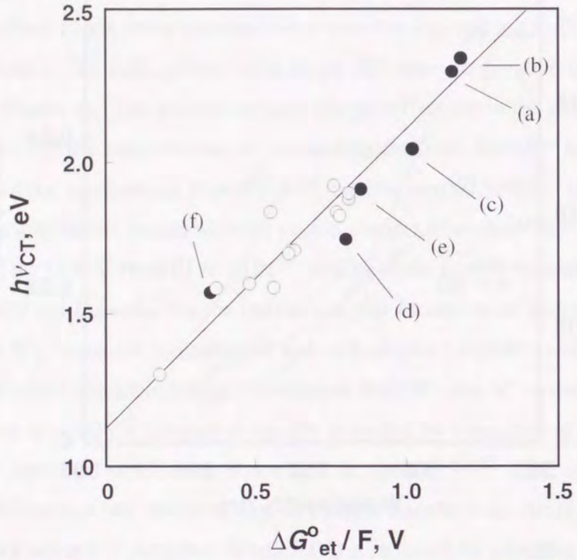

Figure 7. Plot of CT transition energies ($h\nu_{CT}$) of AcrHR–Q complexes (●) and other known CT complexes of Q (○) *vs* $E^{0}_{ox} - E^{0}_{red}$.

The formation constant K_{CT} of the CT complex formed between $AcrH_2$ and chloro-*p*-benzoquinone (ClQ) in MeCN was determined from an increase in the CT absorbance (A) at λ_{max} with an increase in the quinone concentration [Q] according to the Benesi-Hildebrand equation (eq 12),[56] where ε is the extinction coefficient. The K_{CT} values were determined at

$$A = \varepsilon K_{CT}[AcrH_2][ClQ]/(1 + K_{CT}[ClQ]) \quad (12)$$

various temperatures. From the plot of ln K_{CT} vs T^{-1} shown in Figure 8 is determined the heat of formation of the CT complex (ΔH_{CT} = –29 kJ mol^{-1}).

Negative Temperature Dependence of the Rates of Hydride Transfer. The decay of the transient CT band observed in the course of the hydride transfer from $AcrH_2$ to *p*-chloranil in Figure 6d coincides completely with the rise of the absorption band due to the product. However, such a coincidence does not necessarily mean that the CT complex is an

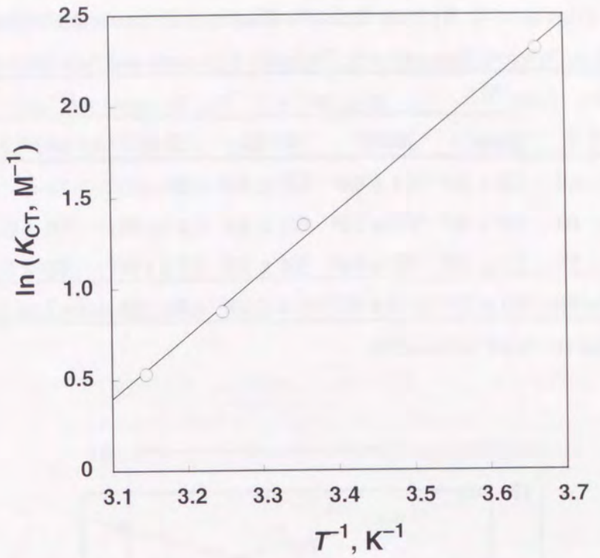

Figure 8. Plot of ln K_{CT} vs T^{-1} for the temperature dependence of K_{CT} of the CT complex formed between $AcrHCH_2Ph$ and chloro-*p*-benzoquinone in MeCN.

intermediate for the hydride transfer reaction as discussed in Introduction. Whether the observed CT complex is a real intermediate for the hydride transfer reaction or a merely innocent bystander in an otherwise dead-end equilibrium could only be distinguishable by the temperature dependence of the rate if one can observe the negative temperature dependence.

The k_{obs} values for the hydride transfer reaction from $AcrHCH_2Ph$ to DDQ in different solvents were determined at various temperatures and they are listed in Table 3. From the Arrhenius plots shown in Figure 9 are obtained the activation enthalpies ($\Delta H^{\neq}_{obs}$) and the activation entropies ($\Delta S^{\neq}_{obs}$) as also listed in Table 3. The k_{obs} value in $CHCl_3$ which is the least polar solvent among the examined solvents is the largest. The negative $\Delta H^{\neq}_{obs}$ value (–13 kJ mol^{-1}) is obtained in $CHCl_3$, and this means *the lower the temperature, the faster the rate of hydride transfer*. The $\Delta H^{\neq}_{obs}$ and $\Delta S^{\neq}_{obs}$ values of other AcrHR derivatives (R = H, Me and Et) were also determined from the temperature dependence of k_{obs}. The Arrhenius plots are shown in Figure 10, where a negative temperature dependence

Table 3. Rate Constants of Hydride Transfer Reaction from $AcrHCH_2Ph$ to DDQ in Various Solvents at Different Temperatures, Dielectric Constants and Activation Parameters

		k_{obs}, M^{-1} s^{-1}				$\Delta H^{\neq}_{obs}$	$\Delta S^{\neq}_{obs}$
solvent	ε	298 K	308 K	318 K	328 K	kJ mol^{-1}	J K^{-1} mol^{-1}
$CHCl_3$	4.8	1.3 x 10^5	1.1 x 10^5	9.8 x 10^4	8.0 x 10^4	–13	–160
CH_2ClCH_2Cl	10	5.5 x 10^4	5.8 x 10^4	6.1 x 10^4	6.4 x 10^4	4	–110
PhCN	25	1.0 x 10^4	1.2 x 10^4	1.4 x 10^4	1.7 x 10^4	13	–89
MeCN	38	1.1 x 10^4	1.2 x 10^4	1.4 x 10^4	1.4 x 10^4	7	–110

[a] The experimental errors are within ±5%.

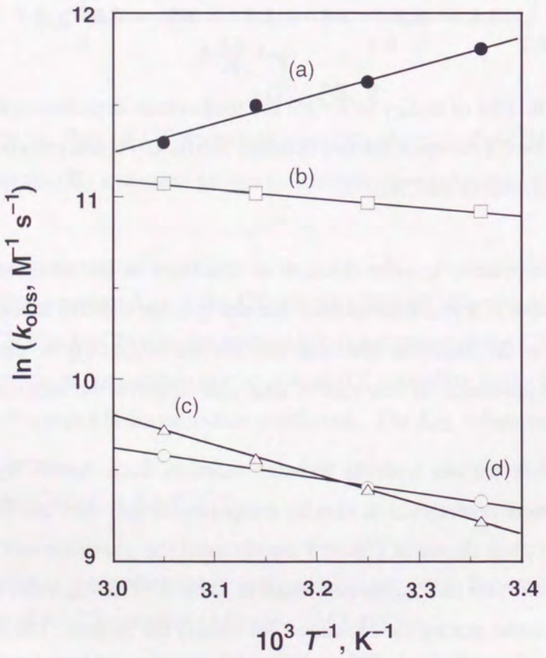

Figure 9. Arrhenius plots of k_{obs} for the reaction of $AcrHCH_2Ph$ (1.1 x 10^{-5} M) with DDQ (2.0 x 10^{-4} M) in (a) $CHCl_3$, (b) CH_2ClCH_2Cl, (c) PhCN and (d) MeCN.

Table 4. Rate Constants of Hydride Transfer Reaction from AcrHR to DDQ in $CHCl_3$ at Different Temperatures and the Activation Parameters

AcrHR	k_{obs}, M^{-1} s^{-1}				$\Delta H^{\neq}_{obs}$	$\Delta S^{\neq}_{obs}$
R	298 K	308 K	318 K	328 K	kJ mol^{-1}	J K mol^{-1}
H	*b*	2.3 x 10^7	1.6 x 10^7	1.1 x 10^7	–32	–170
Me	2.0 x 10^6	1.8 x 10^6	1.8 x 10^6	1.7 x 10^6	–4	–100
Et	7.5 x 10^5	7.6 x 10^5	7.7 x 10^5	7.8 x 10^5	1	–95

[a] The experimental errors k_{obs} of are within ±5%. [b] Too fast to be determined accurately.

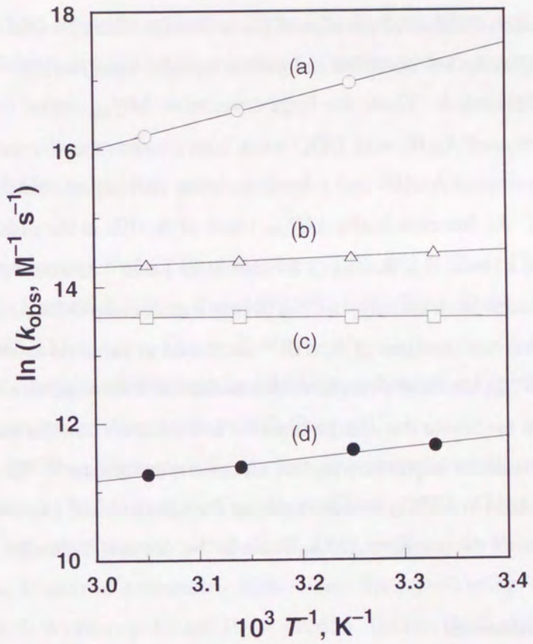

Figure 10. Arrhenius plots of k_{obs} for the reaction of AcrHR [R = (a) H, (b) Me, (c) Et and (d) CH_2Ph; 1.1 x 10^{-5} M] with DDQ (2.0 x 10^{-4} M) in $CHCl_3$.

is clearly observed for the hydride transfer reaction of $AcrH_2$. The $\Delta H^{\neq}_{obs}$ value of AcrHR increases in the order: R = H (–32 kJ mol^{-1}) < R = Me (–4 kJ mol^{-1}) < R = Et (1 kJ mol^{-1}) as listed in Table 4.

The observed negative $\Delta H^{\neq}_{obs}$ values, which should be equal to $\Delta H_{CT} + \Delta H^{\neq}_1$ ($k_{obs} = k_1 K_{CT}$), could only arise when the CT complex lies along the reaction pathway (*vide supra*, eq 1). The ΔH_{CT} values for the AcrHR–DDQ complexes may be more negative than the observed ΔH_{CT} value (–29 kJ mol^{-1}) for the $AcrH_2$ complex with chloro-*p*-benzoquinone which is a weaker electron acceptor than DDQ. Thus, the heat of formation of the CT complex ($\Delta H_{CT} < 0$) may be of greater magnitude than the activation enthalpy for the passage of the CT complex to the transition state ($\Delta H_1^{\neq} > 0$) in eq 1, *i.e.*, $-\Delta H_{CT} > \Delta H_1^{\neq}$ when the $\Delta H^{\neq}_{obs}$ values ($\Delta H^{\neq}_{obs} = \Delta H_{CT} + \Delta H^{\neq}_1$) become negative. As demonstrated by a single correlation between log k_{obs} and log $k_d K^0_{et}$ in Figure 4b, the $\Delta H^{\neq}_1$ value for the hydride transfer reaction consists of the sum of the activation enthalpies for electron transfer from AcrHR to DDQ in the CT complex and proton transfer from $AcrHR^{\bullet+}$ to $DDQ^{\bullet-}$ in the radical ion pair in Scheme 2. Thus, the largest negative $\Delta H^{\neq}_{obs}$ value (–32 kJ mol^{-1}) is obtained for the reaction of $AcrH_2$ with DDQ when both electron transfer and proton transfer are fastest among examined AcrHR and *p*-benzoquinone derivatives and the $\Delta H^{\neq}_1$ value is therefore minimized. An increase in the $\Delta H^{\neq}_{obs}$ value of AcrHR in the order R = H (–32 kJ mol^{-1}) < R = Me (–4 kJ mol^{-1}) < R = Et (1 kJ mol^{-1}) in Table 4 can be well accounted for by an increase in the activation enthalpy for the proton transfer step from $AcrHR^{\bullet+}$ to $DDQ^{\bullet-}$, since the deprotonation rate constant of $AcrHR^{\bullet+}$ decreased in the same order (Table 1). The solvent effects on $\Delta H^{\neq}_{obs}$ are more complicated than the substituent effects. The more polar the solvent, the more favorable the charge transfer and electron transfer steps, but the less favorable the proton transfer step following the electron transfer step.[57] These two opposite effects may be optimized in $CHCl_3$ so as to achieve the smallest $\Delta H^{\neq}_1$ value resulting in the successful observation of the negative $\Delta H^{\neq}_{obs}$ value in this solvent (Table 2).

Summary and Conclusions

The observed negative temperature dependence of the rate of hydride transfer from $AcrH_2$ to DDQ gave an unequivocal evidence for the role of the observed CT complex as an actual intermediate in the hydride transfer reaction. The magnitude of the observed rate constant for the reactions of AcrHR with a hydride acceptor (DDQ or TCNE) varies significantly depending on the type of substituent R in AcrHR at C-9 position and spans a range of 10^7 starting from R = H to Bu^t and CMe_2COOMe. Such large variation in the rate constant is well correlated with the large variation in the deprotonation rate constant of $AcrHR^{\bullet+}$ combined with the small variation in the electron transfer reactivity of AcrHR. Based on these results it is concluded that the overall hydride transfer proceeds via a CT complex formed between AcrHR and the hydride acceptor (A), electron transfer from AcrHR to A in the CT complex, proton transfer from $AcrHR^{\bullet+}$ to $A^{\bullet-}$ and electron transfer from $AcrR^{\bullet}$ to $AH^{\bullet}$ to yield $AcrR^+$ and AH^-. The overall reactivity is determined by the three consecutive steps, *i.e.*, the CT complex formation, the electron transfer and the proton transfer steps, since the electron transfer in the final step is much faster than the previous proton transfer step. The initial electron transfer step in the CT complex may be facilitated by the charge-transfer interaction in the CT complex, since such charge-transfer interaction should result in a decrease in the difference of nuclear configurations before and after the electron transfer step. Thus, this study has provided first comprehensive and confirmative understanding of the mechanism of sequential electron-proton-electron transfer via CT complexes.[58]

References and Notes

(1) Stryer, L. *Biochemistry, 3rd ed*; Freeman: New York, 1988; Chap. 17.

(2) (a) Eisner, U.; Kuthan, J. *Chem. Rev.* **1972**, *72*, 1. (b) Stout, D. M.; Meyer, A. I. *Chem. Rev.* **1982**, *82*, 223.

(3) Fukuzumi, S.; Tanaka, T. *Photoinduced Electron Transfer*; Fox, M. A., Chanon, M., Eds.; Elsevier: Amsterdam; 1988, Part C; Chap. 10.

(4) (a) Sund, H. *Pyridine-Nucleotide Dependent Dehydrogenase*; Walter de Gruyer: West Berlin, 1977. (b) R. M. Kellog, *Top. Curr. Chem.*, 1982, *101*, 111; *Angew. Chem.*, 1984, *96*, 769. (c) Ohno, A.; Ushida, S. Lecture Notes in Bioorganic Chemistry, *Mechanistic Models of Asymmetric Reductions;* Springer-Verlag: Berlin, 1986; p 105. (d) Bunting, J. W. *Bioorg. Chem.* 1991, *19*, 456. (e) He, G.-X.; Blasko, A.; Bruice, T. C. *Bioorg. Chem.* 1993, *21*, 423. (f) Ohno, A. *J. Phys. Org. Chem.* 1995, *8*, 567.

(5) Fukuzumi, S. *Advances in Electron Transfer Chemistry*; Mariano, P. S., Ed.; JAI press; Greenwich, CT, 1992; pp 67-175.

(6) Fukuzumi, S.; Koumitsu, S.; Hironaka, K.; Tanaka, T. *J. Am. Chem. Soc.* **1987**, *109*, 305 and references cited therein.

(7) (a) Fukuzumi, S.; Ishikawa, M.; Tanaka, T. *J. Chem. Soc., Perkin Trans. 2* **1989**, 1811. (b) Fukuzumi, S.; Mochizuki, S.; Tanaka, T. *J. Am. Chem. Soc.* **1989**, *111*, 1497. (c) Ishikawa , M.; Fukuzumi, S. *J. Chem. Soc., Chem. Commun.* **1990**, 1353.

(8) Cheng, J.-P.; Lu, Y.; Zhu, X.; Mu, L. *J. Org. Chem.* **1998**, *63*, 6108.

(9) Ohno, A., Ishikawa, Y., Yamazaki, N., Okamura, M., Kawai, Y, *J. Am. Chem. Soc.* **1998**, *120*, 1186.

(10) (a) Pestovsky, O., Bakac, A., Espenson, J. H. *J. Am. Chem. Soc.* **1998**, *120*, 13422. (b) Pestovsky ,O; Bakac, A.; Espenson, J. H. *Inorg. Chem.* **1998**, *37*, 1616.

(11) Anne, A.; Moiroux, J.; Savéant, J.-M. *J. Am. Chem. Soc.* **1993**, *115*, 10224.

(12) (a) Kreevoy, M. M.; Ostovic, D.; Lee, I.-S. H.; Binder, D. A.; King, G. W. *J. Am. Chem. Soc.* **1988**, *110*, 524. (b) Lee, I.-S. H.; Jeoung, E. H.; Kreevoy, M. M. *J. Am. Chem. Soc.* **1997**, *119*, 2722.

(13) (a) Ohno, A.; Yamamoto, H.; Oka, S.; *J. Am. Chem. Soc.* **1981**, *103*, 2041. (b) Ohno, A.; Shio, T.; Yamamoto, H.; Oka, S. *J. Am. Chem. Soc.* **1981**, *103*, 2045.

(14) (a) Powell, M. F.; Bruice, T. C. *J. Am. Chem. Soc.* **1983**, *105*, 1014, 7139. (b) Chipman, D. M.; Yaniv, R.; van Eikeren, P. *J. Am. Chem. Soc.* **1980**, *102*, 3244.

(15) (a) Carlson, B. W.; Miller, L. L. *J. Am. Chem. Soc.* **1985**, *107*, 479. (b) Miller, L. L.; Valentine, J. R. *J. Am. Chem. Soc.* **1988**, *110*, 3982. (c) Colter, A. K.; Plank, P.; Bergsma, J. P.; Lahti, R.; Quesnel, A. A.; Parsons, A. G. *Can. J. Chem.* **1984**, *62*, 1780. (d) Verhoeven, J. W.; van Gerresheim, W.; Martens, F. M.; van der Kerk, S. M. *Tetrahedron*, **1986**, *42*, 975. (e) Coleman, C. A.; Rose, J. G.; Murray, C. J. *J. Am. Chem. Soc.* **1992**, *114*, 9755.

(16) Fukuzumi, S.; Nishizawa, N.; Tanaka, T. *J. Org. Chem.* **1984**, *49*, 3571.

(17) Fukuzumi, S.; Kondo, Y.; Tanaka, T. *J. Chem. Soc., Perkin Trans. 2* **1984**, 673.

(18) (a) Mulliken, R. S.; Person, W. B. *Molecular Complexes*, a Lecture and Reprint Volume, Wiley-Interscience, New York, 1969. (b) Foster, R. *Organic Charge Transfer Complexes*; Academic Press: New York, 1969.

(19) (a) Kochi, J. K. *Adv. Phys. Org. Chem.* **1994**, *29*, 185. (b) Kochi, J. K. Chimica **1991**, 45, 277. (b) Kochi, J. K. Angew. Chem., Int. Ed. Engl. **1988**, *27*, 1227. (c) Kochi, J. K. *Acc. Chem. Res.* **1992**, *25*, 39. (d) Kochi, J. K. *Acta Chem. Scand.* **1990**, *44*, 409.

(20) (a) Chanon, M.; Tobe, M. *Angew. Chem., Int. Ed. Engl.* **1982**, *21*, 1. (b) Jones, G. II. *In Photoinduced Electron Transfer*; Fox, M. A., Chanon, M., Eds.; Elsevier: Amsterdam, 1988; Part A, p 245. (c) Chanon, M.; Rajzmann, M.; Chanon, F. *Tetrahedron* **1990**, *46*, 6193. (d) Julliard, M.; Chanon, M. *Chem. Rev.* **1983**, *83*, 425.

(21) Sustmann, R.; Korth, H.-G.; Nüchter, U.; Siangouri-Feulner, I.; Sicking, W. *Chem. Ber.* **1991**, *124*, 2811.

(22) (a) Fukuzumi, S.; Mochida, K.; Kochi, J. K. *J. Am. Chem. Soc.* **1979**, *101*, 5961. (b) Fukuzumi, S.; Kochi, J. K. *J. Am. Chem. Soc.* **1980**, *102*, 2141. (c) Fukuzumi, S.; Kochi, J. K. *Tetrahedron* **1982**, *38*, 1035.

(23) Kiselev, V. D.; Miller, J. G. *J. Am. Chem. Soc.* **1975**, *97*, 4036.

(24) A negative temperature dependence of the rates of photoinduced electron transfer reactions of ruthenium(II) complexes has been reported: (a) Kim, H-B.; Kitamura, N.; Kawanishi, Y.; Tazuke, S. *J. Am. Chem. Soc.* **1987**, *109*, 2506. (b) Kim, H.-B.; Kitamura, N.; Kawanishi, Y.; Tazuke, S. *J. Phys. Chem.* **1989**, *93*, 5757.

(25) Brominations of some alkenes in non-polar media were reported to have negative activation energies: Sergeev, G. B.; Serguchev, Yu. A.; Smirnov, V. V. *Russ. Chem. Rev.* **1973**, *42*, 697.

(26) (a) Fukuzumi, S.; Kitano, T. *Chem. Lett.* **1990**, 1275. (b) Fukuzumi, S.; Mochizuki, S.; Tanaka, T. *J. Chem. Soc., Dalton Trans.* **1990**, 695.

(27) Fukuzumi, S.; Tokuda, Y.; Kitano, T.; Okamoto, T.; Otera, J. *J. Am. Chem. Soc.* **1993**, *115*, 8960.

(28) A preliminary report on observation of a negative activation enthalpy for a hydride transfer reaction of a hydride donor other than NADH analogues has appeared: (a) Zaman, K. M.; Yamamoto, S.; Nishimura, N.; Maruta, J.; Fukuzumi, S. *J. Am. Chem. Soc.* **1994**, *116*, 12099. (b) Yamamoto, S.; Sakurai, T.; Liu, Y.; Sueishi, Y. *Phys. Chem. Chem. Phys.* **1999**, *1*, 833.

(29) Roberts, R. M. G.; Ostovic, D.; Kreevoy, M. M. *Faraday Discuss. Chem. Soc.* **1982**, *74*, 257.

(30) Fukuzumi, S.; Kitano, T.; Tanaka, T. *Chem. Lett.* **1989**, 1231.

(31) Otera, J.; Wakahara, Y.; Kamei, H.; Sato, T.; Nozaki, H.; Fukuzumi, S. *Tetrahedron Lett.* **1991**, *32*, 2405.

(32) Bernthsen, A. *Ann.* **1884**, *224*, 1.

(33) Perrin, D. D.; Armarego, W. L. F.; Perrin, D. R. *Purification of Laboratory Chemicals*; Pergamon Press: Elmsford, 1966.

(34) Iida, Y. *Bull. Chem. Soc. Jpn.* **1971**, *44*, 1777.

(35) Webster, O. W.; Mahler, W.; Benson, R. E. *J. Am. Chem. Soc.* **1962**, *84* , 3678.

(36) Mann, C. K.; Barnes, K. K. *Electrochemical Reactions in Nonaqueous Systems*; Marcel Dekker: New York, 1990.

(37) Stewart, J. J. P. *J. Comput. Chem.* **1989**, *10*, 209, 221.

(38) (a) Colter, A. K.; Saito, G.; Sharom, F. J.; Hong, A. P. *J. Am. Chem. Soc.* **1976**, *98*, 7833. (b) Colter, A. K.; Saito, G.; Sharom, F. J. *Can. J. Chem.* **1977**, *55*, 2741.

(39) (a) Gordon, D.; Hove, M. J. *J. Chem. Phys.* **1973**, *59*, 3419. (b) Corvaja, C.; Pasimeni, L.; Brustalon, M. *Chem. Phys.* 1976, *14*, 177. (c) Grampp, G.; Landgraf, S.; Rasmussen, K. *J. Chem. Soc., Perkin Trans. 2* **1999**, 1897.

(40) Phillips, W. D.; Powell, J. C.; Weissman, S. I. *J. Chem. Phys.* **1960**, *33*, 626.

(41) It was confirmed that the rates were not affected by the room light.

(42) The C(9)–C bond cleavage of $AcrHBu^{t\bullet+}$ generated by the electrochemical oxidation of $AcrHBu^{t}$ has also been reported: Anne, A.; Fraoua, S.; Moiroux, J.; Savéant, J.-M. *J. Am. Chem. Soc.* **1996**, *118*, 3938.

(43) The k_d value of $AcrHCH_2Ph^{\bullet+}$ was determined from the k_d value of $AcrHMe^{\bullet+}$ and the ratio of the observed second order rate constant for the proton transfer from $AcrHCH_2Ph^{\bullet+}$ to 3,5-dichloropyridine to that from $AcrHMe^{\bullet+}$; see ref 27. The k_d values of $AcrHR^{\bullet+}$ in which the C(9)-C bond is cleaved exclusively have not been determined accurately.

(44) The proton transfer cannot precede the initial electron transfer from AcrHR to DDQ, since no deprotonation of AcrHR occurs in the presence of pyridine which is a much stronger base than DDQ.

(45) Fukuzumi, S.; Tokuda, Y. *J. Phys. Chem.* **1992**, *96*, 8409.

(46) Hapiot, P.; Moiroux, J.; Savéant, J.-M. *J. Am. Chem. Soc.* **1990**, *112*, 1337.

(47) Rich, P. R.; Bendall, D. S. *Biochim. Biophys. Acta* **1980**, *592*, 506.

(48) The heats of formation of $AcrR^{\bullet}$ and $AcrHR^{\bullet+}$ (R = H and Bu^{t}) were calculated by the PM3 method.

(49) The k_{obs} values are about 10^{10} times larger than the corresponding $k_dK^0_{et}$ values (Figure 4b). Such a large difference may originate from the much larger rate constant of proton transfer from $AcrHR^{\bullet+}$ to a strong base ($A^{\bullet-}$) than the spontaneous deprotonation rate constant k_d, combined with the larger K_{et} value for the radical ion pair formation, in which the large work term is included,[6] than the K^0_{et} value for the free radical ion formation.

(50) Ishikawa, M.; Fukuzumi, S. *J. Chem. Soc., Faraday Trans.* **1990**, *86*, 3531.

(51) (a) Fukuzumi, S.; Kochi, J. K. *J. Am. Chem. Soc.* **1980**, *102*, 7290. (b) Fukuzumi, S.; Wong, C. L.; Kochi, J. K. *J. Am. Chem. Soc.* **1980**, *102*, 2928. (c) Fukuzumi, S.; Kochi, J. K. *J. Am. Chem. Soc.* **1982**, *104*, 7599.

(52) The examined concentration of $AcrHBu^{t}$ (6.0×10^{-3} M) was smaller than the $AcrH_2$ concentration (5.9×10^{-2} M) because of the lower solubility of $AcrHBu^{t}$, when the CT absorbances of the $AcrHBu^{t}$-*p*-chloranil and $AcrHBu^{t}$-DDQ complexes in Figure 6e and 6f, respectively, are smaller than that of the $AcrH_2$–*p*-chloranil complex (Figure 6d).

(53) (a) Foster, R.; Thomson, T. J. *Trans. Faraday Soc.* **1962**, *58*, 860. (b) Zweig, A.; Lancaster, J. E.; Neglia, M. T.; Jura, W. H. *J. Am. Chem. Soc.* **1964**, *86*, 4130.

(54) Fukuzumi, S.; Hironaka, K.; Nishizawa, N.; Tanaka, T. *Bull. Chem. Soc. Jpn.* **1983**, *56*, 2220.

(55) (a) Mann, C. K.; Barnes, K. K. *Electrochemical Reactions in Nonaqueous Systems*, Marcel Dekker, New York, 1970. (b) Seo, E. T.; Nelsonm, R. F.; Fritsch, J. M.; Marcoux, L. S.; Leedy, D. W.; Adams, R. N. *J. Am. Chem. Soc.* **1966**, *84*. 3498. (c) Bock, C. R.; Connor, J. A.; Gutierrez, A. R.; Meyer, T. J.; Whitten, D. G.; Sullivan, B. P.; Nagle, J. K. *J. Am. Chem. Soc.* **1979**, *101*, 4815.

(56) Benesi, H. A.; Hildebrand, J. H. *J. Am. Chem. Soc.* **1949**, *71*, 2703.

(57) Manring, L. E.; Peters, K. S. *J. Am. Chem. Soc.* **1985**, *107*, 6452.

(58) Theoretical confirmation of the participation of a CT complex as a real intermediate has recently been reported for the Diels-Alder reaction of anthracene with TCNE in which an electron transfer process following the CT complex formation plays an important role in determining the overall reactivity[20c]; Wise, K. E.; Wheeler, R. A. *J. Phys. Chem. A* **1999**, *103*, 8279.

Chapter 2

Activation of Carbon–Hydrogen Bond by Photoinduced Electron Transfer

Section 2. 1
A Charge Shift Type of Photoinduced Electron Transfer Reactions of 10-Alkylacridinium Ion Controlled by Solvent Polarity

Abstract: A charge shift type of photoinduced electron transfer reactions from various electron donors to the singlet excited state of 10-decylacridinium cation ($DeAcrH^+$) in a nonpolar solvent (benzene) is found to be as efficient as those of 10-methylacridinium cation ($MeAcrH^+$) and $DeAcrH^+$ in a polar solvent (acetonitrile). Irradiation of the absorption bands of $MeAcrH^+$ in acetonitrile solution containing tetraalkyltin compounds (R_4Sn) results in the efficient and selective reduction of $MeAcrH^+$ to yield the 10-methyl-9-alkyl-9,10-dihydroacridine (AcrHR). The same type of reaction proceeds in benzene when $MeAcrH^+$ is replaced by $DeAcrH^+$ which is soluble in benzene. The photoalkylation of $RAcrH^+$ (R = Me and De) also proceeds in acetonitrile and benzene using 4-*tert*-butyl-1-benzyl-1,4-dihydronicotinamide (Bu^{t}BNAH) instead of R_4Sn, yielding MeAcrHBu^t. The quantum yield determinations, the fluorescence quenching of $RAcrH^+$ by electron donors, direct detection of the reaction intermediates by means of laser flash photolysis experiments indicate that the photoalkylation of $RAcrH^+$ in benzene as well as in acetonitrile proceeds via photoinduced electron transfer from the alkylating agents (R_4Sn and Bu^{t}BNAH) to the singlet excited states of $RAcrH^+$. The limiting quantum yields are determined by the competition between the back electron transfer process and the bond-cleavage process in the radical pair produced by the photoinduced electron transfer. The rates of back electron transfer have been shown to be controlled by the solvent polarity which affects the solvent reorganization energy of the back electron transfer. When the free energy change of the back electron transfer (ΔG^0_{bet}) in a polar solvent is in the Marcus inverted region, the rate of back electron transfer decreases with decreasing the solvent polarity, leading to the larger limiting quantum yield for the photoalkylation reaction. In contrast, the opposite trend is obtained when the ΔG^0_{bet} value is in the normal region: the limiting quantum yield decreases with decreasing the solvent polarity.

Introduction

Electron transfer reactions are normally performed in polar solvents such as acetonitrile, in which the product ions of the electron transfer are stabilized by the strong solvation.[1-5] When a cationic electron acceptor (A^+) is employed in electron transfer reactions with a neutral electron donor (D), the electron transfer from D to A^+ produces a radical cation ($D^{\bullet+}$) and a neutral radical ($A^\bullet$).[6,7] In such a case, the solvation before and after the electron transfer may be largely canceled out when the free energy change of electron transfer is expected to be rather independent of the solvent polarity. On the other hand, the solvent reorganization energy for the electron transfer reaction is expected to decrease with decreasing the solvent polarity.[9] It has been reported that a decrease in the solvent reorganization energy with decreasing the solvent polarity results in an increase in the quantum yield for formation of biphenyl radical cation produced in the photoinduced electron transfer from biphenyl to 10-methylacridinium cation ($MeAcrH^+$).[8] This result indicates that separation within the initially formed radical cation/radical pair can compete more effectively with the back electron transfer in nonpolar solvents as compared to that in polar solvents.[8] Although the utility of photoinduced electron transfer reactions is expected to be considerably extended if charge shift type of electron transfer reactions is developed in nonpolar solvents, there have so far been very few studies on photoinduced electron transfer reactions leading to the stable products in nonpolar solvents in comparison with those in polar solvents.[8,10]

We report herein the first systematic study on photoinduced electron transfer reactions from a variety of neutral electron donors to the singlet excited states of organic cations, 10-methylacridinium cation ($MeAcrH^+$) and 10-decylacridinium cation ($DeAcrH^+$) in polar and nonpolar solvents, respectively. It is found that the photoinduced electron transfer reactions in nonpolar solvents proceed as efficiently as those in polar solvents. It is also found that photoinduced electron transfer reactions of $MeAcrH^+$ and $DeAcrH^+$ with organometallic alkylating agents such as tetraalkyltin compounds (R_4Sn) and 4-*tert*-butyl-1-benzyl-1,4-dihydronicotinamide (Bu^{t}BNAH) which are known as a novel organic alkylating agent[11] lead to the reductive alkylation to yield the corresponding alkylated dihydroacridine (MeAcrHR or DeAcrHR) as a stable product. The efficiency for the product formation determined as the limiting quantum yield is found to be highly dependent on the solvent polarity and the electron donor properties of the alkylating agents. The choice of a series of R_4Sn as electron donors is expected to benefit from an additional advantage other than the ability to act as alkylating reagents, that is the large inner-sphere reorganization energy (λ = 41 kcal mol^{-1})

associated with the electron transfer oxidation.[12,13] The large reorganization energy for the electron transfer oxidation of R_4Sn leads to extend the boundary of the Marcus inverted region to the highly exergonic region (–1.8 eV). Since the one-electron oxidation potentials (E^0_{ox}) of R_4Sn can be finely tuned by the choice of alkyl groups (R), the free energy change of back electron transfer can be so widely altered by changing R and the solvent polarity as to lie in the Marcus normal or inverted region. The reactivities of R_4Sn can also be compared with the organic electron donor (Bu^{t}BNAH) which has a much smaller reorganization energy (22.0 kcal mol^{-1})[14] Thus, the present study provides an excellent opportunity to clarify how the reactivity of charge-shift type of photoinduced electron transfer reactions which lead to stable products can be finely controlled by the solvent polarity.

Experimental Section

Materials. 10-Methylacridinium iodide was prepared by the reaction of acridine with methyl iodide in acetone, and it was converted to the perchlorate salt ($MeAcrH^+ClO_4^-$) by addition of $Mg(ClO_4)_2$ to the iodide salt, and purified by recrystallization from methanol.[15,16] Likewise, 10-decylacridinium hexafluorophosphate was prepared by the reaction of acridine with decyl iodide in acetone and the subsequent methasesis with sliver hexafluorophosphate, followed by recrystallization from methanol.[8] 9-Substituted 10-methylacridinium perchlorate ($MeAcrR^+ClO_4^-$: R = Pr^i, $CHPh_2$ and Ph) was prepared by the reaction of 10-methylacridone in dichloromethane with the corresponding Grignard reagents (RMgX), then addition of sodium hydroxide for the hydrolysis and perchloric acid for the neutralization, and purified by recrystallization from ethanol-diethylether.[17]

Organic electron donors (benzene, toluene, ethylbenzene, cumene, *o*-xylene, *m*-xylene, *p*-xylene, 1,2,3-trimethylbenzene, 1,2,4-trimethylbenzene, 1,3,5-trimethylbenzene 1,2,3,4-tetramethylbenzene, 1,2,3,5-tetramethylbenzene, and 1,2,4,5-tetramethylbenzene, pentamethylbenzene, hexamethylbenzene, triphenylamine, *N,N*-dimethylaniline, ferrocene, decamethylferrocene) were obtained commercially and purified by the standard method.[18] Tetraalkyltin compounds [tetramethyltin (Me_4Sn), tetraethyltin (Et_4Sn) and tetra-*iso*-propyltin (Pr$^i_4$Sn)] were obtained commercially from Aldrich and di-*tert*-butyldimethyltin (Bu$^t_2Me_2Sn$) was prepared by the literature procedure.[12] The *tert*-butylated BNAH (Bu^{t}BNAH) was prepared by the Grignard reaction with BNA^+Cl^-.[11,19] 9-Alkyl-9,10-dihydro-10-methylacridine (AcrHR) was prepared as reported previously.[20] Acetonitrile, dichloromethane, chloroform and benzene used as solvents were purified and dried by the

standard procedure.[18] [$^2H_3$]acetonitrile (CD_3CN) was obtained from EURI SO–TOP, France. Tetrabutylammonium perchlorate (TBAP), obtained from Fluka Fine Chemical, was recrystallized from ethanol and dried in vacuo prior to use. Tetrahexylammonium perchlorate (THAP) was prepared by the addition of $NaClO_4$ to the tetrahexylammonium bromide in acetone, followed by recrystallization from acetone.

Reaction Procedure. Typically, an [$^2H_3$]acetonitrile (CD_3CN) solution (0.8 cm^3) containing $MeAcrH^+$ (1.0×10^{-2} M) in an NMR tube sealed with a rubber septum was deaerated by bubbling with argon gas through a stainless steel needle for 5 min. After an alkylating agent [R_4Sn (2 μL) or Bu^{t}BNAH (2.4 mg)] was added to the solution, the solution was irradiated with a xenon lamp through with a deuterium lamp equipped with a UV-cut filter ($\lambda < 310$ nm) at room temperature. After the reaction was complete, when the solution became colorless, the reaction solution was analyzed by ^{1}H NMR spectroscopy. The ^{1}H NMR measurements were performed using a Japan Electron Optics JNM-GSX-400 (400 MHz) NMR spectrometer. The products for the photochemical reaction of $MeAcrH^+$ with R_4Sn were identified as MeAcrHR by comparing the ^{1}H NMR spectra with those of the authentic samples.[20]

Fluorescence Quenching. Quenching experiments of the fluorescence of $MeAcrH^+$ and $DeAcrH^+$ by electron donors were performed using a Shimadzu RF-5000 fluorescence spectrophotometer. The excitation wavelength was 398 nm for $MeAcrH^+$ and $DeAcrH^+$. The monitoring wavelengths were those corresponding to the maxima of the respective emission bands at λ = 488 and 498 nm, respectively. The solutions were deoxygenated by argon purging for 10 min prior to the measurements. Relative emission intensities were measured for MeCN solution containing $MeAcrH^+$ or $DeAcrH^+$ (5.0×10^{-5} M) with electron donors at various concentrations (3.0×10^{-3} – 2.5 M). There was no change in the shape but there was a change in the intensity of the fluorescence spectrum by the addition of an electron donor. The Stern-Volmer relationship (eq 1) was obtained for the ratio of the emission intensities in the absence

$$I_0 / I = 1 + K_{SV}[D] \qquad (1)$$

and presence of quenchers (I_0/I) and the concentrations of quenchers [D]. The fluorescence lifetime τ of $MeAcrH^+$ and $DeAcrH^+$ were determined as 31 ns in MeCN, 30 ns in $CHCl_3$ and 29 ns in benzene by single photon counting using a Horiba NAES-1100 time-resolved

spectrofluorophotometer. The observed quenching rate constants k_q ($= K_{SV}\tau^{-1}$) were obtained from the Stern-Volmer constants K_{SV} and the emission lifetimes τ.

Electrochemical Measurements. Cyclic voltammetry measurements were performed at 298 K on a BAS 100W electrochemical analyzer in deaerated solvent containing 0.1 M tetrabutylammonium perchlorate (TBAP) or tetrahexylammonium perchlorate (THAP) as supporting electrolyte. A conventional three–electrode cell was used with a gold working electrode (surface area of 0.3 mm^2) and a platinum wire as the counter electrode. The Pt working electrode (BAS) was routinely cleaned by soaking it in concentrated nitric acid, followed by repeating rinsing with water and acetone, drying at 353 K prior to use in order to avoid possible fouling of the electrode surface. The reference electrode was an Ag/0.01 M $AgNO_3$. The cyclic voltammograms were measured with various sweep rates in deaerated MeCN containing 0.10 M TBAP used as a supporting electrolyte at 298 K.

The second harmonic ac voltammetry (SHACV) measurements were performed on a BAS 100B electrochemical analyzer in deaerated MeCN containing 0.10 M $NBu^n_4ClO_4$ as a supporting electrolyte at 298 K to determine the one-electron oxidation potentials of alkylbenzenes and triphenylamine . The platinum working electrode (BAS) was polished with BAS polishing alumina suspension and rinsed with acetone before use. The counter electrode was a platinum wire (BAS). The E^0_{ox} values (*vs.* Ag/Ag^+) are converted to those *vs.* SCE by adding 0.29 V.

ESR Measurements. The $MeAcrPh^•$ was generated by the electron transfer reduction of $MeAcrPh^+ClO_4^-$ ($1.7 \times 10^{-4} - 5.0 \times 10^{-3}$ M) with tetramethylsemiquinone radical anion (2.0×10^{-5} M) generated by comproportionation of tetramethyl-*p*-benzoquinone and tetramethyl-*p*-hydroquinone with tetrabutylammonium hydroxide. The solution containing the radical was transferred to an ESR tube under an atmospheric pressure of Ar. The ESR spectra were measured at various temperatures with a JEOL X-band spectrometer (JES-RE1XE). The ESR spectra were recorded under nonsaturating microwave power conditions. The magnitude of modulation was chosen to optimize the resolution and the signal-to-noise (*S/N*) ratio of the observed spectra. The ESR measurements were also carried out to detect the radical intermediates produced in the photochemical reaction of $MeAcrH^+ClO_4^-$ (1.0×10^{-2} M) with $Bu^t_2Me_2Sn$ (4.5×10^{-2} M) in frozen MeCN at 77 K under irradiation of light with a high pressure mercury lamp (USH–1005D) focusing at the sample cell in the ESR cavity. The *g* values were calibrated with an Mn^{2+} marker and the hyperfine coupling constants (hfc) were determined by computer simulation using a Calleo ESR Version 1.2 program coded by

Calleo Scientific on an Apple Macintosh personal computer.

Quantum Yield Determinations. A standard actinometer (potassium ferrioxalate)[21] was used for the quantum yield determination of the photochemical reactions of $MeAcrH^+$ and $DeAcrH^+$ with R_4Sn and Bu^tBNAH. A square quartz cuvette (10 mm i.d.) which contained a deaerated acetonitrile solution (3.0 cm^3) of $MeAcrH^+$ or $DeAcrH^+$ (5.0×10^{-5} - 1.0×10^{-4} M) and R_4Sn (1.0×10^{-3} - 2.5 M) or Bu^tBNAH (5.0×10^{-4} - 1.0×10^{-3} M) was irradiated with monochromatized light of λ = 398 nm from a Shimadzu RF-5000 fluorescence spectrophotometer. Under the conditions of actinometry experiments, both the actinometer and $MeAcrH^+$ or $DeAcrH^+$ absorbed essentially all the incident light. The light intensity of monochromatized light of λ = 398 nm was determined as 1.8×10^{-8} einstein s^{-1} with the slit width of 20 nm. The photochemical reaction was monitored by using Hewlett Packard 8452A and 8453 Diode-Array spectrophotometers. The quantum yields were determined from the decrease in absorbance due to $MeAcrH^+$ (λ = 358 nm, $\varepsilon = 1.8 \times 10^4$ M^{-1} cm^{-1})[22] and $DeAcrH^+$ (λ = 362 nm, $\varepsilon = 2.0 \times 10^4$ M^{-1} cm^{-1}).

Laser Flash Photolysis. The measurements of transient absorption spectra in the photochemical reactions of $DeAcrH^+$ with R_4Sn in benzene were performed according to the following procedures. The benzene solution was deoxygenated by argon purging for 10 min prior to the measurement. The deaerated benzene solution containing $DeAcrH^+$ (5.0×10^{-5} M) and R_4Sn (1.0×10^{-3} – 2.5 M) was excited by a Nd:YAG laser (Quanta-Ray, GCR-130, 6 ns fwhm) at 355 nm with the power of 30 mJ. A pulsed xenon flash lamp (Tokyo Instruments, XF80-60, 15 J, 60 ms fwhm) was used for the probe beam, which was detected with a Si-PIN module (Hamamatsu, C5331-SPL) after passing through the photochemical quartz vessel (10 mm x 10 mm) and a monochromator. The output from Si-PIN module was recorded with a digitizing oscilloscope (HP 54510B, 300 MHz). The transient spectra were recorded using fresh solutions in each laser excitation. All experiments were performed at 298 K.

Results and Discussion

Photoinduced Electron Transfer from Electron Donors to $MeAcrH^+$ and $DeAcrH^+$. Irradiation of the absorption band of $MeAcrH^+$ results in fluorescence at λ = 488 nm in MeCN and $CHCl_3$. The fluorescence lifetimes were determined by single photon counting. as 31 ns and 30 ns in MeCN and $CHCl_3$, respectively. Due to its limited solubility

of $MeAcrH^+ClO_4^-$, it cannot be used in nonpolar solvents such as benzene. In order to overcome the solubility problem, 10-decylacridinium hexafluorophosphate ($DeAcrH^+PF_6^-$) instead of $MeAcrH^+ClO_4^-$ was dissolved in benzene. The fluorescence maximum of $DeAcrH^+$ (498 nm) in benzene is nearly the same as that of $MeAcrH^+$ in MeCN (488 nm). The fluorescence lifetime of $DeAcrH^+$ in benzene (29 ns) is also nearly the same as that of $MeAcrH^+$ in MeCN (31 ns) (see Supporting Information, S1).

The fluorescence of the singlet excited state ($^1MeAcrH^{+*}$) is quenched efficiently by a variety of electron donors in MeCN and $CHCl_3$.[22,23] The quenching rate constants k_q are determined from the slopes of the Stern-Volmer plots and lifetime of the singlet excited state $^1MeAcrH^{+*}$ (see Supporting Information, S2). The fluorescence of $^1DeAcrH^{+*}$ is also quenched efficiently by the same series of electron donors in benzene and the k_q values thus obtained are summarized in Table 1.

The free energy change of photoinduced electron transfer from electron donors to $^1MeAcrH^{+*}$ (ΔG^0_{et} in eV) is given by eq 2, where e is elementary charge, E^0_{ox} and E^0_{red} are

$$\Delta G^0_{et} = e(E^0_{ox} - E^0_{red}) \qquad (2)$$

the one-electron oxidation potentials of electron donors and the one-electron reduction potential of $^1MeAcrH^{+*}$ (2.32 V), respectiely.[7,22] Since the E^0_{ox} values of electron donors in MeCN have been determined in this study (see Experimental Section), the ΔG^0_{et} values are determined by using eq 2 as listed in Table 1 for comparison. Figure 1a shows a plot of log k_{et} vs ΔG^0_{et} in MeCN, which exhibits a typical feature of an electron-transfer process; the log k_{et} value increases with a decrease in the ΔG^0_{et} value to reach a plateau value corresponding to the diffusion rate constant (2.0×10^{10} M^{-1} s^{-1}) as the photoinduced electron transfer becomes energetically more favorable (i.e., more exergonic).[24]

Photoinduced electron transfer from an electron donor (D) to $^1MeAcrH^{+*}$ may occur as shown in Scheme 1, where k_{12} and k_{21} are diffusion and dissociation rate constants in theencounter complex (D $MeAcrH^{+*}$), k_{et} and k_{-et} are the rate constants of the forward electron transfer from D to $MeAcrH^{+*}$ and the back electron transfer to the ground state.[22,26] The observed rate constant (k_{obs}) of photoinduced electron transfer is given by eq 3. The

Table 1. Fluorescence Quenching Rate Constants (k_q) of $MeAcrH^+$ and $DeAcrH^+$ by Electron Donors in Various Solvents, Oxidation Potential of Electron Donors and the Gibbs Energy Change for Photoinduced Electron Transfer (ΔG^0_{et})

#	electron donor	E^0_{ox} vs SCE [a] in MeCN, V	ΔG^0_{et} [b] eV	k_q, $M^{-1}s^{-1}$		
				MeCN $MeAcrH^+$	$CHCl_3$ $MeAcrH^+$	C_6H_6 $DeAcrH^+$
1	benzene	2.35	0.03	1.3×10^7	7.6×10^6	———
2	toluene	2.20	-0.12	2.4×10^8 [c]	6.6×10^7	3.5×10^7
3	ethylbenzene	2.14	-0.18	4.5×10^8	1.0×10^8	4.5×10^7
4	cumene	2.14	-0.18	2.4×10^8	4.4×10^8	5.7×10^7
5	*m*-xylene	2.02	-0.30	7.7×10^9 [c]	3.5×10^9 [c]	1.8×10^9
6	*o*-xylene	1.98	-0.34	7.9×10^9 [c]	5.5×10^9 [c]	2.0×10^9
7	1,3,5-trimethylbenzene	1.98	-0.34	1.2×10^{10}	5.0×10^9	2.7×10^9
8	*p*-xylene	1.93	-0.39	8.6×10^9 [c]	4.2×10^9 [c]	———
9	1,2,3-trimethylbenzene	1.88 (1.98)	-0.44	1.3×10^{10}	8.1×10^9	3.9×10^9
10	1,2,4-trimethylbenzene	1.79 (1.89)	-0.53	1.3×10^{10}	7.2×10^9	6.2×10^9
11	1,2,3,4-tetramethylbenzene	1.71 (1.81)	-0.61	1.5×10^{10}	7.1×10^9	7.9×10^9
12	1,2,3,5-tetramethylbenzene	1.71 (1.77)	-0.61	1.6×10^{10}	1.3×10^{10}	7.2×10^9
13	1,2,4,5-tetramethylbenzene	1.63 (1.75)	-0.69	1.9×10^{10}	6.7×10^9	9.1×10^9
14	pentamethylbenzene	1.58 (1.68)	-0.74	1.9×10^{10}	9.9×10^9	1.1×10^{10}
15	hexamethylbenzene	1.49 (1.60)	-0.83	2.1×10^{10}	8.4×10^9	1.1×10^{10}
16	triphenylamine	0.84	-1.48	2.2×10^{10}	———	———
17	*N,N*-dimethylaniline	0.71	-1.61	2.6×10^{10}	1.7×10^{10}	1.3×10^{10}
18	ferrocene	0.37	-1.95	———	2.1×10^{10}	———
19	decamethylferrocene	-0.20	-2.52	———	1.6×10^{10}	1.9×10^{10}

[a] Values in parentheses are determined in CH_2Cl_2.

[b] Determined from E^0_{red} of $^1MeAcrH^{+*}$ (= 2.32 V vs SCE in MeCN)[23] and eq 3.

[c] Taken ref. 24

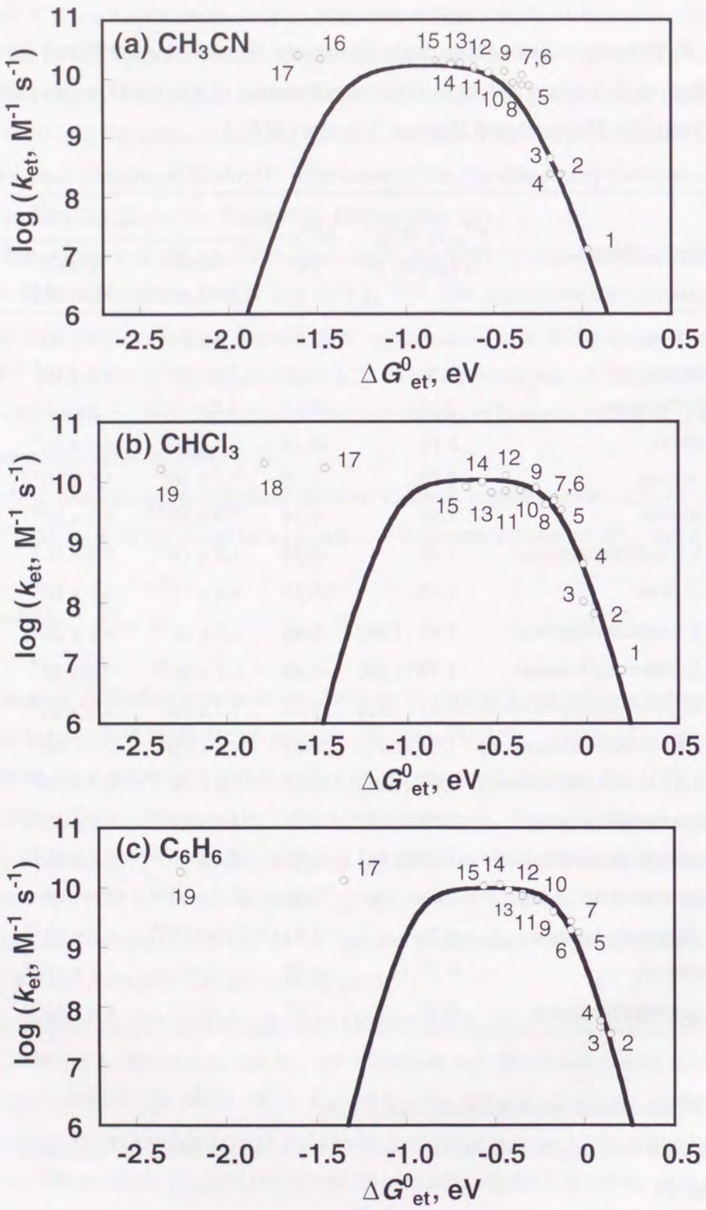

Figure 1. Plots of log k_q vs ΔG^0_{et} for fluorescence quenching of MeAcrH$^+$ (2.0 x 10^{-4} M) by various electron donors in (a) MeCN and (b) $CHCl_3$, and that of DeAcrH$^+$ (2.0 x 10^{-4} M) (c) benzene at 298 K.

Scheme 1

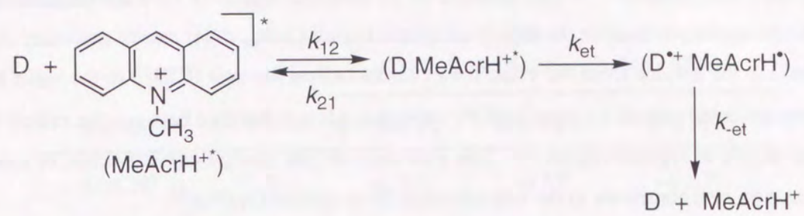

$$k_q = k_{et}k_{12}/(k_{21} + k_{et}) \quad (3)$$

dependence of k_{et} on ΔG^0_{et} for adiabatic outer-sphere electron transfer has well been established by Marcus as given by eq 4, where k is the Boltzmann constant, h is the Planck

$$k_{et} = (kT/h)\exp[-(\lambda/4)(1 + \Delta G^0_{et}/\lambda)^2/kT] \quad (4)$$

constant and λ is the reorganization energy of electron transfer.[7] From eqs 3 and 4 is derived eq 5 where Z [= $(kT/h)(k_{12}/k_{21})$] is the collision frequency which is taken as 1 x 10^{11} M^{-1} s^{-1}.[9]

$$k_q = Z\exp[-(\lambda/4)(1 + \Delta G^0_{et}/\lambda)^2/kT]/(k_{12} + Z\exp[-(\lambda/4)(1 + \Delta G^0_{et}/\lambda)^2/kT]) \quad (5)$$

The k_{12} values in MeCN, $CHCl_3$ and benzene are taken as 2.0 x 10^{10}, 1.2 x 10^{10}, and 1.1 x 10^{10} M^{-1} s^{-1}, respectively.[26]

The dependence of k_q on ΔG^0_{et} for electron transfer quenching of ^{1}MeAcrH^{+*} by electron donors in MeCN is calculated based on eq 5 using the best fit value of λ value (0.88 eV) as shown by the solid line in Figure 1a. The k_q values agree well with the calculated values except for the k_q values in the highly exergonic region, $\Delta G^0_{et} << -1$ eV, which are significantly larger than the calculated values (Figure 1a). The calculated dependence of k_q on ΔG^0_{et} (eq 5) predicts a decrease in the k_q value from a diffusion limited value with increasing the driving force of electron transfer ($-\Delta G^0_{et}$) when the k_{et} values become smaller than the diffusion limited value in the Marcus inverted region ($\Delta G^0_{et} < -\lambda$), provided that the λ value is constant in a series of electron transfer reactions.[9] The absence of a Marcus inverted region

has well been recognized in forward photoinduced electron transfer reactions.[24] In the case of back electron transfer reactions, however, the observation of the Marcus-inverted region has been well established.[27-30] The absence of an inverted region in forward photoinduced electron transfer reactions in the highly exergonic region ($\Delta G^0_{et} < -\lambda$) can be explained by an increase in the λ value from the value for a contact radical ion pair (CRIP) to the value for a solvent separated radical ion pair (SSRIP) which has a larger distance between the radical ions in the highly exergonic region.[30] The existence of low energy excited states of radical cations may also contribute to the non-existence of an inverted region.[31]

The solvent independent ΔG^0_{et} value is confirmed by determination of the E^0_{ox} values of electron donors and E^0_{red} values of acridinium ions in solvents with different polarity. The E^0_{ox} values of alkylbenzene derivatives have been determined in MeCN and CH_2Cl_2 as listed in Table 1 (see the values in parentheses). The E^0_{red} values of 10-methyl-9-substituted acridinium ions instead of $MeAcrH^+$ have also been determined in MeCN, CH_2Cl_2, $CHCl_3$ and benzene, since the reversible redox couples can be obtained for the 9-substituted derivatives in contrast to the case of $MeAcrH^+$. The E^0_{red} values are also listed in Table 2. The E^0_{ox} values in a less polar solvent (CH_2Cl_2) are shifted to the positive direction by about 0.1 V due to the less solvation of the radical cations as compared to that in MeCN (Table 1). Similar positive shifts are observed for the E^0_{red} values of acridinium ions in CH_2Cl_2 as compared to the E^0_{red} values in MeCN and the larger shifts are observed in $CHCl_3$ and benzene (Table 2). Thus, the ΔG^0_{et} values obtained as the difference between the E^0_{ox} and E^0_{red} values (eq 2) become rather solvent independent because of the cancellation of the solvation. However, the cancellation is not complete, since the positive shifts in the E^0_{ox} values are slightly larger than the shifts in the E^0_{red} values.

The dependence of k_q on ΔG^0_{et} for electron transfer quenching of $^1RAcrH^{+*}$ by aromatic electron donors in $CHCl_3$ and benzene is also calculated based on eq 5 as shown in Figure 1b and Figure 1c, respectively. The ΔG^0_{et} values $CHCl_3$ and benzene are evaluated from the values in MeCN [ΔG^0_{et} (MeCN)] by using eq 6, where the constant value C, which is

$$\Delta G^0_{et} = \Delta G^0_{et}\,(\mathrm{MeCN}) + C \qquad (6)$$

dependent on the solvent, is determined by fitting the data to eq 5. The best fit values of λ and C are determined as $\lambda = 0.62$ eV, C = 0.16 eV in $CHCl_3$ and $\lambda = 0.53$ eV, C = 0.27 eV in

Table 2. One-Electron Reduction Potentials $E^0(MeAcrR^+/MeAcrR^\bullet)$ of $MeAcrR^+ClO_4^-$ Determined by the Cyclic Voltammograms in Deaerated Various Solvents at 298 K

		$E^0(MeAcrR^+/MeAcrR^\bullet)$, V *vs* SCE		
Solvent	ε	R = $PhCH_2$	R = Ph	R = Pr^i
MeCN[a]	37.5	–0.50[c]	–0.55[c]	–0.63[c]
CH_2Cl_2[a]	7.8	–0.44[c]	–0.49[c]	–0.54[c]
$CHCl_3$[a]	4.8	–0.44[c]	–0.47[c]	–0.52[c]
C_6H_6[b]	2.3	–0.42[d]	–0.45[d]	–0.42[d]

[a] Containing 0.1 M TBAP. [a] Containing 0.5 M THAP. [a] Sweep rate is 50 mV s^{-1}. [b] Sweep rate is 10 mV s^{-1}.

benzene.[32] The λ value decreases from the value in MeCN (0.88 eV) with decreasing the solvent polarity due to the smaller solvent reorganization energy, whereas the ΔG^0_{et} value increases, since the difference in solvation between aromatic donor radical cations and acridinium ion decreases with decreasing the solvent polarity.

Electron Transfer Self-Exchange Reactions between $MeAcrPh^\bullet$ and $MeAcrPh^+$ in Different Solvents. The decrease in the solvent reorganization energy of electron transfer with decreasing the solvent polarity is examined by determining the rate constants of electron transfer self-exchange reactions between 9-phenyl-10-methylacridinium ion ($MeAcrPh^+$) and the corresponding one-electron reduced radical ($MeAcrPh^\bullet$) in solvents with different polarity. The $MeAcrPh^\bullet$ radical was produced by the electron transfer reduction of $MeAcrPh^+$ by tetramethylsemiquinone radical anion (eq 7). ESR spectra for $MeAcrPh^\bullet$ were

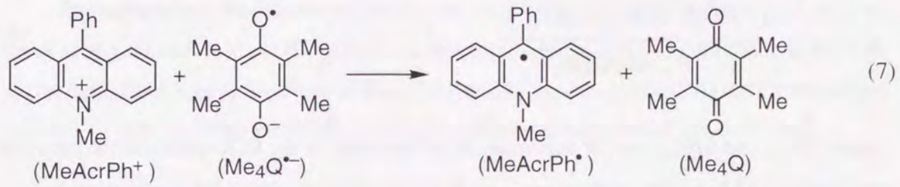

(7)

persistent for several hours in deaerated MeCN. The hyperfine splitting constants and the maximum slope linewidths (ΔH_{msl}) were determined from a computer simulation of the ESR spectra as shown in Figure 2. The ΔH_{msl} value thus determined increases linearly with an increase in the concentration of $MeAcrPh^+$ in MeCN as shown in Figure 3. Such linewidth

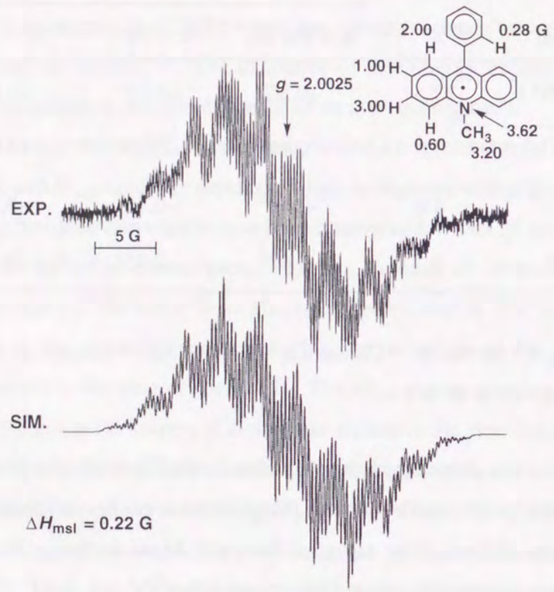

Figure 2. ESR spectrum of $MeAcrPh^•$ in deaerated MeCN at 298 K and the computer simulation spectrum.

variations of the ESR spectra can be used to investigate the rate processes involving the radical species.[33] The rate constants (k_{ex}) of the electron transfer self-exchange reactions between $MeAcrPh^+$ and $MeAcrPh^•$ were determined using eq 8,

$$k_{ex} = \frac{1.57 \times 10^7 \, (\Delta H_{msl} - \Delta H^0_{msl})}{(1 - P_i)\,[MeAcrPh^+]} \qquad (8)$$

where ΔH_{msl} and ΔH^0_{msl} are the maximum slope linewidth of the ESR spectra in the presence and absence of $MeAcrPh^+$, respectively, and P_i is a statistical factor which can be taken as

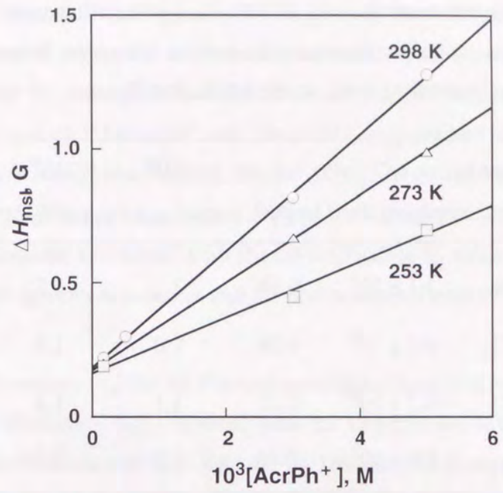

Figure 3. Plots of ΔH_{msl} vs $[MeAcrPh^+]$ for the ESR spectra of $MeAcrPh^•$ in deaerated MeCN at various temperatures.

Arrhenius plots as listed in Table 3. The small $\Delta S^{\neq}$ values in Table 3 are consistent with the outer-sphere electron transfer reactions. The reorganization energies (λ) of the electron transfer reactions are obtained from the k_{ex} values using eq 9 where k_{diff} is the diffusion rate constant which corresponds to k_{12} in Scheme 1 ($k_{diff} = 2.0 \times 10^{10}$ M^{-1} s^{-1} in

$$[(k_{ex})^{-1} - (k_{diff})^{-1}] = Z^{-1} \exp(\lambda / 4kT) \qquad (9)$$

MeCN, 2.0×10^{10} M^{-1} s^{-1} in CH_2Cl_2, 1.2×10^{10} M^{-1} s^{-1} in $CHCl_3$ and 1.1×10^{10} M^{-1} s^{-1} in benzene, respectively).[26] The λ values thus determined are also listed in Table 3. It is clearly shown that the λ value decreases with decreasing the solvent polarity.[35]

Photochemical Reactions of $MeAcrH^+$ and $DeAcrH^+$ with R_4Sn. Irradiation of the absorption band of $MeAcrH^+ClO_4^-$ in a deaerated MeCN solution containing R_4Sn with xenon lamp for 1 h gave the alkyl adduct (MeAcrHR) as shown in eq 10 (see Experimental Section).[36] The quantum yields (Φ) of the photochemical reactions of $MeAcrH^+$ and

Table 3. Electron Transfer Self-Exchange Rate Constants (k_{ex}), the Rreorganization Energies (λ), and the Activation Parameters ($\Delta H^{\neq}$ and $\Delta S^{\neq}$) for the MeAcrPh•/MeAcrPh+ System

Solvent	k_{ex}	λ	$\Delta H^{\neq}$	$\Delta S^{\neq}$
	$M^{-1}s^{-1}$	eV	kcal mol^{-1}	cal $K^{-1}mol^{-1}$
MeCN	3.1×10^9	0.34	2.2	3.7
CH_2Cl_2	4.1×10^9	0.28	1.0	1.3
CH_3Cl	4.2×10^9	0.27	1.1	1.3
C_6H_6	5.9×10^9	0.21	1.9	0.5

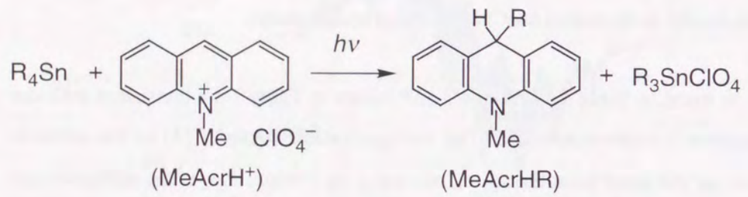

(MeAcrH+) (MeAcrHR) (10)

DeAcrH+ with R_4Sn were determined from the spectral change under irradiation of monochromatized light of λ_{max} = 398 nm (see Experimental Section). The Φ value increases with an increase in the concentration of R_4Sn [R_4Sn] to approach a limiting value (Φ_∞) in accordance with eq 11 (see Supporting Information, S4). Equation 11 is rewritten by

$$\Phi = \Phi_\infty K_{obs}[R_4Sn] / (1 + K_{obs}[R_4Sn]) \quad (11)$$

eq 12 which predicts a linear correlation between Φ^{-1} and $[R_4Sn]^{-1}$. From the slopes and

$$\Phi^{-1} = \Phi_\infty{}^{-1}[1 + (K_{obs}[R_4Sn])^{-1}] \quad (12)$$

intercepts of linear plots are obtained the Φ_∞ and K_{obs} values. The K_{obs} values can be

converted to the corresponding rate constants (k_{obs}) using the relation $K_{obs} = k_{obs}\tau$ provided that the excited state of MeAcrH+ or DeAcrH+ involved in the photochemical reaction is singlet. The k_{obs} and Φ_∞ values thus determined are listed in Table 4.

The fluorescence of ^{1}MeAcrH+* and ^{1}DeAcrH+* is quenched efficiently by electron transfer from R_4Sn in MeCN and benzene, respectively. The quenching rate constants k_q are also listed in Table 4, where the k_{obs} values derived from the dependence of Φ on [R_4Sn] in both MeCN and benzene agree well with the corresponding k_q values of the fluorescence quenching. Such an agreement indicates that the photochemical reaction proceeds via

Table 4. The Constants (k_q) for the Fluorescence Quenching of RAcrH+ with R_4Sn, the Observed Rate Constants (k_{obs}) Derived from the Dependence of the Quantum Yields on [R_4Sn] in the Photoalkylation of RAcrH+ by Tetraalkyltin Compounds in MeCN and Benzene at 298 K, and the Driving Force of Back Electron Transfer ($-\Delta G^0_{bet}$) from RAcrH• to $R_4Sn^{\bullet+}$ in MeCN

R_4Sn	Solvent	k_q, M^{-1} s^{-1}	k_{obs}, M^{-1} s^{-1}	Φ_∞	$-\Delta G^0_{bet}$, eV [a]
Me_4Sn	benzene	1.1×10^8	1.1×10^8	0.0088	
	MeCN	3.3×10^8	4.2×10^8	0.00042	2.11
Et_4Sn	benzene	3.3×10^9	2.1×10^9	0.028	
	MeCN	1.5×10^{10}	2.4×10^9	0.007	1.67
$Pr^i{}_4Sn$	benzene	7.3×10^9	5.0×10^9	0.027	
	MeCN	1.8×10^{10}	8.0×10^9	0.028	1.43
$Bu^t{}_2Me_2Sn$	benzene	1.1×10^{10}	1.7×10^{10}	0.0055	
	MeCN	1.1×10^{10}	1.4×10^{10}	0.021	1.29

[a] $-\Delta G^0_{bet}$ values in benzene can be estimated based on eq 6 where ΔG^0_{et} is replaced by ΔG^0_{bet}.

photoinduced electron transfer from R_4Sn to the singlet excited states (^{1}MeAcrH+* and ^{1}DeAcrH+*).

The formation of DeAcrH$^{\bullet}$ in photoinduced electron transfer from Et_4Sn to $^1DeAcrH^{+*}$ in MeCN is confirmed by the laser flash photolysis of the $DeAcrH^+$-Et_4Sn system as shown in Figure 4a. The laser excitation (355 nm from a Nd:YAG laser) of $DeAcrH^+$ (8.0×10^{-5} M) in deaerated MeCN and benzene solutions containing Et_4Sn (8.2×10^{-3} M) gives transient absorption of DeAcrH$^{\bullet}$ which is essentially the same as that of MeAcrH$^{\bullet}$ (a broad absorption band between 450 and 540 nm).[22,37] The formation of DeAcrH$^{\bullet}$ in photoinduced electron transfer from the weakest electron donor employed in this study, i.e., Me_4Sn to $DeAcrH^+$ has also been confirmed in benzene as shown in Figure 4b. Thus, the photochemical reaction of $RAcrH^+$ (R = Me and De) with R_4Sn proceeds via photoinduced electron transfer from R_4Sn to $^1RAcrH^{+*}$ as shown in Scheme 2.

The photochemical reaction is initiated by photoinduced electron transfer (k_{et}) from R_4Sn to $^1RAcrH^{+*}$ to give the radical cation-acridinyl radical pair ($R_4Sn^{\bullet+}$ $RAcrH^{\bullet}$). The Sn-C bond of $R_4Sn^{\bullet+}$ is known to be cleaved to give the alkyl radical,[38-41] which is coupled

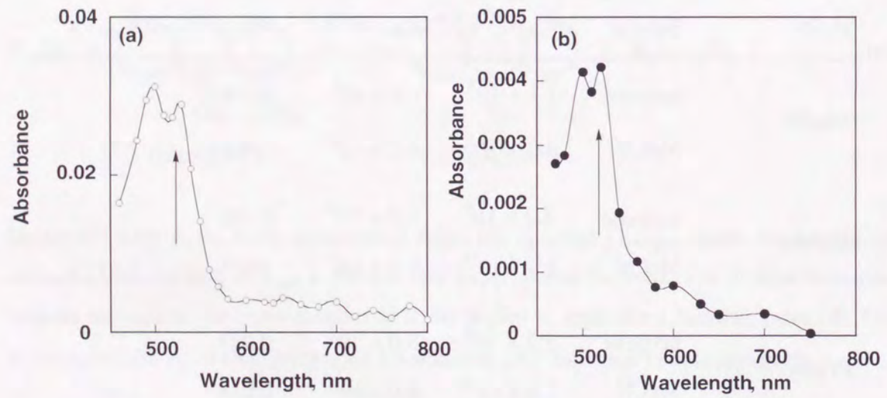

Figure 4. (a) Transient absorption spectra of DeAcrH$^{\bullet}$ generated in electron transfer from Et_4Sn (8.2×10^{-3} M) to $DeAcrH^+$ (8.0×10^{-5} M) in MeCN at 150 μs after laser exciation (355 nm) at 298 K (b) Transient absorption spectra of DeAcrH$^{\bullet}$ generated in electron transfer from Me_4Sn (1.0×10^{-1} M) to $DeAcrH^+$ (5.0×10^{-4} M) in benzene at 150 μs after laser exciation (355 nm) at 298 K.

Scheme 2

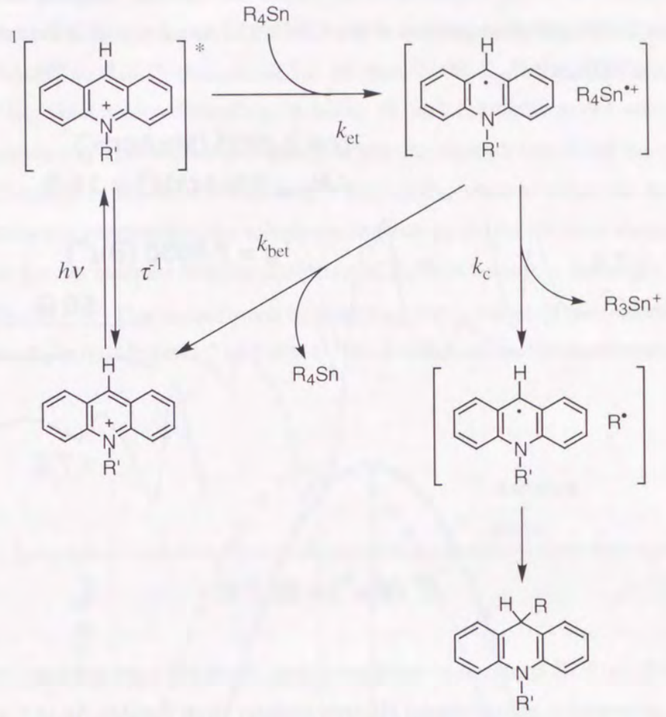

within the cage to yield the adduct selectively without dimerization of free RAcrH$^{\bullet}$ radicals escaped from the cage,[42] in competition with the back electron transfer to the ground state (k_{bet}). In such case, the limiting quantum yield Φ_∞ is determined by the competition between the cleavage of C-Sn bond of $R_4Sn^{\bullet+}$ in the radical cation/radical pair (k_c) and the back electron transfer from RAcrH$^{\bullet}$ to $R_4Sn^{\bullet+}$ (k_{bet}) as given by eq 13.

$$\Phi_\infty = k_c/(k_{bet} + k_c) \tag{13}$$

In the case of $Bu^t{}_2Me_2Sn$, the Sn-Bu^t bond of $Bu^t{}_2Me_2Sn^{\bullet+}$ is cleaved selectively as compared to the Sn-Me bond,[11] to give MeAcrH(Bu^t) rather than MeAcrHMe (see Experimental Section). This is confirmed by the ESR spectrum observed in photoinduced electron transfer from $Bu^t{}_2Me_2Sn$ to the singlet excited state of $MeAcrH^+$ observed in frozen

MeCN at 77 K under photoirradiation with a high-pressure mercury lamp as shown in Figure 5. The ten-line isotropic spectrum is ascribed to the hyperfine coupling of an unpaired electron with the 9 equivalent protons of $Bu^{t\bullet}$.[41,43] The broad signal at the center can be assigned due to $MeAcrH^{\bullet}$.[44]

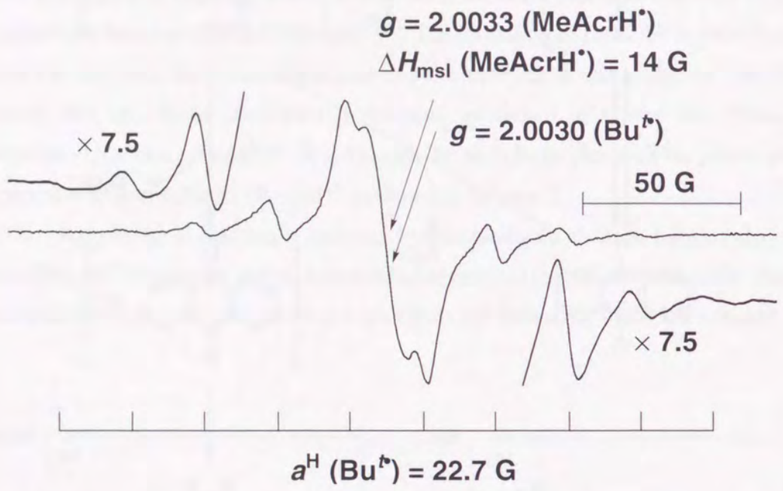

Figure 5. (a) ESR spectrum of acridinyl radical ($MeAcrH^{\bullet}$) and *tert*-butyl radical ($Bu^{t\bullet}$) generated in photoinduced electron transfer from $Bu^t_2Me_2Sn$ (4.5×10^{-2} M) to the siglet excited state of $MeAcrH^+$ (1.0×10^{-2} M) observed in frozen MeCN at 77 K under irradiation of UV light by using high-pressure marcury lamp.

Solvent Dependence of the Limiting Quantum Yield. The Φ_∞ value varies drastically depending on the alkyl group (R) of R_4Sn and solvents from the smallest value (4.2×10^{-4}) for Me_4Sn in MeCN to the largest value (2.8×10^{-2}) for Pr^i_4Sn in MeCN as shown in Table 4. It is interesting to note that the Φ_∞ value of Me_4Sn in benzene is 21 times larger than the corresponding value in MeCN. However, this is reversed for $Bu^t_2Me_2Sn$, the Φ_∞ value in a polar solvent (MeCN) is 38 times larger than the corresponding value in a nonpolar solvent (benzene). The ratio of the Φ_∞ value in benzene to that in MeCN changes systematically from Me_4Sn to $Bu^t_2Me_2Sn$ with decreasing the driving force ($-\Delta G^0_{bet}$) of back electron transfer from $RAcrH^{\bullet}$ to $R_4Sn^{\bullet+}$. The driving force is obtained from the

difference between the E^0_{ox} value of R_4Sn and E^0_{red} value of $RAcrH^+$ (eq 2),[45] and the $-\Delta G^0_{bet}$ values are listed in Table 4. Since the cleavage rate of C-Sn bond of $R_4Sn^{\bullet+}$ (k_c) may be independent of solvent polarity,[41] the Φ_∞ value is determined by the back electron transfer rate from $RAcrH^{\bullet}$ to $R_4Sn^{\bullet+}$ (k_{bet}) in eq 13; the smaller the k_{bet} value, the larger is the Φ_∞ value. The k_{bet} value varies depending on ΔG^0_{bet} of back electron transfer according to the Marcus equation (eq 4) as shown in Figure 6 where the dependence of log k_{bet} vs ΔG^0_{bet} in MeCN and benzene is drawan schematically.[9] The $-\Delta G^0_{bet}$ value at which the maximum k_{bet} value is obtained corresponds to the reloganization energy (λ) for the back electron transfer. The λ value for the electron transfer oxidation of R_4Sn is known to be large (λ = 41 kcal mol^{-1} = 1.78 eV).[12,13] This is confirmed by analyzing the k_q values of photoinduced electron transfer from R_4Sn to $^1MeAcrH^{+*}$ in Table 4. The λ value can be obtained from the

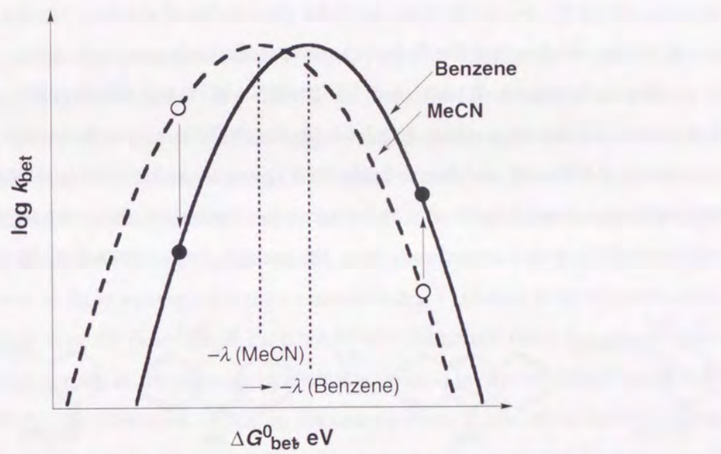

Figure 6. Dependence of log k_{bet} on ΔG^0_{bet} in MeCN (solid line) and benzene (broken line). The lines are drawn schemiatically based on eq 4. The ΔG^0_{bet} value at which k_{bet} is maximum corresponds to $-\lambda$ (eq 4).

k_q and ΔG^0_{et} values using eq 5. The λ values thus evaluated are λ = 1.95 eV and 1.82 eV for Me_4Sn and Et_4Sn in MeCN, respectively.[46] These values agree with the reported large value.[12,13] In such a case, the $-\Delta G^0_{et}$ value is changed from the value in the Marcus inverted

region in the case of Me_4Sn to the normal region up to 1.2 eV which is significantly smaller than the λ value in the case of $Bu^t_2Me_2Sn$. According to the Marcus equation (eq 4), the k_{bet} value decreases with decreasing the λ value in the inverted region, whereas the k_{bet} value increases in the normal region (Figure 6). The λ value is expected to decrease with decreasing the solvent polarity (Table 3). In fact, the λ values evaluated from the k_q and ΔG^0_{et} values in benzene using eq 5 (λ = 1.52 eV and 1.30 eV for Me_4Sn and Et_4Sn, respectively) are significantly smaller than those in MeCN (*vide supra*).[47] This is the reason why the Φ_∞ value of Me_4Sn in benzene is much larger than the corresponding value in MeCN, whereas this is reversed for $Bu^t_2Me_2Sn$, the Φ_∞ value of which in MeCN is 38 times larger than the corresponding value in benzene (Table 4). Thus, whether the back electron transfer is in the Marcus inverted region or in the normal region determines whether the Φ_∞ value increases or decreases with decreasing the solvent polarity. In such a case, the solvent dependence of Φ_∞ would be reversed if the photoinduced electron transfer system with the much smaller λ value than the R_4Sn-RAcrH$^+$ system is chosen (*vide infra*).

Photochemical Reactions of Bu^{t}BNAH with MeAcrH$^+$ and DeAcrH$^+$. Irradiation of the absorption band of MeAcrH$^+$ClO$_4^-$ in a deaerated MeCN solution containing Bu^{t}BNAH with xenon lamp for 1h gave an adduct [MeAcrHBu^t] as shown in eq 14 (see Experimental Section). The same type of reaction occurs when MeAcrH$^+$ClO$_4^-$ is replaced by DeAcrH$^+$ in benzene. Thus, the product derived from RAcrH$^+$ is the same as

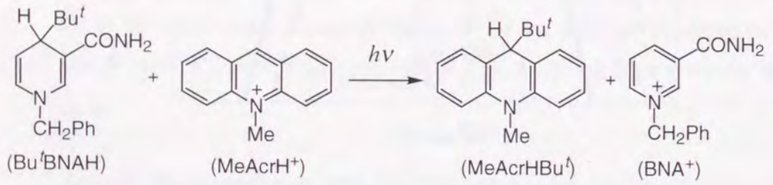

(14)

obtained in the photochemical reaction with $Bu^t_2Me_2Sn$. The quantum yields (Φ) of the photochemical reactions of MeAcrH$^+$ and DeAcrH$^+$ with Bu^{t}BNAH were determined from the spectral change under irradiation of monochromatized light of λ_{max} = 398 nm (see Experimental Section). The Φ_∞ and k_{obs} values are determined as the case of the photochemical reactions with R_4Sn and they are listed in Table 5 (see Supporting Information, Figure S6). In contrast with the case of $Bu^t_2Me_2Sn$ (Table 4), the Φ_∞ value increases with decreasing the solvent polarity and the Φ_∞ value in benzene is *20 times larger* than that in MeCN.

Table 5. The Constants (k_q) for the Fluorescence Quenching of RAcrH$^+$ with Bu^{t}BNAH, and the Observed Rate Constants (k_{obs}) Derived from the Dependence of the Quantum Yields on [Bu^{t}BNAH] in the Photochemical Reaction of RAcrH$^+$ with Bu^{t}BNAH

Solvent	k_q, $M^{-1}s^{-1}$	k_{obs}, $M^{-1}s^{-1}$	Φ_∞
MeCN	2.1×10^{10}	2.3×10^{10}	0.04
$CHCl_3$	2.0×10^{10}	1.9×10^{10}	0.12
C_6H_6	2.3×10^{10}	2.1×10^{10}	0.81

The k_q values are also determined independently by the fluorescence quenching via electron transfer from Bu^{t}BNAH to ^{1}MeAcrH^{+*} and ^{1}DeAcrH^{+*} and they are also listed in Table 5 in which the k_q values agree with the k_{obs} values. Such an agreement indicates that the photochemical reaction of RAcrH$^+$ with Bu^{t}BNAH proceeds via photoinduced electron transfer from Bu^{t}BNAH to ^{1}RAcrH^{+*} as shown in Scheme 3. The photoinduced electron transfer from Bu^{t}BNAH to ^{1}RAcrH^{+*} produces the radical cation/radical pair (Bu^{t}BNAH$^{\bullet+}$ RAcrH$^\bullet$). Savéant et al. have reported that the electrochemical oxidation of Bu^{t}BNAH results in the selective C(4)-C bond cleavage of Bu^{t}BNAH$^{\bullet+}$.[48] Although there are two possible modes of the carbon-carbon bond cleavage in such reactions to generate (a) Bu$^{t\bullet}$ and BNA$^+$ or (b) Bu^{t+} and BNA$^\bullet$, the formation of Bu$^{t\bullet}$ in the one-electron oxidation of Bu^{t}BNAH has been confirmed by applying a rapid mixing flow electron spin resonance (ESR) technique.[49] Thus, cleavage of Bu^{t}BNAH$^{\bullet+}$ gives Bu$^{t\bullet}$ that is coupled immediately with MeAcrH$^\bullet$ to yield the adduct (MeAcrHBu^t) in competition with the back electron transfer from MeAcrH$^\bullet$ to Bu^{t}BNAH$^{\bullet+}$ (Scheme 2).

By applying the steady-state approximation to the reactive species in Scheme 2, the dependence of Φ on [Bu^{t}BNAH] can be derived as given by eq 15, which agrees with the observed dependence of Φ on [Bu^{t}BNAH]. The limiting quantum yields Φ_∞ corresponds to

$$\Phi = [k_c/(k_c + k_{bet})]k_{et}\tau[Bu^tBNAH]/(1 + k_{et}\tau[Bu^tBNAH]) \quad (15)$$

$k_c/(k_c + k_{bet})$. In such a case the Φ_∞ value is determined by the competition between the C(4)-C bond cleavage (k_c) and the back electron transfer (k_{bet}). Since the reorganization energy (λ) of photoinduced electron transfer reactions of BNAH and derivatives in MeCN is

Scheme 2

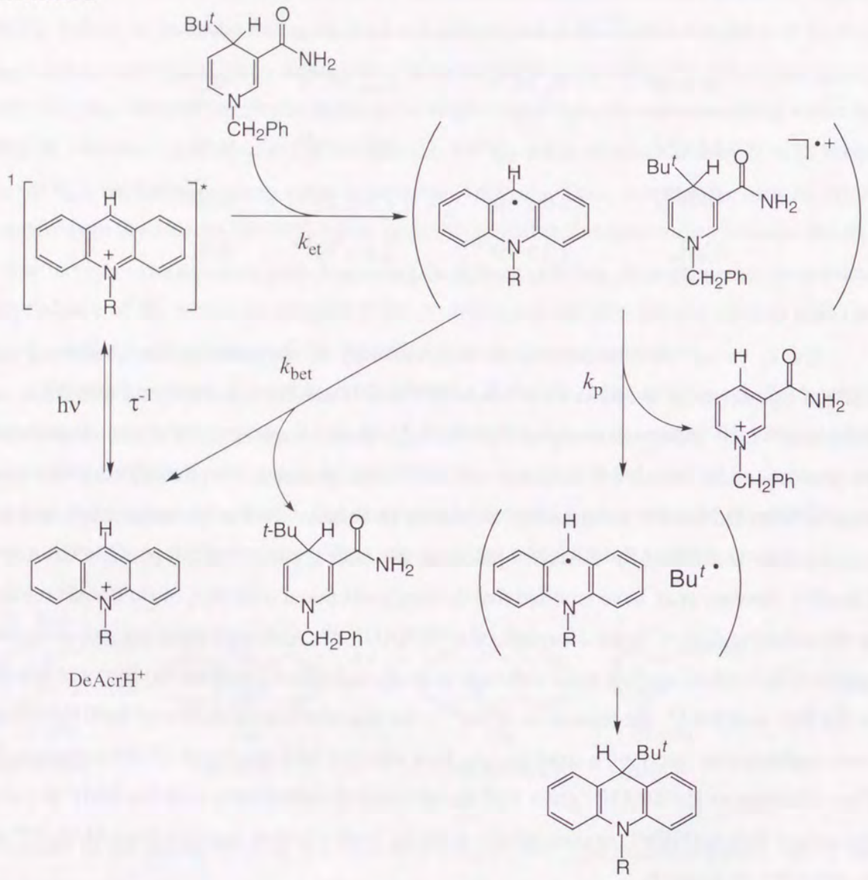

relatively small (λ = 0.5 eV),[14] the back electron transfer from MeAcrH$^\bullet$ to Bu^{t}BNAH$^{\bullet+}$ should be in the Marcus inverted region ($-\Delta G^0_{bet}$ = 1.1 eV >> 0.5 eV) in contrast with the case of $Bu^t_2Me_2Sn$ ($-\Delta G^0_{bet}$ = 1.1 eV << 1.8 eV). Thus, the solvent reorganization energy should decrease with decreasing the solvent polarity, leading to the decrease in the back electron transfer rate in the Marcus inverted region as shown in Figure 6 and thereby an

increase in the Φ_∞ value (Table 5).

Summary and Conclusions

The present study has shown that the reactivity of charge-shift type of photoinduced electron transfer reactions which lead to stable products can be finely controlled by the solvent polarity. The photoinduced electron transfer from electron donors to ^{1}RAcrH^{+*} occurs efficiently even in a non-polar solvent as well as in a polar solvent to yield the stable adducts between RAcrH$^\bullet$ and radicals produced by the bond-cleavage of the radical cations to yield the stable adducts. The limiting quantum yield increases with decreasing the solvent polarity when the back electron transfer from RAcrH$^\bullet$ to the radical cations is in the Marcus inverted region, whereas the yield decreases when the back electron transfer is in the Marcus normal region.

References

(1) *Electron Transfer in Chemistry*; Balzani, V., Ed.; Wiley-VCH: Weinheim, 2001; Vol. 1-5.

(2) *Photoinduced Electron Transfer*; Fox, M. A., Chanon, M., Eds.; Elsevier: Amsterdam, 1988.

(3) Eberson, L. *Electron Transfer Reactions in Organic Chemistry; Reactivity and Structure*; Springer: Heidelberg, 1987; Vol. 25.

(4) (a) Müller, F.; Mattay, J. *Chem. Rev.* **1993**, *93*, 99. (b) Mella, M.; Fagnoni, M.; Freccero, M.; Fasani, E.; Albini, A. *Chem. Soc. Rev.* **1998**, *27*, 81.

(5) (a) Julliard, M.; Chanon, M.; *Chem. Rev.* **1983**, *83*, 425. (b) Lewis, F. D. *Acc. Chem. Res.* **1986**, *19*, 401. (c) Yoon, U. C.; Mariano, P. S. *Acc. Chem. Res.* **1992**, *25*, 233. (d) Kavarnos, G. J.; Turro, N. J. *Chem. Rev.* **1986**, *86*, 401. (e) Gaillard, E. R.; Whitten, D. G. *Acc. Chem. Res.* **1996**, *29*, 292.

(6) Fukuzumi, S. In *Advances in Electron Transfer Chemistry*; Mariano, P. S., Ed.; JAI Press: Greenwich, 1992; Vol. 2, p. 65.

(7) Fukuzumi, S.; Tanaka, T. In *Photoinduced Electron Transfer*; Fox, M. A., Chanon, M., Eds.; Elsevier: Amsterdam, 1988; Part C, p. 578.

(8) Todd, W. P.; Dinnocenzo, J. P.: Farid, S.; Goodman, J. L.; Gould, I. R. *J. Am. Chem. Soc.* **1991**, *113*, 3601.

(9) (a) Marcus, R. A. *Ann. Rev. Phys. Chem.* **1964**, *15*, 155. (b) Marcus, R. A. *Angew. Chem., Int. Ed. Engl.* **1993**, *32*, 1111. (c) Eberson, L. *Adv. Phys. Org. Chem.* **1982**, *18*, 79.

(10) Although the radical/radical cation pair was observed in benzene in competition with return electron transfer in photoinduced charge shift reaction from biphenyl to 10-decylacridinium cation ($DeAcrH^+$), no product in such nonpolar solvent was reported in ref 8.

(11) Fukuzumi, S.; Suenobu, T.; Patz, M.; Hirasaka, T.; Itoh, S.; Fujitsuka, M.; Ito, O. *J. Am. Chem. Soc.* **1998**, *120*, 8060.

(12) Fukuzumi, S.; Wong, C. L.; Kochi, J. K. *J. Am. Chem. Soc.* **1980**, *23*, 2928.

(13) Fukuzumi, S.; Kuroda, S.; Tanaka, T. *J. Chem. Soc., Perkin Trans. 2* **1986**, 25.

(14) Patz, M.; Kuwahara, Y.; Suenobu, T.; Fukuzumi, S. *Chem. Lett.* **1997**, 567.

(15) Roberts, R. M. G.; Ostovic, D.; Kreevoy, M. M. *Faraday Discuss. Chem. Soc.* **1982**, *74*, 257.

(16) Fukuzumi, S.; Koumitsu, S.; Hironaka, K.; Tanaka, T. *J. Am. Chem. Soc.* **1987**, *109*, 305.

(17) Fukuzumi, S.; Ohkubo, K.; Tokuda, Y.; Suenobu, T. *J. Am. Chem. Soc.* **2000**, *122*, 4286.

(18) Perrin, D. D.; Armarego, W. L. F. *Purification of Laboratory Chemicals*; Butterworth-Heinemann: Oxford, 1988.

(19) Anne, A. *Heterocycles* **1992**, *34*, 2331.

(20) Fukuzumi, S.; Tokuda, Y.; Kitano, T.; Okamoto, T.; Otera, J. *J. Am. Chem. Soc.* **1993**, *115*, 8960.

(21) (a) Hatchard, C. G.; Parker, C. A. *Proc. R. Soc. London, Ser. A* **1956**, *235*, 518. (b) Calvert, J. C.; Pitts, J. N. In *Photochemistry*; Wiley: New York, 1966; p. 783.

(22) Fujita, M.; Ishida, A.; Takamuku, S.; Fukuzumi, S. *J. Am. Chem. Soc.* **1996**, *118*, 8566.

(23) Ohkubo, K.; Fukuzumi, S. *Org. Lett.* **2000**, *2*, 3647.

(24) (a) Rehm, A.; Weller, A. *Ber. Bunsenges Phys. Chem.* **1969**, *73*, 834. (b) Rehm, A.; Weller, A. *Isr. J. Chem.* **1970**, *8*, 259.

(25) In Scheme 1, the back electron transfer to the excited state is neglected when the back electron transfer to the ground state is much faster than the back electron transfer to the excited state.

(26) Kavarnos, G. J. *Fundamentals of Photoinduced Electron Transfer*; Wiley-VCH: New York, 1993.

(27) (a) Closs, G. L.; Miller, J. R. *Science* **1988**, *240*, 440. (b) Miller, J. R.; Calcaterra, L. T.; Closs, G. L. *J. Am. Chem. Soc.* **1984**, *106*, 3047. (c) Asahi, T.; Mataga, N. *J. Phys. Chem.* **1989**, *93*, 6575. (d) Gould, I. R.; Ege, D.; Moser, J. E.; Farid, S. *J. Am. Chem. Soc.* **1990**, *112*, 4290. (e) Gould, I. R.; Farid, S. *Acc. Chem. Res.* **1996**, *29*, 522.

(28) (a) McLendon, G. *Acc. Chem. Res.* **1988**, *21*, 160. (b) Winkler, J. R.; Gray, H. B. *Chem. Rev.* **1992**, *92*, 369. (c) McLendon, G.; Hake, R. *Chem. Rev.* **1992**, *92*, 481.

(29) (a) Rau, H.; Frank, R.; Greiner, G. *J. Phys. Chem.* **1986**, *90*, 2476. (b) Stevens, B.; Biver, C. J., III; McKeithan, D. N. *Chem. Phys. Lett.* **1991**, *187*, 590. (c) Kikuchi, K.; Takahashi, Y.; Katagiri, T.; Niwa, T.; Hoshi, M.; Miyashi, T. *Chem. Phys. Lett.* **1991**, *180*, 403.

(30) Mataga, N.; Miyasaka, H., In *Electron Transfer from Isolated Molecules to Biomolecules Part 2*; Jortner, J., Bixon, M., Eds.; Wiley: New York, 1999; p. 431.

(31) Mataga, N.; Konda, Y.; Asahi, T.; Miyasaka, H.; Okada, T.; Kakitani, T. *Chem. Phys.* **1988**, *127*, 239.

(32) Since the redox potentials have been determined in the presence of the high concentration of electrolyte (Table 1 and Table 3), the positive shifts of the redox potentials in less polar solvents may be larger in the absence of electrolyte as compared to those in its absence. This may be the reason why the estimated *C* value is larger than that expected from the difference in the redox potentials determined in the presence of the high concentration of electrolyte.

(33) (a) Chang, R. *J. Chem. Educ.* **1970**, *47*, 563. (b) Cheng, K. S.; Hirota, N. In *Investigation of Rates and Mechanisms of Reactions*; Hammes, G. G., Ed.; Wiley-Interscience: New York, 1974; Vol. VI, p 565.

(34) Fukuzumi, S.; Nakanishi, I.; Suenobu, T.; Kadish, K. M. *J. Am. Chem. Soc.* **1999**, *121*, 3468.

(35) The difference in the λ values for the electron transfer self-exchange of $MeAcrPh^+/MeAcrPh^\bullet$ between MeCN and benzene (0.13 eV) is smaller than the corresponding difference for the electron transfer reactions from aromatic electron donors to the singlet excited state of acridinium ion (0.27 eV). This is consistent with the smaller solvation of acridinium ion as compared to aromatic donor radical cations due to the more delocalized charge.

(36) Fukuzumi, S.; Kuroda, S.; Tanaka, T. *J. Chem. Soc., Chem. Commun.* **1986**, 1553.

(37) (a) Peters, K. S.; Pang, E.; Rudzki, J. *J. Am. Chem. Soc.* **1982**, *104*, 5535. (b) Poulos, A. T.; Hammond, G. S.; Burton, M. E. *Photochem. Photobiol.* **1981**, *34*, 169.

(38) The transient absorption spectrum of $Et_4Sn^{\bullet+}$ is not observed because of the facile Sn-C bond cleavage of $Et_4Sn^{\bullet+}$; see: ref 40.

(39) Fukuzumi, S.; Mochida, K.; Kochi, J. K. *J. Am. Chem. Soc.* **1979**, *101*, 5961.

(40) (a) Walther, B. W.; Williams, F.; Lau, W.; Kochi, J. K. *Organometallics* **1983**, *2*, 688. (b) Symons, M. C. R. *Chem. Soc. Rev.* **1984**, *13*, 393.

(41) Fukuzumi, S.; Kochi, J. K. *J. Org. Chem.* **1980**, *45*, 2654.

(42) No dimer formation was observed in the present case, indicating that the radical coupling in the cage is highly efficient as compared to the escape of radicals from the cage. In the case of the photochemical reaction of diphenylmethane with $MeAcrH^+$, however, the dimers, $(MeAcrH)_2$ and $(Ph_2CH)_2$ were formed in addition to the adduct; see: ref 22.

(43) Fessenden, R. W.; Schuler, R. H. *J. Chem. Phys.* **1963**, *39*, 2147. (b) Ascough, R. B.; Thomson, C. *Trans. Faraday Soc.* **1962**, *58*, 1477. (c) Krusic, P. J.; Kochi, J. K. *J. Am. Chem. Soc.* **1968**, *90*, 7155.

(44) (a) Fukuzumi, S.; Fujita, M.; Noura, S.; Ohkubo, K.; Suenobu, T.; Araki, Y.; Ito, O. *J. Phys. Chem. A* **2001**, *105*, in press.

(45) The E^0_{red} value of $DeAcrH^+$ is assumed to be the same as that of $MeAcrH^+$. See ref. 8.

(46) The λ value of Pr^i_4Sn is also determined as 1.82 eV. However, the evaluation of the λ value from the k_q value which is close to the diffusion-limit involves a large experimental error.

(47) The ΔG^0_{et} values in benzene are evaluated from those in MeCN by using eq 6.

(48) Anne, A.; Moiroux, J.; Savéant, J.-M. *J. Am. Chem.* Soc. **1993**, *115*, 10224.

(49) Takada, N.; Itoh, S.; Fukuzumi, S. *Chem. Lett.* **1996**, 1103.

Section 2. 2

100 % Selective Oxygenation of *p*-Xylene to *p*-Tolualdehyde via Photoinduced Electron Transfer

Abstract: The 100 % selective oxygenation of *p*-xylene to *p*-tolualdehyde is initiated by photoinduced electron transfer from *p*-xylene to the singlet excited state of 10-methyl-9-phenylacridinium ion under visible light irradiation, leading to yield *p*-tolualdehyde exclusively as the final oxygenated product. The reason for the high selectivity in the photocatalytic oxygenation of *p*-xylene is discussed based on the photoinduced electron transfer mechanism.

Introduction: Selective oxygenation of ring-substituted toluenes to aromatic aldehydes has been one of the most important organic reactions in industrial chemistry because of useful applications of aromatic aldehydes as key chemical intermediates for production of a variety of fine or specialty chemicals such as pharmaceutical drugs, dyestuffs, pesticides, and perfume compositions.[1] A number of methods using inorganic oxidants such as chromium(IV),[2] cobalt(III),[3] manganese(III),[4] cerium(IV),[5] benzeneseleninic anhydride,[6] or peroxydisulfate/copper ion[7] have so far been reported for oxygenation of ring-substituted toluenes to aromatic aldehydes. However, their synthetic utility has been limited because of low yield and poor selectivity. In addition, the use of stoicihometric amounts of inorganic oxidants results in the generation of copious amounts of inorganic waste, which causes serious pollution of environment. The electrochemical recycle of these oxidants has been reported to avoid the stoicihometric use of toxic inorganic oxidants.[8,9] However, the development of catalytic alternatives employing clean oxidants such as O_2 is highly desired.[10]

This study reports that 10-methyl-9-phenylacridinium perchlorate ($AcrPh^+ClO_4^-$, green color) acts as an efficient photocatalyst for highly selective oxygenation of *p*-xylene to *p*-tolualdehyde under visible light irradiation via photoinduced electron transfer from *p*-xylene to the singlet excited state of $AcrPh^+$ ($^1AcrPh^{+*}$). In contrast to the oxidation by inorganic oxidants, the rate of photoinduced electron transfer is highly sensitive to the oxidation potentials of electron donors, and thus, no further oxidation of *p*-tolualdehyde has occurred via photoinduced electron transfer from *p*-tolualdehyde to $^1AcrPh^{+*}$, leading to formation of

p-tolualdehyde as the sole oxygenated product of *p*-xylene.

Result and Discissions

Visible light irradiation of the absorption band (λ_{max} = 358 and 417 nm) of 10-methylacridinium perchlorate ($AcrH^+ClO_4^-$: 10 mM) in oxygen-saturated acetonitrile containing *p*-xylene (30 mM) with a Xenon lamp through a UV cut-off filter ($\lambda > 310$ nm) results in formation of *p*-tolualdehyde accompanied by disappearance of *p*-xylene. After 24 h irradiation, the yield of *p*-tolualdehyde was 37 %.[11] The product yield is improved to 66 %, when the solvent, acetonitrile is replaced by a less polar solvent, chloroform-*d*, under otherwise the same experimental conditions. The photocatalyst $AcrH^+$ remained largely unchanged, but a small amount of the adduct, 9-*p*-xylenyl-10-methyl-9,10-dihydroacridine [$AcrH(CH_2C_6H_4CH_3$-*p*)], was produced after the photooxygenation reaction. The photooxygenated product yield is further improved to 100% when $AcrH^+$ is replaced by $AcrPh^+$ in chloroform as shown in Table 1. There was no dioxygenated product after the prolonged photoirradiation. It was confirmed that there was no adduct formation between the photocatalyst, $AcrPh^+$ and *p*-xylene. Thus, the 100 % selective photooxygenation of *p*-xylene to *p*-tolualdehyde has been accomplished by using $AcrPh^+$ as a photocatalyst in chloroform. The photoirradiation time to obtain 100 % yield *p*-tolualdehyde (3.0×10^{-2} M) was reduced from 24 h to 10 h when a xenon lamp was replaced by a high-pressure Hg lamp through an acetophenone-methanol filter ($\lambda > 300$ nm).

Other isomers, *o*- and *m*-xylene, are also converted to *o*- and *m*-tolualdehyde, respectively (Table 1). The product yields of *o*-, *m*-, *p*-tolualdehyde and benzaldehyde after 10 h photoirradiation of an oxygen saturated chloroform solution of xylenes and toluene (3.0×10^{-2} M) containing $AcrPh^+$ (1.0×10^{-2} M) with a high-pressure Hg lamp ($\lambda > 300$ nm) decreases in order: *p*- > *o*- > *m*-xylene > toluene. The selectivity for tolualdehyde decreases in order: *p*- (100 %) > *m*- (99 %) > *o*-xylene (94 %). The further oxygenation of *m*- and *o*-xylene occurs to yield small amounts of the corresponding phthalaldehyde. In the case of *p*-xylene, it was confirmed that no photooxygenation of *p*-tolualdehyde occurs when *p*-tolualdehyde was used as a starting material.

We have previously reported that oxygenation of ring-substituted toluenes to aromatic aldehydes proceeds via photoinduced electron transfer from toluenes to the singlet excited

Table 1. Photooxygenation of Xylenes and Toluene (3.0×10^{-2} M), Catalyzed by $AcrPh^+$ (1.0×10^{-2} M) with O_2 in O_2-Saturated Chloroform at 298 K[a]

		selectivity	
	conversion	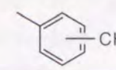	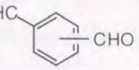
p-xylene	100 %	100 %	0 %
m-xylene	67 %	99 %	1 %
o-xylene	70 %	94 %	6 %
toluene	3 %[b]	100 %[b]	

[a] Irradiation time is 10 h. [b] Benzaldehyde.

state of 10-methylacridinium ion ($^1AcrH^{+*}$) as shown in Scheme 1 for the case of *p*-xylene.[12] The photoinduced electron transfer from *p*-xylene to $^1AcrH^{+*}$ (k_{et}) is followed by the deprotonation of *p*-xylene radical cation in competition with the back electron transfer (k_b) to the reactant pair to produce *p*-xylenyl radical which couples with $AcrH^•$ in the absence of oxygen to yield the adduct [$AcrH(CH_2C_6H_4CH_3$-*p*)].[12] In the presence of oxygen, *p*-xylenyl radical is readily trapped by oxygen to give *p*-xylenylperoxyl radical that is reduced by back electron transfer from $AcrH^•$ to yield *p*-xylenyl hydroperoxide, accompanied by regeneration of $AcrH^+$ (Scheme 1). The hydroperoxide decomposes to yield *p*-tolualdehyde selectively.[12]

The 100 % selective photocatalytic oxygenation of *p*-xylene is made possible by the difference in the reactivity of *p*-xylene and the oxygenated product, *p*-tolualdehyde as indicated by the following fluorescence quenching experiments. The fluorescence lifetimes (τ) of $AcrH^+$ (λ_{em} = 488 nm) in the absence and presence of xylenes, toluene or the corresponding aldehydes were determined using the time resolved fluorescence spectrofluorophotometer. The rate constants of fluorescence quenching k_q ($= K_q\tau^{-1}$) by photoinduced electron transfer are determined from the slopes of the linear Stern-Volmer plots of τ_0/τ (τ_0 = 37 ns in MeCN[13]) vs the quencher concentration. The k_q values thus determined are listed in Table 2.

Scheme 1

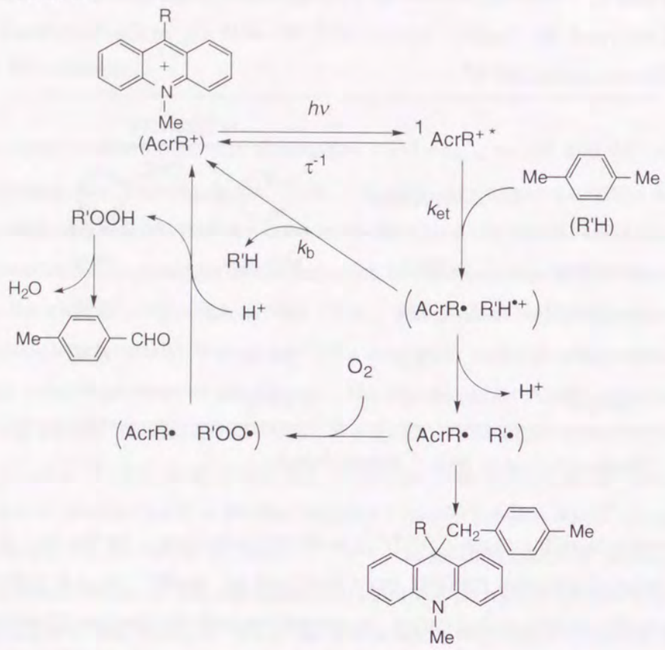

Table 2. Fluorescence Quenching Rate Constants of $AcrH^+$ with Xylenes, Toluene and Aldehydes in Deaerated MeCN at 298 K

	k_q, $M^{-1}s^{-1}$	
	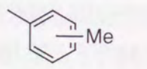	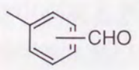
p-xylene	8.6×10^9	a
m-xylene	7.7×10^9	5.2×10^7
o-xylene	7.9×10^9	3.8×10^8
toluene	2.4×10^8	a

[a] Too slow to be determined accurately.

The $^1AcrH^{+*}$ fluorescence was quenched efficiently by electron transfer from xylenes to $^1AcrH^{+*}$, whereas no quenching was observed by *p*-tolualdehyde ($k_q << 1 \times 10^7$ M^{-1} s^{-1}). The k_q value decreases in order: *p*-xylene > *o*-xylene > *m*-xylene > *o*-tolualdehyde > toluene > *m*-tolualdehyde >> *p*-tolualdehyde (not observed). This order is consistent with the order of the monooxygenated and dioxygenated product yields in Table 1. Thus, the faster the photoinduced electron transfer, the larger is the product yield. However, the k_q value for *p*-xylene determined in chloroform (4.2×10^9 M^{-1} s^{-1}) is smaller than the value in acetonitrile in Table 2, in contrast to the improved product yield in chloroform as compared to that in a more polar solvent acetonitrile (*vide supra*). The improved product yield in chloroform may result from a decrease in the reorganization energy for the electron transfer with decreasing the solvent polarity, which results in the slower back electron transfer from $AcrH^•$ to *p*-xylene radical cation in Scheme 1 (*vide infra*). Since the deprotonation of *p*-xylene radical cation, which leads to the oxygenated product, competes with the back electron transfer, the slower back electron transfer results in the larger product yield.

The reorganization energies are evaluated by determining the rate constants of electron transfer self-exchange reactions between 9-phenyl-10-methylacridinium ion ($AcrPh^+$) and the corresponding one-electron reduced radical ($AcrPh^•$) in acetonitrile and chloroform. The $AcrPh^•$ radical was produced by the electron transfer reduction of $AcrPh^+$ by tetramethylsemiquinone radical anion. The ESR spectrum of $AcrPh^•$ was persistent for several hours in deaerated acetonitrile. The hyperfine splitting constants and the maximum slope linewidths (ΔH_{msl}) were determined from a computer simulation of the ESR spectra. The ΔH_{msl} value thus determined increases linearly with an increase in the concentration of $AcrPh^+$ in MeCN. Such linewidth variations of the ESR spectra can be used to investigate the rate processes involving the radical species. The rate constants (k_{ex}) of the electron transfer exchange reactions between $AcrPh^+$ and $AcrPh^•$ were determined using eq 1, where ΔH^0_{msl} is the maximum slope linewidth of the ESR spectra in the absence of $AcrPh^+$, respectively,

$$k_{ex} = \frac{1.57 \times 10^7 \, (\Delta H_{msl} - \Delta H^0_{msl})}{(1 - P_i) \, [AcrPh^+]} \qquad (1)$$

and P_i is a statistical factor which can be taken as nearly zero.[14] The reorganization energies (λ) of the electron transfer reactions are obtained from the k_{ex} values using eq 2 ($Z = 10^{11}$ $M^{-1}s^{-1}$), where the effect of diffusion ($k_{diff} = 2.0 \times 10^{10}$ $M^{-1}s^{-1}$

$$[(k_{ex})^{-1} - (k_{diff})^{-1}] = Z^{-1} \exp(\lambda / 4k_B T) \quad (2)$$

in MeCN and 1.2 x 10^{10} $M^{-1}s^{-1}$ in chloroform, respectively) is taken into account, and k_B is the Boltzmann constant. The λ value in chloroform is determined as 0.27 eV which is smaller than the value in MeCN (0.34 eV).

Since the λ values (0.27, 0.34 eV) are much smaller than the driving force of the back electron transfer ($-\Delta G^0_{et}$ = 2.36 eV) from AcrH$^\cdot$ (E^0_{ox} vs SCE = -0.43 V)[15] to *p*-xylene radical cation (E^0_{red} = 1.93 V)[16] the back electron transfer is deeply in the Marcus inverted region, where the back electron transfer rate is expected to slow down with decreasing the λ value.[17] The slower back electron transfer rate with decreasing the solvent polarity leads to increase the product yield as observed experimentally.

The further improvement of the product yield by employing AcrPh$^+$ instead of AcrH$^+$ can also be ascribed to the slower back electron transfer rate for the former than the latter. In the Marcus inverted region, the back electron transfer becomes slower with increasing the driving force. Since the E^0_{ox} value of AcrPh$^\cdot$ (E^0_{ox} vs SCE = -0.55 V)[18] is more negative than the value of AcrH$^\cdot$ (E^0_{ox} vs SCE = -0.43 V),[15] the driving force of the back electron transfer from AcrPh$^\cdot$ (2.48 eV) is larger than that from AcrH$^\cdot$ (2.36 eV). The larger driving force results in the slower back electron transfer, leading to the improved product yield.

The enhanced stability of AcrPh$^+$ as a photocatalyst as compared to AcrH$^+$ is ascribed to the steric effect of phenyl group of AcrPh$^\cdot$ which hampers the radical coupling with the deprotonated radicals, that is the deactivation process of the photocatalyst in Scheme 1.

In conclusion, the use of AcrPh$^+$ as a photocatalyst in chloroform has enabled us to accomplish the 100 % selective photooxygenation of *p*-xylene to *p*-tolualdehyde as well as highly selective photooxygenation of other isomers to the corresponding aromatic aldehydes.

References

(1) (a) Franz, G.; Sheldon, R. A. in *Ullmann's Encyclopedia of Industrial Chemistry*; 5th Ed.; VCH: Weinheim, 1991. (b) Sheldon, R. A.; Kochi, J. K. in *Metal Catalyzed Oxidation of Organic Compounds*, Academic Press, New York, 1981, Chapter 10.

(2) (a) Clarke, R.; Kuhn, A. T.; Okoh, E. *Chem. Br.* **1975**, *11*, 59. (b) Periasamy, M.; Bhatt, M. V. *Tetrahedron Lett.* **1978**, 4561.

(3) Ballard, R. E.; McKillop, A. *U.S. Patent 4* **1984**, *482*, 438.

(4) Udupa, H. V. K. *Trans. Soc. Adv. Electrochem. Sci. Technol.* **1976**, *11*, 143.

(5) (a) Baciocchi, E.; Giacco, T. D.; Roi, C.; Sebastiani, G. V. *Tetrahedron Lett.* **1985**, *28*, 3353. (b) Ho, T.-L. *Synthesis* **1973**, 347. (c) Syper, L. *Tetrahedron Lett.* **1966**, 4493.

(6) Barton, D. H. R.; Hui, R. A. H. F.; Lester, D. J.; Ley, S. V. *Tetrahedron Lett.* **1976**, 3331.

(7) Bhatt, M. V.; Perumal, P. T. *Tetrahedron Lett.* **1981**, *22*, 2605.

(8) (a) Steckhan, E. *Angew. Chem., Int. Ed. Engl.* **1986**, *25*, 683. (b) (b) Kreh, R. P.; Spotniz, R. M.; Lundquist, J. T. *J. Org. Chem.* **1989**, *54*, 1526.

(9) For the direct anodic oxidation, see: (a) Brinkhaus, K.-H. G.; Steckhan, E. *Tetrahedron* **1986**, *42*, 553. (b) Nishiguchi, I.; Hirashima, T. *J. Org. Chem.* **1985**, *50*, 539. (c) Torii, S.; Shiroi, T. *J. Synth. Org. Chem., Jpn.* **1979**, 37, 914.

(10) (a) Sheldon, R. A. *J. Chem. Tech. Biotechnol.* **1997**, *68*, 381. (b) Sheldon, R. A. *Chem. Ind. (London)* **1997**, 12. (c) *Oxygenases and Model Systems*; Funabiki, T., Ed.; Kluwer: Dordrecht, 1997.

(11) The products were analyzed by ^{1}H NMR spectroscopy.

(12) Fujita, M.; Ishida, A.; Takamuku, S.; Fukuzumi, S. *J. Am. Chem. Soc.* **1996**, *118*, 8566.

(13) Poulos, A. T.; Hammond, G. S.; Burton, M. E. *Photochem. Photobiol.* **1981**, *34*, 169.

(14) Cheng, K. S.; Hirota, N. *Investigation of Rates and Mechanisms of Reactions*; Hammes, G. G., Ed.; Wiley-Interscience: New York, 1974; Vol. VI, p 565.

(15) Fukuzumi, S.; Koumitsu, S.; Hironaka, K.; Tanaka, T. *J. Am. Chem. Soc.* **1987**, *109*, 305.

(16) The E^0_{ox} value of *p*-xylene, which corresponds to the E^0_{red} value of the radical cation was determined by the second harmonic ac voltammetry (SHACV) measurements. The SHACV method is known to provide a superior approach to the direct evaluation of the one-electron redox potentials in the presence of a follow-up chemical reaction; Arnett, E. M.; Amarnath, K.; Harvey, N. G.; Cheng, J.-P. *J. Am. Chem. Soc.* **1990**, *112*, 344.

(17) (a) Marcus, R. A. *Ann. Rev. Phys. Chem.* **1964**, *15*, 155. (b) Marcus, R. A. *Angew. Chem., Int. Ed. Engl.* **1993**, *32*, 1111.

(18) The E^0_{ox} value of AcrPh$^\bullet$, which corresponds to the E^0_{red} value of AcrPh$^+$ was determined by the CV measurements in acetonitrile; Fukuzumi, S.; Ohkubo, K.; Tokuda, Y.; Suenobu, T. *J. Am. Chem. Soc.* **2000**, *122*, 4286.

Chapter 3

Activation of Metal–Carbon and Metal–Oxygen Bond by Electron Transfer

Section 3. 1

Activation Parameters for Cobalt–Carbon Bond Cleavage of Organocobalt(III, IV) Complexes with Dimethylglyoxime and Porphyrin Ligands

Abstract. The electron transfer oxidation and subsequent cobalt–carbon bond cleavage of vitamin B_{12} model complexes were investigated using cobaloximes, $(DH)_2Co^{III}(R)(L)$, where DH^- = the anion of dimethylglyoxime, R = Me, Et, Ph, $PhCH_2$ and $PhCH(CH_3)$, L = a substituted pyridine, as coenzyme B_{12} model complexes and $[Fe(bpy)_3](PF_6)_3$ or $[Ru(bpy)_3](PF_6)_3$ (bpy = 2,2'–bipyridine) as an oxidant. The rapid one–electron oxidation of $(DH)_2Co^{III}(R)(L)$ with the oxidant gives the corresponding Co(IV) complexes, $[(DH)_2Co^{IV}(R)(L)]^+$, which were identified by the ESR spectra. This is followed by the rate-determining homolytic cleavage of Co(IV)–C bond of $[(DH)_2Co^{IV}(R)(L)]^+$, resulting in formation of alkyl radical ($R^\bullet$). In the absence of oxygen, $R^\bullet$ is oxidized by the oxidant to produce R^+ that is readily trapped by coordinated pyridine to yield alkylpyridinium ion (Rpy^+). In the presence of oxygen, however, the oxidation of $(DH)_2Co(PhCH_2)(py)$ with one equiv of $[Ru(bpy)_3](PF_6)_3$ leads to yield the oxygenated products, benzaldehyde and benzylhydroperoxide, via the reaction of oxygen with benzyl radical produced by the homolytic cleavage of Co(IV)–C bond of $[(DH)_2Co^{IV}(PhCH_2)(py)]^+$. A comparison of activation enthalpies ($\Delta H^{\neq}$) and entropies ($\Delta S^{\neq}$) for the Co(IV)–C bond cleavage of $[(DH)_2Co^{IV}(R)(L)]^+$ with those of $(DH)_2Co^{III}(R)(L)$ reveals that the Co(IV)–C bond becomes significantly weaker as compared to corresponding Co(III)–C bond. There is a large compensation effect between the $\Delta H^{\neq}$ and $\Delta S^{\neq}$ values for cleavage of Co–C bond in a series of $(DH)_2Co^{III}(R)(L)$ and $[(DH)_2Co^{IV}(R)(L)]^+$, when the $\Delta S^{\neq}$ values vary significantly spanning a range of 100 entropy unit. In contrast, the $\Delta S^{\neq}$ values for cleavage of Co–C bond in the corresponding porphyrin complexes, $(TPP)Co^{III}(R)(L)$ and $[(TPP)Co^{IV}(R)(L)]^+$ where TPP^{2-} = the dianion of tetraphenylporphyrin, remain constant irrespective the difference in the $\Delta H^{\neq}$ values. Such a remarkable difference depending on the type of macrocyclic ligands is discussed in terms of the different flexibility of the ligand responding to the steric pressures of axial ligands. The implication in the enzymatic activation of the Co–C bond of coenzyme B_{12} is also discussed.

Introduction

Coenzyme B_{12} (5'–deoxyadenosylcobalamin, AdoCbl)–dependent rearrangements are initiated by homolytic dissociation of the cobalt–carbon bond to generate 5'deoxyadenosyl radical.[1] The Co(III)–C bond dissociation energies of various B_{12} model complexes have been determined by Halpern et al. in relation with the homolytic mechanisms of coenzyme B_{12}–dependent rearrangement.[2–5] The nonenzymatic thermal homolysis of AdoCbl has also been extensively studied by Finke et al. and the activation parameters ($\Delta H^{\neq}$ and $\Delta S^{\neq}$) of homolytic Co(III)–C bond dissociation have been reported as 33 ± 2 kcal mol^{-1} and 11 ± 2 cal mol^{-1} K^{-1}, respectively.[6,7] Under enzymatic reaction conditions, however, the enzyme enhances the rate of Co–C bond cleavage by a factor up to 10^{12} as compared to that of the free coenzyme.[2–9] Brown et al. have determined the temperature dependence of the ribonucleotide triphosphate reductase (RTPR)-catalyzed process and the $\Delta H^{\neq}$ and $\Delta S^{\neq}$ values are obtained as 20 ± 1 kcal mol^{-1} and 13 ± 4 cal mol^{-1} K^{-1}, respectively.[10] This indicates that the enzymatic activation of the Co–C bond is achieved enthalpically, since the entropy of activation is essentially the same as that for the nonenzymatic thermal homolysis of AdoCbl.[10] In contrast, however, a largely positive $\Delta S^{\neq}$ value (96 cal mol^{-1} K^{-1}) has recently been determined by Stubbe and coworkers for the RTPR enzymatic Co–C bond homolysis, and thereby entropic rather than enthalpic factors have been suggested to make the largest contribution in the enzymatic activation of the Co–C bond.[11] In addition, a decrease in the activation enthalpy is often accompanied by the concomitant decrease in the entropy of activation.[12]

There have been many mechanisms proposed so far as to the origin of the enormous enhancement for the Co–C bond cleavage.[13–18] Enzymatic compression of the axial Co–N bond has been proposed to cause transmission of steric compression to the Co–C bond which is activated by the "butterfly" type upward deformation of the corrin–ring plane.[15,16] Such deformation may be made possible by the flexibility of the corrin ring, which has been shown to be in sharp contrast with the rigidity of porphyrin ring.[4] However, the X–ray

crystal structure of coenzyme B_{12} dependent methylmalonyl–CoA (MMCoA) mutase has revealed that B_{12}'s appended 5,6–dimethylbenzimidazole base is not bound directly to cobalt in MMCoA mutase as previously believed, but that a protein side–chain histidine imidazole serves as the axial base coordinated with cobalt.[19] Since then, the actual role of the axial base in both Co–C homolysis and heterolysis has been studied extensively.[18,20]

On the other hand, it has been reported that the Co(II)–C bond of methylcobalamin is significantly weakened as compared to the Co(III)–C bond.[21] Although electron transfer reduction of AdoCbl is hardly predicted for the mechanism of any adenosylcobalamin–dependent or methylcobalamin–dependent enzymes, the comparison of homolysis rates for reduced and unreduced cobamides provided valuable insight into the nature of Co–C bond.[21] The Co(II)–C homolysis rate was too fast to be determined at room temperature and the rate was determined electrochemically at low temperatures below –30 °C.[22] The one–electron reduction of methylcobalamin leads to populate the Co–C σ^* orbital, thus facilitating the cleavage.[22] Alternatively the one–electron oxidation may lead to depopulate the Co–C σ orbital, also facilitating the Co–C bond cleavage as shown by Halpern et al.[23,24] However, the Co(IV)–C bond dissociation energies have yet to be determined. In this context, we have recently reported the one–electron oxidized organocobalt porphyrins ($[(TPP)Co(R)(L)]^+$, TPP^{2-} = the dianion of tetraphenylporphyrin, R = alkyl or aryl groups; L = substituted pyridines) have d^5 cobalt(IV) character depending on R or L and that the dissociation energies of the Co(IV)–C bond are significantly smaller than those of the corresponding Co(III)–C bond.[25] We have also reported facile homolytic cleavage for Co(IV)–C bond of dialkylcobalt(IV) complexes as compared to the slow cleavage of the corresponding dialkylcobalt(III) complexes, which require thermal or photochemical activation.[26]

We report herein the activation parameters for the Co(IV)–C bond cleavage of a series of σ–bonded organocobaloximes, $[(DH)_2Co^{IV}(R)(L)]^+$ (DH^- = the anion of dimethylglyoxime, R = Me, Et, Ph, $PhCH_2$ and $PhCH(CH_3)$, and L = substituted pyridines) produced by the electron transfer oxidation of $(DH)_2Co^{III}(R)(L)$ with a one–electron oxidant, $[Fe(bpy)_3](PF_6)_3$ (bpy = 2,2'–bipyridine) or $[Ru(bpy)_3](PF_6)_3$ in acetonitrile (MeCN). The present data permits an extensive comparison of the activation parameters ($\Delta H^{\neq}$ and $\Delta S^{\neq}$) between the Co(IV)–C and Co(III)–C bond cleavage of a series of organocobalt complexes with a flexible ligand (DH^-) and a rigid ligand (TPP^{2-}). Such an extensive comparison of the activation parameters provides valuable insight into the essential role of the flexible corrin ring in the enzymatic activation of B_{12}, although the one–electron oxidation of coenzyme B_{12} model complexes has no proven biological role at present. The present study should also be significant for organometallic chemistry, where the factors controlling the strengths of metal–carbon bonds remain to be clarified.[27–29]

Experimental Section

Materials. Cobalt chloride and iron sulfate were purchased from Nakarai Tesque. Dimethylglyoxime and 2,2'–bipyridine were purchased from Wako Pure Chemicals. Organocobaloximes, $(DH)_2Co(R)(L)$ (R = Me, Et, Ph, $PhCH_2$ and $PhCH(CH_3)$, L = various pyridines and H_2O) were prepared by following literature method.[30–32] It is purified by a Soxhlet extraction with dichloromethane, then recrystallized with dichloromethane/acetone. ^1H NMR (300 MHz, CD_3CN): $(DH)_2Co(Me)(py)$: δ 0.60 (s, 3H), 2.06 (s, 12H), 7.41 (t, 2H, *J* = 6.0 Hz), 7.83 (t, 1H, *J* = 6.0 Hz), 8.47 (d, 2H, *J* = 6.0 Hz), 18.63 (br s, 2H); $(DH)_2Co(Me)$(2–Mepy): δ 1.26 (s, 3H), 2.23 (s, 12H), 2.72 (s, 3H), 7.78 (t, 1H, *J* = 8.5 Hz), 7.85 (d, 1H, *J* = 8.5 Hz), 8.33 (t, 1H, *J* = 8.5 Hz), 8.55 (t, 1H, *J* = 8.5 Hz), 18.36 (br s, 2H); $(DH)_2Co(Me)(3,5–Cl_2py)$: δ 0.67 (s, 3H), 2.13 (s, 12H), 7.57 (s, 1H), 8.00 (s, 1H), 8.37 (d, 1H, *J* = 8.5 Hz), 8.55 (s, 1H, *J* = 8.5 Hz), 18.38 (br s, 2H); $(DH)_2Co(Me)(3–n–Bupy)$: δ 0.57 (s, 3H), 0.88 (t, 3H, *J* = 7.3 Hz), 1.24 (m, 2H, *J* = 7.3 Hz), 1.51 (m, 2H, *J* = 7.3 Hz), 2.04 (s, 12H), 2.57 (t, 2H, *J* = 7.3 Hz), 2.72 (s, 3H), 7.29 (dd, 1H, *J* = 7.8 and 5.5 Hz), 7.64 (d, 1H, *J* = 7.3 Hz), 8.33 (t, 1H, *J* = 8.5 Hz), 8.23 – 8.32 (m, 2H), 18.60 (br s, 2H); $(DH)_2Co(Me)$(3–Brpy): δ 0.63 (s, 3H), 2.05 (s, 12H), 7.34 (dd, 1H, *J* = 8.3 and 5.5 Hz), 7.89 (d, 1H, *J* = 8.3 Hz), 8.00 (ddd, 1H, *J* = 8.3, 2.5 and 1.4 Hz), 8.44 (dd, 1H, *J* = 5.3 and 1.1 Hz), 8.54 (d, 1H, *J* = 8.3 Hz), 18.54 (br s, 2H); $(DH)_2Co(Me)$(4–Mepy): δ 0.46 (s, 3H), 2.05 (s, 12H), 2.94 (s, 3H), 6.52 (d, 2H, *J* = 7.1 Hz), 7.87 (d, 2H, *J* = 7.1 Hz), 18.60 (br s, 2H); $(DH)_2Co(Me)(3,4–Me_2py)$: δ 0.55 (s, 3H), 2.05 (s, 12H), 2.17 (s, 3H), 2.24 (s, 3H), 7.15 (d, 2H, *J* = 5.5 Hz), 8.10 (s, 1H, *J* = 7.1 Hz), 8.12 (s, 1H, *J* = 5.5 Hz), 18.60 (br s, 2H); $(DH)_2Co(Me)$(3–Clpy): δ 0.63 (s, 3H), 2.05 (s, 12H), 7.40 (dd, 1H, *J* = 8.4 and 5.3 Hz), 7.86 (ddd, 1H, *J* = 8.4 , 2.3 and 1.2 Hz), 8.40 (dd, 1H, *J* = 5.5 and 1.4 Hz), 8.44 (d, 1H, *J* = 2.3 Hz), 18.60 (br s, 2H); $(DH)_2Co(Me)$(3–Mepy): δ 0.57 (s, 3H), 2.05 (s, 12H), 2.26 (s, 3H), 7.28 (dd, 1H, *J* = 7.8 and 5.3 Hz), 7.63 (d, 1H, *J* = 7.6 Hz), 8.25 (s, 1H), 8.26 (d, 1H, *J* = 7.6 Hz), 18.60 (br s, 2H); $(DH)_2Co(Me)$(4–CNpy): δ 0.60 (s, 3H), 2.05 (s, 12H), 7.57 (d, 2H, *J* = 6.9 Hz), 8.30 (d, 2H, *J* = 6.9 Hz), 18.37 (br s, 2H); $(DH)_2Co(Et)(py)$: δ 0.26 (t, 3H, J = 7.7 Hz), 2.09 (q, 2H, *J* = 7.7 Hz), 7.34 (t, 2H, *J* = 7.7 Hz), 7.85 (t, 1H, *J* = 7.7 Hz), 8.22 (d, 2H, *J* = 7.7 Hz), 18.98 (br

s, 2H); $(DH)_2Co(Ph)(py)$: δ 2.04 (s, 12H), 6.8 – 8.8 (m, 10H), 18.41 (br s, 2H); $(DH)_2Co(PhCH_2)(py)$: δ 2.07 (br s, 12H), 3.86 (s, 2H) 7.4 – 8.7 (m, 10H), 19.14 (br s, 2H). Since the $(DH)_2Co(R)(L)$ are light sensitive,[30,33] the compounds were kept in the dark and all experiments were carried out in the dark.

Tris(2,2'–bipyridine)iron(III) hexafluorophosphate $[Fe(bpy)_3](PF_6)_3$, was prepared from a reaction between iron(II)sulfate heptahydrate and 2,2'–bipyridine followed by oxidation of the resulting iron(II) complex by ceric sulfate in aqueous H_2SO_4.[34] Tris(2,2'–bipyridine)ruthenium dichloride hexahydrate, $[Ru(bpy)_3]$-Cl_2•$6H_2O$ was obtained commercially from Aldrich. The oxidation of $[Ru(bpy)_3]Cl_2$ with lead dioxide in aqueous H_2SO_4 gives $[Ru(bpy)_3]^{3+}$ which was isolated as the PF_6 salt, $[Ru(bpy)_3](PF_6)_3$.[35] Pyridine and substituted pyridines (3,5–dichloropyridine, 4–cyanopyridine, 3–chloropyridine, 3–picoline, 3,4–lutidine, 4–(dimethylamino)pyridine, 3–bromopyridine, 2–picoline, 4–picoline, 4–aminopyridine and 3–*n*–butylpyridine) were obtained commercially and purified using standard methods.[36] Tetrabutylammonium perchlorate (TBAP), obtained from Fluka Fine Chemical, was recrystallized from ethanol and dried in vacuo prior to use. Acetonitrile used as a solvent were purified and dried by the standard procedure.[36] Acetonitrile–d_3 (CD_3CN) was obtained from EURI SO–TOP, France.

Reaction Procedure. Typically, $(DH)_2Co(R)(L)$ (1.0×10^{-3} M) and $[Fe(bpy)_3](PF_6)_3$ (2.0×10^{-3} M) were added to an NMR tube which contained deaerated CD_3CN (0.60 cm^3) under an atmospheric pressure of argon. The products were identified by the ^1H NMR spectra by comparing with those of authentic samples. ^1H NMR spectra were measured on a JEOL NMR spectrometer, GSX–400 (400 MHz) and JEOL JMN–AL300 (300 MHz). Chemical shifts of ^1H NMR were expressed in parts per million downfield from tetramethylsilane as an internal standard (δ = 0). ^1H NMR (400 MHz, CD_3CN): *N*–methylpyridinium ion: δ 4.30 (s, 3H), 8.0–9.2 (m, 5H). *N*–ethylpyridinium ion: δ 1.57 (t, 3H, J = 7.3 Hz) 4.54 (q, 2H, J = 7.3 Hz), 7.5–9.0 (m, 5H).

The products of the reaction of $(DH)_2Co(PhCH_2)(py)$ (1.0×10^{-3} M) and $[Ru(bpy)_3](PF_6)_3$ (1.0×10^{-3} M) in oxygen–saturated CD_3CN were determined by the ^1H NMR spectra. ^1H NMR (300 MHz, CD_3CN): benzylhydroperoxide: δ 4.89 (s, 2H), 7.3–7.5 (m, 5H); benzaldehyde: δ (m, 5H), 7.3–8.0 (m, 5H), 9.98 (s, 1H).

Kinetic Measurements. Kinetic measurements of the oxidation of $(DH)_2Co(R)(L)$ with $[Fe(bpy)_3](PF_6)_3$ in MeCN were performed on a Hewlett–Packard 8453 photodiode array spectrophotometer and a Shimadzu UV–160A spectrophotometer which was

thermostated at from 298 K to 328 K. Typically, deaerated MeCN solution of $[Fe(bpy)_3](PF_6)_3$ (1.0×10^{-4} M) was added to an MeCN solution of $(DH)_2Co(Me)(py)$ (1.7×10^{-5} M) by means of a microsyringe in quartz cuvette (i.d. 10 mm) under Ar with stirring. All kinetic measurements were carried out where the concentrations of $[Fe(bpy)_3](PF_6)_3$ were maintained at > 10–fold excess of the concentrations of $(DH)_2Co(R)(L)$. Rates of the oxidation of $(DH)_2Co(R)(L)$ with $[Fe(bpy)_3](PF_6)_3$ in MeCN were monitored by measuring the increase of absorbance due to $[Fe(bpy)_3]^{2+}$ at λ_{max} = 520 nm ($\varepsilon_{max} = 8.7 \times 10^3$ M^{-1} cm^{-1}) in MeCN at 298 K.[37] The first–order rate constants were determined by least–square curve fits using a personal computer. The first–order plots were linear for 3 or more half–lives with the correlation coefficient $\rho > 0.999$.

Cyclic Voltammetry. Cyclic voltammetry measurements were performed at 298 K on a BAS 100W electrochemical analyzer in deaerated MeCN containing 0.1 M NBu_4ClO_4 as supporting electrolyte. A conventional three–electrode cell was used with a gold working electrode (surface area of 0.3 mm^2) and a platinum wire as the counter electrode. The Pt working electrode (BAS) was polished with a BAS polishing alumina suspension and rinsed with acetone before use. The measured potentials were recorded with respect to the $Ag/AgNO_3$ (0.01 M) reference electrode. All potentials (vs Ag/Ag^+) were converted to values *vs* SCE by adding 0.29 V.[38] The $E_{1/2}$ value of ferrocene used as a standard is 0.37 V vs SCE in MeCN under the present experimental conditions. All electrochemical measurements were carried out under an atmospheric pressure of argon.

ESR Measurements. ESR spectra of $[(DH)_2Co(R)(L)]^+$ in frozen MeCN were measured at 153 K with a JEOL X–band spectrometer JES–RE1XE and were recorded under nonsaturating microwave power conditions. The magnitude of the modulation was chosen to optimize the resolution and the signal to noise ratio (S/N) of the observed spectra. The g values were calibrated using a Mn^{2+} marker and the hyperfine coupling constants were determined by a computer simulation using a Calleo ESR II program coded by Calleo Scientific Software Publishers.

Results and Discussion

One–Electron Oxidation Potentials of $(DH)_2Co(R)(L)$ and $(TPP)Co(R)(L)$. The one–electron oxidation potentials (E^0_{ox} vs SCE) of $(DH)_2Co^{III}(R)(H_2O)$ in an aqueous solution were reported previously as 0.849 V (R = *p*–$CH_3C_6H_4CH_2$) and 0.902 V (R = Me).[23] The E^0_{ox} values of $(DH)_2Co^{III}(R)(L)$ (R = Me, Et, Ph, $PhCH_2$ and $PhCH(CH_3)$, L = various pyridines and H_2O) in MeCN were also readily determined by the cyclic voltammograms which give the reversible one–electron redox waves. No second oxidation wave was observed in the potential region less than 1.5 V. The E^0_{ox} values of $(DH)_2Co^{III}(Me)(L)$ with different axial base ligands (L) are listed in Table 1 together with the pK_a values of L.[39] The E^0_{ox} values of $(DH)_2Co^{III}(R)(py)$ with different R groups (R = Me, Et, Ph, $PhCH_2$ and $PhCH(CH_3)$, py = pyridine) are listed in Table 2. The cyclic voltammograms of all $(DH)_2Co(R)(L)$ complexes in Table 1 and Table 2 gave reversible waves in MeCN even at slow scan rate (20 mV s^{-1}) at 298 K, indicating that the Co–C bond cleavage in $[(DH)_2Co(R)(L)]^+$ occurs at much slower rate than the cyclic voltammetry time scale.

The E^0_{ox} values of $(DH)_2Co(Me)(L)$ are nearly constant irrespective of pK_a value of L,[38] as shown in Figure 1a. This is in sharp contrast with those of $(TPP)Co(R)(L)$ which decrease with an increase in pK_a of L as shown in Figure 1b.[25] Such a difference in the dependence of E^0_{ox} on pK_a between $(DH)_2Co(Me)(L)$ and $(TPP)Co(R)(L)$ may result from the difference in the flexibility of $(DH)_2$ and TPP rings. As the pK_a of L increases, the electron density on the metal also increases, leading to the negative shift of the E^0_{ox} value in the case of $(TPP)Co(Me)(L)$ as shown in Figure 1b. In the case of $(DH)_2Co(Me)(L)$, however, the stronger binding of L with the larger pK_a value results in the deformation of $(DH)_2$ ring, which leads to the weaker binding of Co with nitrogens of $(DH)_2$ rings. These two opposite effects are canceled out to make the E^0_{ox} value constant irrespective of pK_a of L as shown in Figure 1a.

Oxidation of $(DH)_2Co^{III}(R)(L)$ with $[Fe(bpy)_3]^{3+}$. Oxidation of $(DH)_2Co^{III}(R)(L)$ has been performed using $[Fe(bpy)_3]^{3+}$ as an oxidant. Since the one–electron reduction potential of $[Fe(bpy)_3]^{3+}$ in MeCN (E^0_{red} = 1.04 V *vs* SCE) is more positive than the E^0_{ox} values of $(DH)_2Co^{III}(R)(L)$ but less positive than the second oxidation potentials, only one–electron oxidation of $(DH)_2Co^{III}(R)(L)$ is expected to occur. However, the initial fast one–electron oxidation of $(DH)_2Co^{III}(R)(L)$ with more than two equivalents

Table 1. One-Electron Oxidation Potentials (E^0_{ox} vs SCE) of $(DH)_2Co(Me)(L)$ (L = Substituted Pyridines and Water), $g_{//}$ and $A_{//(Co)}$ Values of $[(DH)_2Co(Me)(L)]^+$, Rate Constants (k_{obs}) and Activation Parameters for the Co(IV)–C Bond Cleavage of $[(DH)_2Co(Me)(L)]^+$ in MeCN

no.	L	pK_a[a]	E^0_{ox} V	$g_{//}$	$A_{//(Co)}$ G	k_{obs}[b] s^{-1}	$\Delta H^{\neq}$ kcal mol^{-1}	$\Delta S^{\neq}$ cal K^{-1} mol^{-1}
1a	3,5-Cl_2py	0.67	0.84	2.0206	26.7	1.4×10^{-3}	9.4	-40
2a	4-CNpy	1.86	0.80	2.0215	26.4	7.9×10^{-4}	14.8	-23
3a	3-Clpy	2.81	0.84	2.0206	26.3	8.8×10^{-4}	14.9	-24
4a	3-Brpy	2.84	0.83	2.0199	26.2	5.4×10^{-4}	14.3	-25
5a	py	5.28	0.85	2.0212	26.3	5.0×10^{-4}	14.9	-24
6a	3-Mepy	5.79	0.82	2.0213	26.7	2.7×10^{-4}	10.3	-40
7a	2-Mepy	5.96	0.81	nd	nd	1.9×10^{-3}	2.6	-62
8a	4-Mepy	5.98	0.84	2.0244	26.6	5.2×10^{-4}	15.8	-21
9a	3,4-Me_2py	6.46	0.82	2.0211	26.9	6.8×10^{-4}	7.3	-49
10a	4-Me_2Npy	9.71	0.80	2.0216	29.1	2.5×10^{-4}	12.4	-33
11a	3-*n*-Bupy		0.81	nd	nd	1.9×10^{-3}	6.1	-51
12a	H_2O	7.00	0.86	2.0254[c]	27.3[c]	1.9×10^{-2}	19.2	-7

[a] Taken from ref 38. [b] 298 K. [c] Determined in MeOH/MeCN (1:1 v/v)

Table 2. One–Electron Oxidation Potentials (E^0_{ox} vs SCE) of $(DH)_2Co(R)(py)$, $g_{//}$ and $A_{//(Co)}$ Values of $[(DH)_2Co(R)(py)]^+$, Rate Constants (k_{obs}) and Activation Parameters for the Co(IV)–C Bond Cleavage of $[(DH)_2Co(R)(py]^+$ in MeCN

no.	R	E^0_{ox} V	$g_{//}$	$A_{//(Co)}$ G	k_{obs}[a] s^{-1}	$\Delta H^{\neq}$ kcal mol^{-1}	$\Delta S^{\neq}$ cal K^{-1} mol^{-1}
5b	$PhCH(CH_3)$	nd	nd	nd	7.1×10^{-3}	4.0	-55
5c	$PhCH_2$	0.80	2.0344	26.4	1.5×10^{-3}	12.1	-31
5d	Et	0.82	2.0319	26.6	5.8×10^{-4}	13.5	-28
5e	Ph	0.86	2.0223	26.2	2.5×10^{-4}	18.8	-12

[a] 298 K.

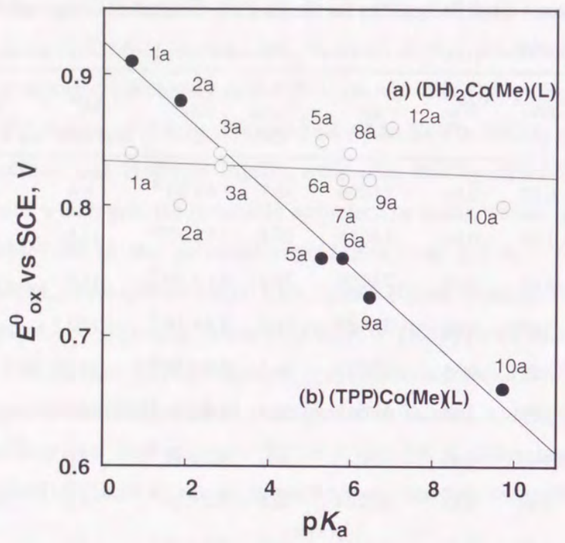

Figure 1. Dependence of the one–electron oxidation potential (E^0_{ox}) of (a) $(DH)_2Co(Me)(L)$ (O) and (b) (TPP)Co(Me)(L) (●) on pK_a of L.

of $[Fe(bpy)_3]^{3+}$ is followed by the second one–electron oxidation which is much slower than the first oxidation. A typical example for the spectral change is shown in Figure 2, where the absorption band due to $[Fe(bpy)_3]^{2+}$ appears stepwise in the oxidation of $(DH)_2Co(Me)(py)$ with $[Fe(bpy)_3]^{3+}$. The stoichiometry of the two–electron oxidation of reaction is given by eq 1 based on the product analysis (see Experimental Section).

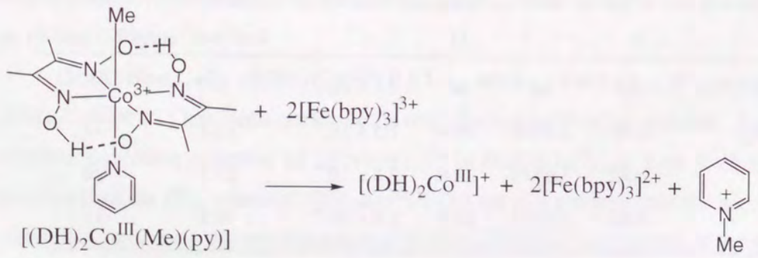

(1)

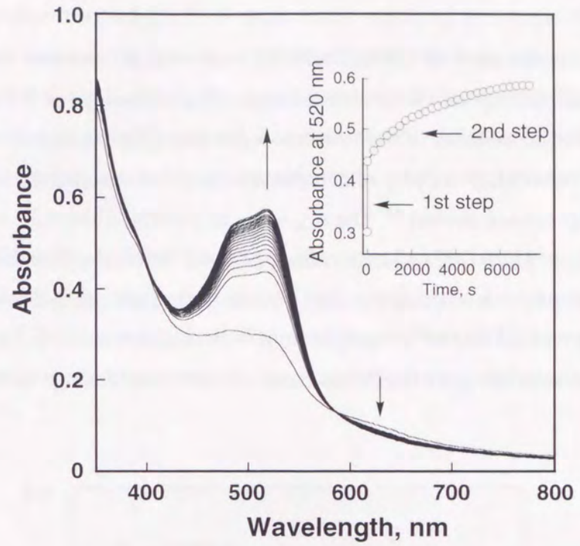

Figure 2. Visible spectral change observed in electron transfer from $(DH)_2Co(Me)(py)$ (1.7×10^{-5} M) to $Fe(bpy)_3(PF_6)_3$ (1.0×10^{-4} M) in MeCN at 298 K at prolonged reaction time (0 – 6000 sec, 300 sec interval). Inset shows time dependence of absorbance at 520 nm.

The first one–electron oxidation of $(DH)_2Co(R)(L)$ with $[Fe(bpy)_3]^{3+}$ was too fast to be monitored even by using a stopped–flow technique. The one–electron oxidized products of $(DH)_2Co(R)(H_2O)$ have previously been identified as the corresponding organocobalt(IV) species based on the ESR spectra measured in aqueous methanol solution.[24,40,41] The one–electron oxidized complexes, $[(DH)_2Co(Me)(L)]^+$ with a series of L and $[(DH)_2Co(R)(py)]^+$ with different R groups, were produced by the one–electron oxidation of $(DH)_2Co(R)(L)$ with $[Fe(bpy)_3]^{3+}$, and the ESR spectra were measured in frozen MeCN at 153 K. The ESR spectra revealed the characteristic patterns of eight hyperfine lines due to the interaction of the unpaired electron with one cobalt nucleus ($I = 7/2$). The ESR parameters ($g_{//}$ and $A_{//(Co)}$) are also listed in Tables 1 and 2. The $g_{//}$ and $A_{//(Co)}$ values are rather insensitive of the type of R and pK_a of L, and they are essentially the same as those of $[(DH)_2Co(R)(H_2O)]^+$, which have previously been identified as the corresponding organocobalt(IV) species.[24,40–42] Thus, the

site of electron removal from all $(DH)_2Co(R)(L)$ complexes is the cobalt atom rather than the $(DH)_2$ ligand.

In contrast to the case of $(DH)_2Co(R)(L)$, the site of electron removal from (TPP)Co(R)(L) has been reported to be changed depending on the type of R and pK_a of L.[39] Figure 3a shows the dependence of the isotropic hyperfine coupling constant due to ^{59}Co (A_{Co}) of $[(TPP)Co(Me)(L)]^+$ on pK_a of L (open circles),[25] in comparison with $A_{//(Co)}$ of $[(DH)_2Co(Me)(L)]^+$ (closed circles).[43] The A_{Co} value of $[(TPP)Co(Me)(L)]^+$ increases from 7.9 G (L = 3,5–Cl_2py, pK_a = 0.67) with increasing pK_a of L to reach a constant value (ca. 12 G) in the region of pK_a > 3, whereas the $A_{//(Co)}$ value is constant irrespective of pK_a of L. Since the A_{Co} value of $[(TPP)Co^{III}]^{2+}$ porphyrin π radical cation is 6.0 G,[44] an increase in A_{Co} from this value indicates more Co(IV) character in $[(TPP)Co(Me)(L)]^+$ with increasing

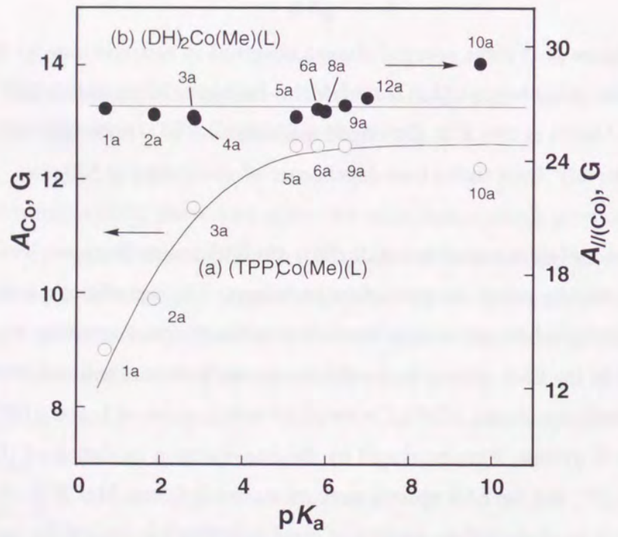

Figure 3. Dependence of the hyperfine coupling constant (A_{Co} or $A_{//(Co)}$) of (a) $[(TPP)Co(Me)(L)]^+$ (O) and (b) $[(DH)_2Co(Me)(L)]^+$ (●) on pK_a of L.

the basicity of L (pK_a) to reach the pure Co(IV) oxidation state which has the A_{Co} value of 12 G.[43] The porphyrin ligand (TPP) is more easily oxidized as compared with the $(DH)_2$ ligand, but an increase in the basicity of the axial ligand results in a change of the oxidation site from the TPP ligand in part to the metal center only as the electron density on the metal increases. In the case of $(DH)_2$ ligand, however, there is no contribution from the ligand center oxidation and the oxidation site remains on the metal irrespective of pK_a of L (Figure 3b).

Rates of Co(IV)–C Bond Cleavage. The rate of second one–electron oxidation step of $(DH)_2Co(PhCH_2)(py)$ obeys first–order kinetics and the first–order rate constant (k_{obs}) remains the same with variation of the $[Fe(bpy)_3]^{3+}$ concentration used in excess as shown in Figure 4. The first–order kinetics has also been reported for the oxidative decomposition of

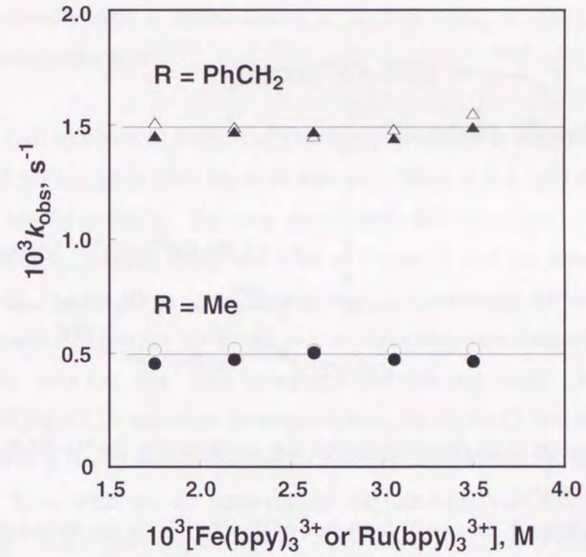

Figure 4. Plots of k_{obs} vs $[Fe(bpy)_3{}^{3+}]$ or $[Ru(bpy)_3{}^{3+}]$ in the second electron transfer oxidation of $(DH)_2Co(R)(py)$ (R = Me and $PhCH_2$) (1.7 x 10^{-5} M) with $[Fe(bpy)_3{}^{3+}]$ (O and Δ) or $[Ru(bpy)_3{}^{3+}]$ (● and ▲) in deaerated MeCN at 298 K.

$(DH)_2Co(R)(H_2O)$ at room temperature.[24] The k_{obs} value was determined as 1.5 x 10^{-3} s^{-1} at 298 K and the same value was obtained in the oxidation of $(DH)_2Co(PhCH_2)(py)$ with a stronger oxidant, $[Ru(bpy)_3]^{3+}$ (E^0_{red} vs SCE = 1.24 V).[28] Such a constant dependence of k_{obs} on the oxidant concentration indicates that the rate–determining step for the second one–electron oxidation is the cleavage of the Co–C bond of $[(DH)_2Co(PhCH_2)(py)]^+$ to give alkyl radical which may be rapidly oxidized by the oxidant to produce methyl cation that is readily trapped by coordinated pyridine to yield alkylpyridinium ion (Rpy^+), as shown in Scheme 1.[45] The electron transfer from generated alkyl radical to $[Fe(bpy)_3]^{3+}$ should proceed efficiently since the one–electron oxidation potentials (E^0_{ox}) of $R^\bullet$ (e.g., $PhCH_2^\bullet$: E^0_{ox} vs SCE = 0.73 V)[46]. are lower than the one–electron reduction potential of $[Fe(bpy)_3]^{3+}$ in MeCN (E^0_{red} = 1.04 V *vs* SCE).

Scheme 1

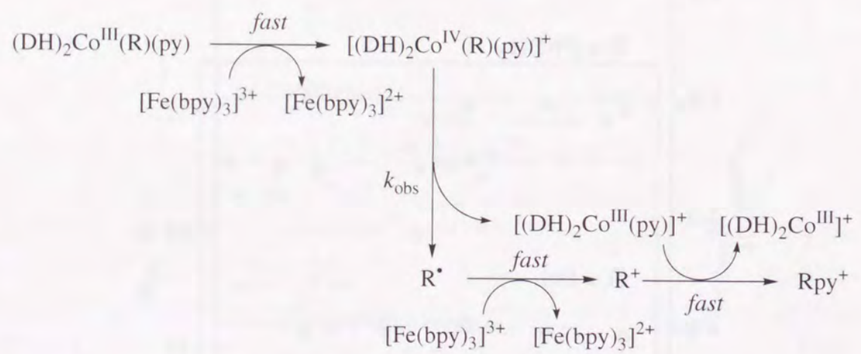

The quantitative formation of alkylpyridinium ion was confirmed by the ^1H–NMR spectrum (see Experimental Section).

According to Scheme 1, the rate of formation of $[Fe(bpy)_3]^{2+}$ at the second step should be the same as the rate of disappearance of $[(DH)_2Co(R)(py)]^+$ (eq 2). The rate of

$$d[[Fe(bpy)_3]^{2+}]/dt = k_{obs}\{[2[(DH)_2Co(R)(py)]]_0 - [[Fe(bpy)_3]^{2+}]\}$$
$$= -d[[(DH)_2Co(R)(py)]^+]/dt = k_{obs}[[(DH)_2Co(R)(py)]^+] \qquad (2)$$

disappearance of $[(DH)_2Co(R)(py)]^+$ was monitored by ESR as shown in Figure 5,

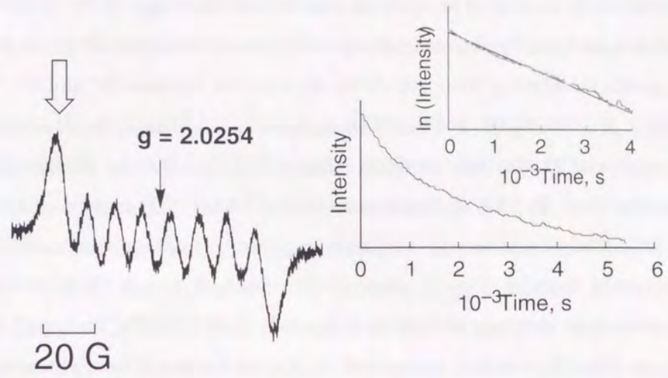

Figure 5. ESR spectrum of $[(DH)_2Co^{IV}(Me)(L)]^+$ produced in the reaction of $(DH)_2Co(Me)(L)$ (1.0 x 10^{-3} M) with $Ru(bpy)_3(PF_6)_3$ (1.0 x 10^{-3} M) in deaerated MeCN at 298 K. Decay of the ESR signal of $[(DH)_2Co^{IV}(Me)(L)]^+$ and first-order plot.

where the ESR spectrum of $[(DH)_2Co^{IV}(Me)(py)]^+$ produced in the one-electron oxidation of $(DH)_2Co(Me)(L)$ (1.0 x 10^{-3} M) with $Ru(bpy)_3(PF_6)_3$ (1.0 x 10^{-3} M) was measured in deaerated MeCN at 298 K. The slow decay of the ESR signal of $[(DH)_2Co^{IV}(Me)(py)]^+$ obeys first-order kinetics (eq 2, see inset of Figure 5) and the observed first-order rate constant (k_{obs} = 4.9 x 10^{-4} s^{-1}) agrees with the k_{obs} value (5.0 x 10^{-4} s^{-1}) obtained from the rate of formation of $[Fe(bpy)_3]^{2+}$ at the second step within experimental errors (± 5%). Such agreement between the rate constants determined from the decay rates of $[(DH)_2Co^{IV}(Me)(L)]^+$ and those determined from the rates of formation of $[Fe(bpy)_3]^{2+}$ at the second step (eq 2) was confirmed for a series of substituted pyridines (L) as listed in Table 1. Thus, what we are observing as the rate of second electron transfer to form $[Fe(bpy)_3]^{2+}$ is the cleavage rate of Co^{IV}-C bond of $[(DH)_2Co^{IV}(R)(L)]^+$ produced in the first rapid electron transfer from $[(DH)_2Co^{IV}(R)(L)]$ to $[Fe(bpy)_3]^{3+}$, since the subsequent electron transfer from $R^\bullet$ to $[Fe(bpy)_3]^{3+}$ to produce $[Fe(bpy)_3]^{2+}$ is much faster than the cleavage rate (Scheme 1).

Alternatively the Co(IV)–C bond may be cleaved heterolytically to produce R^+ and $[(DH)_2Co^{II}(L)]^-$ which is rapidly oxidized by $[Fe(bpy)_3]^{3+}$ to produce the same products as the case in Scheme 1. Whether the Co(IV)–C bond is cleaved homolytically or heterolytically

may be determined by the trap of the cleaved product with dioxygen (O_2). If the Co(IV)–C bond is cleaved homolytically, the cleaved radical R$^\bullet$ would be trapped by O_2 to produce the oxygenated products, whereas there would be no reaction between R$^+$ and O_2. Thus, the reaction of $(DH)_2Co(PhCH_2)(py)$ (1.0 mM) with one equiv of $[Ru(bpy)_3]^{3+}$ was performed in O_2–saturated MeCN and the products were identified by the NMR spectra (see Experimental Section). In 24 h the conversion of $(DH)_2Co(PhCH_2)(py)$ was 34 % and the oxygenated products, benzaldehyde (PhCHO) and benzyl hydroperoxide ($PhCH_2OOH$), were obtained in 26 % and 8 % yield, respectively. Such oxygenated products could only arise *via* the homolytic cleavage of Co(IV)–C bond in $[(DH)_2Co(PhCH_2)(py)]^+$ to produce benzyl radical ($PhCH_2^\bullet$) which is trapped by O_2 to produce benzylperoxyl radical ($PhCH_2OO^\bullet$) as shown in Scheme 2.

Scheme 2

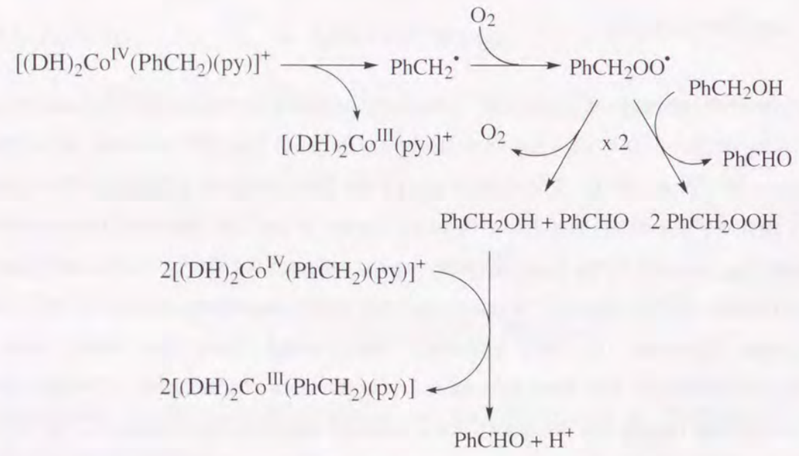

The disproportionation of $PhCH_2OO^\bullet$ is known to yield $PhCH_2OH$ and PhCHO accompanied by the release of O_2.[47] The hydrogen transfer from $PhCH_2OH$ to $PhCH_2OO^\bullet$ also yield $PhCH_2OOH$ and PhCHO (Scheme 2). Benzyl alcohol is further oxidized by $[(DH)_2Co^{IV}(PhCH_2)(py)]^+$ to yield PhCHO,[26a] accompanied by regeneration of $(DH)_2Co^{III}(PhCH_2)(py)$ (Scheme 2). This is the reason why PhCHO is obtained as the major oxygenated product together with the small amount of $PhCH_2OOH$.[26a,48] Thus, it can be concluded that the cleavage of Co(IV)–C bond occurs homolytically rather than

heterolytically.[24,49,50] The Co(IV)–C bond cleavage in $[(TPP)Co(R)(L)]^+$ has also been reported to occur homolytically, since the products derived from free radical R$^\bullet$ were detected.[25]

Mechanism of Homolytic Cleavage of Co(V)–C Bond. The k_{obs} values for the Co(IV)–C homolytic cleavage of $[(DH)_2Co(Me)(L)]^+$ in Table 1 have no apparent correlation with the basicity of the axial ligand L as shown in Figure 5 (open circles). In contrast to such a scattered relation between log k_{obs} and pK_a of L, the corresponding k_{obs} value of $[(TPP)Co(Me)(L)]^+$ first increases with increase in pK_a, reaches a maximum for 3–chloropyridine (no. 3a), and then decreases in the pK_a region larger than that of 3–chloropyridine (pK_a = 2.81, see closed circles in Figure 6). Such a change in he dependence of k_{obs} on pK_a is related to the change of the oxidation site of $[(TPP)Co(Me)(L)]^+$ as discussed based on the dependence of A_{Co} on pK_a of L in Figure 3 (*vide supra*). The larger the pK_a value up to the value of 3–chloropyridine (2.81), the more the Co(IV) character in $[(TPP)Co(Me)(L)]^+$, the faster the Co–C cleavage. In the larger pK_a region (> 3), however, the site of electron transfer remains the same, yielding the pure Co(IV) oxidation state, $[(TPP)Co^{IV}(Me)L]^+$, when the k_{obs} value decreases with an increase in pK_a. These results indicate that the reactivity of Co–C bond cleavage is determined by the electron density on the cobalt: the smaller the electron density, the larger the cleavage reactivity of the Co–C bond. Thus, the homolytic cleavage of the Co(IV)–C bond has been proposed to occur via a rate–determining intramolecular electron transfer from R to Co as shown in Scheme 3.[25,29] The intramolecular electron transfer mechanism is also consistent with the larger cleavage rate of $[(TPP)Co(R)]^+$ with increasing the donor ability of R: R = Ph < Me < Et < Bu.[25] In contrast to the case of R = Me in Figure 5b, the k_{obs} value of R = R = Ph continues to increase with increasing pK_a of L, when the Co(IV) character keeps increasing because of the weak donor ability of the σ–bonded Ph as compared to that of Me.[25] The homolytic cleavage of the Co(IV)–C bond is followed by the migration of R to a nitrogen of the porphyrin ring to give the *N*–aryl or *N*–alkyl Co(II) porphyrins which are further oxidized to yield the Co(III) complexes (Scheme 3).[25]

The intramolecular electron transfer mechanism can also be adopted for the homolytic cleavage of the Co(IV)–C bond of $[(DH)_2Co^{IV}(R)(L)]^+$ (Scheme 3). In contrast to the case of $[(TPP)Co^{IV}(Me)L]^+$, however, an increase in the pK_a value does not simply result in an increase in the electron density on the metal, since the stronger binding of L with the larger pK_a value results in the deformation of $(DH)_2$ ring, which leads to the weaker binding of Co

Scheme 3

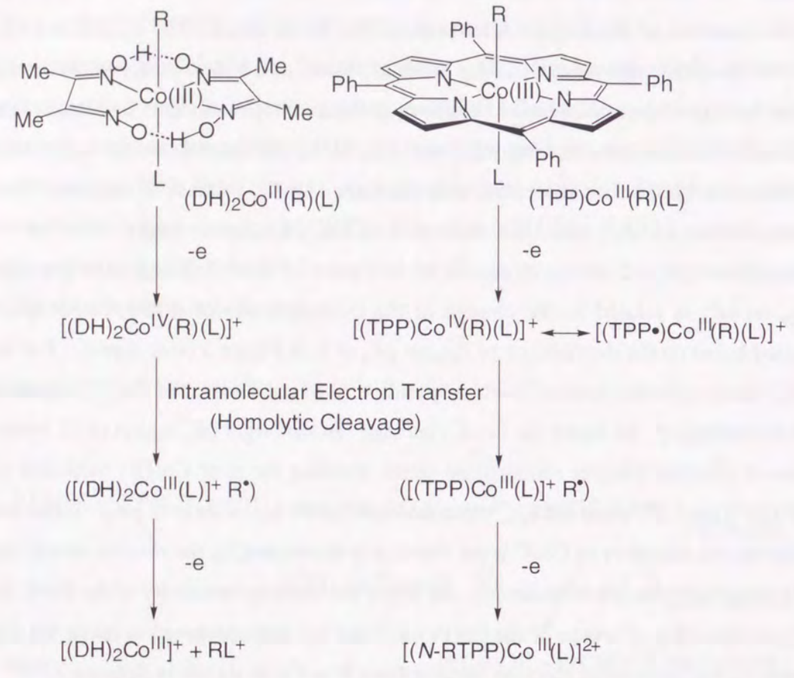

with nitrogens of $(DH)_2$ rings as indicated by the constant E^0_{ox} value irrespective of pK_a of L (Figure 1a). This may be the reason why there is no apparent correlation between k_{obs} and pK_a (open circles in Figure 5). The rate–determining homolysis of the Co(IV)–C bond to produce R• is followed by the one–electron oxidation of R• and the subsequent reaction with the axial base L yields $[(DH)_2Co^{III}]^+$ and RL^+ (Scheme 3).

The k_{obs} values were determined for various $[(DH)_2Co(R)(L)]^+$ where R = Me, Et, Ph, $PhCH_2$ and $PhCH(CH_3)$, L = a series of substituted pyridines in MeCN at different temperatures. The activation enthalpies ($\Delta H^{\neq}$) and entropies ($\Delta S^{\neq}$) for the Co–C bond dissociation of $[(DH)_2Co^{IV}(R)(L)]^+$ were then determined form the slopes and intercepts of Eyring plots of k_{obs}, respectively. The typical Eyring plots are shown in Figure 7, where an isokinetic temperature is observed. The observation of such an isokinetic temperature strongly suggests that the mehcanism for the Co-C bond cleavage is the same for various

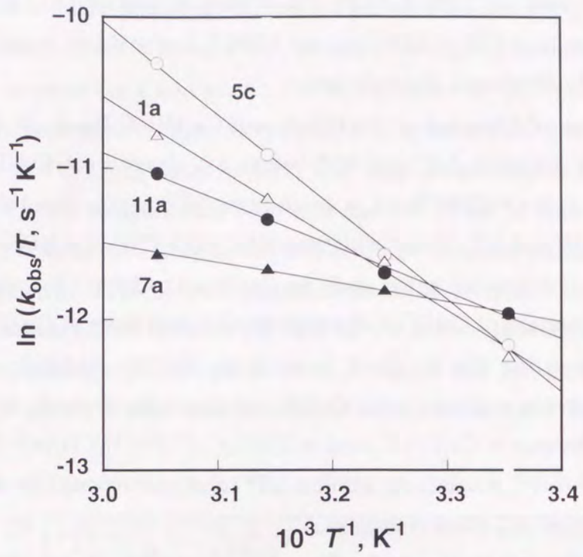

Figure 6. Eyring plots of k_{obs} for Co(IV)–C bond cleavage of $[(DH)_2Co(PhCH_2)(py)]^+$ (5c, ○), $[(DH)_2Co(Me)(3,4\text{–}Cl_2py)]^+$ (1a, △), $[(DH)_2Co(Me)(3\text{–}Bupy)]^+$ (11a, ●) and $[(DH)_2Co(Me)(2\text{–}Mepy)]^+$ (7a, ▲) (3.0×10^{-5} M) in deaerated MeCN at various temperatures.

$[(DH)_2Co^{IV}(R)(L)]^+$. Other $\Delta H^{\neq}$ values also vary significantly depending on the type of R and L with the compensated change in the $\Delta S^{\neq}$ values. The $\Delta H^{\neq}$ and $\Delta S^{\neq}$ values for a series of $[(DH)_2Co(R)(L)]^+$ are listed in Tables 1 and 2.

The $\Delta S^{\neq}$ values for bond-cleavage processes are generally expected to be positive. However, all the $\Delta S^{\neq}$ values determined for the cleavage of Co(IV)–C bond of $[(DH)_2Co^{IV}(R)(L)]^+$ are negative. Since it has been confirmed that the rate-determining step for the second one–electron oxidation step of $(DH)_2Co^{III}(R)(L)$ is the homolytic cleavage of Co(IV)–C bond of $[(DH)_2Co^{IV}((R)(L)]^+$ (*vide supra*), the negative $\Delta S^{\neq}$ values for the Co(IV)–C suggest that the elongation of the Co–C bond is accompanied by the shortening of other bonds. In fact, according to the X-ray structures,[51] the longer Co–C bond (2.064 Å) of $(DH)_2Co(PhCH_2)(py)$ as compared to the Co–C bond of $(DH)_2Co(Me)(py)$ (1.999 Å) is accompanied by the shorter Co-N bonds (1.878 Å (average) for four Co–N bonds of

$(DH)_2Co(PhCH_2)(py)$ and 2.056 Å for the Co–py bond as compared to 1.896 Å (average) for four Co-N bonds of $(DH)_2Co(Me)(py)$ and 2.069 Å for the Co–py bond). The relation between $\Delta H^{\neq}$ and $\Delta S^{\neq}$ values is discussed later.

Comparison of Cleavage of Co(III)–C and Co(IV)–C Bond. Halpern et al.[4,12] have previously reported $\Delta H^{\neq}$ and $\Delta S^{\neq}$ values for cleavage of Co(III)–C bond in $(DH)_2Co^{III}(R)(L)$ (R = $PhCH(CH_3)$, L = 4–substituted pyridine) as listed in Table 3. The corresponding $\Delta H^{\neq}$ and $\Delta S^{\neq}$ values for cleavage of Co(IV)–C bond in $[(DH)_2Co^{IV}(R)(L)]^+$ (R = $PhCH(CH_3)$) determined in this study are also listed in Table 3 for comparison. The $\Delta H^{\neq}$ values for cleavage of Co(IV)–C bond are smaller than those of Co(III)–C by 14–21 kcal mol^{-1}, suggesting that the Co–C bond in the Co(IV) oxidation state becomes significantly weaker as compared to the Co(III) oxidation state. It should be noted that the $\Delta H^{\neq}$ value for cleavage of Co(IV)–C bond in $[(DH)_2Co^{IV}(PhCH(CH_3))(4\text{–}NH_2py)]^+$ is as small as 3.0 kcal mol^{-1}, which is the smallest $\Delta H^{\neq}$ value ever reported for the Co–C bond cleavage of coenzyme B_{12} model complexes.

The $\Delta H^{\neq}$ values can be converted to $D_{Co\text{–}R}$ by using eq 2, where F_c is the ratio of

$$D_{Co\text{–}R} = \Delta H^{\neq} - F_c \Delta H^{\neq}_{\eta} \qquad (2)$$

Table 3. Rate Constants (k_{obs}) and Activation Parameters for the Co(IV)–C Bond Cleavage of $[(DH)_2Co(PhCH(CH_3))(L)]^+$ in MeCN

		Co(IV) – C			Co(III) – C [a]		
L	pK_a [b]	k_{obs} [c] s^{-1}	$\Delta H^{\neq}$ kcal mol^{-1}	$\Delta S^{\neq}$ cal K^{-1} mol^{-1}	k_{obs} [c] s^{-1}	$\Delta H^{\neq}$ kcal mol^{-1}	$\Delta S^{\neq}$ cal K^{-1} mol^{-1}
4-CNpy	1.86	5.2×10^{-3}	6.5	-42	1.3×10^{-3}	20.1	-4
py	2.81	7.1×10^{-3}	4.0	-55	7.3×10^{-4}	21.6	0
4-Mepy	5.28	6.2×10^{-3}	6.0	-49	6.0×10^{-4}	21.8	1
4-NH_2py	9.30	4.4×10^{-4}	3.0	-64	4.0×10^{-4}	23.8	4

[a] Taken from ref 2b. [b] Taken from ref 38. [c] 298 K.

cage recombination to the sum of all competing cage processes and $\Delta H^{\neq}_{\eta}$ is the activation enthalpy for viscous flow.[6,52] Since $0 < F_c < 1$ and $1 < \Delta H^{\neq}_{\eta} < 2$ kcal mol^{-1}, the $F_c \Delta H^{\neq}_{\eta}$ value may be taken as 1 ± 1 kcal mol^{-1}. The $D_{Co\text{–}R}$ values for $[(DH)_2Co^{IV}(R)(L)]^+$ are therefore smaller than those for the corresponding Co(III) complexes, $(DH)_2Co^{III}(R)(L)$ by 14–21 kcal mol^{-1}. The $D_{Co\text{–}R}$ values for $[(TPP)Co^{IV}(R)]^+$ are also smaller than those for the corresponding Co(III) complexes by 5–11 kcal mol^{-1}.[25] Thus, in both TPP and $(DH)_2$ cases the Co–C bond in the higher oxidation state Co(IV) complex becomes significantly weaker as compared to that in the lower oxidation state Co(III) complex.

Compensation Effects between $\Delta H^{\neq}$ and $\Delta S^{\neq}$. A relation between $\Delta H^{\neq}$ and $\Delta S^{\neq}$ for the Co–C bond cleavage of $[(DH)_2Co^{IV}(R)(L)]^+$ where R = Me, Et, Ph, $PhCH_2$ and $PhCH(CH_3)$, L = a series of substituted pyridines is summarized as a plot between $\Delta H^{\neq}$ L.

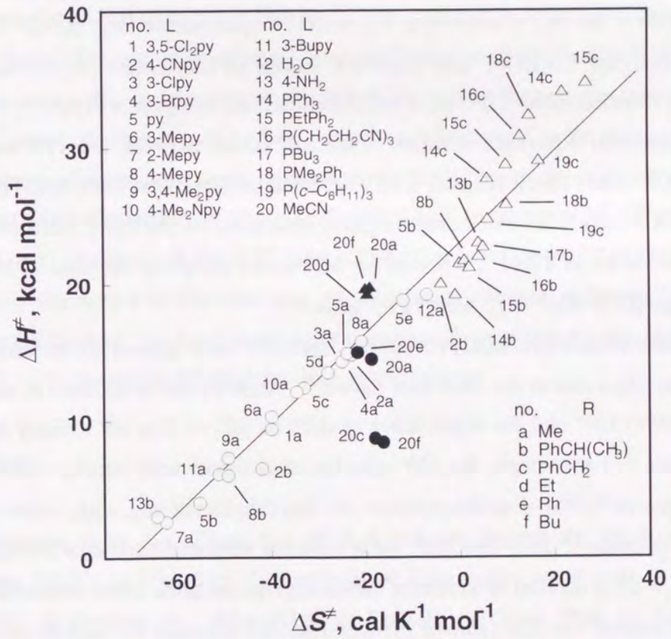

Figure 7. Plots of $\Delta H^{\neq}$ vs $\Delta S^{\neq}$ for homolytic Co(IV)–C bond cleavage of $[(DH)_2Co^{IV}(R)(L)]^+$ (○), $(DH)_2Co^{III}(R)(L)$ (Δ), $[(TPP)Co^{IV}(R)(L)]^+$ (●), and $(TPP)Co^{III}(R)(L)$ (▲).

and $\Delta S^{\neq}$ in Figure 7. There are large compensation effects between the $\Delta H^{\neq}$ and$\Delta S^{\neq}$ values for cleavage of Co(IV)–C bond in $[(DH)_2Co^{IV}(R)(L)]^+$ in Figure 7, where $\Delta H^{\neq}$ increases linearly with increasing $\Delta S^{\neq}$. Since the observed variation of $\Delta H^{\neq}$ is large enough to be determined accurately (see Figure 6), the compensation effects are genuine and reflect systematic dependence of structural features of the transition state for the Co(IV)–C bond cleavage. Such compensation effects between the $\Delta H^{\neq}$ and $\Delta S^{\neq}$ values are also observed for cleavage of Co(III)–C bond in $(DH)_2Co^{III}(R)(L)$, although both the $\Delta H^{\neq}$ and $\Delta S^{\neq}$ values are significantly larger than those for cleavage of Co(IV) bond.[12] Taken together, there is a unified linear correlation between the $\Delta H^{\neq}$ and $\Delta S^{\neq}$ values for cleavage of Co–C bond in a series of both $(DH)_2Co^{III}(R)(L)$ and $[(DH)_2Co^{IV}(R)(L)]^+$ in Figure 7, where the $\Delta S^{\neq}$ values vary significantly spanning a range of 100 entropy unit which covers from highly negative values to positive values. Such a unified linear correlation strongly indicates that the Co-C cleavage mechanism is the same irrespective of the oxidation state of Co and types of R and

In contrast to the case of coenzyme B_{12} model complexes, however, the $\Delta S^{\neq}$ values for cleavage of both the Co(III)–C and Co(IV)–C bonds of alkylcobalt porphyrins remain constant with variation in the $\Delta H^{\neq}$ values (closed circles and triangles in Figure 7). However, there is a significant difference in terms of the $\Delta S^{\neq}$ values between the TPP and $(DH)_2$ ligands: the $\Delta S^{\neq}$ values for cleavage of Co(IV)–C bond of $[(DH)_2Co^{IV}(PhCH(CH_3))(L)]^+$ (–51 ~ –68 cal K^{-1} mol^{-1}) are much more negative than those of Co(III)–C bond (4 ~ –4 cal K^{-1} mol^{-1}) as shown in Table 3, whereas the $\Delta S^{\neq}$ values are about the same (–20 cal K^{-1} mol^{-1}) between $[(TPP)Co^{IV}(R)]^+$ and (TPP)Co(R).[25]

In the case of alkylcobalt(III) porphyrins, the $\Delta H^{\neq}$ value generally increases with an increase in the pK_a value of the axial base ligand.[12] Such a trend is not seen in the case of $[(DH)_2Co^{IV}(Me)(L)]^+$ and the dependence of $\Delta H^{\neq}$ on pK_a of L is not entirely simple as shown in Figure 7. For example, the $\Delta H^{\neq}$ value becomes significantly smaller when pyridine (no. 5a) is replaced by 3,4–dimethylpyridine (no. 9a) despite the larger pK_a value (6.46) as compared to pyridine (5.28). The $\Delta H^{\neq}$ value with the strongest axial coordination by 4–Me_2Npy (pK_a = 9.71, no.10a) in which the substituent has no steric effect toward the $(DH)_2$ ligand is also smaller than the value of pyridine (no. 5a); compare 13b and 5b in Figure 7. Thus, the steric pressure of the substituent as well as the strong axial coordination of a strong base (L) forces the flexible $(DH)_2$ ligand to bend away from L and toward R may cause the significant conformational deflection,[4,15,16] resulting in a decrease in the $\Delta H^{\neq}$ value for the Co–C cleavage, which is accompanied by a decrease in the $\Delta S^{\neq}$ value. In contrast, the

porphyrin ligand is sufficiently rigid and thereby the geometrical freedom is not affected by the σ–bonded R or the axial base (L) coordination to maintain the $\Delta S^{\neq}$ values for cleavage of both the Co(III)–C and Co(IV)–C bonds rather constant.

Summary and Conclusions

The present results have made it possible for the first time to compare the $\Delta H^{\neq}$ and $\Delta S^{\neq}$ values for cleavage of both Co(III)–C and Co(IV)–C bonds in an extensive series of coenzyme B_{12} model complexes, $(DH)_2Co(R)(L)$, and the corresponding organocobalt porphyrins, (TPP)Co(R)(L). It has been shown that the $\Delta H^{\neq}$ values for the Co–C bond cleavage of coenzyme B_{12} model complexes can be easily decreased by formation of the higher oxidation state, Co(IV), the stronger donor ability of the σ–bonded R, the steric pressure of the substituent as well as the axial coordination of a strong base (L) complex, but that an decrease in the $\Delta H^{\neq}$ value is compensated by the concomitant decrease in the $\Delta S^{\neq}$ value (open circles and triangles in Figure 7). This indicates that the Co–C bond weakening in terms of enthalpy is readily achieved by the deformation of the flexible $(DH)_2$ ligand but that it is accompanied by a decrease in the probability to have the optimized conformation for the Co–C bond cleavage, resulting in a compensating decrease in the entropy term. Such compensation effects show sharp contrast to the Co–C bond cleavage for organocobalt porphyrins where the porphyrin ring is sufficiently rigid to maintain the $\Delta S^{\neq}$ value constant irrespective of the change in the $\Delta H^{\neq}$ value (closed circles and triangles in Figure 7). Thus, the protein–coenzyme interaction may play an important role in fixing the optimized conformation for the Co–C bond cleavage of coenzyme B_{12} and thereby preventing a decease in the $\Delta S^{\neq}$ value in order to enhance the Co–C bond cleavage.

References

(1) (a) Babior, B. M. *Acc. Chem. Res.* **1975**, *8*, 376. (b) Dolphin, D., Ed. *B_{12}*; Wiley: New York, 1982. (c) Schneider, Z.; Stroinski, A. *Comprehensive B_{12}*; de Gruyter, Berlin, 1987. (d) Toscano, P. J.; Marzilli, L. G. *Prog. Inorg. Chem.* **1984**, *31*, 105. (e) Finke, R. G.; Schiraldi, D. A.; Mayer, B. J. *Coord. Chem. Rev.* **1984**, *54*, 1. (f) Randaccio, L.; Pahor, N. B.; Zangrando, E. Marzilli, L. G. *Chem. Soc. Rev.* **1989**, *18*, 225. (g) Marzilli, L. G. In *Bioinorganic Catalysis*; Reedijk, J., Ed.; Marcel Dekker: New York, 1993; pp 227-259.

(2) (a) Halpern, J. *Science* **1985**, *227*, 869. (b) Halpern, J. *Acc. Chem. Res.* **1982**, *15*, 238.

(3) (a) Tsou, T. -T.; Loots, M.; Halpern, J. *J. Am. Chem. Soc.* **1982**, *104*, 623. (b) Ng, F. T. T.; Rempel, G. L.; Halpern, J. *J. Am. Chem. Soc.* **1982**, *104*, 621. (c) Ng, F. T. T.; Rempel, G. L.; Halpern, J. *Inorg. Chim. Acta* **1983**, *77*, L65. (d) Halpern, J.; Kim, S. -H.; Leung, T. W. *J. Am. Chem. Soc.* **1984**, *106*, 8317. (e) Geno, M. K.; Halpern, J. *J. Chem. Soc., Chem. Commun.* **1987**, 1052. (f) Ng, F. T. T.; Rempel, G. L.; Mancuso, C.; Halpern, J. *Organometallics* **1990**, *9*, 2762.

(4) Geno, M. K.; Halpern, J. *J. Am. Chem. Soc.* **1987**, *109*, 1238.

(5) Collman, J. P.; McElwee-White, L.; Brothers, P. J.; Rose, E. *J. Am. Chem. Soc.* **1986**, *108*, 1332.

(6) (a) Finke, R. G.; Hay, B. P. *Inorg. Chem.* **1984**, *23*, 3041. (b) Finke, R. G.; Hay, B. P. *Inorg. Chem.* **1985**, *24*, 1278. (c) Hay, B. P.; Finke, R. G. *J. Am. Chem. Soc.* **1986**, *108*, 4820. (d) Hay, B. P.; Finke, R. G. *J. Am. Chem. Soc.* **1987**, *109*, 8012. (e) Koenig, T. W.; Hay, B. P.; Finke, R. G. *Polyhedron.* **1988**, *7*, 1499.

(7) Waddington, M. D.; Finke, R. G. *J. Am. Chem. Soc.* **1993**, *115*, 4629.

(8) (a) Hollaway, M. R.; White, H. A.; Joblin, K. N.; Johnson, A. W.; Lappert, M. F.; Wallis, O. C. *Eur. J. Biochem.* **1978**, *82*, 143. (b) Toscano, P. J.; Seligson, A. L.; Curran, M. T.; Skrobutt, A. T.; Sonnenberger, D. C. *Inorg. Chem.* **1989**, *28*, 166.

(9) (a) Licht, S. S.; Gerfen, G. J.; Stubbe, J. *Science* **1996**, *271*, 477. (b) Padmakumar, R.; Padmakumar, R.; Banerjee, R. *Biochemistry* **1997**, *36*, 3713.

(10) Brown, K. L.; Li, J. *J. Am. Chem. Soc.* **1998**, *120*, 9466.

(11) Licht, S. S.; Lawrence, C. C.; Stubbe, J. *Biochemistry* **1999**, *38*, 1234.

(12) Halpern, J. *Bull. Chem. Soc. Jpn.* **1988**, *61*, 13.

(13) (a) Kräutler, B, Keller, W.; Kratky, C. *J. Am. Chem. Soc.* **1989**, *111*, 8936. (b) Kräutler, B.; Konrat, R.; Stupperich, E.; Färber, G.; Gruber, K.; Kratky, C. *Inorg. Chem.* **1994**, *33*, 4128. (c) Garr, C. D.; Finke, R. G. *Inorg. Chem.* **1993**, *32*, 4414.

(14) Pratt, J. M. *Chem. Soc. Rev.* **1985**, *14*, 161.

(15) Banerjee, R. *Chem. Biol.* **1997**, *4*, 175.

(16) (a) Hill, H. A. O.; Pratt, J. M.; Wiliams, R. J. P. *Chem. Br.* **1969**, *5*, 156. (b) Grate, J. H.; Schrauzer, G. N. *J. Am. Chem. Soc.* **1979**, *101*, 4601.

(17) (a) Nie, S.; Marzilli, L. G.; Yu, N.-T. *J. Am. Chem. Soc.* **1989**, *111*, 9256. (b) Nie, S.; Marzilli, P. A.; Marzilli, L. G.; Yu, N.-T. *J. Am. Chem. Soc.* **1990**, *112*, 6084.

(18) (a) Garr, C. D.; Sirovatka, J. M.; Finke, R. G. *Inorg. Chem.* **1996**, *35*, 5912. (b) Garr, C. D.; Sirovatka, J. M.; Finke, R. G. *J. Am. Chem. Soc.* **1996**, *118*, 11142. (c) Sirovatka, J. M.; Finke, R. G. *J. Am. Chem. Soc.* **1997**, *119*, 3057. (d) Sirovatka, J. M.; Finke, R. G. *Inorg. Chem.* **1999**, *38*, 1697.

(19) Mancia, F.; Keep, N. H.; Nakagawa, A.; Leadlay, P. F.; McSweeney, S.; Rasmussen, B.; Bösecke, P.; Diat, O.; Evans, P. R. *Structure* **1996**, *4*, 339.

(20) Jensen, M. P.; Halpern, J. *J. Am. Chem. Soc.* **1999**, *121*, 2181.

(21) (a) Martin B. D.; Finke, R. G. *J. Am. Chem. Soc.* **1990**, *112*, 2419. (b) Martin B. D.; Finke, R. G. *J. Am. Chem. Soc.* **1992**, *114*, 585. (c) Finke, R. G.; Martin, B. D. *J. Inorg. Biochem.* **1990**, *40*, 19.

(22) Lexa, D.; Savéant, J.-M. *J. Am. Chem. Soc.* **1978**, *100*, 3220. (b) Lexa, D.; Savéant, J.-M. *Acc. Chem. Res.* **1983**, *16*, 235.

(23) Halpern, J.; Chan, M. S.; Hanson, J.; Roche, T. S.; Topich, J. A. *J. Am. Chem. Soc.* **1975**, *97*, 1606.

(24) Vol'pin, M. E.; Levitin, I. Y.; Sigan, A. L.; Halpern, J.; Tom, G. M. *Inorg. Chim. Acta.* **1980**, *41*, 271.

(25) Fukuzumi, S.; Miyamoto, K.; Suenobu, T.; Van Caemelbecke, E.; Kadish, K. M. *J. Am. Chem. Soc.* **1998**, *120*, 2880.

(26) (a) Ishikawa, K.; Fukuzumi, S.; Goto, T.; Tanaka, T. *J. Am. Chem. Soc.* **1990**, 112, 1577. (b) Fukuzumi, S.; Ishikawa, K.; Tanaka, T. *Organometallics* **1987**, *6*, 358. (c) Ishikawa, K.; Fukuzumi, S.; Tanaka, T. *Bull. Chem. Soc. Jpn.* **1987**, *60*, 563. (d) Fukuzumi, S.; Kitano, T.; Ishikawa, M.; Matsuda, Y. *Chem. Phys.* **1993**, *176*, 337.

(27) (a) Collman, J. P.; Hegedus, L. S.; Norton, J. R.; Finke, R. G. *Principles and Applications of Organotransition Metal Chemistry*; University Science Books: Mill Valley, CA, 1987. (b) Guilard, R.; Kadish, K. M. *Chem. Rev.* **1988**, *88*, 1121.

(28) Fukuzumi, S.; Nakanishi, I.; Tanaka, K.; Suenobu, T.; Tabard, A.; Guilard, R.; Van Caemelbecke, E.; Kadish, K. M. *J. Am. Chem. Soc.* **1999**, *121*, 785.

(29) Fukuzumi, S.; Nakanishi, I.; Tanaka, K.; Tabard, A.; Guilard, R.; Van Caemelbecke, E.; Kadish, K. M. *Inorg. Chem.* **1999**, *38*, 5000.

(30) Schrauzer, G. N. *Inorganic Synthesis* **1968**, *11*, 61.

(31) Ishikawa, K.; Fukuzumi, S.; Tanaka, T. *Inorg. Chem.* **1989**, *28*, 1661.

(32) Tada, M.; Nakamura, T.; Matsumoto, M. *J. Am. Chem. Soc.* **1988**, *110*, 4647.

(33) Ishikawa, K.; Fukuzumi, S.; Goto, T.; Tanaka, T. *J. Chem. Soc., Dalton Trans.* **1990**, 85.

(34) (a) Wong, C. L.; Kochi, J. K. *J. Am. Chem. Soc.* **1979**, *101*, 5593. (b) Fukuzumi, S.; Wong, C. L.; Kochi, J. K. *J. Am. Chem. Soc.* **1980**, *102*, 2928.

(35) DeSimone, R. E.; Drago, R. S. *J. Am. Chem. Soc.* **1970**, *92*, 2343.

(36) Perrin, D. D.; Armarego, W. L. F. *Purification of Laboratory Chemicals*; Butterworth-Heinemann: Oxford, 1988.

(37) Ford-Smith, M. H.; Sutin, N. *J. Am. Chem. Soc.* **1961**, *83,* 1830.

(38) Mann, C. K.; Barnes, K. K. *Electrochemical Reactions in Nonaqueous Systems*; Marcel Dekker: New York, 1990.

(39) Shoefield, K. S. *Hetero-Aromatic Nitrogen Compounds*; Plenum Press: New York, 1967; p 146.

(40) Halpern, J.; Topich, J.; Zamaraev, K. I. *Inorg. Chim. Acta.* **1976**, *20*, L21.

(41) Topich, J., Halpern, J. *Inorg. Chem.* **1979**, *18*, 1339.

(42) For stable Co(IV) complexes, see: (a) Anson, F. C.; Collins, T. J.; Coots, R. J.; Gipson, S. L.; Richmond, T. G. *J. Am. Chem. Soc.* **1984**, *106*, 5037. (b) Collins, T. J.; Powell, R. D.; Slebodnick, C.; Uffelman, E. S. *J. Am. Chem. Soc.* **1991**, *113*, 8419. (c) Will, S.; Lex, J.; Vogel, E.; Adamian, V. A.; Van Caemelbecke, E.; Kadish, K. M. *Inorg. Chem.* **1996**, *35*, 5577.

(43) Since the $A_{\perp(Co)}$ value of $[(DH)_2Co(Me)(py)]^+$ is about 5 G and $A_{//(Co)}$ = 26 G, the isotropic value (A_{Co}) is obtained using the relation, $A_{Co} = (2A_{\perp(Co)} + A_{//(Co)})/3$, as 12 G which is approximately the same as the value of $[(TPP)Co(Me)(Py)]^+$.

(44) (a) Ohya-Nishiguchi, H.; Khono, M.; Yamamoto, K. *Bull. Chem. Soc. Jpn.* **1981**, *54*, 1923. (b) Ichimori, K.; Ohya-Nishiguchi, H.; Hirota, N.; Yamamoto, K. *Bull. Chem. Soc. Jpn.* **1985**, *58*, 623.

(45) Vol'pin, M. E.; Levitin, I. Y.; Sigan, A. L.; Nikitaev, A. T. *J. Organomet. Chem.* **1985**, *279*, 263.

(46) (a) Wayner, D. D. M.; McPhee, D. J.; Griller, D. *J. Am. Chem. Soc.* **1988**, *110,* 132. (b) Sim, B. A.; Milne, P. H.; Griller, D.; Wayner, D. D. M. *J. Am. Chem. Soc.* **1990**, *112*, 6635.

(47) Howard, J. A. *Adv. Free-Radical Chem.* **1972**, *4*, 49.

(48) (a) Fujita, M.; Ishida, A.; Takamuku, S.; Fukuzumi, S. *J. Am. Chem. Soc.* **1996**, *118*, 8566. (b) Fujita, M.; Fukuzumi, S. *J. Mol. Catal.* **1994**, *90*, L225.

(49) Reisenhofer, E.; Costa, G. *Inorg. Chim. Acta* **1981**, *49*, 121.

(50) Tamblyn, W. H.; Klingler, R. J.; Hwang, W. S.; Kocih, J. K. *J. Am. Chem. Soc.* **1981**, *112*, 3161.

(51) (a) Bresciani-Pahor, N.; Randaccio, L.; Zangrando, E.; Antolini, L. *Acta Crystallogr., Sect. C. (Cr. Str. Commun.)* **1988**, *44*, 2052. (b) Bigotto, A.; Zangrando, E.; Randaccio, L. *J. Chem. Soc., Dalton Trans.* **1976**, 96.

(52) (a) Koenig, T. W.; Finke, R. G. *J. Am. Chem. Soc.* **1988**, *110*, 2657. (b) Garr, C. D.; Finke, R. G. *J. Am. Chem. Soc.* **1992**, *114*, 10440.

Section 3. 2

Photoalkylation of C_{60} by Alkylcobalt(III) Complexes

Abstract: Photolysis of a benzonitrile solution of alkylcobalt(III) complexes, $[RCo(DH)_2py]$ (R = Me and $PhCH_2$, $(DH)_2$ = bis(dimethylglyoximato), py = pyridine) in the presence of C_{60} by using visible light results in alkylation of C_{60} to yield R_2C_{60}. The excited state of $[RCo(DH)_2py]$ rather than C_{60} is responsible for the photoalkylation of C_{60}, since the action spectrum for formation of R_2C_{60} agrees with the absorption spectrum of $[RCo(DH)_2py]$ which is quite different from that of C_{60}. The photoalkylation of C_{60} is retarded by a radical trapping reagent such as 2,2,6,6-tetramethyl-1-piperidinyloxyl radical (TEMPO). This indicates that photoalkylation of C_{60} proceeds via photocleavage of cobalt–carbon bond of $[RCo(DH)_2py]$. The intermediate benzyl radical produced by the photocleavage reaction of $[PhCH_2Co(DH)_2py]$ is detected by ESR.

Introduction

Buckminsterfullerene (C_{60}) and the homologs are known to act as an electrophile and thus it functionalization by the reaction with various nucleophiles has been studied extensively.[1,2] Since C_{60} is relatively weak electrophile, strong alkylating reagents such as alkyllithium have so far been employed for alkylation of C_{60}.[3,4] The use of the photo-excited state of C_{60} has further expanded the scope of the reactions with nucleophiles.[5-7] We have recently reported that the photoinduced electron transfer process from various alkylating reagents to $^3C_{60}^*$ leads to alkylation of C_{60}.[8-10] Alternatively the photo-excited states of alkylmetals may be utilized for alkylation of C_{60} via photocleavage of metal–carbon bond. Photocleavage of metal–carbon bonds of transition-metal alkyls which are stable thermally has merited special attention,[11,12] and such reactions of alkylcobalt(III) complexes have been subjected to detailed scrutiny in relation to the enzymatic function of coenzyme B_{12}.[13,14]

In this study we report that the photocleavage of cobalt–carbon bonds of alkylcobalt(III) complexes, $[RCo(DH)_2py]$ (R = Me and $PhCH_2$, $(DH)_2$ = bis(dimethylglyoximato), py = pyridine) in the presence of C_{60} results in formation of R_2C_{60}. The reaction mechanism is discussed based on detection of the reactive intermediate by ESR as well as the effect of a radical trapping reagent on the photoalkylation of C_{60} by

$[RCo(DH)_2py]$.

Experimental Section

Materials. Alkylcobalt(III) complexes, $[RCo(DH)_2py]$ (R = Me and $PhCH_2$) were prepared by following the literature method.[15] C_{60} (>99.95 % pure) was purchased from Science Laboratories Co., Ltd., Japan, and used as received. C_{60} of 99.99% purity was obtained from Texas Fullerenes Corp. and used for the spectral measurements. Benzonitrile (PhCN; 99.9 %) was purchased from Aldrich, and purified by successive distillation over P_2O_5 prior to use. A radical trapping reagent, 2,2,6,6-tetramethyl-1-piperidinyloxyl radical (TEMPO), was purchased from Wako Pure Chemical Ind. Ltd., Japan. Tetra-*n*-butylammonium perchlorate (TBAP) was purchased from Sigma Chemical Co., recrystallized from ethanol, and dried under vacuum at 40 °C prior to use.

Reaction Procedure. Typically, to a solution of C_{60} (10.1 mg, 0.014 mmol) in deaerated PhCN (50 mL) under an atmospheric pressure of argon was added $[MeCo(DH)_2py]$ (5.4 mg, 0.014 mmol), and the solution was irradiated with a Xe lamp equipped with a UV-cut filter (λ < 300 nm) for 3 h. After evaporation under reduced pressure, the residue was separated by washing it with acetonitrile and centrifuged to give 1,2-Me_2C_{60}. ^1H NMR spectra were measured on a JEOL GSX-400 (400 MHz) spectrometer. Chemical shifts of ^1H NMR were expressed in parts per million downfield from tetramethylsilane as an internal standard (δ = 0). ^1H NMR (400 MHz, $CS_2/CDCl_3$, 4:1 v/v) δ 3.02 (s, 6H). The UV–visible spectral change associated with the photochemical reaction were monitored with the use of a Hewlett Packard 8453 diode array spectrophotometer. UV-Vis (λ_{max}, PhCN) 435, 710 nm.

The irradiation wavelength dependence of the photochemical reaction rates were determined by irradiating monochromatized light from a Shimadzu RF-5000 fluorescence spectrophotometer.

ESR Measurements. ESR spectra of a photolyzed PhCN solution of C_{60} and $[PhCH_2Co(DH)_2py]$ were taken on a JEOL JES-RE1XE and were recorded under nonsaturating microwave power conditions. The magnitude of the modulation was chosen to optimize the resolution and the signal to noise ratio (S/N) of the observed spectra. The *g* values were calibrated using a Mn^{2+} marker.

Cyclic Voltammetry. Redox potentials in MeCN containing 0.1 M TBAP as

supporting electrolyte were determined at room temperature by cyclic voltammetry under deaerated conditions using a three electrode system and a BAS 100B electrochemical analyzer. The working and counter electrodes were platinum while $Ag/AgNO_3$ (0.01 M) was used as the reference electrode. All potentials are reported as V vs SCE. The $E_{1/2}$ value of ferrocene used as a standard is approximately 0.37 V vs SCE in MeCN under our solution conditions.

Results and Discussion

Irradiation of a PhCN solution containing $[MeCo(DH)_2py]$ and C_{60} with visible light results in formation of 1,2-Me_2C_{60} (eq 1). No reaction occurs in the dark. Figure 1 shows the visible-near IR spectral change observed in the photochemical reaction where the appearance of new absorption bands at 435 nm and 710 nm are diagnostic for 1,2-alkyl adducts of C_{60}.[8,16] The ^1H NMR signal at δ 3.02 (s, 6H) of 1,2-Me_2C_{60} (in $CS_2/CDCl_3$, 4:1 v/v) agrees with that reported previously.[17]

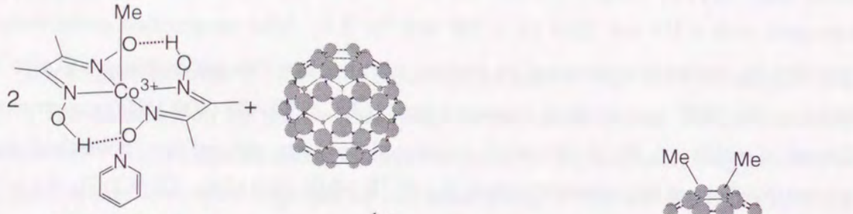

$$[MeCo(DH)_2py] \xrightarrow[PhCN]{h\nu} 2\,[Co(DH)_2py] + \text{1,2-}Me_2C_{60} \quad (1)$$

When $[MeCo(DH)_2py]$ is replaced by $[PhCH_2Co(DH)_2py]$, the regioselectivity of the C_{60} adduct is changed from the 1,2-isomer to the 1,4-isomer (eq 2). The new absorption band at 450 nm in Figure 2, which is diagnostic for 1,4-alkyl adducts of

$$2\,[(PhCH_2)Co(DH)_2py] + C_{60} \xrightarrow[PhCN]{h\nu} 2\,[Co(DH)_2py] + 1,4\text{–}(PhCH_2)_2C_{60} \quad (2)$$

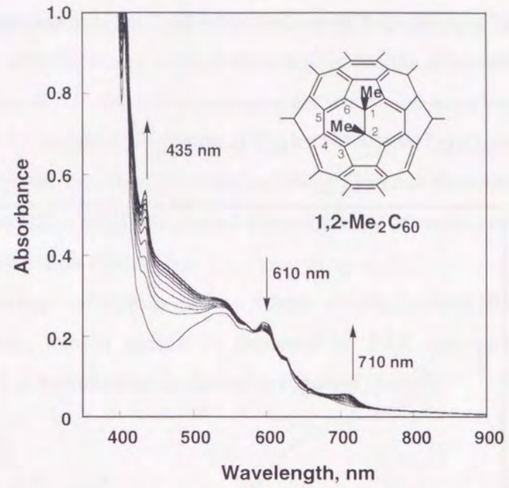

Figure 1. Electronic absorption spectra observed in the photoalkylation of C_{60} (2.8 x 10^{-4} M) with $[MeCo(DH)_2py]$ (1.0 x 10^{-3} M) in deaerated PhCN at 298 K.

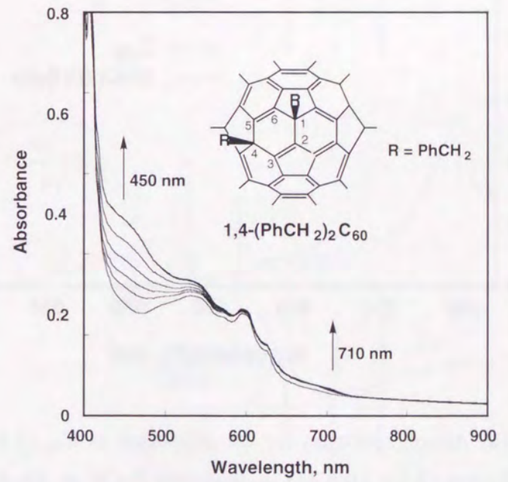

Figure 2. Electronic absorption spectra observed in the photoalkylation of C_{60} (2.8 x 10^{-4} M) with $[PhCH_2Co(DH)_2py]$ (2.4 x 10^{-4} M) in deaerated PhCN at 298 K.

C_{60},[18,19] agrees with that of 1,4-$(PhCH_2)_2C_{60}$ shown by X-ray crystallography to exist as the 1,4-isomer.[20] The preference of formation of 1,4-isomer is ascribed to the steric effect of two benzyl groups.[20]

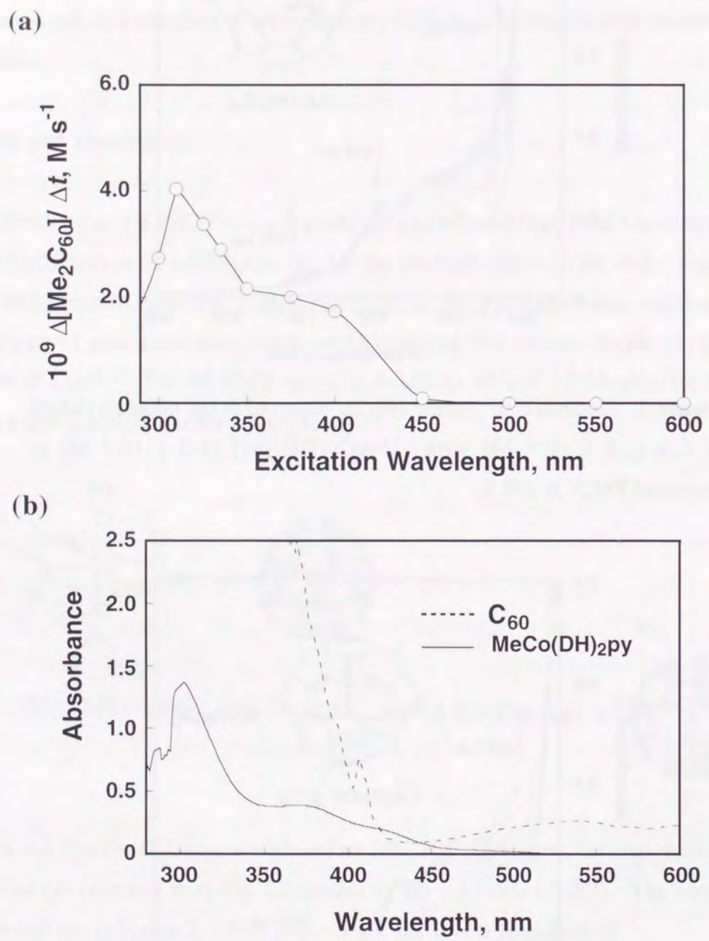

Figure 3. (a) Action spectrum for the alkylation of C_{60} (2.8×10^{-4} M) by $[MeCo(DH)_2py]$ (3.5×10^{-4} M) in deaerated PhCN at 298 K. (b) UV-Vis spectra of $[MeCo(DH)_2py]$ (1.8×10^{-4} M) and C_{60} (2.8×10^{-4} M) in PhCN at 298 K.

Reaction Mechanism. Visible light irradiation of a benzonitrile solution of $[MeCo(DH)_2py]$ and C_{60} results in photoexcitation of both $[MeCo(DH)_2py]$ and C_{60}. In order to determine which excited state is responsible for the photoalkylation of C_{60}, the photochemical rates were determined by changing the irradiation wavelength. Figure 3 shows the action spectrum for the photoalkylation of C_{60} by $[MeCo(DH)_2py]$, which agrees with the shape of the absorption spectrum of $[MeCo(DH)_2py]$ rather than that of C_{60} (compare Figure 3a and Figure 3b). Thus, the photoalkylation may proceed via the excited state of $[MeCo(DH)_2py]$ rather than that of C_{60}.

The photocleavage of cobalt–carbon bonds of alkylcobalt(III) complex are well established. In fact, benzyl radical is detected by ESR during photoirradiation of $[PhCH_2Co(DH)_2py]$ in benzonitrile as shown in Figure 4 (part a).

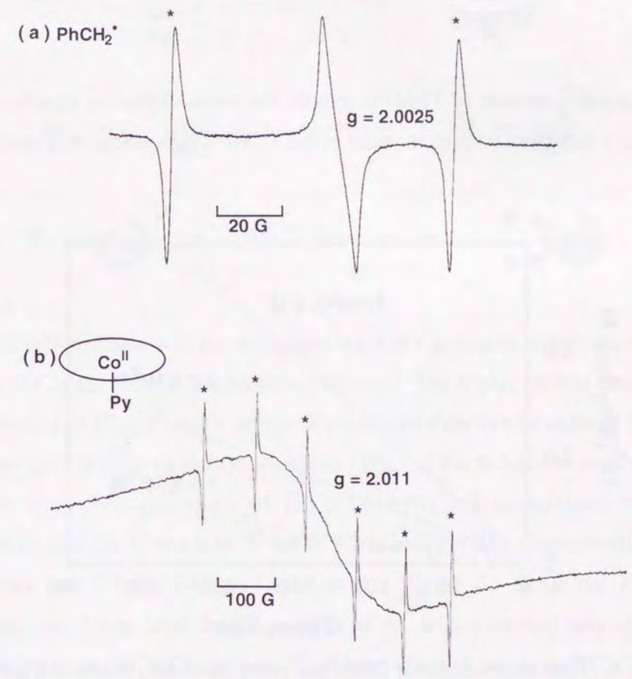

Figure 4. ESR spectra of (a) benzyl radical and (b) $[Co(DH)_2py]$ produced by photoirradiation of $[PhCH_2Co(DH)_2py]$ in propionitrile at 193 K. The astersk denotes an Mn^{2+} ESR marker.

The g value (2.0025) agrees with that of benzyl radical,[21] although the hyperfine structure is not resolved because of the large modulation required to detect the unstable radical species. The Co(II) complexes produced by the homolytic cleavage of the cobalt–carbon bond of $[PhCH_2Co(DH)_2py]$ is also detected by ESR as shown in Figure 4 (part b).[22]

In the case of $[MeCo(DH)_2py]$, methyl radical produced by the photocleavage of cobalt–carbon bond is too unstable to be detected by ESR. However, a radical trapping reagent such as TEMPO can trap methyl radical produced by the photocleavage of cobalt–carbon bond of $[MeCo(DH)_2py]$ as shown in eq 3. Figure 5 shows the effect of TEMPO on the photoalkylation of C_{60} by $[MeCo(DH)_2py]$.

$$[MeCo(DH)_2py] + \underset{\text{TEMPO}}{\overset{\bullet}{O}\!-\!N} \xrightarrow[PhCN]{h\nu} [Co(DH)_2py] + \underset{}{OMe\!-\!N} \qquad (3)$$

Addition of a small amount of TEMPO retards the photoalkylation significantly and the retarding effect is increased with an increase in the TEMPO concentration (Figure 5).

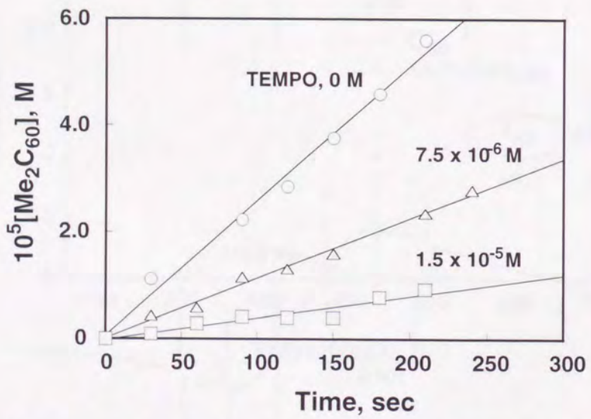

Figure 5. Time dependence of $[Me_2C_{60}]$ in the photoalkylation of C_{60} (1.0 x 10^{-4} M) with $[MeCo(DH)_2py]$ (1.2 x 10^{-4} M) in the absence and presence of different concentrations of TEMPO in deaerated PhCN at 298 K.

This indicates that photocleavage of cobalt–carbon bond to produce alkyl radical is essential for the photoalkylation of C_{60} to occur.

Based on the above results, the mechanism of photoalkylation of C_{60} by $[RCo(DH)_2py]$ (R = Me and $PhCH_2$) may be given by Scheme 1. Irradiation of the absorption band of $[RCo(DH)_2py]$ results in cleavage of the cobalt–carbon bond to produce alkyl radical. The alkyl radical is known to add to C_{60} to give $RC_{60}^{\bullet}$ which can be detected by ESR.[23,24] The radical coupling between $RC_{60}^{\bullet}$ and $R^{\bullet}$ yields the final product, R_2C_{60}, the isomer distribution of which is determined by the steric interaction between two R groups.

Scheme 1

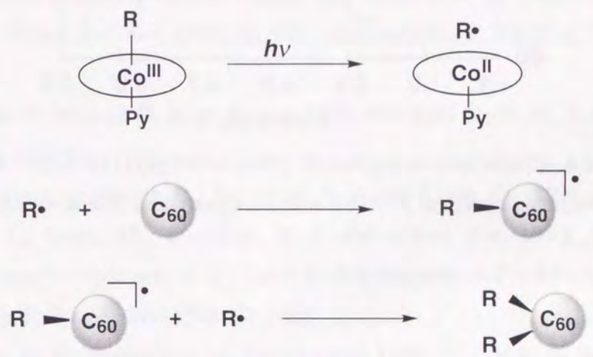

Alternatively irradiation of the absorption band of C_{60} results in formation of the triplet excited state of C_{60} via the fast intersystem crossing.[5] The triplet excited state of C_{60} has a reduction potential of E^0_{red} = 1.14 V versus SCE and can therefore be reduced by a variety of reductants provided that the oxidation potentials (E^0_{ox}) of the reductants are lower than 1.14 V.[5,8,9] The oxidation potentials of $[RCo(DH)_2py]$ are determined by the cyclic voltammograms as 0.85 V and 0.86 V for R = Me and $PhCH_2$, respectively. The cyclic voltammogram of $[MeCo(DH)_2py]$ is shown in Figure 6. Since the E^0_{ox} valuesof $[RCo(DH)_2py]$ are lower than the E^0_{red} value of the triplet excited sate of C_{60} ($^3C_{60}^*$), electron transfer from $[RCo(DH)_2py]$ to $^3C_{60}^*$ may occur to produce $[RCo(DH)_2py]^+$ and $C_{60}^{\bullet-}$ as shown in Scheme 2. The cobalt–carbon bond of $[RCo(DH)_2py]^+$ is known to be cleaved to produce $R^{\bullet}$,[25] which may lead to the alkyl adduct of C_{60}. However, the lifetime

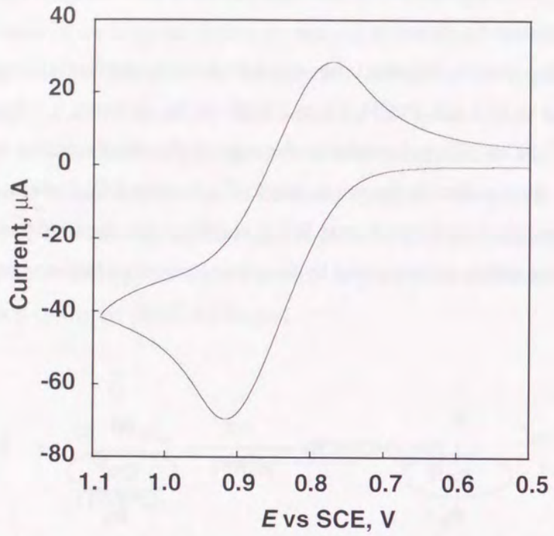

Figure 6. Cyclic voltammogram of [MeCo(DH)$_2$py] (1.0 x 10^{-2} M) in MeCN containing TBAP (0.10 M) with Au electrode at 298 K; sweep rate 0.1 V s^{-1}.

Scheme 2

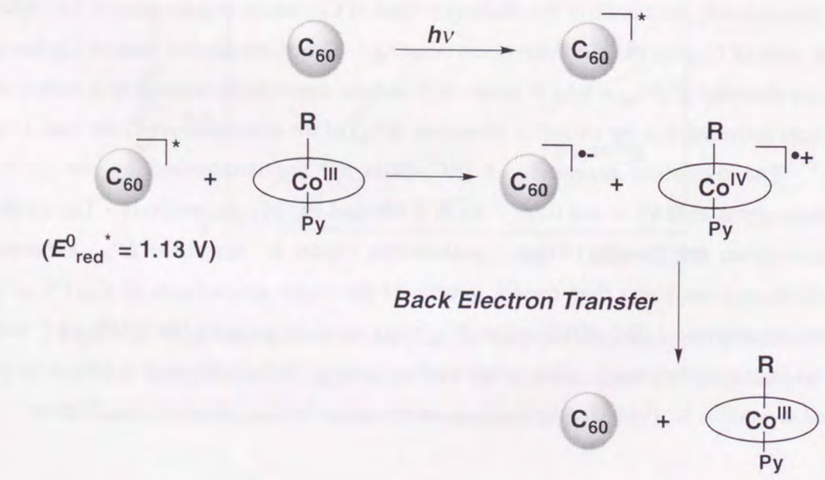

of [RCo(DH)$_2$py]$^+$ is long enough so that the CV wave is reversible even at a low scan rate (0.1 V s^{-1}) as shown in Figure 6. In such a case, cleavage of the cobalt–carbon bond of [RCo(DH)$_2$py]$^+$ is too slow to compete with the
fast back electron transfer from $C_{60}^{\bullet-}$ to [RCo(DH)$_2$py]$^+$, resulting in no net reaction as shown in Scheme 2. This may be the reason why only the excited sate of [RCo(DH)$_2$py] is responsible for the photoalkylation of C_{60} by [RCo(DH)$_2$py].

References and Notes

(1) (a) Hirsh, A. *Angew. Chem. Int. Ed. Engl.* **1993**, *32*, 1138. (b) Hirsh, A. T*he Chemistry of the Fullerenes*, Georg Thieme Verlag: New York, 1994. (c) Diederich, F.; Issacs, L.; Philp, D. *Chem. Soc. Rev.* **1994**, *23*, 243. (d) Diederich, F.; Thilgen, C. *Science* **1996**, *271*, 317.

(2) (a) Taylor R.; Walton, D. R. M. *Nature* **1993**, *363*, 685. (b) Wudl, F. *Acc. Chem. Res.* **1992**, *25*, 157.

(3) (a) Sawamura, M.; Iikura, H.; Nakamura, E. *J. Am. Chem. Soc.* **1996**, *118*, 12850. (b) Murata Y.; Shiro, M.; Komatsu, K. *J. Am. Chem. Soc.* **1997**, *119*, 8117. (c) Timmerman, P.; Anderson, H. L.; Faust, R.; Nierengarten, J.-F.; Habicher, T.; Seiler, P.; Diederich, F. *Tetrahedron* **1996**, *52*, 4925.

(4) (a) Meier M. S.; Poplawska, M. *Tetrahedron* **1996**, *52*, 5043. de la Cruz,, P.; de la Hoz, A.; Langa, F.; Illescas, B.; Martin, N. *Tetrahedron* **1997**, *53*, 2599 . (b) Zhang X.; Foote, C. S. *J. Am. Chem. Soc.* **1995**, *117*, 4271.

(5) (a) Arbogast, J. W.; Foote, C. S.; Kao, M. *J. Am. Chem. Soc.* **1992**, *114*, 2277. (b) Foote, C. S. *Top. Curr. Chem.* **1994**, *169*, 347.

(6) (a) Williams, R. M.; Zwier, J. M.; Verhoeven, J. W. *J. Am. Chem. Soc.* **1995**, *117*, 4093. (b) Guldi, D. M.; Maggini, M.; Scorrano, G.; Prato, M. *J. Am. Chem. Soc.* **1997**, *119*, 974.

(7) (a) Lem, G.; Schuster, D. I.; Courtney, S. H.; Lu, Q.; Wilson, S. R. *J. Am. Chem. Soc.* **1995**, *117*, 554. (b) Siedschlag, C.; Luftmann, H.; Wolff, C.; Mattay, J. *Tetrahedron* **1997**, *53*, 3587. (c) Wilson, S. R.; Kaprinidis, N.; Wu, Y.; Schuster, D. I. *J. Am. Chem. Soc.* **1993**, *115*, 8495. (d) Akasaka, T.; Ando, W.; Kobayashi, K.; Nagase, S. *J. Am. Chem. Soc.* **1993**, *115*, 10366. (e) Akasaka, T.; Mitsuhida, E.; Ando, W.; Kobayashi, K.; Nagase, S. *J. Am. Chem. Soc.* **1994**, *116*, 2627. (f) Averdung J.; Mattay, J.

Tetrahedron **1996**, *52*, 5407. (g) Kusukawa, T.; Shike, A.; Ando, W. *Tetrahedron* **1996**, *52*, 4995. (h) Schuster, D. I. Cao, J.; Kaprinidis, N.; Wu, Y.; Jensen, A. W.; Lu, Q.; Wang, H.; Wilson, S. R. *J. Am. Chem. Soc.* **1996**, *118*, 5639. (i) Liou K.-F.; Cheng, C.-H. *Chem. Commun.* **1996**, 1423.

(8) (a) Mikami, K.; Matsumoto, S.; Ishida, A.; Takamuku, S.; Suenobu, T.; Fukuzumi, S. *J. Am. Chem. Soc.* **1995**, *117*, 11134. (b) Mikami, K.; Matsumoto, S.; Tonoi, T.; Suenobu, T.; Ishida, A.; Fukuzumi, S. *Synlett*, **1997**, 85.

(9) Fukuzumi, S.; Suenobu, T.; Patz, M.; Hirasaka, T.; Itoh, S.; Fujitsuka, M.; Ito, O. *J. Am. Chem. Soc.* **1998**, *120*, 8060.

(10) Fukuzumi, S.; Suenobu, Fujitsuka, M.; Ito, O.; Tonoi, T.; Matsumoto, S.; Mikami, K. *J. Organomet. Chem.* **1999**, *574*, 32 .

(11) Geoffroy, G. L.; Wrighton, M. S. *Organometallic Photochemistry*; Academic Press, New York, 1979.

(12) Fukuzumi, S.; Ishikawa, K.; Tanaka, T. *Organometallics* **1987**, *6*, 358.

(13) (a) Chagivertz A. M.; Grissom, C. B. *J. Am. Chem. Soc.* **1993**, *115*, 12152. (b) Grissom, C. B. *Chem. Rev.* **1995**, *95*, 3.

(14) Endicott J. F.; Netzel, T. L. *J. Am. Chem. Soc.* **1979**. *101*, 4000.

(15) Schrauzer, G. N. *Inorg. Synth.* **1968**, *11*, 61.

(16) (a) Creegan, K. M.; Robbins, J. L.; Robbings, W. K.; Millar, J. M.; Sherwood, R. D.; Tindall, P. J.; Cox, D. M.; Smith A. B. III; MaCauley, J. P. Jr.; Jones, D. R.; Gallagher, R. T. *J. Am. Chem. Soc.* **1992**, *114*, 1103. (b) Smith, A. B. III; Strongin, R. M.; Brard, L.; Furst, G. T.; Romanow, W. J.; Owens, K. G.; King, R. C. *J. Am. Chem. Soc.* **1993**, *115*, 5829.

(17) Caron, C.; Subramanian, R.; D'Souza, F.; Kim, J.; Kutner, W.; Jones, M. T.; Kadish, K. M. *J. Am. Chem. Soc.* **1993**, *115*, 8505.

(18) (a) Murata, Y.; Komatsu, K.; Wan, T. S. M.; *Tetrahedron Lett.* **1996**, *37*, 7061. (b) Miki, S.; Kitao, M.; Fukunishi, K. *Tetrahedron Lett.* **1996**, *37*, 2049. (c) Gonzalez, R.; Wudl, F.; Pole, D. L.; Sharma, P. K.; J. Warkentin, *J. Org. Chem.* **1996**, *61*, 5837.

(19) Fukuzumi, S.; Suenobu, T.; Hirasaka, T.; Arakawa, R.; Kadish, K. M. *J. Am. Chem. Soc.* **1998**, *120*, 9220.

(20) Subramanian, R.; Kadish, K. M.; Vijayashree, M. N.; Gao, X.; Jones, M. T.; Miller, M. D.; Krause, K. L.; Suenobu, T.; Fukuzumi, S. *J. Phys. Chem.* **1996**, *100*, 16327.

(21) (a) Dixon W. T.; Norman, R. O. C. *J. Chem. Soc.* **1964**, 4857. (b) Carrington, A.; Smith, I. C. P. *Mol. Phys.* **1965**, *9*, 137.

(22) Nishida Y.; Shimohori, H. *Bull. Chem. Soc. Jpn.* **1973**, *46*, 2406.

(23) Morton, J. R.; Negri, F.; Preston, K. F. *Acc. Chem. Res.* **1998**, *31*, 63.

(24) Fukuzumi, S.; Nakanishi, I.; Suenobu, T.; Kadish, K. M. *J. Am. Chem. Soc.* **1999**, *121*, 3468.

(25) Halpern, J.; Chan, M. S.; Hanson, J.; Roche, T. S.; Topich, J. A. *J. Am. Chem. Soc.* **1975**, *97*, 1606.

Chapter 3. 3

Regioreversed Thermal and Photochemical Reduction of 10-Methylacridinium and 1-Methylquinolinium Ions by Organosilanes and Oraganostannanes

Abstract: Irradiation of the absorption band of 10-methylacridinium ion ($AcrH^+$) in acetonitrile containing allylic silanes and stannanes results in the efficient and selective reduction of 10-methylacridinium ion to yield the allylated dihydroacridines. In the photochemical reactions of $AcrH^+$ with unsymmetric allylsilanes, the allylic groups are introduced selectively at α-position. Likewise the reactions with unsymmetric allylstannanes afforded the α-adducts predominantly, but the γ–adducts were also obtained as minor products. In contrast to this, the thermal reduction of $AcrH^+$ and 1-methylquinolinium ion (QuH^+) by unsymmetric allylstannanes gave only the γ–adducts. Thermal reduction of QuH^+ by tributyltin hydride or hydrosilanes in the presence of fluoride anion also occurs to yield 1-methyl-1,2-dihydroquinoline selectively. On the other hand, the photoreduction of QuH^+ derivatives by tributyltin hydride and tris(trimethylsilyl)silane yields the corresponding 1,4-dihydroquinolines exclusively. The difference in the mechanisms for the regioreversed thermal and photochemical reduction of $AcrH^+$ and QuH^+ is discussed in terms of nucleophilic vs electron transfer pathways. The photochemical reactions proceed via photoinduced electron transfer from organosilanes and organostannanes to the singlet excited states of $AcrH^+$ and QuH^+, followed by the radical coupling of the resulting radical pair in competition with the back electron transfer to the ground state. The rate constants of photoinduced electron transfer obtained from the fluorescence quenching of $AcrH^+$ and QuH^+ by organosilane and organostannane donors agree with those obtained from the dependence of the quantum yields on the donor concentrations for the photochemical reactions. The electron transfer rate constants are well analyzed in light of the Marcus theory of adiabatic outer-sphere electron transfer, leading to the evaluation of the reorganization energy ($\lambda = 0.90$ eV) of the electron transfer reactions. The transient spectra of the radical pair produced by the photoinduced electron transfer from organosilanes to the singlet excited state of $AcrH^+$ have been successfully detected in laser flash photolysis of the $AcrH^+$-organosilane systems. The rate constants of back electron transfer to the ground state have been determined, leading to the evaluation of the reorganization energy for the back electron transfer, which agrees with the value for the forward electron transfer.

Introduction

The carbon-carbon bond formation via photoinduced electron transfer reactions of organosilanes and organostannanes have attracted growing interest not only because of the mechanistic aspects but also in view of their synthetic utility.[1–6] A pioneering work by Mariano et al.[1,2] has demonstrated that desilylation processes from organosilanes attendant upon the photoinduced electron transfer oxidation constitute effective methods for site selective generation of organic radicals which can serve as intermediates for the C-C bond formation. On the other hand, organosilanes and organostannanes have been frequently used as key reagents for many synthetically important transformations. In particular, Lewis acid-promoted carbon-carbon bond formation reactions of organosilanes and organostannanes have found considerable interest in organic synthesis in recent years.[7-12] Hydrosilanes and hydrostannanes are also commonly used as convenient hydride reagents in the reduction of various substrates.[10–13] Although these metal hydrides are also regarded as potential electron donors as well as hydride or hydrogen donors,[14] little is known about the actual roles in the electron-transfer reactions. No mechanistic comparison has so far been made between the thermal and photochemical reactions of organosilanes and organostannanes with the same substrates. Of many hydride acceptors, nicotinamide adenine dinucleotide (NAD^+) and its analogs are particularly important in regard to the vital role in biological redox processes. The regioselective reduction of NAD^+ analogs has attracted considerable interest in relation with the biological hydride reduction occurring selectively at the C-4 position.[15,16]

We report herein that the photochemical reduction of 10-methylacridinium ion ($AcrH^+$) by allylic silanes and stannanes occurs efficiently and regioselectively to afford the allylated dihydroacridines in which the allylic group is introduced at the α-position but that the thermal reduction by allylic stannanes occurs with the reversed regioselectivities to give the γ-adducts.[17] *Reversed* regioselectivities in the photoreduction of NAD^+ analogs (1-methylquinolinium ions) by hydrostannanes and hydrosilanes are also reported as compared to those in the thermal reduction by hydrostannanes and hydrosilanes. We could observe the transient absorption spectra in the visible region successfully to clarify the detailed mechanism of the regioselective photochemical reduction of $AcrH^+$ by organosilanes. Thus, this study provides excellent opportunities to compare directly the regioselectivities in both the thermal and photochemical reduction of NAD^+ analogs by the organometallic compounds and

to gain comprehensive and confirmative understanding for their mechanistic difference which leads to the regioreversed addition.

Experimental Section

Materials. 10-Methylacridinium iodide was prepared by the reaction of acridine with methyl iodide in acetone, and was converted to the perchlorate salt ($AcrH^+ClO_4^-$) by addition of magnesium perchlorate to the iodide salt. $AcrH^+ClO_4^-$ was purified by recrystallization from methanol.[18,19] Likewise, 1-methylquinolinium perchlorate ($QuH^+ClO_4^-$), 1,2-dimethylquinolinium perchlorate (2-$MeQuH^+ClO_4^-$) and 1,4-dimethylquinolinium perchlorate (4-$MeQuH^+ClO_4^-$) were prepared by the reaction of the corresponding quinoline derivatives with methyl iodide in acetone, followed by the metathesis with magnesium perchlorate.[18,19] Allyltrimethylsilane and benzyltrimethylsilane were obtained commercially. The other organosilane and organostannane compounds were prepared according to the literature method.[20] Hydrosilanes employed in this study are commercially available. An inorganic oxidant used in this study, tris(1,10-phenanthroline)iron(III) hexafluorophosphate, $[Fe(phen)_3](PF_6)_3$, was prepared according to the literature.[21] Organic oxidants (9,10-dicyanoanthracene, naphthalene, pyrene and 2,3-dichloro-5,6-dicyano-*p*-benzoquinone) were obtained commercially and purified by the standard method.[22] Tetrabutylammonium fluoride was also obtained commercially. An acetonitrile and dichloromethane used as solvents were purified and dried by the standard procedure.[22] An $[^2H_3]$acetonitrile (99.5 %, Aldrich) was used without further purification.

Reaction Procedure. Typically, an $[^2H_3]$acetonitrile (CD_3CN) solution (0.8 cm^3) containing $AcrH^+$ (1.0×10^{-2} M) in an NMR tube sealed with a rubber septum was deaerated by bubbling with argon gas through a stainless steel needle for 5 min. After an organosilane or organostannane compound (2-5 μL) was added to the solution by means of a microsyringe and mixed, the solution was irradiated with a high pressure mercury lamp through acetophenone-methanol filter transmitting $\lambda > 300$ nm at room temperature or in refrigerant methanol thermostated at 233 K by Cryocool CC-100. After the reaction was complete, when the solution became colorless, the reaction solution was analyzed by ^1H NMR spectroscopy. When dichloromethane was used as a solvent, the solvent was pumped off after the reaction. The residue was dried in vacuum and dissolved in CD_3CN, which was then analyzed by ^1H NMR.

Thermal reduction of $AcrH^+$ by an organostannane compound was started by adding an organostannane compound (2×10^{-2} M) to an $[^2H_3]$acetonitrile (CD_3CN) solution (0.8 cm^3) containing $AcrH^+$ (1×10^{-2} M) in an NMR tube. After the reactions were complete, the products were also analyzed by ^1H NMR.

The reaction of QuH^+ (1.0×10^{-1} M) and Ph_3SiH (3.0×10^{-1} M) was started by adding a CD_3CN solution (0.3 cm^3) of tetrabutylammonium fluoride (2.0 M) to a deaerated CD_3CN solution (0.8 cm^3) in an NMR tube sealed with a rubber septum by means of a microsyringe and mixed. After the reaction was complete in 1 h, the reaction solution was analyzed by ^1H NMR spectroscopy. In the case of photoreduction of 1-methylquinolinium ion (QuH^+), a deaerated CD_3CN solution (0.6 cm^3) of QuH^+ (1.0×10^{-2} M) and tris(trimethylsilyl)silane (1.5×10^{-2} M) in an NMR tube was irradiated with a high pressure mercury lamp for 50 min.

The ^1H NMR measurements were performed using a Japan Electron Optics JNM-PS-100 (100 MHz) and JNM-GSX-400 (400 MHz) NMR spectrometers. ^1H NMR (CD_3CN): $AcrH(CH_2CH{=}CH_2)$ δ 2.26 (t, 2H, J = 7.3 Hz), 3.36 (s, 3H), 3.96 (t, 1H, J = 7.3 Hz), 4.76 (dd, 1H, J = 2.0, 17 Hz), 4.87 (dd, 1H, J = 2.0, 10.3 Hz), 5.68 (m, 1H), 6.9-7.2 (m, 8H). $AcrH(CH_2CH{=}CMe_2)$ δ 0.89 (s, 3H), 0.93 (s, 3H), 2.21 (t, 2H, J = 7.3 Hz), 3.40 (s, 3H), 3.89 (t, 1H, J = 7.3 Hz), 5.10 (t, 1H, J = 7.3 Hz), 6.95-7.29 (m, 8H). $AcrH(CMe_2CH{=}CH_2)$ δ 0.84 (s, 6H), 3.30 (s, 3H), 3.73 (s, 1H), 4.45 (dd, 1H, J = 2.0, 17.6 Hz), 4.74 (dd, 1H, J = 2.0, 10.7 Hz), 5.69 (dd, 1H, J = 10.7, 17.6 Hz), 6.9-7.2 (m, 8H). $AcrH(CH(Ph)CH{=}CH_2)$ δ 3.24 (s, 3H), 3.39 (t, 1H, J = 8.7 Hz), 4.19 (d, 1H, J = 8.3 Hz), 4.65 (dd, 1H, J = 2.0, 17.8 Hz), 4.84 (dd, 1H, J = 2.0, 10.3 Hz), 6.0-6.2 (m, 1H), 6.6-7.4 (m, 13H). $AcrH(CH_2CH{=}CHPh)$ δ 2.2 (m, 2H), 3.37 (s, 3H), 4.10 (t, 1H, J = 6.8 Hz), 6.0-7.4 (m, 15H). $AcrH(cyclo\text{-}C_6H_{11})$ δ 0.8-2.0 (m, 11H), 3.34 (s, 3H), 3.61 (d, 1H, J = 8.7 Hz), 6.6-7.4 (m, 8H). $AcrH(CH_2Ph)$ δ 2.80 (d, 2H, J = 7.3 Hz), 3.32 (s, 3H), 4.19 (t, 1H, J = 7.3 Hz), 6.7-7.3 (m, 13H). 1,2-QuH_2 δ 2.72 (s, 3H), 3.98 (d, J = 3.5 Hz, 2H), 5.73 (m, 1H), 6.32 (d, J = 4.2 Hz, 1H), 6.5-7.1 (m, 4H). 1,4-QuH_2 δ 3.01 (s, 3H), 3.52 (d, J = 3.3 Hz, 2H), 4.51 (m, 1H), 5.73 (d, J = 9.6 Hz, 1H), 6.7-7.2 (m, 4H). 2-Me-1,2-QuH_2 δ 1.05 (d, J = 5.3 Hz, 3H), 2.81 (s, 3H), 4.08 (m, 1H), 5.72 (dd, J = 9.1 Hz, J = 4.2 Hz, 1H), 6.31 (d, J = 9.1 Hz, 1H), 6.5-7.1 (m, 4H). 2-Me-1,4-QuH_2 δ 2.05 (s, 3H), 3.20 (s, 3H), 3.48 (d, J = 3.3 Hz, 2H), 5.95 (m, 1H), 6.8-7.4 (m, 4H). 4-Me-1.2-QuH_2 δ 1.95 (s, 3H), 2.70 (s, 3H), 3.86 (d, J = 4.1 Hz, 2H), 5.60 (t, J = 4.1 Hz, 1H), 6.5-7.1 (m, 4H). 4-Me-1,4-QuH_2 δ 1.15 (d, J = 6.5 Hz, 3H), 3.02 (s, 3H), 3.40 (m, 1H), 6.6-7.4 (m, 6H).

Kinetic Measurements. Kinetic measurements were performed under deaerated conditions using a Shimadzu UV-160A, UV-2200, or a Hewlett Packard diode array spectrophotometer, which was thermostated at 298 K. Rates of the electron transfer reactions from organostannanes to ferricenium ion in MeCN were followed by the decrease in absorbance due to ferricenium ion in the long-wavelength region (600-700 nm).[23] A typical procedure for the kinetic measurements of the thermal reactions of $AcrH^+$ and X-QuH^+ with organostannanes is following. An acetonitrile (0.40 cm^3) solution of 2.7 x 10^{-3} M $AcrH^+$ or X-QuH^+ contained in a 1-mm quartz cuvette was placed in a cell holder of the spectrophotometer, which was thermostated at 298 K . Allylstannane was added (2 x 10^{-2} - 6 x 10^{-2} M) by means of a microsyringe with shaking. Rates of the reduction of $AcrH^+$ and X-QuH^+ were followed by the disappearance of the absorbance (λ = 415 nm and 315 nm) due to $AcrH^+$ to X-QuH^+, respectively. The pseudo-first-order plot for each reaction was linear for 3 or more half-lives with the correlation coefficient $\rho > 0.999$.

Quantum Yield Determinations. A standard actinometer (potassium ferrioxalate)[24] was used for the quantum yield determination of the photoreduction of $AcrH^+$ and X-QuH^+ by organometallic compounds. A square quartz cuvette (10 mm i.d.) which contained an acetonitrile solution (3.0 cm^3) of $AcrH^+$ and X-QuH^+ (3.1 x 10^{-4} - 6.0 x 10^{-4} M) and an organometallic compound (5 x 10^{-4} - 4 x10^{-3} M) was irradiated with monochromatized light of λ = 358 and 320 nm from a Hitachi 650-10S fluorescence spectrophotometer, respectively. Under the conditions of actinometry experiments, both the actinometer and $AcrH^+$ or X-QuH^+ absorbed essentially all the incident light. The light intensity of monochromatized light of λ = 358 nm and 320 nm was determined as 1.1 x 10^{-8} einstein s^{-1} and 3.8 x 10^{-8} einstein s^{-1} with the slit width of 20 nm, respectively. The photochemical reaction was monitored by using a Shimadzu UV-160A or UV-2200 spectrophotometer. The quantum yields were determined from the decrease in absorbance due to $AcrH^+$ (λ = 396 nm, ε = 3.5 x 10^3 M^{-1} cm^{-1}) and QuH^+ (λ = 338 nm, ε = 1.8 x 10^3 M^{-1} cm^{-1}). When the contribution of thermal reactions cannot be neglected, the quantum yields were determined by subtracting the rate of thermal reactions in the dark from that of the photochemical reaction.

Fluorescence Quenching. Quenching experiments of the fluorescence of 10-methylacridinium ion, 9,10-dicyanoanthracene, naphthalene, and pyrene by organosilanes and organostannanes were performed using a Hitachi 650-10S fluorescence spectrophotometer. The excitation wavelengths were 360, 315, 390, 300, 365 nm for $AcrH^+$, QuH^+, 9,10-dicyanoanthracene, naphthalene, and pyrene in MeCN, respectively. The monitoring

wavelengths were those corresponding to the maxima of the emission bands at λ = 488, 398, 460, 335, and 420 nm, respectively. The solutions were deoxygenated by argon purging for 10 min prior to the measurements. Relative emission intensities were measured for MeCN solution containing $AcrH^+$ or QuH^+ (5.0 x 10^{-5} M) with organometals at various concentrations (1.5 x 10^{-2} - 6.2 x 10^{-2} M). There was no change in the shape but there was a change in the intensity of the fluorescence spectrum by the addition of an organometal. The Stern-Volmer relationship (eq 1) was obtained for the ratio of the emission intensities in the absence and

$$I_0 / I = 1 + K_{SV}[D] \quad (1)$$

presence of organometals (I_0/I) and the concentrations of organometals [D]. The fluorescence lifetime τ of $AcrH^+$ was determined as 37 ns in MeCN by single photon counting using a Horiba NAES-1100 time-resolved spectrofluorophotometer. The observed quenching rate constants k_q ($= K_{SV}\tau^{-1}$) were obtained from the Stern-Volmer constants K_{SV} and the emission lifetimes τ. When organometals such as allyltributylstannane which reacts thermally with $AcrH^+$ are employed as quenchers, the Stern-Volmer constant (K_{SV}) was determined from the ratio of the lifetime in the absence and presence of organometals (τ_0/τ) by use of a single photon counting using a Horiba NAES-1100 time-resolved spectrofluorophotometer (eq 2).

$$\tau_0 / \tau = 1 + K_{SV}[D] \quad (2)$$

Laser Flash Photolysis. The measurements of transient absorption spectra in the photochemical reactions of $AcrH^+$ with $PhCH_2SiMe_3$ or CH_2=$CHCH_2SiMe_3$ in MeCN were performed according to the following procedures. The MeCN solution was deoxygenated by argon purging for 10 min prior to the measurement. The deaerated MeCN solution containing $AcrH^+$ (1.7 x 10^{-3} M) and organosilanes (2.8 x 10^{-2} M) was excited by a Nd:YAG laser (Quanta-Ray, GCR-130, 6 ns fwhm) at 355 nm with the power of 30 mJ. A pulsed xenon flash lamp (Tokyo Instruments, XF80-60, 15 J, 60 ms fwhm) was used for the probe beam, which was detected with a Si PIN photodiode (Hamamatsu, S1722-02) after passing through the photochemical quartz vessel (10 mm x 5 mm) and a monochromator. The output from the Si PIN photodiode was recorded with a digitizing oscilloscope (HP 54510B, 300

MHz). The transient spectra were recorded using fresh solutions in each laser excitation. All experiments were performed at 298 K.

ESR Measurements. ESR spectra of the photolyzed $AcrH^+ClO_4^-$ and $PhCH_2SiMe_3$ (or ferrocene) in frozen MeCN were taken on a JEOL JES-RE1XE and were recorded under nonsaturating microwave power conditions. The magnitude of the modulation was chosen to optimize the resolution and the signal to noise ratio (S/N) of the observed spectra. The *g* values were calibrated using an Mn^{2+} marker.

Theoretical Calculations. Semiempirical calculations were performed using the MOPAC program (Ver. 6) which is incorporated in the MOLMOLIS program (Ver. 2.8) by Daikin Industries, Co. Ltd. The PM3 Hamiltonian was used for the semiempirical MO calculations.[25] Final geometries and energetics were optimized by minimizing the total molecular energy with respect to all structural variables. The heats of formation (ΔH_f) were calculated with the restricted Hartree Fock (RHF) formalism using a key word "PRECISE". The *ab initio* calculations were performed at the Becke3LYP/6-31+G* or MP2/6-31++G* level[26,27] with GAUSSIAN 98.[28]

Results and Discussion

Photoaddition of Organosilanes and Organostannanes with 10-Methylacridinium Ion. Irradiation of the absorption band of 10-methylacridinium perchlorate ($AcrH^+ClO_4^-$) in deaerated methanol solution containing allylsilane for 3.5 h gave an adduct [$AcrH(CH_2CH{=}CH_2)$] as shown in (eq 3). Such photoaddition reactions with

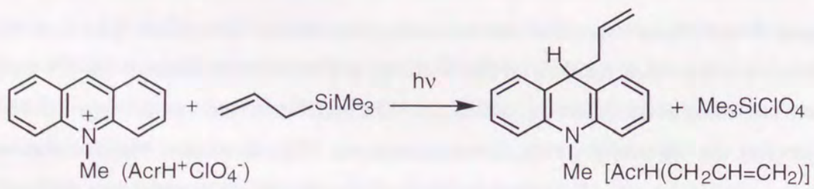

(3)

$AcrH^+$ also occur efficiently using other organosilanes and organostannanes. The products are well identified by the ^1H NMR spectra (see Experimental Section). The product yields under various reaction conditions are summarized in Table 1.

Table 1. Photoreduction of $AcrH^+$ (1.0×10^{-2} M) by Organosilanes and Organostannanes (1.5×10^{-2} M) in Deaerated MeCN

allylmetal	condition	time (h)	product (yield (%))
$CH_2{=}CHCH_2SiMe_3$	a	3.5	$AcrH(CH_2CH{=}CH_2)$ (60)
$Me_2C{=}CHCH_2SiMe_3$	a	3.5	$AcrH(CH_2CH{=}CMe_2)$ (60)
$PhCH_2SiMe_3$	a	1.5	$AcrH(CH_2Ph)$ (100)
$CH_2{=}CHCH_2SnPh_3$	a	1.5	$AcrH(CH_2CH{=}CH_2)$ (85)
$PhCH_2SnPh_3$	a	1.0	$AcrH(CH_2Ph)$ (100)
$CH_2{=}CHCH_2SnBu_3$	a	0.5	$AcrH(CH_2CH{=}CH_2)$ (100)
$Me_2C{=}CHCH_2SnBu_3$	a	0.5	$AcrH(CH_2CH{=}CMe_2)$ (80)
			$AcrH(CMe_2CH{=}CH_2)$ (20)
$Me_2C{=}CHCH_2Sn(cyc\text{-}C_6H_{11})_3$	a	1.0	$AcrH(CH_2CH{=}CMe_2)$ (67)
			$AcrH(CMe_2CH{=}CH_2)$ (16)
			$AcrH(cyc\text{-}C_6H_{11})$ (17)
$PhCH{=}CHCH_2SnBu_3$	a	0.5	$AcrH(CH_2CH{=}CHPh)$ (57)
			$AcrH(C(H)PhCH{=}CH_2)$ (43)
$Me_2C{=}CHCH_2SnBu_3$	b	1.0	$AcrH(CH_2CH{=}CMe_2)$ (81)
			$AcrH(CMe_2CH{=}CH_2)$ (19)
$Me_2C{=}CHCH_2SnBu_3$	c	1.0	$AcrH(CH_2CH{=}CMe_2)$ (100)
$Me_2C{=}CHCH_2Sn(cyc\text{-}C_6H_{11})_3$	c	1.0	$AcrH(CH_2CH{=}CMe_2)$ (71)
			$AcrH(CMe_2CH{=}CH_2)$ (11)
			$AcrH(cyc\text{-}C_6H_{11})$ (18)

[a] In MeCN at 298 K. [b] In MeCN at 233 K. [c] $[AcrH^+] = 6.1 \times 10^{-3}$ M, [organometal] = 1×10^{-2} M in CH_2Cl_2 at 298 K. [d] Irradiation with a xenon lamp through a filter (Y-43) cutting off $\lambda < 420$ nm.

When an unsymmetrical allylic silane, *e.g*, prenyltrimethylsilane is employed, the allylic group is introduced at the α-position to yield AcrH($CH_2CH{=}CMe_2$) exclusively and no γ-adduct [AcrH($CMe_2CH{=}CH_2$)] has been formed (eq 4). In the case of prenyltributylstannane, however, γ-adduct (20 %) is formed as well as α-adduct which is the

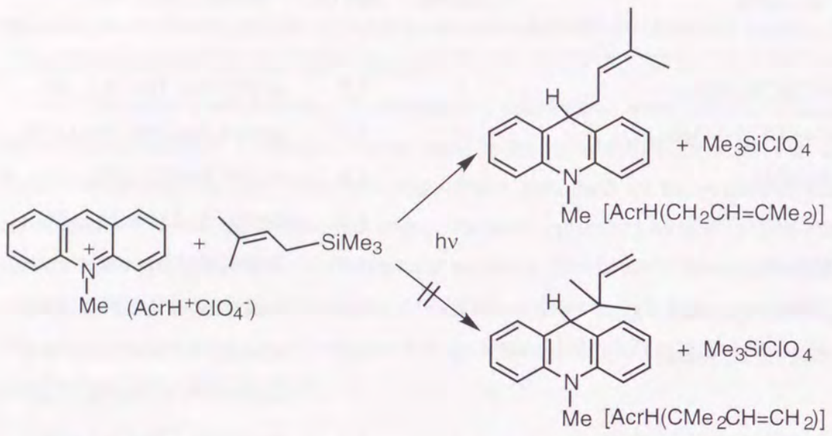

(4)

major product. Although the addition reaction of prenyltributylstannane with $AcrH^+$ also occurs thermally to yield the γ-adduct exclusively as described later, the photoaddition reaction was carried out under the experimental conditions such that the contribution of the thermal reaction can be neglected. In fact, essentially the same selectivity ratio of the α- to γ-adduct was obtained at a much lower reaction temperature (233 K) when the contribution of the thermal reaction, if any, should be completely neglected as compared to the reaction at 298 K (Table 1). The yield of γ-adduct is increased to 43 % that is comparable with that of α-adduct (57 %) when tributyl-*trans*-cinnamylstannane is employed (Table 1).

When the butyl group of prenyltributylstannane is replaced by the more electron donating cyclohexyl group, the adduct derived from the cleavage of the Sn-cyclohexyl group is also obtained together with the α- and γ- adducts of the allylic group (Table 1). The ratio of the α- to γ-adduct increases when CH_2Cl_2 instead of MeCN is used as a solvent (Table 1).

The photoalkylation also occurs selectively in the case of organosilanes containing an electron donating alkyl group, e.g., benzyltrimethylsilane to yield the benzyl adduct (Table 1). We have previously reported that photoalkylation of $AcrH^+$ by tetraalkyltin compounds (R_4Sn, R = Et, Bu, and Pr^i) to yield AcrHR.[29]

Thermal Reduction of 10-Methylacridinium Ion by Allylic Stannanes. It is found that 10-methylacridinium ion ($AcrH^+$) is readily reduced by allyltributyltin to yield selectively 9-allyl-10-methyl-9,10-dihydroacridine [AcrH($CH_2CH{=}CH_2$)] in MeCN as

Table 2. Addition Reaction of Allylic Stannanes with $AcrH^+$ in MeCN in the Dark

allylic stannane (concentration (M))	[$AcrH^+$] (M)	time (h)	product (yield (%))
$CH_2{=}CHCH_2SnBu_3$[a] (8.0×10^{-2})	6×10^{-2}	1	AcrH($CH_2CH{=}CH_2$) (100)
$Me_2C{=}CHCH_2SnBu_3$[a] (2.0×10^{-2})	1×10^{-2}	10	AcrH($CMe_2CH{=}CH_2$) (100)
$Me_2C{=}CHCH_2Sn(cyc\text{-}C_6H_{11})_3$[a] ($3.8 \times 10^{-2}$)	1×10^{-2}	10	AcrH($CMe_2CH{=}CH_2$) (100)
$PhCH{=}CHCH_2SnBu_3$[a] (1.5×10^{-2})	1×10^{-2}	10	AcrH(C(H)PhCH=CH_2)(100)
$Me_2C{=}CHCH_2SnBu_3$[b] (2.9×10^{-2})	4×10^{-3}	10	AcrH($CMe_2CH{=}CH_2$) (100)
$Me_2C{=}CHCH_2Sn(cyc\text{-}C_6H_{11})_3$[b] ($3.7 \times 10^{-2}$)	4×10^{-3}	10	AcrH($CMe_2CH{=}CH_2$) (100)

[a] In MeCN. [b] In CH_2Cl_2.

shown in Table 2. In contrast to the photochemical reaction (Table 1), the thermal reaction of $AcrH^+$ with prenyltributylstannane yields only the γ-adduct (eq 5). Likewise the thermal reduction of $AcrH^+$ by tributyl-*trans*-cinnamylstannane also yield the γ-adduct exclusively (Table 2).

Rates of the reduction of $AcrH^+$ by allylic stannanes were followed by the disappearance of the absorbance ($\lambda = 415$ nm) due to $AcrH^+$ (see Experimental Section). The rates obeyed ordinary second-order kinetics, showing the first-order dependence on the concentration of each reactant. The observed second-order rate constants (k_{obs}) are listed in

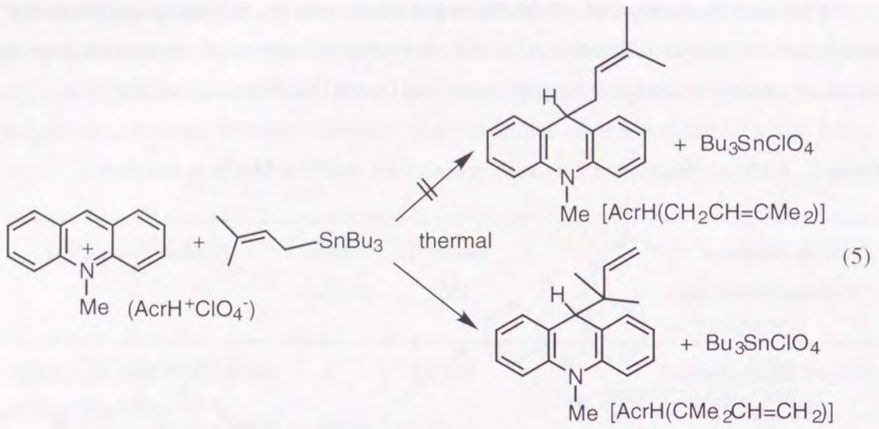

(5)

Table 3. The Observed Rate Constants (k_{obs}) of Thermal Reduction of AcrH$^+$ (2.7 x 10^{-3} M) by Allylic Stannanes in MeCN at 298 K

allylstannane	k_{obs}, M^{-1} s^{-1}
CH_2=$CHCH_2SnBu_3$	6.4 x 10^{-2}
Me_2C=$CHCH_2SnBu_3$	1.4 x 10^{-2}
PhCH=$CHCH_2SnBu_3$	5.2 x 10^{-3}

Table 3. The k_{obs} valuedecreases with the γ-substitution by the bulky groups (Me_2 and Ph), demonstrating a significant steric effect of the substituent at the carbon where the C-C bond is formed with AcrH$^+$.

Thermal Hydride Reduction of NAD$^+$ Analogs. Upon mixing QuH$^+$ (8.0 x 10^{-5} mol) with Bu_3SnH (1.9 x 10^{-4} mol) in acetonitrile (0.80 cm^3) at 298 K, QuH$^+$ was readily reduced to yield initially 1-methyl-1,2-dihydroquinoline (1,2-QuH_2: 80% in 30 min), which was gradually isomerized to the corresponding 1,4-isomer (1,4-QuH_2: 70% in 70 min) as shown in eq 6. The 1,2- and 1,4-isomers can also be differentiated by their absorption spectra (λ_{max} = 350 and 250 nm, respectively). Figure 1 shows the electronic spectra observed in the reduction of QuH$^+$ by Bu_3SnH in MeCN. Under the experimental conditions of a low concentration of QuH$^+$ (2.0 x 10^{-3} M), the absorbance due to the initial product, the 1,2-

isomer (λ_{max} = 350 nm) increases, accompanied by the decrease in absorbance due to QuH$^+$ (λ_{max} = 315 nm) with a clean isosbestic point. The reduction of 1,4-dimethylquinolinium ion (4-MeQuH$^+$) by Bu_3SnH also occurs efficiently to yield exclusively the corresponding 1,2-isomer (4-Me-1,2-QuH_2) which does not isomerize to the 1,4-isomer. These products were well identified from their ^{1}H NMR spectra (see Experimental Section). The isomerization

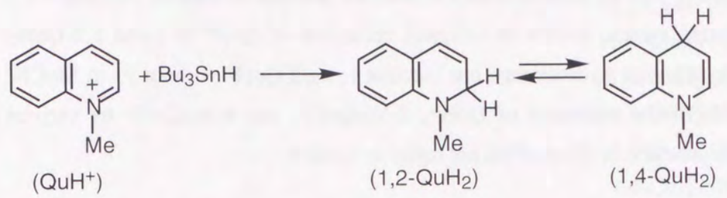

(6)

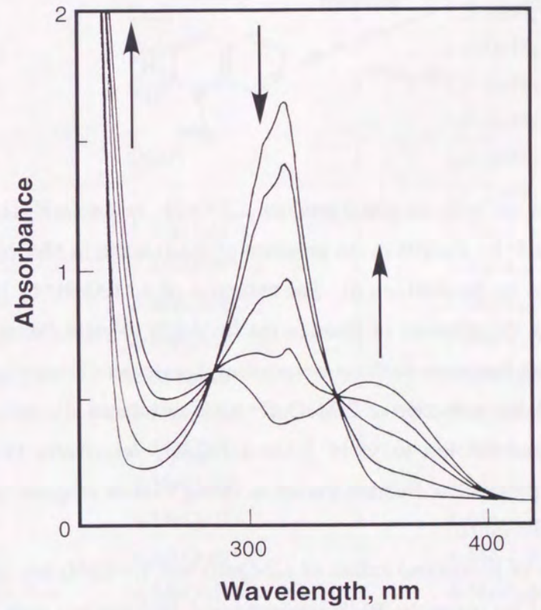

Figure 1. Electronic absorption spectra observed in the reduction of QuH$^+$ (2.0 x 10^{-3} M) by Bu_3SnH (2.0 x 10^{-2} M) in MeCN at 298 K; time interval: 0, 10, 30, 45 and 60 min.

from 1,2-QuH_2 to 1,4-QuH_2 has been reported to occur by the reaction of the 1,2-isomer with

QuH^+ in reduction of quinolinium salts with $NaBH_4$.[30] When QuH^+ is replaced by 1,2-dimethylquinolinium ion (2-MeQuH^+) in which the C-2 position is blocked by methyl group, no reaction with Bu_3SnH has occurred at 298 K.

Various hydrosilanes are known to be capable of reducing carbonyl compounds in the presence of fluoride ion, when penta-coordinate hydrosilicates $[R_3SiHF]^-$ are formed as reactive intermediates.[31] In the present system as well, the addition of fluoride ion ($Bu_4N^+F^-$) to the Ph_3SiH-QuH^+ system results in efficient reduction of QuH^+ to yield 1,2-QuH_2 selectively (eq 7), although hydrosilanes are inactive toward QuH^+ without F^- in MeCN. The product yields of the reduction of QuH^+, 2-MeQuH^+, and 4-MeQuH^+ by various hydrosilanes in the presence of fluoride ion are listed in Table 4.

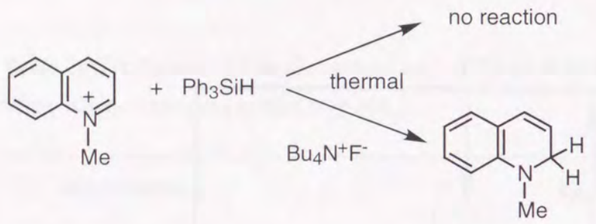

(7)

The isomerization from the initial product, 1,2-QuH_2, to 1,4-QuH_2 is also observed in the reduction of QuH^+ by Ph_3SiH in the presence of fluoride ion in MeCN (Table 4) as the case of the reduction by Bu_3SnH (eq 6). The reduction of 4-MeQuH^+ by hydrosilanes also occurs efficiently in the presence of fluoride ion in MeCN to yield exclusively 4-Me-1,2-QuH_2 which does not isomerize to the corresponding 1,4-isomer (Table 4). In contrast with the case of Bu_3SnH, the reduction of 2-MeQuH^+ by hydrosilanes also occurs efficiently in the presence of fluoride ion to yield 2-Me-1,2-QuH_2 selectively (Table 4). Thus, hydrosilanes in the presence of fluoride ion act as strong hydride reagents as compared with the hydrostannane, Bu_3SnH.

The ΔH_f (heat of formation) values of 1,2-QuH_2 and 1,4-QuH_2 are calculated as 37.3 and 34.1 kcal mol^{-1} by using the PM3 semiempirical MO method with the geometrical parameters optimized (See Experimental Section). Thus, the initial nucleophilic attack of Bu_3SnH and hydrosilanes in the presence of fluoride ion occurs preferentially at the C-2 position in the case of QuH^+ to yield the 1,2-isomer, which then isomerizes to the thermodynamically stable form, 1,4-isomer.

Table 4. Regioselective Reduction of QuH^+ Derivatives by Hydrosilanes in the Presence of $Bu_4N^+F^-$ (0.2 M) and that by Bu_3SnH in MeCN at 298K

metal hydride (M)	QuH^+ derivative (0.1M)	time (h)	product (yield (%))
Ph_3SiH (0.2)	QuH^+	1	1,2-QuH_2 (100)
		3	1,2-QuH_2 (94)
			1,4-QuH_2 (6)
		24	1,2-QuH_2 (58)
			1,4-QuH_2 (42)
		100	1,2-QuH_2 (39)
			1,4-QuH_2 (61)
Ph_2SiH_2 (0.3)	QuH^+	1	1,2-QuH_2 (55)
			1,4-QuH_2 (45)
$PhMe_2SiH$ (0.3)	QuH^+	1	1,2-QuH_2 (100)
$(MeO)_3SiH$ (0.3)	QuH^+	2	1,2-QuH_2 (100)
$(TMS)_3SiH$ (0.3)	QuH^+	2	1,2-QuH_2 (87)
			1,4-QuH_2 (13)
Bu_3SnH (0.24)[a]	QuH^+	1	1,2-QuH_2 (40)
			1,4-QuH_2 (60)
Ph_3SiH (0.2)	2-MeQuH^+	3	2-Me-1,2-QuH_2 (100)
Ph_2SiH_2 (0.3)	2-MeQuH^+	1	2-Me-1,2-QuH_2 (100)
$PhMe_2SiH$ (0.3)	2-MeQuH^+	1	2-Me-1,2-QuH_2 (100)
$(MeO)_3SiH$ (0.3)	2-MeQuH^+	2	2-Me-1,2-QuH_2 (100)
$(TMS)_3SiH$ (0.3)	2-MeQuH^+	2	2-Me-1,2-QuH_2 (100)
Bu_3SnH (0.24)[a]	2-MeQuH^+	1	no reaction
Ph_3SiH (0.2)	4-MeQuH^+	3	4-Me-1,2-QuH_2 (100)
Ph_2SiH_2 (0.3)	4-MeQuH^+	1	4-Me-1,2-QuH_2 (100)
$PhMe_2SiH$ (0.3)	4-MeQuH^+	1	4-Me-1,2-QuH_2 (100)
$(MeO)_3SiH$ (0.3)	4-MeQuH^+	2	4-Me-1,2-QuH_2 (100)
$(TMS)_3SiH$ (0.3)	4-MeQuH^+	2	4-Me-1,2-QuH_2 (100)
Bu_3SnH (0.24)[a]	4-MeQuH^+	1	4-Me-1,2-QuH_2 (100)

[a] In the absence of $Bu_4N^+F^-$

Photochemical Reduction of Quinolinium Ions by Bu_3SnH and $(TMS)_3SiH$.

As described above, no thermal reduction of 2-MeQuH$^+$ by Bu_3SnH occurs because of the steric effect of methyl group at the C-2 position. Irradiation of the absorption band of 2-MeQuH$^+$ (λ_{max} = 315 nm) in deaerated MeCN containing Bu_3SnH with monochromatized light of λ = 320 nm, however, results in efficient reduction of 2-MeQuH$^+$ to yield the corresponding 1,4-isomer (2-Me-1,4-QuH_2) exclusively (eq 8). In contrast to the thermal reduction of QuH$^+$ by Bu_3SnH, no 1,2-isomer has been formed during the photochemical reaction.

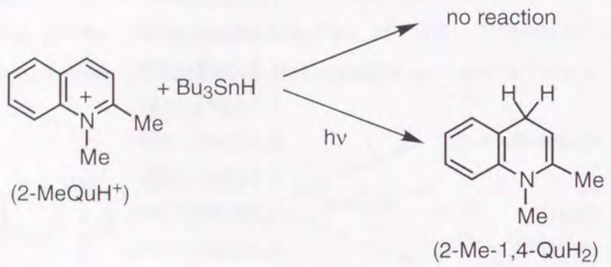

(8)

When Bu_3SnH is replaced by $(TMS)_3SiH$, no thermal reduction of X-QuH$^+$ (X = H, 2-Me and 4-Me) by $(TMS)_3SiH$ has occurred at 298 K. As is the case of the photochemical reaction of 2-MeQuH$^+$ with Bu_3SnH, irradiation of the absorption band of X-QuH$^+$ in deaerated MeCN containing $(TMS)_3SiH$ and H_2O (5.0 M) results in the efficient reduction of X-QuH$^+$ to yield the corresponding 1,4-isomer (X-1,4-QuH_2) exclusively (H_2O was added to trap the silyl cation). Figure 2 shows the electronic spectra observed in the photoreduction of QuH$^+$ by $(TMS)_3SiH$ in deaerated MeCN. In contrast to the thermal reduction of QuH$^+$ by Bu_3SnH (Figure 1), the absorbance due to the initial product, the 1,4-isomer (λ_{max} = 250 nm) increases, accompanied by the decrease in absorbance due to QuH$^+$ (λ_{max} = 315 nm) with a clean isosbestic point. The photoreduction of 2-MeQuH$^+$, 4-MeQuH$^+$ and by $(TMS)_3SiH$ also occurs efficiently to yield the corresponding 1,4-isomers. In the case of the photoreduction of 10-methylacridinium ion (AcrH$^+$) by $(TMS)_3SiH$, 10-methyl-9,10-dihydroacridine ($AcrH_2$) is obtained exclusively. The product yields of the photoreduction of these NAD$^+$ analogs by $(TMS)_3SiH$ are listed in Table 5.

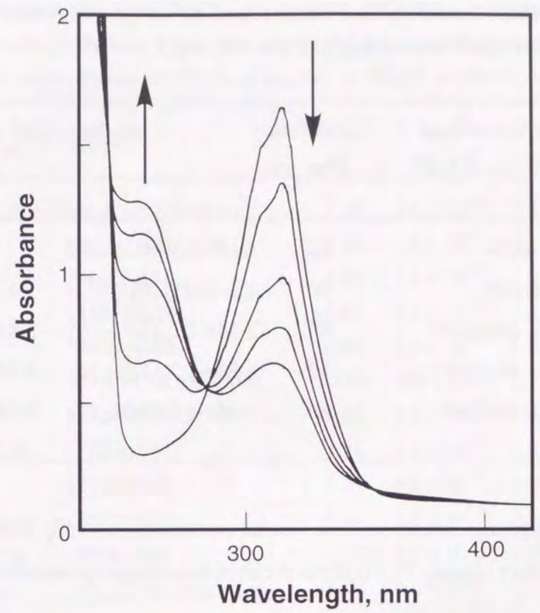

Figure 2. Electronic absorption spectra observed in the photoreduction of QuH$^+$ (2.0 x 10^{-3} M) by $(TMS)_3SiH$ (2.0 x 10^{-2} M) in MeCN at 298 K; time interval: 0, 10, 30, 40 and 50 min.

Photoinduced Electron Transfer. Irradiation of the absorption bands of AcrH$^+$ and QuH$^+$ in MeCN causes fluorescence at 488 and 398 nm, respectively. The fluorescence of AcrH$^+$ is known to be quenched by electron transfer from various organic electron donors to the singlet excited state (AcrH^{+*}).[32] The fluorescence of AcrH$^+$, QuH$^+$, 2-MeQuH$^+$ and 4-MeQuH$^+$ is also quenched efficiently by electron donors including organosilanes and organostannanes employed in this study. The rate constants (k_{obs}) of the fluorescence quenching are determined from the slopes of the Stern-Volmer plots and lifetime of the singlet excited state [AcrH^{+*} (τ = 37 ns), QuH^{+*} (20 ns), 2-MeQuH^{+*} (15 ns) and 4-MeQuH^{+*} (19 ns)], which were determined by the single photon counting measurements (see Experimental Section). The free energy change of photoinduced electron transfer from

Table 5. Photoreduction of NAD^+ Analogs by $(TMS)_3SiH$ and Bu_3SnH in Deaerated MeCN at 298 K under Irradiation of Light of $\lambda = 320$ nm

metal hydride (0.02 M)	NAD^+ analog (0.02 M)	irradiation time, min	product (yield , %)	
$(TMS)_3SiH$	$AcrH^+$	60	$AcrH_2$ (100)	
$(TMS)_3SiH$	QuH^+	50	1,2-QuH_2 (0)	1,4-QuH_2 (62)
$(TMS)_3SiH$	2-MeQuH^+	60	2-Me-1,2-QuH_2 (0)	2-Me-1,4-QuH_2 (60)
$(TMS)_3SiH$	4-MeQuH^+	50	4-Me-1,2-QuH_2 (0)	4-Me-1,4-QuH_2 (50)
Bu_3SnH	2-MeQuH^+	60	2-Me-1,2-QuH_2 (0)	2-Me-1,4-QuH_2 (70)

organosilanes and organostannanes to these singlet excited states (ΔG^0_{et} in eV) is given by eq 9, where e is elementary charge, E^0_{ox} is the one-electron oxidation potentials of

$$\Delta G^0_{et} = e(E^0_{ox} - E^0_{red}) \quad (9)$$

organosilanes[6a,33] and organostannanes,[17] and E^0_{red} is the one-electron reduction potentials of the singlet excited states, $AcrH^{+*}$ and X-QuH^{+*} (X = H, 2-Me and 4-Me).[34] The ΔG^0_{et} values are largely negative as listed in Table 6, indicating that the fluorescence quenching occurs efficiently via photoinduced electron transfer from organosilanes and organostannanes to $AcrH^{+*}$ and X-QuH^{+*}. The rate constants (k_{obs}) of the fluorescence quenching via photoinduced electron transfer are listed in Table 6, where the k_{obs} values are in the range of 1.0×10^{10} - 1.7×10^{10} M^{-1} s^{-1}, being close to the diffusion limit in MeCN at 298 K.[35] The k_{obs} values for photoinduced electron transfer and thermal electron transfer reactions of organosilanes and organostannanes are also included in Table 6. A plot of log k_{obs} vs ΔG^0_{et} is shown in Figure 3 which demonstrates a typical dependence of the rate constant for outer-sphere electron transfer reactions on the free energy change of electron transfer (ΔG^0_{et}); the log k_{obs} value increases with a decrease in ΔG^0_{et} to reach a diffusion-limited value ($k_{obs} = 2.0 \times 10^{10}$ M^{-1} s^{-1}).[35]

Table 6. Free Energy Change of Electron Transfer (ΔG^0_{et}), Rate Constants (k_{obs}) of Electron Transfer, and Limiting Quantum Yields (Φ_∞) for the Photochemial Reactions of $AcrH^+$ and QuH^+ Derivatives with Organosilanes and Organostannanes in MeCN at 298 K

acceptor	E^0_{red},[a] V	donor[b]	ΔG^0_{et},[c] eV	k_{obs},[d] M^{-1} s^{-1}	k_{obs},[e] M^{-1} s^{-1}	Φ_∞[f]
$AcrH^{+*}$	2.32	$Me_2C{=}CHCH_2SnBu_3$	-1.43	1.8×10^{10}	1.4×10^{10}	1.8×10^{-1}
		$CH_2{=}CHCH_2SnBu_3$	-1.26	1.8×10^{10}	1.4×10^{10}	1.5×10^{-1}
		$(TMS)_3SiH$	-1.02	1.2×10^{10}	1.7×10^{10}	8.0×10^{-2}
		$(TMS)_3SiD$	-1.02	1.2×10^{10}	1.7×10^{10}	3.6×10^{-2}
		$PhCH_2SiMe_3$	-0.94	1.2×10^{10}	1.0×10^{10}	1.7×10^{-2}
		$Me_2C{=}CHCH_2SiMe_3$	-0.93	9.0×10^{9}	1.1×10^{10}	7.0×10^{-3}
		$CH_2{=}CHCH_2SiMe_3$	-0.82	1.2×10^{10}	1.0×10^{10}	8.0×10^{-3}
QuH^{+*}	2.54	$(TMS)_3SiH$	-1.24	1.0×10^{10}	1.3×10^{10}	8.0×10^{-2}
		$(TMS)_3SiD$	-1.24	1.0×10^{10}	1.3×10^{10}	4.2×10^{-2}
2-MeQuH^{+*}	2.46	$(TMS)_3SiH$	-1.16	1.3×10^{10}	1.7×10^{10}	9.6×10^{-2}
4-MeQuH^{+*}	2.51	$(TMS)_3SiH$	-1.21	1.0×10^{10}	1.2×10^{10}	7.6×10^{-2}
DCA^*	1.91	$Me_2C{=}CHCH_2SnBu_3$	-1.02	1.5×10^{10}		
		$CH_2{=}CHCH_2SnBu_3$	-0.85	1.5×10^{10}		
		$(TMS)_3SiH$	-0.61	6.5×10^{9}		
		$PhCH_2SiMe_3$	-0.53	6.7×10^{9}		
		$Me_2C{=}CHCH_2SiMe_3$	-0.52	9.0×10^{9}		
		$CH_2{=}CHCH_2SiMe_3$	-0.41	3.1×10^{9}		
naphthalene*	1.46	$Me_2C{=}CHCH_2SnBu_3$	-0.57	6.8×10^{9}		
		$CH_2{=}CHCH_2SnBu_3$	-0.40	1.4×10^{9}		
		$Me_2C{=}CHCH_2SiMe_3$	-0.07	1.8×10^{8}		
		$CH_2{=}CHCH_2SiMe_3$	0.04	1.5×10^{7}		
pyrene*	1.23	$Me_2C{=}CHCH_2SnBu_3$	-0.34	5.2×10^{9}		
		$CH_2{=}CHCH_2SnBu_3$	-0.17	1.5×10^{8}		
		$(TMS)_3SiH$	0.07	1.2×10^{7}		
		$PhCH_2SiMe_3$	0.15	9.1×10^{6}		
		$Me_2C{=}CHCH_2SiMe_3$	0.16	2.3×10^{7}		
$Fe(phen)_3^{3+}$	0.98	$(TMS)_3SiH$	0.32	1.0×10^{3}		
$FeCp_2^+$	0.37	$Me_2C{=}CHCH_2SnMe_3$	0.52	5.0		
		$CH_2{=}CHCH_2SnBu_3$	0.69	8.0×10^{-3}		

[a] E^0_{red} vs SCE, taken from refs 6a, 33 and 34. [b] The E^0_{ox} values are taken from refs 6a and 17. [c] Determined from $\Delta G^0_{et} = E^0_{ox} - E^0_{red}$. [d] Determmined from the fluorescence quenching rate constants for photoinduced electron transfer and electron transfer rate constants for thermal electron transfer reactions. [e] Determined from the dependennce of the quantum yield on the donor concentration.

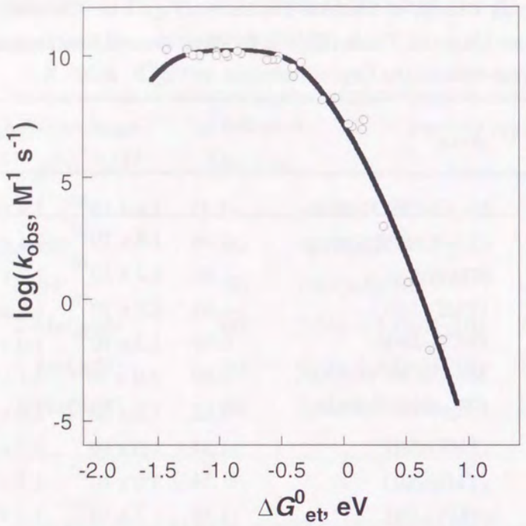

Figure 3. Plot of log k_{obs} vs ΔG^0_{et} for photoinduced and thermal electron transfer reactions of organosilanes and organostannanes in MeCN at 298 K. The data are taken from Table 6. The solid line is drawn based on eq 12 using λ = 0.90 eV.

A general scheme for photoinduced electron transfer from an electron donor (D) to an excited-state acceptor (A^*) is given in eq 10, where k_{12} and k_{21} are diffusion and dissociation

$$D + A^* \underset{k_{21}}{\overset{k_{12}}{\rightleftharpoons}} (D\,A^*) \xrightarrow{k_{et}} (D^{\bullet+}\,A^{\bullet-}) \xrightarrow{k_{bet}} D + A \qquad (10)$$

rate constants in the encounter complex ($D\,A^*$), k_{et} and k_{bet} are the rate constants of forward electron transfer from D to A to produce the radical ion pair ($D^{\bullet+}\,A^{\bullet-}$) and back electron transfer to the ground state.[6a,35-37] The observed rate constant (k_{obs}) of photoinduced electron transfer is given by eq 11. The dependence of k_{et} on ΔG^0_{et} for adiabatic outer-sphere electron transfer

$$k_{obs} = k_{et}k_{12}/(k_{21} + k_{bet}) \qquad (11)$$

has been well established by Marcus as given by eq 12, where k is the Boltzmann constant, h

$$k_{et} = (kT/h)\exp[-(\lambda/4)(1 + \Delta G^0_{et}/\lambda)^2/kT] \qquad (12)$$

is the Planck constant and λ is the reorganization energy of electron transfer.[38-40] From eqs 11 and 12 is derived eq 13, where k_{12} in MeCN is known as 2.0 x 10^{10} M^{-1} s^{-1},[35] and Z [= $(kT/h)(k_{12}/k_{21})$] is the collision frequency taken as 1 x 10^{11} M^{-1} s^{-1}.[38] A linear plot of

$$[kT\ln Z(k_{obs}^{-1} - k_{12}^{-1})]^{1/2} = \lambda^{1/2}/2 + \Delta G^0_{et}/(2\lambda^{1/2}) \qquad (13)$$

$[kT\ln Z(k_{obs}^{-1} - k_{12}^{-1})]^{1/2}$ ($= \Delta G^{\neq}_{et}$) vs ΔG^0_{et} (eq 13) is shown in Figure 4, where the k_{obs} values with $\Delta G^0_{et} < -0.53$ eV are not included because of the large uncertainty of the $k_{obs}^{-1} - k_{12}^{-1}$ values. From the intercept at $\Delta G^0_{et} = 0$, the λ value is obtained as 0.90 eV. The slope of the linear correlation in Figure 4 (0.48 $eV^{-1/2}$) agrees with the value expected from eq 13,

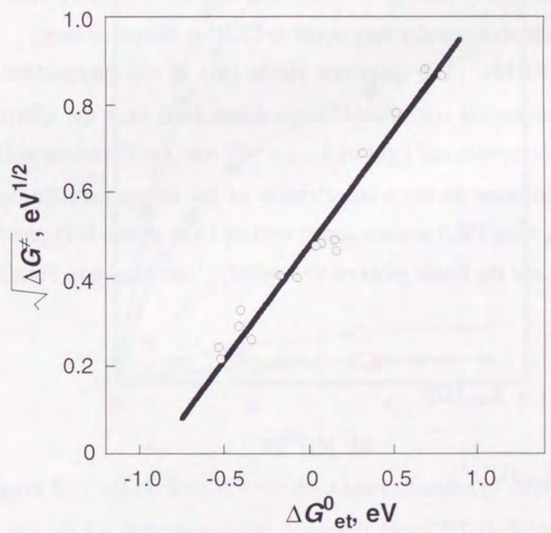

Figure 4. Plot of $(\Delta G^{\neq}_{et})^{1/2}$ ($= [kT\ln Z(k_{obs}^{-1} - k_{12}^{-1})]^{1/2}$) vs ΔG^0_{et} (see eq 13). The k_{obs} values with $\Delta G^0_{et} < -0.53$ eV in Table 6 are not included because of the large uncertainty of the $k_{obs}^{-1} - k_{12}^{-1}$ values.

$1/(2\lambda^{1/2}) = 0.48\ eV^{-1/2}$.

The dependence of k_{obs} on ΔG^0_{et} is calculated based on eq 13 using the λ value (0.89 eV) as shown by the solid line in Figure 3. The k_{obs} values with $\Delta G^0_{et} < -0.53$ eV which were not included in Figure 4 agree well with the calculated values except for the k_{obs} value at $\Delta G^0_{et} = -1.43$ eV, which is slightly larger than the calculated value (Figure 3). The calculated dependence of k_{obs} on ΔG^0_{et} (eq 13) predicts a decrease in the k_{obs} value from a diffusion limited value with increasing the driving force of electron transfer ($-\Delta G^0_{et}$) when the k_{et} values become smaller than the diffusion limited value in the Marcus inverted region ($\Delta G^0_{et} < -\lambda$), provided that the λ value is constant in a series of electron transfer reactions.[38] The absence of a Marcus inverted region has well been recognized in forward photoinduced electron transfer reactions.[35] In the case of back electron transfer reactions, however, the observation of the Marcus-inverted region has been well established.[41,42] The absence of an inverted region in forward photoinduced electron transfer reactions in the highly exergonic region ($\Delta G^0_{et} < -\lambda$) is explained by an increase in the λ value from the value for a contact radical ion pair (CRIP) or a solvent separated radical ion pair (SSRIP) which has a larger distance between the radical ions in the highly exergonic region.[41d,43] In the case of back electron transfer reactions, electron transfer may occur in CRIP as discussed later.

Quantum Yields. The quantum yields (Φ) of the photoaddition reactions of organometallic compounds with $AcrH^+$ were determined from the spectral change under irradiation of monochromatized light of $\lambda_{max} = 358$ nm (see Experimental). The Φ values increase with an increase in the concentration of the organometallic compound [D], to approach a limiting value (Φ_∞) in accordance with eq 14 as shown in Figure 5. Equation 14 is rewritten by eq 15 and the linear plots of Φ^{-1} and $[D]^{-1}$ are shown in Figure 6. From slopes and

$$\Phi = \Phi_\infty K_{obs}[D] / (1 + K_{obs}[D]) \quad (14)$$

$$\Phi^{-1} = \Phi_\infty^{-1}[1 + (K_{obs}[D])^{-1}] \quad (15)$$

intercepts are obtained the Φ_∞ and K_{obs} values. The K_{obs} values can be converted to the corresponding rate constants (k_{obs}) provided that the excited state of $AcrH^+$ involved in the photochemical reaction is singlet ($AcrH^{+*}$; $k_{obs} = K_{obs}\tau^{-1}$, $\tau = 37$ ns). The k_{obs} values were also obtained for the photoreduction of X-QuH^+ by $(TMS)_3SiH$ from the linear plots of Φ^{-1}

and $[(TMS)_3SiH]^{-1}$ (Figure 7). The k_{obs} values are listed in Table 6, where the k_{obs} values agree well with the corresponding values determined independently by the fluorescence quenching. Such agreement strongly indicates that the photoreduction of $AcrH^+$ and X-QuH^+ by organosilanes and organostannanes proceeds via photoinduced electron transfer from these organometallic compounds to the singlet excited states, $AcrH^{+*}$ and X-QuH^{+*}.

Regioreversal Addition via Photoinduced Electron Transfer. Based on the above results the reaction mechanism for the photoaddition reactions of allylic silanes and stannanes with $AcrH^+$ is summarized as shown representatively for the photoaddition of $Me_2C{=}CHCH_2SnBu_3$ with $AcrH^+$ (eq 3) in Scheme 1. The reaction is initiated by photoinduced electron transfer (k_{obs}) from the allylic stannane to the singlet excited state ($^1AcrH^{+*}$) to give the radical cation-acridinyl radical pair ($Me_2C{=}CCHCH_2SnBu_3^{\bullet+}$ $AcrH^{\bullet}$).

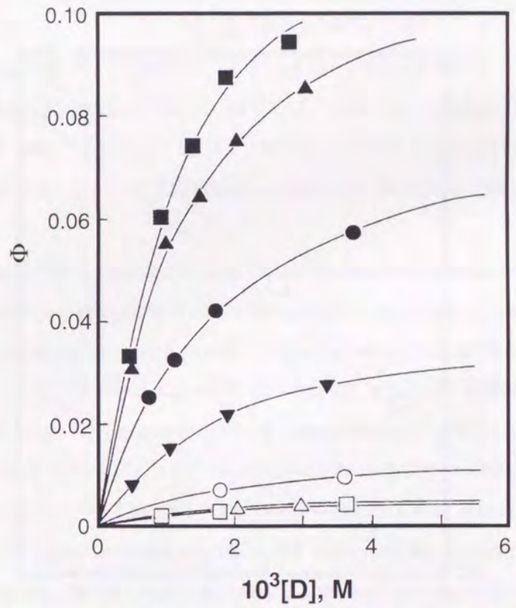

Figure 5. Plots of Φ vs [D] for the photoreduction of $AcrH^+$ (3.1×10^{-4} M) by organometallic donors [$CH_2{=}CHCH_2SiMe_3$ (Δ), $Me_2C{=}CHCH_2SiMe_3$ (□), $PhCH_2SiMe_3$ (○), $CH_2{=}CHCH_2SnPh_3$ (▼), $PhCH_2SnPh_3$ (●), $CH_2{=}CHCH_2SnBu_3$ (▲), $Me_2C{=}CHCH_2SnBu_3$ (■)] in deaerated MeCN at 298 K.

The metal-carbon bonds of radical cations of organostannanes and organosilanes are known to be cleaved to give the alkyl or allyl radicals.[15c,44-47] The bond cleavage has been shown to occur via an S_N2 reaction with a nucleophilic solvent such as MeCN (Scheme 1).[45-47] Thus, the radicals produced by the photoinduced electron transfer oxidation with $AcrH^{+*}$ may be coupled within the cage to yield the adducts selectively without dimerization of free $AcrH^{\bullet}$ radicals escaped from the cage, in competition with the back electron transfer to the ground state (k_{bet}). A similar mechanism has been proposed by Mariano et al. for the photoaddition reaction of allylic silanes with pyrrolinium ions.[1,2] The identical regiochemical outcome in the photoaddition of 1,1- and 3,3-dimethylallyl silanes to give the same adduct indicates that the free allyl radical produced by desilylation of the organosilane radical cation is responsible for the product formation step rather than the carbon-carbon bond formation between the organosilane radical cation and pyrrolidinyl radical.[1,2] If the free allyl radicals are

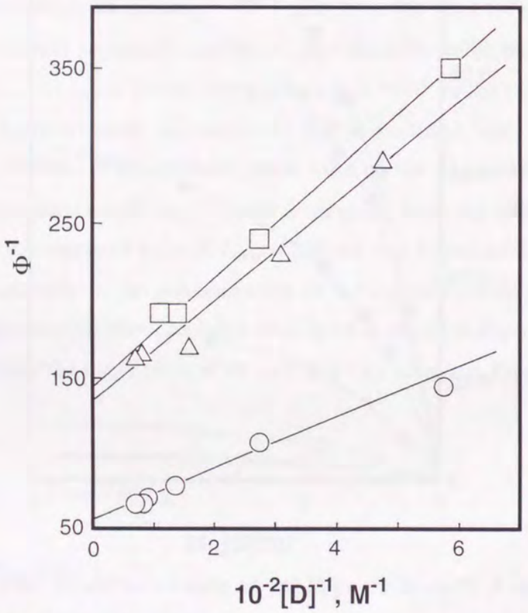

Figure 6. Plots of Φ^{-1} vs $[D]^{-1}$ for the photoreduction of $AcrH^+$ (3.1×10^{-4} M) by organometallic donors [CH_2=$CHCH_2SiMe_3$ (Δ), Me_2C=$CHCH_2$-$SiMe_3$ (□), $PhCH_2SiMe_3$ (○)] in deaerated MeCN at 298 K.

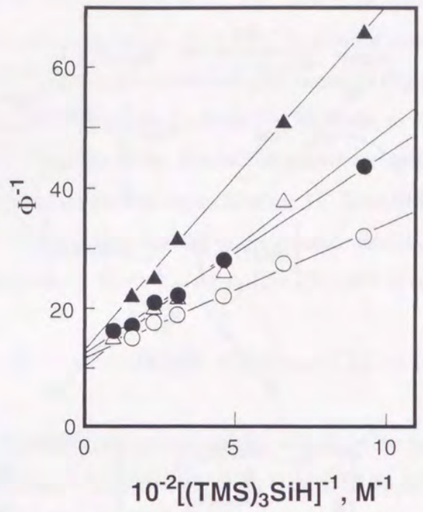

Figure 7. Plots of Φ^{-1} vs $[(TMS)_3SiH]^{-1}$ for the photoreduction of $AcrH^+$ (2.9×10^{-4} M) (○), QuH^+ (6.0×10^{-4} M) (●), 2-$MeQuH^+$ (6.0×10^{-4} M) (Δ) and 4-$MeQuH^+$ (6.0×10^{-4} M) (▲) by $(TMS)_3SiH$ in deaerated MeCN at 298 K.

responsible for the product formation step in the photoaddition reactions with $AcrH^+$, the regioselectivity would be independent of the metal moieties. Although the regioselectivity of photoaddition of prenylsilane with $AcrH^+$ is the same as that of the photoaddition with pyrrolinium ion (*i.e.*, the selective formation of γ-adduct, eq 2), the different regioselectivities are obtained in the case of photoaddition of unsymmetrical allylic stannanes (Table 1). Moreover, the ratios of the yields of the α- to γ-adducts vary depending on the substituents of allylic stannanes (Table 1).[48] Thus, the C-C bond formation may occur in the cage in which the trialkylmetal ion exists in proximity of $AcrH^{\bullet}$ affecting the regioselectivity for the C-C bond formation with the prenyl radical (Scheme 1). If the back electron transfer occurs in the cage as shown in Scheme 1, the decay of $AcrH^{\bullet}$ in the radical pair should follow first-order kinetics rather than second-order kinetics for the out-of-cage radicals. This was confirmed by the laser flash experiments (*vide infra*).

The direct observation of the radical pair of $AcrH^{\bullet}$ in Scheme 1 has been hampered due to the strong fluorescence of $AcrH^+$ exhibiting negative absorption at 488 nm in which the transient absorption spectrum of $AcrH^{\bullet}$ should be observed.[49]

Scheme 1

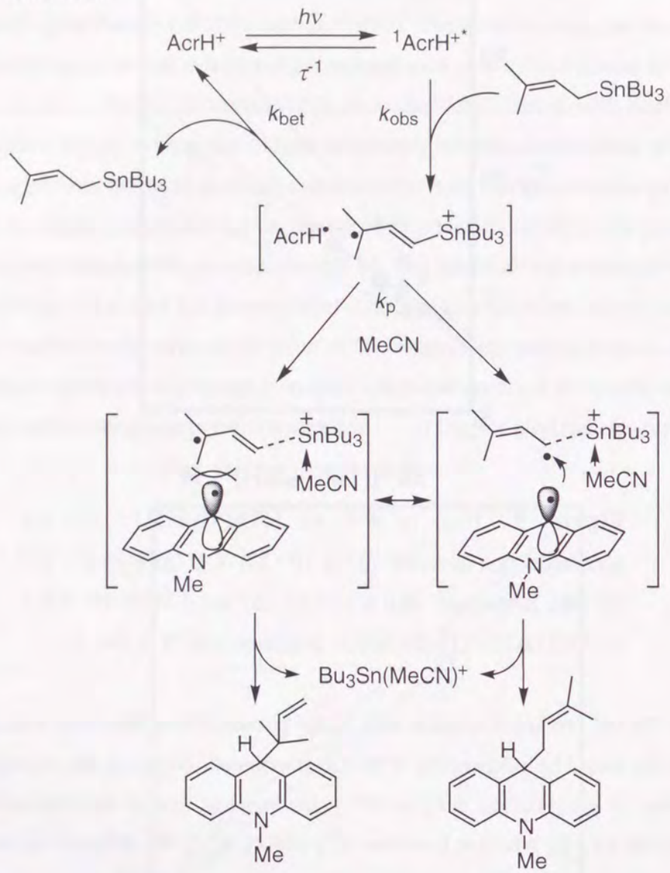

Thus, the back electron transfer in Scheme 1 should be sufficiently slow to be able to detect AcrH• produced in the photoinduced electron transfer reactions from organosilanes and organostannanes to AcrH+*. Laser flash irradiation (355 nm form a Nd:YAG laser) of AcrH+ (5.0×10^{-5} M) in deaerated MeCN solution containing CH_2=$CHCH_2SiMe_3$ and $PhCH_2SiMe_3$ gave transient absorption band at λ_{max} = 500 nm due to AcrH•,[49] as shown in Figure 8a and 8b, respectively. The absorption band due to $PhCH_2SiMe_3$•+ (λ_{max} = 530 nm)[47] is overlapped in Figure 8b. The formation of AcrH• in photoinduced electron transfer from $PhCH_2SiMe_3$ to AcrH+* is also confirmed by the ESR spectrum measured under irradiation of a frozen MeCN solution containing $PhCH_2SiMe_3$ and AcrH+ with a high-

pressure mercury lamp at 143 K (Figure 9).[50] The same ESR spectrum with the g value of 2.0032 was obtained by photoirradiation of an MeCN solution containing an electron donor (ferrocene) and AcrH+.[51,52] Thus, the observed ESR signal in Figure 9 is assigned to AcrH• produced by photoinduced electron transfer from $PhCH_2SiMe_3$ to AcrH+*. The absorption at λ = 500 nm decays obeying first-order kinetics as shown in insets of Figure 8 as expected for the back electron transfer within the cage (Scheme 1). Thus, the decay rate of the radical pair corresponds to the back electron transfer to the ground state (k_{bet}) and the bond-cleavage process (k_p) to yield the product. Since $k_{bet} >> k_p$ (*i.e.*, $\Phi_\infty << 1$ in eq 16), the first-order

$$\lambda = 2[-kT\ln(hk_{bet}/kT)] - \Delta G^0_{et} - [(\Delta G^0_{et} - 2[-kT\ln(hk_{bet}/kT)])^2 - (\Delta G^0_{et})^2]^{1/2} \quad (16)$$

decay rates in insets of Figure 8a and 8b correspond mainly to the back electron transfer from AcrH• to CH_2=$CHCH_2SiMe_3$•+ (k_{bet} = 2.9 x 10^7 s^{-1}) and $PhCH_2SiMe_3$•+ (k_{bet} = 7.9 x 10^7 s^{-1}), respectively.[53] From eq 12 is derived the reorganization energy of back electron transfer as given by eq 16. The λ values for the back electron transfer from AcrH• to CH_2=$CHCH_2SiMe_3$•+ and $PhCH_2SiMe_3$•+ are obtained from the k_{bet} values using eq 16 as 0.80 and 0.89 eV, respectively.[54] The λ values thus determined agree with the averaged λ value (0.90 eV) for forward photoinduced electron transfer from organosilanes and organostannanes (Figure 4).

According to Scheme 1, the quantum yield is expressed by eq 17, which agrees well with

$$\Phi = [k_p k_{obs}\,\tau/(k_p + k_{bet})]\,[D]/(1 + k_{obs}\,\tau\,[D]) \quad (17)$$

the experimental result (eq 14). The limiting quantum yield Φ_∞ is then expressed by eq 18,

$$\Phi_\infty = k_p/(k_p + k_{bet}) \quad (18)$$

where the competition between the rates of bond-cleavage of the organometallic radical cation (k_p) and the back electron transfer (k_{bet}) determines the limiting quantum yield. Thus, the small Φ_∞ values of organosilanes as compared to those of the organostannane counterparts shown in Table 6 may well be ascribed to the stronger Si-C bonds than the Sn-C bonds.[50] The faster back electron transfer from AcrH• to organosilane radical cations as expected from the more favorable energetics judging from the higher oxidation potentials of organosilanes

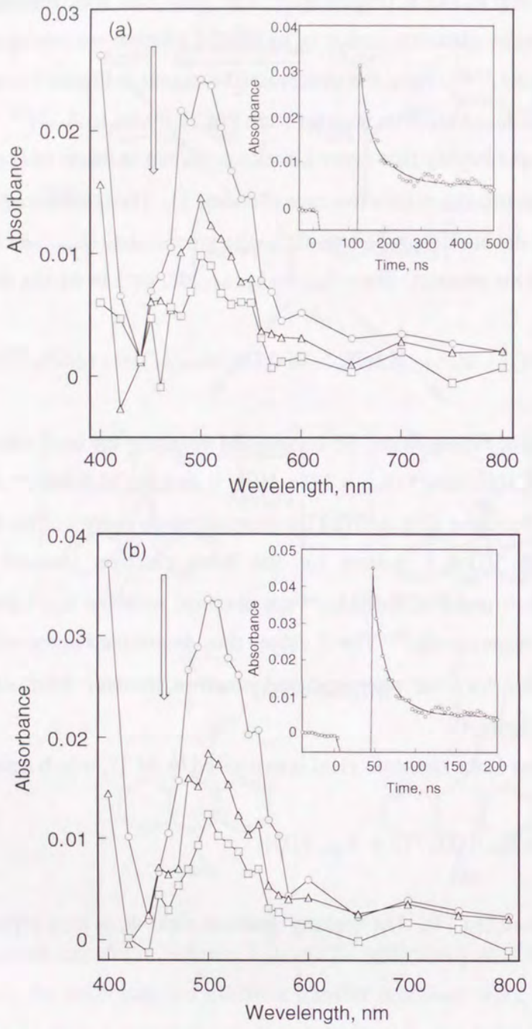

Figure 8. Transient absorption spectra observed in the photoreduction of $AcrH^+$ (1.7×10^{-4} M) with (a) $CH_2{=}CHCH_2SiMe_3$ (2.8×10^{-2} M) at 160 ns (○), 200 ns (Δ) and 650 ns (□) and (b) $PhCH_2SiMe_3$ (2.8×10^{-2} M) at 50 ns (○), 70 ns (Δ) and 100 ns (□) after laser excitation in deaerated MeCN at 298 K. Inset: Kinetic trace for $AcrH^•$ produced in the photoinduced electron transfer reactions from (a) $CH_2{=}CHCH_2SiMe_3$ and (b) $PhCH_2SiMe_3$ to $AcrH^{+*}$ at $\lambda = 500$ nm after laser excitation in deaerated MeCN at 298 K.

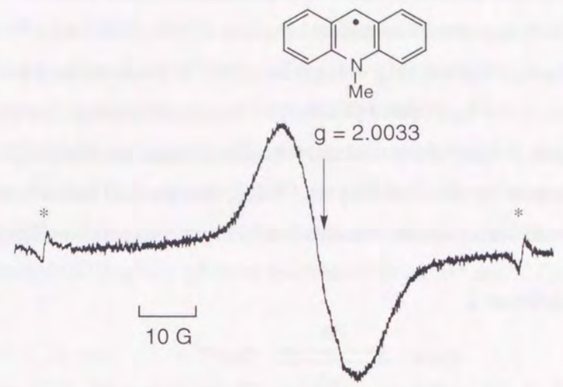

Figure 9. ESR spectrum of frozen MeCN containing $AcrH^+ClO_4^-$ (1.0×10^{-2} M) and $PhCH_2SiMe_3$ (5.0×10^{-2} M) with a high pressure mercury lamp at 143 K. The asterisk (*) denotes an Mn^{2+} ESR marker.

than those of organostannane counterparts may also contribute the smaller Φ_∞ values.

The photoreduction of X-QuH^+ by $(TMS)_3SiH$ may also occur *via* photoinduced electron transfer from $(TMS)_3SiH$ to ^{1}X-QuH^{+*} as shown representatively for the reaction between $(TMS)_3SiH$ and QuH^+ in Scheme 2. The reaction is initiated by photoinduced electron transfer from $(TMS)_3SiH$ to $^1QuH^{+*}$ to give the metal hydride radical cation-quinolinyl radical pair, followed by the hydrogen transfer in the cage, in competition with the back electron transfer to the reactant pair, to yield the hydride adduct selectively without dimerization of free $QuH^•$ radicals escaped from the cage.

According to Scheme 2, the dependence of Φ on the $(TMS)_3SiH$ concentration may be expressed by eq 19, where k_{obs} and k_{bet} are the rate constants of photoinduced electron transfer

$$\Phi = [k_H k_{obs}\tau / (k_H + k_{bet})]\,[(TMS)_3SiH] / (1 + k_{obs}\tau\,[(TMS)_3SiH]) \qquad (19)$$

and the back electron transfer, respectively, τ is the lifetime of ^{1}X-QuH^{+*} and k_H is the rate constant of hydrogen transfer from $(TMS)_3SiH^{•+}$ to X-$QuH^•$. The existence of rate-determining hydrogen transfer step following the photo-induced electron transfer in Scheme

2 is confirmed by the deuterium isotope effect determined as $\Phi_H/\Phi_D = 1.9$ (in Table 6) from the ratio of the limiting quantum yields (Φ_∞) of $(TMS)_3SiH$ and $(TMS)_3SiD$, which corresponds to $(k_H/k_D)[(k_D + k_b)/(k_H + k_{bet})]$ in eq 19. In contrast, no kinetic isotope effect has been observed in the k_{obs} values (Table 6). Similar Φ_∞ values irrespective of methyl substituents in Table 6 show sharp contrast with the diminished reactivity of 2-MeQuH$^+$ in the thermal reduction by Bu_3SnH (eq 6). Thus, the thermal reduction of X-QuH$^+$ by Bu_3SnH may proceed *via* a polar mechanism exhibiting the significant steric effect of

Scheme 2

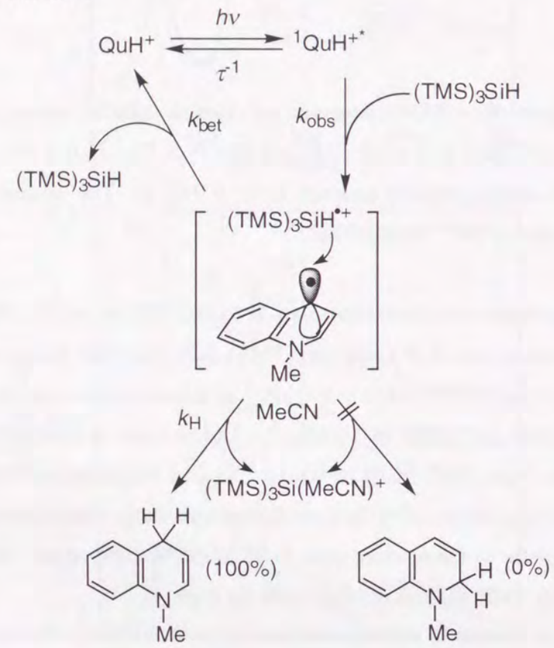

methyl group at the C-2 carbon where the C-H bond is formed with X-QuH$^+$. In contrast, no significant steric effects have been observed in the photochemical reactions *via* the photoinduced electron transfer. The spin density of QuH$^\bullet$ with the optimized geometry is calculated using density functional theory at the Becke3LYP/6-31+G* level (see Experimental Section).[26,27] Since the spin density of QuH$^\bullet$ is greatest at the C-4 position (0.54) as compared to the value at the C-2 position (0.39), the hydrogen transfer from the metal hydride radical cation to QuH$^\bullet$ occurs at the C-4 position to yield the corresponding

1,4-isomer exclusively.[55] In contrast to the spin density, the MP2/6-31++G* calculation indicates that the charge density of QuH$^+$ is greatest at the C-2 position (0.16) as compared to the value at the C-4 position (0.003).[56] Thus, the nucleophilic attack of Bu_3SnH occurs at the C-2 position to yield the corresponding 1,2-isomer selectively.

In conclusion, the photoinduced electron transfer from organosilanes and organostannanes to AcrH^{+*} and X-QuH^{+*} provides a unique reaction pathway for regioselective addition of organosilanes and organostannanes, which is reversed in the corresponding thermal nucleophilic addition reactions with AcrH$^+$ and X-QuH$^+$.

References

(1) (a) Mariano, P. S. *Photoinduced Electron Transfer*; Fox, M. A., Chanon, M., Ed.; Elsevier: Amsterdam, 1988; Part C, p.372. (b) Mariano, P. S. *Acc. Chem. Res.* **1983**, *16*, 130. (c) Mariano, P. S. *Synthetic Organic Chemistry*; Horspool, W. M., Ed.; Plenum Press: London, 1984.

(2) (a) Ohga, K.; Mariano, P. S. *J. Am. Chem. Soc.* **1982**, *104*, 617. (b) Ohga, K.; Yoon, U. C.; Mariano, P. S. *J. Org. Chem.* **1984**, *49*, 213. (c) Su, Z.; Mariano, P. S.; Falvey, D. E.; Yoon, U. C.; Oh, S. W. *J. Am. Chem. Soc.* **1998**, *120*, 10676. (d) Takahashi, Y.; Miyashi, T.; Yoon, U. C.; Oh, S. W.; Mancheno, M.; Su, Z.; Falvey, D. F.; Mariano, P. S. *J. Am. Chem. Soc.* **1999**, *121*, 3926.

(3) (a) Mattes, S. L.; Farid, S. *Acc. Chem. Res.* **1982**, *15*, 80. (b) Eaton, D. F. *J. Am. Chem. Soc.* **1980**, *102*, 3278, 3280. (c) Lan, J. Y.; Schuster, G. B. *Advances in Electron Transfer Chemistry*; Mariano, P. S. Ed.; JAI Press: Greenwich, 1991; Vol. 1.

(4) (a) Fukuzumi, S. *Electron Transfer in Chemistry*, Vol. 5; Balzani, V., Ed.; Wiley-VCH: Weinheim, **2000**, in press. (b) Fukuzumi, S. *Bull. Chem. Soc. Jpn.* **1997**, *70*, 1. (c) Fukuzumi, S.; Itoh, S. *Advances in Photochemistry*, Vol. 25; Neckers, D. C.; Volman, D. H.; von Bünau, G., Eds.; Wiley: New York, 1998, pp 107-172.

(5) (a) Sakurai, H.; Sakamoto, K.; Kira, M. *Chem. Lett.* **1984**, 1213. (b) Nakadaira, Y.; Komatsu, N.; Sakurai, H. *Chem. Lett.* **1985**, 1781. (c) Mizuno, K.; Ikeda, M.; Otsuji, Y. *Tetrahedron Lett.* **1985**, *26*, 461. (d) Mizuno, K.; Kobata, T.; Maeda, R.; Otsuji, Y. *Chem. Lett.* **1990**, 1821. (e) Fukuzumi, S.; Kitano, T.; Mochida, K. *Chem. Lett.* **1989**, 2177. (f) Fukuzumi, S.; Kitano, T.; Mochida, K. *Chem. Lett.* **1990**, 1774. (g) Fukuzumi, S.; Kitano, T.; Mochida, K. *J. Chem. Soc., Chem. Commun.* **1990**, 1236.

(6) (a) Fukuzumi, S.; Fujita, M.; Otera, J.; Fujita, Y. *J. Am. Chem. Soc.* **1992**, *114*, 10271.

(b) Fukuzumi, S.; Okamoto, T.; Otera, J. *J. Am. Chem. Soc.* **1994**, *116*, 5503. (c) Mikami, K.; Matsumoto, S.; Ishida, A.; Takamuku, S.; Suenobu, T.; Fukuzumi, S. *J. Am. Chem. Soc.* **1995**, *117*, 11134. (d) Mikami, K.; Matsumoto, S.; Okubo, Y.; Fujitsuka, M.; Ito, O.; Suenobu, T.; Fukuzumi, S. *J. Am. Chem. Soc.* **2000**, *122*, 2236.

(7) (a) Yamamoto, H. *Lewis Acid Chemistry: A Practical Approach*; Oxford University Press: Oxford, 1999. (b) *Selectivities in Lewis Acid Promoted Reactions*; Schinzer, D., Ed.; Kluwer Academic Publishers: Dordrecht, The Netherlands, 1989. (c) Santelli, M.; Pons, J.-M. *Lewis Acids and Selectivity in Organic Synthesis*; CRC Press: Boca Raton, FL, 1995.

(8) (a) Colvin, E. W. *Silicon in Organic Synthesis*; Butterworths: London, 1981. (b) Mukaiyama, T. *Angew, Chem., Int. Ed. Engl.* **1977**, *16*, 817. (c) Mukaiyama, T.; Murakami, M. *Synthesis* **1987**, 1043. (d) Gennari, C. *Selectivities in Lewis Acid Promoted Reactions*; Schinzer, D. Ed.; Kluwer Academic Publ.: Dordrecht, 1989; Chapter 4, p 53. (e) Heathcock, C. H. *Aldrichim. Acta* **1990**, *23*, 99. (f) Hosomi, A. *Acc. Chem. Res.* **1988**, *21*, 200.

(9) (a) Yamamoto, Y. *Acc. Chem. Res.* **1987**, *20*, 243. (b) Naruta, Y. *J. Am. Chem. Soc.* **1980**, *102*, 3774.

(10) (a) Davies, A. G. *Organotin Chemistry*; VCH: Weinheim, Germany, 1997; p 327. (b) Smith, P. J., Ed. *Chemistry of Tin, 2nd ed.*; Blackie: London, U. K., 1997; p 578.

(11) (a) Kursanov, D. N.; Parnes, Z. N.; Loim, N. M. *Synthesis* **1974**, 633. (b) Weber, W. P. In *Silicon Reagents for Organic Synthesis*; Springer-Verlag: London, 1983. (c) Corey, J. Y.; Braddock-Wilking, J. *Chem. Rev.* **1999**, *99*, 175.

(12) (a) Neumann, W. P. *Synthesis* **1987**, 665. (b) Curran, D. P. *Synthesis* **1988**, 417. (c) Jasperse, C. P.; Curran, D. P.; Fevig, T. L. *Chem. Rev.* **1991**, *91*, 1237. (d) Giese, B. *Radicals in Organic Synthesis: Formation of Carbon-Carbon Bonds*; Pergamon Press: Oxford, U.K., 1986. (d) Ryu, I.; Sonoda, N.; Curran, D. P. *Chem. Rev.* **1996**, *96*, 177. (e) Komatsu, M.; Ryu, I. *Chem. Rev.* **1999**, *99*, 1991.

(13) Chatgilialoglu, C. *Acc. Chem. Res.* **1992**, *25*, 188.

(14) (a) Kochi, J. K. *Organometallic Mechanisms and Catalysis*; Academic Press: New York, 1978; p. 501. (b) Klingler, R. J.; Mochida, K.; Kochi, J. K. *J. Am. Chem. Soc.* **1979**, *101*, 6626. (c) Yang, D.; Tanner, D. D. *J. Org. Chem.* **1986**, *51*, 2267.

(15) (a) Stout, D. M.; Meyer, A. I. *Chem. Rev.* **1982**, *82*, 223. (b) Fukuzumi, S.; Tanaka, T. *Photoinduced Electron Transfer*; Fox, M. A., Chanon, M., Ed.; Elsevier: Amsterdam,

1988; Part C, p. 578. (c) Fukuzumi, S. *Advances in Electron Transfer Chemistry*; Mariano, P. S. Ed.; JAI Press: Greenwich, 1992; Vol. 2, p 65.

(16) (a) Franke, M.; Steckhan, E. *Angew. Chem., Int. Ed. Engl.* **1988**, *27*, 265. (b) Westerhausen, D.; Herrmann, S.; Hummel, W.; Steckhan, E. *Angew. Chem., Int. Ed. Engl.* **1992**, *31*, 1529. (c) Ishitani, O.; Inoue, N.; Koike, K.; Ibusuki, T. *J. Chem. Soc., Chem. Commun.* **1994**, 367.

(17) A preliminary report has appeared: Fukuzumi, S.; Fujita, M.; Otera, J. *J. Chem. Soc., Chem. Commun.* **1993**, 1536.

(18) Roberts, R. M. G.; Ostović , D.; Kreevoy, M. M. *Faraday Discuss. Chem. Soc.* **1982**, *74*, 257.

(19) Fukuzumi, S.; Koumitsu, S.; Hironaka, K.; Tanaka, T. *J. Am. Chem. Soc.* **1987**, *109*, 305.

(20) Hosomi, A.; Shirahata, A.; Sakurai, H. *Chem. Lett.* **1978**, 901.

(21) Fukuzumi, S.; Tokuda, Y.; Kitano, T.; Okamoto, T.; Otera, J. *J. Am. Chem. Soc.* **1993**, *115*, 8960.

(22) Perrin, D. D.; Armarego, W. L. F. *Purification of Laboratory Chemicals*; Butterworth-Heinemann: Oxford, 1988.

(23) (a) Ishikawa, K.; Fukuzumi, S.; Goto, T.; Tanaka, T. *J. Am. Chem. Soc.* **1990**, *112*, 1578. (b) Fukuzumi, S.; Ishikawa, K.; Hironaka, K.; Tanaka, T. *J. Chem. Soc., Perkin Trans. 2* **1987**, 751.

(24) (a) Hatchard, C. G.; Parker, C. A. *Proc. R. Soc. London, Ser. A* **1956**, *235*, 518. (b) Calvert, J. C.; Pitts, J. N. *Photochemistry*; Wiley: New York, 1966; p 783.

(25) Sterwart, J. J. P. *J. Comput. Chem.* **1989**, *10*, 209, 221.

(26) (a) Becke, A. D. *J. Chem. Phys.* **1993**, *98*, 5648. (b) Lee, C.; Yang, W.; Parr, R. G. *Phys. Rev. B* **1988**, *37*, 785.

(27) Hehre, W. J.; Radom, L.; Schleyer, P. v. R.; Pople, J. A. *Ab Initio Molecular Orbital Theory*; Wiley: New York, 1986.

(28) Frisch, M. J.; Trucks, G. W.; Schlegel, H. B.; Scuseria, G. E.; Robb, M. A.; Cheeseman, J. R.; Zakrzewski, V. G.; Montgomery, J. A., Jr.; Stratmann, R. E.; Burant, J. C.; Dapprich, S.; Millam, J. M.; Daniels, A. D.; Kudin, K. N.; Strain, M. C.; Farkas, O.; Tomasi, J.; Barone, V.; Cossi, M.; Cammi, R.; Mennucci, B.; Pomelli, C.; Adamo, C.; Clifford, S.; Ochterski, J.; Petersson, G. A.; Ayala, P. Y.; Cui, Q.; Morokuma, K.; Malick, D. K.; Rabuck, A. D.; Raghavachari, K.; Foresman, J. B.; Cioslowski, J.; Ortiz,

J. V.; Baboul, A. G.; Stefanov, B. B.; Liu, G.; Liashenko, A.; Piskorz, P.; Komaromi, I.; Gomperts, R.; Martin, R. L.; Fox, D. J.; Keith, T.; Al-Laham, M. A.; Peng, C. Y.; Nanayakkara, A.; Gonzalez, C.; Challacombe, M.; Gill, P. M. W.; Johnson, B.; Chen, W.; Wong, M. W.; Andres, J. L.; Gonzalez, C.; Head-Gordon, M.; Replogle, E. S.; Pople, J. A. *Gaussian 98 (Revision A.7)* Gaussian, Inc.; Pittsburgh PA, 1998.

(29) Fukuzumi, S.; Kuroda, S.; Tanaka, T. *J. Chem. Soc., Chem. Commun.* **1987**, 120.

(30) (a) Roberts, R. M. G.; Ostović , D.; Kreevoy, M. M. *J. Org. Chem.* **1983**, *48*, 2053. (b) Romoff, T. T.; Sampson, N. S.; van Eikeren, P. *J. Org. Chem.* **1987**, *52*, 4454. (c) Kim, D.; Lee, I.-S. H.; Kreevoy, M. M. *J. Am. Chem. Soc.* **1990**, *112*, 1889.

(31) (a) Fujita, M.; Hiyama, T. *J. Org. Chem.* **1988**, *53*, 5405. (b) Corriu, R. J. P.; Perz, R.; Reye, C. *Tetrahedron* **1983**, *39*, 999. (c) Fujita, M.; Hiyama, T. *J. Am. Chem. Soc.* **1984**, *106*, 4629. (d) Fujita, M.; Hiyama, T. *J. Am. Chem. Soc.* **1985**, *107*, 8294.

(32) (a) Fujita, M.; Ishida, A.; Takamuku, S.; Fukuzumi, S. *J. Am. Chem. Soc.* **1996**, *118*, 8566. (b) Fujita, M.; Fukuzumi, S. *J. Chem. Soc., Perkin Trans. 2* **1993**, 1915.

(33) Fukuzumi, S.; Noura, S. *J. Chem. Soc., Chem. Commun.*, **1994**, 287.

(34) The one-electron reduction potentials of $AcrH^{+*}$, QuH^{+*}, 2-$MeQuH^{+*}$ and 4-$MeQuH^{+*}$ were determined from the one-electron reduction potentials of the ground state[33] and the excitation energies, which are obtained from the frequencies of the absorption and emission maxima.[15b]

(35) (a) Rehm, A.; Weller, A. *Ber. Bunsenges Phys. Chem.* **1969**, *73*, 834. (b) Rehm, A.; Weller, A. *Isr. J. Chem.* **1970**, *8*, 259.

(36) When A^* is replaced by A, eq 10 is also applied for thermal electron transfer reactions.

(37) In eq 10, the back electron transfer to the excited state is neglected when the back electron transfer to the ground state is much faster than the back electron transfer to the excited state.

(38) (a) Marcus, R. A. *Annu. Rev. Phys. Chem.* **1964**, *15*, 155. (b) Marcus, R. A. *J. Chem. Phys.* **1956**, *24*, 966. (c) Marcus, R. A. *Angew. Chem., Int. Ed. Engl.* **1993**, *32*, 1111.

(39) For nonadiabatic electron transfer, see: Marcus, R. A.; Sutin, N. *Biochim. Biophys. Acta* **1985**, *811*, 265.

(40) In eq 12, the work term of the product ions is neglected, since an electrostatic interaction in the radical ion pair is known to be small in a polar solvent such as MeCN.

(41) (a) Closs, G. L.; Miller, J. R. *Science* **1988**, *240*, 440. (b) Miller, J. R.; Calcaterra, L. T.; Closs, G. L. *J. Am. Chem. Soc.* **1984**, *106*, 3047. (c) Asahi, T.; Mataga, N. *J. Phys. Chem.* **1989**, *93*, 6575. (d) Gould, I. R.; Ege, D.; Moser, J. E.; Farid, S. *J. Am. Chem. Soc.* **1990**, *112*, 4290. (e) Gould, I. R.; Farid, S. *Acc. Chem. Res.* **1996**, *29*, 522.

(42) (a) McLendon, G. *Acc. Chem. Res.* **1988**, *21*, 160. (b) Winkler, J. R.; Gray, H. B. *Chem. Rev.* **1992**, *92*, 369. (c) McLendon, G.; Hake, R. *Chem. Rev.* **1992**, *92*, 481. (d) Mataga, N.; Miyasaka, H. *Electron Transfer from Isolated Molecules to Biomolecules Part 2*; Jortner, J., Bixon, M., Ed.; Wiley: New York, 1999, p 431.

(43) (a) Rau, H.; Frank, R.; Greiner, G. *J. Phys. Chem.* **1986**, *90*, 2476. (b) Stevens, B.; Biver, C. J., III; McKeithan, D. N. *Chem. Phys. Lett.* **1991**, *187*, 590. (c) Kikuchi, K.; Takahashi, Y.; Katagiri, T.; Niwa, T.; Hoshi, M.; Miyashi, T. *Chem. Phys. Lett.* **1991**, *180*, 403.

(44) (a) Fukuzumi, S.; Mochida, K.; Kochi, J. K. *J. Am. Chem. Soc.* **1979**, *101*, 5961. (b) Fukuzumi, S.; Wong, C. L.; Kochi, J. K. *J. Am. Chem. Soc.* **1980**, *102*, 2928.

(45) Dinnocenzo, J. P.; Farid, S.; Goodman, J. L.; Gould, L. R.; Todd, W. P. *Mol. Cryst. Liq. Cryst.* **1991**, *194*, 151.

(46) (a) Cermenati, L.; Freccero, M.; Venturello, P.; Albini, A. *J. Am. Chem. Soc.* **1995**, *117*, 7869. (b) Dinnocenzo, J. P.; Farid, S.; Goodman, J. L.; Gould, I. R.; Todd, W. P.; Mattes, S. L. *J. Am. Chem. Soc.* **1989**, *111*, 8973.

(47) Dockery, K. P.; Dinnocenzo, J. P.; Farid, S.; Goodman, J. L.; Gould, I. R.; Todd, W. P. *J. Am. Chem. Soc.* **1997**, *119*, 1876.

(48) In the case of $Me_2C{=}CHCH_2Sn(cyc\text{-}C_6H_{11})_3$, the $cyc\text{-}C_6H_{11}$-Sn bond is also cleaved to give the adduct, $AcrH(cyc\text{-}C_6H_{11})$ (Table 1). However, cleavage of the $Me_2C{=}CHCH_2$-Sn bond is much more favored than the $cyc\text{-}C_6H_{11}$-Sn bond when the statistical factor is taken into account.

(49) (a) Peters, K. S.; Pang, E.; Rudzki, J. *J. Am. Chem. Soc.* **1982**, *104*, 5535. (b) Poulos, A. T.; Hammond, G. S.; Burton, M. E. *Photochem. Photobiol.* **1981**, *34*, 169.

(50) Butcher, E.; Rhodes, C. J.; Standing, M.; Davidson, R. S.; Bowser, R. *J. Chem. Soc., Perkin Trans. 2* **1992**, 1469.

(51) The ESR signal due to $PhCH_2SiMe_3^{\bullet+}$ may be overlapped with the $AcrH^{\bullet}$ signal, since the *g* value of $PhCH_2SiMe_3^{\bullet+}$ (2.003)[50] is nearly the same as the value of $AcrH^{\bullet}$. The detected radicals are stable after cutting off the light at 143 K. This indicates that an intermolecular electron transfer occurs after the photoinduced electron transfer from the organosilane to $AcrH^{+*}$ to give the organosilane radical cation and $AcrH^{\bullet}$, which are separated with a long distance at 143 K, preventing the back electron transfer to the

ground state.

(52) The ESR signal due to ferricenium ion was too broad to be detected under the present experimental conditions.

(53) The k_{bet} value is apparently inconsistent with the large second-order rate constant of the Si-C bond cleavage of $PhCH_2SiMe_3^{\bullet+}$ with MeCN (3.2×10^9 M^{-1} s^{-1}) in dichloromethane, which leads to a short lifetime of the free radical cation ($PhCH_2SiMe_3^{\bullet+}$) in neat MeCN (< 10^{-9} s).[47] However, the Si-C bond cleavage rate of $PhCH_2SiMe_3^{\bullet+}$ in the cage (Scheme 1) may be much slower than the rate for the free radical cation to ensure the observed back electron transfer from $AcrH^{\bullet}$ to $PhCH_2SiMe_3^{\bullet+}$ in the cage, since the Si-C bond cleavage rate has been shown to be very sensitive to the steric nature of the alkyl substituents at silicon.[47]

(54) The ΔG^0_{bet} values of back electron transfer from $AcrH^{\bullet}$ to $CH_2{=}CHCH_2SiMe_3^{\bullet+}$ and $PhCH_2SiMe_3^{\bullet+}$ are -1.93 and -1.86 eV (obtained from the E^0_{ox} value of $AcrH^{\bullet}$ and the E^0_{ox} values of $CH_2{=}CHCH_2SiMe_3$ and $PhCH_2SiMe_3$),[6a,19] respectively and these are in the Marcus inverted region ($\Delta G^0_{bet} < -\lambda$). The other solution of eq 16 gives a λ value in the normal region ($\Delta G^0_{bet} > -\lambda$), which is inconsistent with the results on the forward electron transfer reactions in Figure 3.

(55) In the photochemical reduction of QuH^+ by $(TMS)_3SiH$, no thermal isomerization of 1,4-QuH_2 to 1,2-QuH_2 was observed. The thermal isomerization rate is shown to be sensitive to the type of metal hydrides used as hydride donors (see Table 4).

(56) The semiempirical MNDO calculation gave a similar result: the charge density of QuH^+ is greatest at the C-2 position (0.18) as compared to the value at the C-4 position (0.098).

Section 3. 4

Comparison between Electron Transfer and Nucleophilic Reactivities of Ketene Silyl Acetals with Cationic Electrophiles

Abstract: The products and kinetics for the reactions of ketene silyl acetals with a series of *p*-methoxy substituted trityl cations have been examined and they are compared with those of outer-sphere electron transfer reactions from 10,10'-dimethyl-9,9',10,10'-tetrahydro-9,9'-biacridine [$(AcrH)_2$] to the same series of trityl cations as well as other electron acceptors. The C-C bond formation in the reaction of β,β-dimethyl-substituted ketene silyl acetal (**1**: $Me_2C{=}C(OMe)OSiMe_3$) with trityl cation salt ($Ph_3C^+ClO_4^-$) takes place between **1** and the carbon of *para*-position of phenyl group of Ph_3C^+, whereas a much less sterically hindered ketene silyl acetal (**3**: $H_2C{=}C(OEt)OSiEt_3$) reacts with Ph_3C^+ at the central carbon of Ph_3C^+ The kinetic comparison indicates that the nucleophilic reactivities of ketene silyl acetals are well correlated with the electron transfer reactivities provided that the steric demand at the reaction center for the C–C bond formation remains constant.

Introduction

Carbon-carbon bond formation reactions of organosilanes have found considerable interest in organic synthesis.[1-4] The nucleophilic reactivities of organosilanes in polar reactions have been evaluated extensively based on the rate constants for the reactions with carbocations.[5-7] On the other hand, the electron transfer reactivities of organosilanes have been determined based on the rate constants for the electron transfer reactions with one-electron oxidants.[8-10] The importance of electron transfer processes has now been well recognized in many areas of chemistry.[11-13] It has previously been shown that nucleophilic reactivities are largely correlated with the one-electron oxidation potentials of nucleophiles, which are one of the most important factors to determine the electron transfer reactivities.[14] However, the nucleophilic reactivity is often affected by the steric demand at the reaction center.[8] In the case of ketene silyl acetals, β-methyl-substitution increases the electron transfer reactivity whereas an increase in the steric demand would affect the nucleophilic reactivity.[8] Thus, an exact comparison between the nucleophilic and electron transfer reactivities of ketene silyl acetals should be made by using the same series of electrophiles or electron acceptors in order to keep the steric demand at the reaction center constant.

This study reports products and kinetics for the reactions of β,β-dimethyl-substituted ketene silyl acetal and a much less sterically hindered ketene silyl acetal with a series of *p*-methoxy substituted trityl cations $[(MeOC_6H_4)_x(C_6H_5)_{(3-x)}C^+]$ (x = 0–3) and these data are directly compared with those of outer-sphere electron transfer reactions from 10,10'-dimethyl-9,9',10,10'-tetrahydro-9,9'-biacridine $[(AcrH)_2]$[15] to the same series of trityl cations as well as other electron acceptors. The present study provides valuable insight into the electron transfer vs nucleophilic reactivities of ketene silyl acetals.

Results and Discussion

The reactions of β,β-dimethyl-substituted ketene silyl acetal (**1**) with less sterically hindered benzhydryl cation salts $Ar_2CH^+X^-$ (X = BF_4 or OTf) as compared to trityl cation are known to produce the corresponding esters in which the central carbon of benzhydryl cation is connected to **1** via nucleophilic addition of **1** to benzhydryl cation followed by the facile desilylation of the intermediate siloxy substituted carbenium ion as shown in Scheme 1.[5,6] In contrast, we have found that C–C bond formation in the reaction of **1** with trityl

Scheme 1

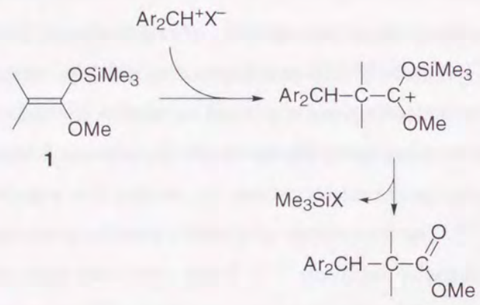

cation salt ($Ph_3C^+ClO_4^-$) takes place between **1** and the carbon of *para*-position of phenyl group of Ph_3C^+ (see Experimental Section) rather than the central carbon to yield a different type of ester **2** (eq 1).

When **1** is replaced by a much less sterically hindered ketene silyl acetal (**3**: $H_2C{=}C(OEt)OSiEt_3$), C–C bond formation occurs at the central carbon of Ph_3C^+ (eq 2).[8] Thus, the steric demand at the reaction center for the C–C bond formation results

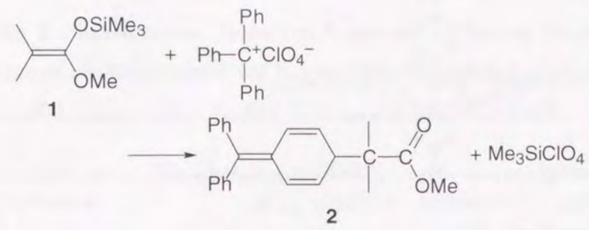

(1)

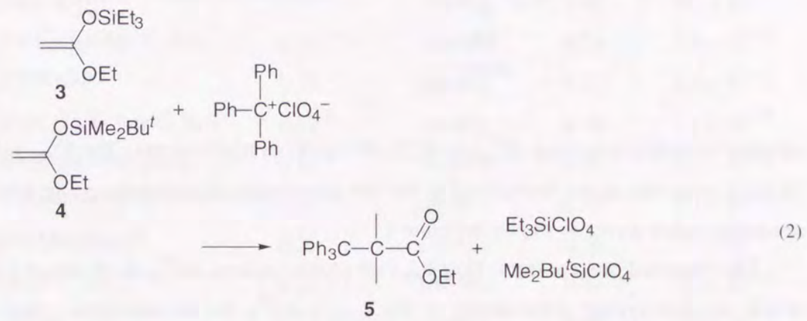

(2)

in a change in the type of products. In order to examine the contribution of an electron transfer pathway in the reactions of ketene silyl acetals with trityl cations, the rates were determined by using a stopped-flow technique and the observed rate constants are compared with those of outer-sphere electron transfer reactions from $(AcrH)_2$ to the same series of trityl cations as well as other electron acceptors.

The reactions of $(AcrH)_2$ with various electron acceptors including trityl cations are known to occur via an outer-sphere electron transfer from $(AcrH)_2$ to the acceptors, followed by the facile C–C bond cleavage to produce $AcrH^•$ which can rapidly transfer an electron to the acceptors to yield two equivalents of $AcrH^+$ and trityl radical (eq 3).[15]

Trityl radical produced was detected by the ESR spectrum. The electron transfer rates were determined from the appearance of absorbance due to $AcrH^+$ (λ_{max} = 358 nm, ε_{max} = 18000 M^{-1} cm^{-1}) as reported previously.[15] The rates obey second-order kinetics, showing first-order dependence on each reactant concentration. The observed second-order rate constants (k_{obs}) of electron transfer from $(AcrH)_2$ to a variety of one-electron oxidants are listed in Table 1. The free energy change of electron transfer (ΔG^0_{et} in eV) was determined from the one-electron oxidation potential of $(AcrH)_2$ (E^0_{ox} = 0.62 V vs SCE)[15] and the one–

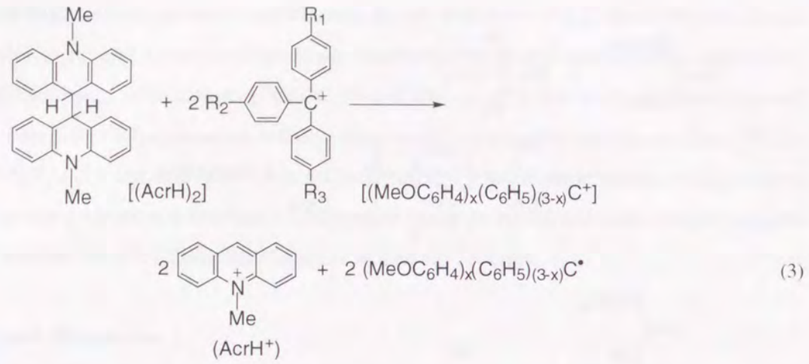

(3)

electron reduction potentials (E^0_{red} vs SCE) of a series of trityl cations. The E^0_{red} values of a series of trityl cations are determined by the fast scanning cyclic voltammograms which show reversible redox waves as shown in Figure 1.

The observed rate constants (log k_{obs}) are plotted against ΔG^0_{et} as shown in Figure 2a, which exhibits typical dependence of log k_{obs} vs ΔG^0_{et} for an endergonic outer-sphere electron transfer, *i.e.*, log k_{obs} increases linearly with increasing ΔG^0_{et} with a slope of $-1/2.3kT$ (= –16.9 at 298 K, k is the Boltzmann constant).

The rates of reactions of ketene silyl acetals with trityl cations were determined from the disappearance of absorbance due to trityl cations (*e.g.*, $Ph_3C^+ClO_4^-$; λ_{max} = 400 nm, ε_{max} = 3800 M^{-1} cm^{-1}) as shown in Figure 3. The disappearance rate obey pseudo-first-order kinetics in the presence of large excess ketene silyl acetal (see inset in Figure 3) and the pseudo-first-order rate constants increases linearly with increasing ketene silyl acetal concentration. The observed second-order rate constants determined from the slope of plots of the pseudo-first-order rate constant vs ketene silyl acetal concentration are also listed in Table 1.

The ΔG^0_{et} values for electron transfer from ketene silyl acetals to trityl cations were determined from the E^0_{ox} values of ketene silyl acetals[8b,16] and the E^0_{red} values of trityl cations. A plot of log k_{obs} vs ΔG^0_{et} for the reactions of **1** with trityl cations shown in Figure 2b has a good parallel linear correlation with the plot for outer-sphere electron transfer reactions from $(AcrH)_2$ to trityl cations (Figure 2a). The slope is almost identical between these two different types of reactions: one is the addition of **1** to trityl cations and the other is the outer-sphere electron transfer. However, it is unlikely that the addition of **1** to

Table 1. One-Electron Reduction Potentials of Various Oxidant, and free energy change of electron transfer (ΔG^0_{et}) and Rate Constant (k_{obs}) in the Reaction of Trityl Cation Derivatives with $(AcrH)_2$ in Deaerated MeCN at 298 K.

no.	oxidant	E^0_{red} vs SCE, V	reductant	ΔG^0_{et}, eV	k_{obs}, M^{-1} s^{-1}
1a	$[Fe(C_5H_5)_2]^+$	0.37 [a]	$(AcrH)_2$	0.25	2.3×10^5 [a]
2a	$[Fe(C_5H_5)(HgClC_5H_4)]^+$	0.36 [a]	$(AcrH)_2$	0.26	2.8×10^5 [a]
3a	$[(TPP)Co]^+$	0.35 [a]	$(AcrH)_2$	0.27	1.8×10^5 [a]
4a	$[Fe(C_5H_5)(t\text{-amyl}C_5H_4)]^+$	0.32 [a]	$(AcrH)_2$	0.30	1.1×10^5 [a]
5a	$[Fe(C_5H_5)(BuC_5H_4)]^+$	0.31 [a]	$(AcrH)_2$	0.31	8.1×10^4 [a]
6a	2,3-Dicyano-*p*-benzoquinone	0.28 [a]	$(AcrH)_2$	0.34	1.1×10^4 [a]
7a	$[Fe(MeC_5H_4)_2]^+$	0.26 [a]	$(AcrH)_2$	0.36	2.1×10^4 [a]
8a	$[Fe(BuC_5H_4)_2]^+$	0.25 [a]	$(AcrH)_2$	0.37	2.0×10^4 [a]
9a	TCNE	0.22 [a]	$(AcrH)_2$	0.40	3.8×10^3 [a]
10a	Ph_3C^+	0.21	$(AcrH)_2$	0.41	4.2×10^3
11a	TCNQ	0.19 [a]	$(AcrH)_2$	0.43	3.8×10^3 [a]
12a	$(p\text{-}MeOC_6H_4)Ph_2C^+$	0.05	$(AcrH)_2$	0.57	1.9
13a	*p*-chloranil	0.01 [a]	$(AcrH)_2$	0.61	2.4 [a]
14a	*p*-bromanil	0.00 [a]	$(AcrH)_2$	0.62	2.3 [a]
15a	$(p\text{-}MeOC_6H_4)_2PhC^+$	-0.07	$(AcrH)_2$	0.69	9.0×10^{-2}
16a	$(p\text{-}MeOC_6H_4)_3C^+$	-0.21	$(AcrH)_2$	0.83	$<10^{-3}$
10b	Ph_3C^+	0.21	**1**	0.69	4.2×10^4
12b	$(p\text{-}MeOC_6H_4)Ph_2C^+$	0.05	**1**	0.85	3.3×10^3
15b	$(p\text{-}MeOC_6H_4)_2PhC^+$	-0.07	**1**	0.97	7.9
16b	$(p\text{-}MeOC_6H_4)_3C^+$	-0.21	**1**	1.11	6.1×10^{-2}
15c	$(p\text{-}MeOC_6H_4)_2PhC^+$	-0.07	**3**	1.37	5.0×10^2
16c	$(p\text{-}MeOC_6H_4)_3C^+$	-0.21	**3**	1.51	1.9×10
10c	Ph_3C^+	0.21	**4**	1.07	3.4×10^4
16c	$(p\text{-}MeOC_6H_4)_3C^+$	-0.21	**4**	1.49	2.1×10

[a] Taken from ref. 15b.

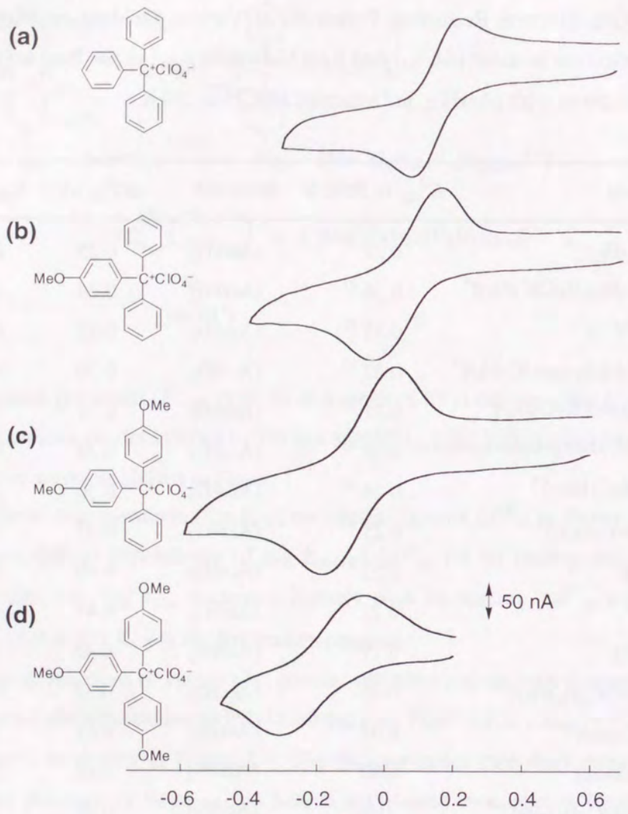

Figure 1. Cyclic coltammograms of (a) $Ph_3C^+ClO_4^-$ (b) $(MeOC_6H_4)Ph_2C^+ClO_4^-$ (c) $(MeOC_6H_4)_2PhC^+ClO_4^-$ (d) $(MeOC_6H_4)_3C^+ClO_4^-$ (2.0 x 10^{-2} M) in deaerated MeCN containing $Bu_4NClO_4^-$ (0.10 M) with a gold microelectrode at 298 K; sweep rate 100 V s^{-1}.

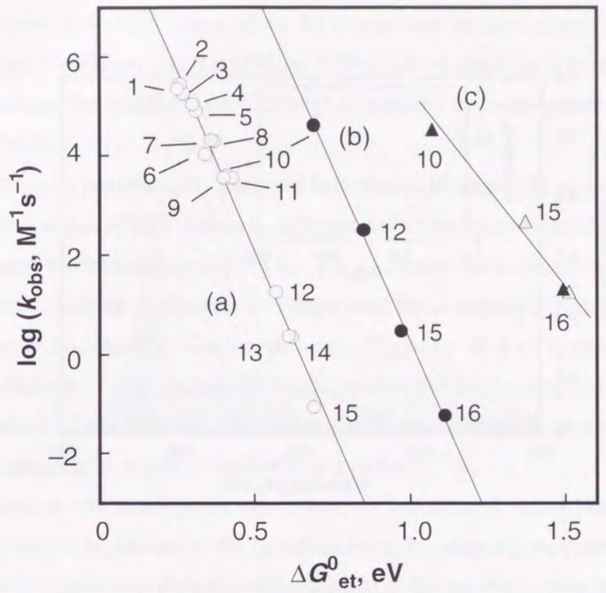

Figure 2. Plots of log k_{obs} vs ΔG^0_{et} for the reaction of (a) $(AcrH)_2$ (○), (b) $(CH_3)_2C{=}C(OMe)OSiMe_3$ (●), (c) $CH_2{=}C(OEt)OSiEt_3$ (Δ), $CH_2{=}C(OEt)OSiMe_2Bu^t$ (▲) with the various oxidants at 298 K. 1 Fc^+, 2 (1-HgCl)Fc^+, 3 $[(TPP)Co]^+$, 4 (1-*t*-amyl)Fc^+, 5 1-BuFc^+, 6 2,3-dicyano-*p*-benzoquinone, 7 1,1'-Me_2Fc^+, 8 1,1'-Bu_2Fc^+, 9 tetracyanoethylene, 10 Ph_3C^+, 11 7,7',8,8'-tetracyano-*p*-quinodimethane, 12 $(MeOC_6H_4)(C_6H_5)_2C^+$, 13 *p*-chloranil, 14 *p*-bromanil, 15 $(MeOC_6H_4)_2(C_6H_5)C^+$, 16 $(MeOC_6H_4)_3C^+$. Fc = ferrocene, TPP^{2-} = the dianion of tetraphenylporphyrin.

trityl cations proceeds via an outer-sphere electron transfer, since the k_{obs} values are at least by a five orders magnitude larger than those expected from the outer-sphere electron transfer reactions. Thus, there should be an orbital interaction (the difference in 10^5 in k_{obs} corresponds to the energy of ca. 7 kcal mol^{-1}) in the radical pair which would be produced by the electron transfer reaction. Such a reaction may be best described as an inner-sphere electron transfer from **1** to trityl cation, followed by the C–C bond formation leading to the formal nucleophilic addition of **1** to trityl cation as shown in Scheme 2. It has not been

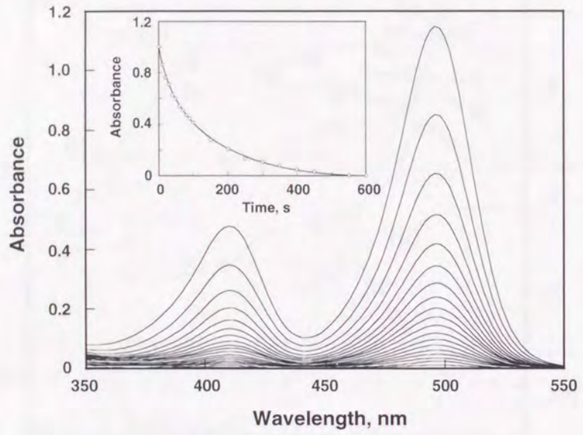

Figure 3. Visible spectral change observed in the reaction of (p-$MeOC_6H_4)_2PhC^+ClO_4^-$ (3.0 x 10^{-5} M) with $(CH_3)_2C{=}C(OMe)$-$OSiMe_3$ (**1**: 2.4 x 10^{-3} M) in deaerated MeCN at 298 K (20 s interval). Inset: Plots of time dependence of the decay in absorbance at 496 nm due to (p-$MeOC_6H_4)_2PhC^+$.

Scheme 2

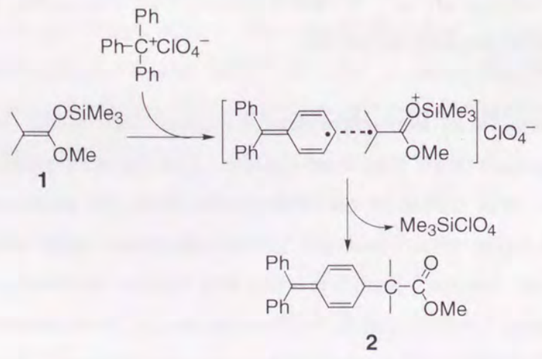

strictly ruled out that the reaction of **1** with trityl cation simply is an ionic reaction at the least hindered position of the trityl cation, since the charge may be delocalized into the aromatic ring. In such a case, however, it would be difficult to account for a good parallel linear correlation between the reactions of **1** with trityl cations and the outer-sphere electron transfer reactions in Figure 2.

In the case of a less sterically hindered ketene silyl In acetal (**3**), however, the type of product in the reaction of trityl cation is different from that obtained in the reaction with a sterically hindered ketene silyl acetal (eq 1). The k_{obs} values of the reactions of **3** with trityl cations (Figure 2c) are by more than 10^{12} larger than those expected from the outer-sphere electron transfer correlation. The much larger reactivity of **3** as compared to **1** in the nucleophilic addition to trityl cations shows sharp contrast with the reversed reactivity in the electron transfer reactions in which the reactivity of **3**, which has the more positive E^0_{ox} value (1.30 V),[8b] is expected to be much smaller than **1** (0.83 V).[8b] .

In conclusion, the nucleophilic reactivities of ketene silyl acetals vary significantly depending on the steric demand at the reaction center, but they are well correlated with the electron transfer reactivities when the steric demand at the reaction center for the C–C bond formation remains constant (Figure 2).

Experimental

Materials. Trityl cation derivatives were prepared by the corresponding triphenylmethylchloride or triphenylmethanol with perchloric acid in acetic anhydride.[17] The purity of trityl cation derivatives thus obtained was checked by elemental analysis and ^1H NMR spectra. ^1H NMR measurements were performed with a JNM-GSX-400 (400 MHz) NMR spectrometer. Anal. Calcd for $C_{19}H_{15}O_4Cl$, $Ph_3C^+ClO_4^-$; C, 66.58; H, 4.41. Found: C, 65.78; H, 7.15. Anal. Calcd for $C_{20}H_{17}O_5Cl$, $(MeOC_6H_4)Ph_2C^+ClO_4^-$; C, 64.44; H, 4.60. Found: C, 64.15; H, 4.54. Anal. Calcd for $C_{21}H_{19}O_6Cl$, $(MeOC_6H_4)_2PhC^+ClO_4^-$; C, 62.62; H, 4.75. Found: C, 61.20; H, 4.68. Anal. Calcd for $C_{22}H_{21}O_7Cl$, $(MeOC_6H_4)_3C^+ClO_4^-$; C, 61.05; H, 4.89. Found: C, 60.52; H, 4.81. ^1H NMR (CD_3CN, 400 MHz) δ (Me_4Si, ppm) $Ph_3C^+ClO_4^-$, 7.2-8.3 (m, 15H); $(MeOC_6H_4)Ph_2C^+ClO_4^-$, 4.22 (s, 3H), 7.4-8.1 (m, 14H); $(MeOC_6H_4)_2PhC^+ClO_4^-$, 4.12 (s, 6H), 7.3-8.1 (m, 13H); $(MeOC_6H_4)_3C^+ClO_4^-$, 4.07 (s, 9H), 7.2-8.1 (m, 12H). Methyl trimethylsilyl dimethylketene acetal ($Me_2C{=}C(OMe)OSiMe_3$, **1**) was were obtained commercially from Aldrich. 2–Ethoxy–2–butenyldimethyl-t-butylsilane ($CH_2{=}C(OEt)O$-$SiMe_2Bu^t$ and 2–Ethoxy–2–

butenyltriehylsilane (CH_2=C(OEt)OSiEt_3, **3**) were prepared as described in the literature.[18] The silicon reagents were purified by vacuum distillation. 10,10'-dimethyl-9,9',10,10'-tetrahydro-9,9'-biacridine [$(AcrH)_2$] was prepared from the reduction 10-methylacridinium perchlorate ($AcrH^+ClO_4^-$) with $Me_3SnSnMe_3$ in MeCN at 333 K, and purified by recrystallization from the mixture of acetonitrile and chloroform. Anal. Calcd for $C_{28}H_{24}N_2$; C, 86.56; H, 6.23; N, 7.21. Found: C, 86.56; H, 6.29; N, 7.15. ^{1}H NMR ($CDCl_3$, 400 MHz) δ (Me_4Si, ppm) 3.08 (s, 6H), 3.95 (s, 2H), 6.5-7.3 (m, 16H). 10-methylacridinium iodide ($AcrH^+I^-$) was prepared by the reaction of acridine with methyl iodide in acetone,[19] and it was converted to the perchlorate salt ($AcrH^+ClO_4^-$) by the addition of magnesium perchlorate to the iodide salt, and purified by recrystallization from methanol.[20] Acetonitrile and dichloromethane used as solvent, were purchased from Wako Pure Chemical Ind. Ltd., Japan, and distilled over P_2O_5 prior to use.[21] *p*-Benzoquinone was purchased from Tokyo Kasei Organic Chemicals, and purified by the standard methods.[21] Acetonitrile-d_3 and chloroform-*d* were obtained from EURI SO-TOP, CEA, France. Trifluoroacetic acid was also obtained commercially. Tetrabutylammonium perchlorate (TBAP), obtained from Fluka Fine Chemical, was recrystallized from ethanol and dried in vacuo prior to use.

Spectral and Kinetic Measurements. The reactions of the trityl cation derivatives with the various nucleophiles in deaerated MeCN were monitored with a Hewlett Packard 8452 diode array spectrophotometer when the rates were slow enough to be determined accurately. The rates were determined from appearance of the absorbance due to $AcrH^+$ (λ_{max} = 358 nm, ε_{max} = 1.8 x 10^4 M^{-1} cm^{-1}) or the trityl cation derivatives (*e.g.*, $Ph_3C^+ClO_4^-$, λ_{max} = 400 nm, ε_{max} = 3.8 x 10^3 M^{-1} cm^{-1}). The kinetic measurements for faster reactions such as the reaction of $Ph_3C^+ClO_4^-$ with $(AcrH)_2$ were carried out with a Union RA-103 stopped-flow spectrophotometer which was thermostated at 298 K under deaerated conditions. The concentration of the trityl cation derivatives or the various nucleophiles was maintained at more than 15-fold excess of the other reactant to attain pseudo-first-order conditions. Pseudo-first-order rate constants were determined by a least-squares curve fit using an NEC microcomputer. The first-order plots of ln ($A_\infty - A$) vs time (A_∞ and A are the final absorbance and the absorbance at the reaction time, respectively) were linear for three or more half-lives with the correlation coefficient, $\rho > 0.999$. In each case, it was confirmed that the rate constants derived from at least 5 independent measurements agreed within an experimental error of ±5 %.

Reaction Procedure. Typically, $Ph_3C^+ClO_4^-$ (1.0 x 10^{-2} M) and Me_2C=C(OMe)OSi-Me_3 (1.0 x 10^{-2} M) were added to an NMR tube which contained deaerated CD_3CN solution (0.60 cm^3) under an atmospheric pressure of argon. The products of was identified by the ^{1}H NMR spectra by comparing with those of authentic samples. The ^{1}H NMR measurements were performed using a JNM-GSX-400 (400 MHz) NMR spectrometer. **2**: ^{1}H NMR (CD_3CN, 298 K, 400 MHz); δ(Me_4Si, ppm): 1.17 (s, 6H), 3.50 (tt, 1H, J = 4.4 and 2.2 Hz), 3.67 (s, 3H), 5.72 (td, 2H, J = 10.6 and 1.8 Hz), 6.54 (qd, 2H, J = 10.6 and 1.8 Hz), 7.11-7.36 (m, 10H). The assignment was confirmed by an NOE experiment in which the signal at 3.50 ppm is coupled with that at 1.17 ppm. *p*-Methoxy substituted **2**: 1.16 (s, 6H), 3.46 (m, 1H), 3.76 (s, 3H), 4.21 (s, 3H), 6.37-6.56 (m, 4H), 6.80-7.38 (m, 9H).

Electrochemical Measurements. Electrochemical measurements of trityl cation derivatives were performed on a BAS 100B electrochemical analyzer in deaerated acetonitrile containing 0.10 M $Bu^n_4NClO_4$ as a supporting electrolyte at 298 K. The gold working microelectrode (id = 10 μm, BAS) was polished with BAS polishing alumina suspension and rinsed with acetone before use. The counter electrode was a platinum wire (BAS). The measured potentials were recorded with respect to the $Ag/AgNO_3$ (1.0 x 10^{-2} M) reference electrode. The E^0_{red} values (vs Ag/Ag^+) are converted to those vs SCE by adding 0.29 V.[22]

References

(1) (a) Mukaiyama, T.; Murakami, M. *Synthesis* **1987**, 1043. (b) Reetz, M. T. *Angew. Chem., Int. Ed. Engl.* **1982**, *21*, 96; **1984**, *23*, 556. (b) Yamamoto, H. In *Lewis Acid Chemistry; A Practical Approach*; Oxford University Press: Oxford, 1999.

(2) (a) Hosomi, A. *Acc. Chem. Res.* **1988**, *21*, 200-206. (b) Yamamoto, Y. *Acc. Chem. Res.* **1987**, *20*, 243.

(3) Fleming, I. In *Comprehensive Organic Synthesis*; Trost, B. M., Fleming, I., Eds.; Pergamon Press: Oxford, 1991; Vol. 2, pp 563-593.

(4) Santelli, M.; Pons, J.-M. *Lewis Acids and Selectivity in Organic Synthesis*; CRC Press: Boca Raton, FL, 1995.

(5) (a) Mayr, H.; Patz, M. *Angew. Chem., Int. Ed. Engl.* **1994**, *33*, 938-957. (b) Bartl, J.; Steenken, S.; Mayr, H. *J. Am. Chem. Soc.* **1991**, *113*, 7710.

(6) Patz, M.; Mayr, H. *Tetrahedron Lett.* **1993**, *34*, 3393-3396.

(7) Burfeindt, J.; Patz, M.; Müller, M.; Mayr, H. *J. Am. Chem. Soc.* **1998**, *120*, 3629.

(8) (a) Sato, T.; Wakahara, Y.; Otera, J.; Nozaki, H.; Fukuzumi, S. *J. Am. Chem. Soc.* **1991**, *113*, 4028. (b) Fukuzumi, S.; Fujita, M.; Otera, J.; Fujita, Y. *J. Am. Chem. Soc.* **1992**, *114*, 10271. (c) Otera, J.; Fujita, Y.; Sato, T.; Nozaki, H.; Fukuzumi, S.; Fujita, M. *J. Org. Chem.* **1992**, 57, 5054.

(9) Fukuzumi, S.; Itoh, S. In *Advances in Photochemistry*, Vol. 25; Neckers, D. C.; Volaman, D. H.; von Bünau, G., Eds.; Wiley: New York, 1998; pp 107-172.

(10) (a) Fukuzumi, S.; Fujita, M.; Otera, J. *J. Org. Chem.* **1993**, *58*, 5405. (b) Fukuzumi, S.; Okamoto, T.; Otera, J. *J. Am. Chem. Soc.* **1994**, *116*, 5503.

(11) (a) *Photoinduced Electron Transfer*; Fox, M. A., Chanon, M., Eds.; Elsevier: Amsterdam, 1988; Parts A-D. (b) *Advances in Electron Transfer Chemistry*; Mariano, P. S., Ed.; JAI Press: Greenwich, 1991, 1992, 1994-1996, 1999; Vols. 1-6.

(12) *Electron Transfer in Chemistry*; Balzani, V., Ed.; Wiley-VCH: Weinheim, 2000; Vols. 1-5.

(13) (a) Kochi, J. K. *Angew. Chem., Int. Ed. Engl.* **1988**, *27*, 1227. (b) Rathore, R.; Kochi, J. K. *Adv. Phys. Org. Chem.* **2000**, *35*, 193-318.

(14) Patz, M.; Mayr, H.; Maruta, J.; Fukuzumi, S. *Angew. Chem., Int. Ed. Engl.* **1995**, *34*, 1225.

(15) (a) Fukuzumi, S.; Kitano, T.; Ishikawa, M. *J. Am. Chem. Soc.* **1990**, *112*, 5631. (b) Fukuzumi, S.; Tokuda, Y.; Fujita, M. *J. Phys. Chem.* **1992**, *96*, 8413.

(16) The E^0_{ox} values have been estimated based on free energy relationsships for outer-sphere electron transfer reactions of ketene silyl acetals.[8b]

(17) Dauben, H. J.; Honnen, L. R.; Harmon, K. M. *J. Org. Chem.* **1960**, *25*, 1442.

(18) (a) Ireland, R. E.; Wipf, P.; Armstrong, J. D. *J. Org. Chem.* **1991**, *56*, 680. (b) Gennari, C.; Beretta, M. G.; Bernardi, A.; Moro, G.; Scolastico, C.; Todeschini, R. *Tetrahedron*, **1986**, *42*, 893. (c) Hosomi, A.; Shirahata, A.; Sakurai, H. *Chem. Lett.* **1978**, 901.

(19) Fukuzumi, S.; Ishikawa, M.; Tanaka, T. *Tetrahedron* **1986**, *42*, 1021.

(20) Fukuzumi, S.; Koumitsu, S.; Hironaka, K.; Tanaka, T. *J. Am. Chem. Soc.* **1987**, *109*, 305

(21) Perrin, D. D.; Armarego, W. L. F. *Purification of Laboratory Chemicals*; Butterworth-Heinemann: Oxford, 1988.

(22) Mann, C. K.; Barnes, K. K. *Electrochemical Reactions in Nonaqueous Systems*; Marcel Dekker: New York, 1990.

Chapter 4

Activation Metal–Metal Bond by Electron Transfer

Photochemical Generation of Cyclopentadienyliron Dicarbonyl Anion by an NAD Dimer Analogue

Abstract. Irradiation of the absorption band of an NAD (nicotinamide adenine dinucleotide) dimer analogue, 1-benzyl-1,4-dihydronicotinamide dimer, $(BNA)_2$, in acetonitrile containing cyclopentadienyliron dicarbonyl dimer, $[CpFe(CO)_2]_2$, results in generation of two equivalents of cyclopentadienyliron dicarbonyl anion, $[CpFe(CO)_2]^-$, accompanied by the oxidation of $(BNA)_2$ to yield two equivalents of BNA^+. The studies on the quantum yields, the electrochemistry, and the transient absorption spectra have revealed that the photochemical generation of $[CpFe(CO)_2]^-$ by $(BNA)_2$ proceeds via photoinduced electron transfer from the triplet excited state of $(BNA)_2$ to $[CpFe(CO)_2]_2$.

Introduction

Cyclopentadienyliron dicarbonyl anion, $[CpFe(CO)_2]^-$ ($Cp = \eta^5$–C_5H_5) has played an important role in the development of inorganic and organometallic chemistry,[1-3] since it is readily alkylated, acylated, or metalated by reaction with an appropriate electrophile.[1-3] However, strong reducing reagents such as Na/Hg amalgam,[4] Na/K alloy,[5] Na dispersion,[6] and trialkylborohydrides[7] have so far been required to produce $[CpFe(CO)_2]^-$ by the chemical reductive cleavage of cyclopentadienyliron dicarbonyl dimer, $[CpFe(CO)_2]_2$. Alternatively $[CpFe(CO)_2]^-$ can be produced by the electrochemical reduction of $[CpFe(CO)_2]_2$ at highly negative potentials.[8,9] On the other hand, photochemistry of metal carbonyl compounds has provided a valuable synthetic technique in organometallic chemistry.[10-17] In particular, photochemistry of $[CpFe(CO)_2]_2$ has received much attention since there are a diversity of reaction pathways leading to mononuclear, dinuclear, and even ionic products.[12,15-17] Loss of CO and homolysis of the Fe–Fe bond are primary photochemical processes known for $[CpFe(CO)_2]_2$.[12-17] However, there has so far been no report on the photochemical reduction of $[CpFe(CO)_2]_2$ by an electron donor to produce $[CpFe(CO)_2]^-$.

We report herein a convenient method for generation of $[CpFe(CO)_2]^-$ by the

photochemical reduction of $[CpFe(CO)_2]_2$ by a unique organic two-electron donor, that is an NAD (nicotinamide adenine dinucleotide) dimer analogue, 1-benzyl-1,4-dihydronicotinamide dimer $[(BNA)_2]$.[18,19] Combination of the photochemical and electrochemical results obtained in this study provides confirmative bases to elucidate the reaction mechanism of the photochemical reduction of $[CpFe(CO)_2]_2$ by $(BNA)_2$.

Experimental Section

Materials. Cyclopentadienyliron dicarbonyl dimer, $[CpFe(CO)_2]_2$ ($Cp = \eta^5$–C_5H_5), was purchased from Tokyo Kasei Organic Chemicals, Japan and from Aldrich, France, for the experiments performed in Osaka and in Paris, respectively. In both cases it was used as received. Pentamethylcyclopentadienyliron dicarbonyl dimer, $[Cp^*Fe(CO)_2]_2$ ($Cp^* = \eta^5$–C_5Me_5), was obtained from Strem Chemicals, Inc., U.S.A. $[CpFe(CO)_2]^-NBu_4^+$ used in the voltammetric experiments was prepared by *pre*-electrolysis in a two-compartment cell of a solution of $[CpFe(CO)_2]_2$ at –1.6 V *vs* SCE in deaerated acetonitrile in the presence of 0.3 M NBu_4BF_4; ten milliliters of the electrolyzed solution were transferred with a syringe to the voltammetric cell. 1-Benzyl-1,4-dihydronicotinamide dimer $[(BNA)_2]$ was prepared according to the literature.[20] Acetonitrile (MeCN) used as solvents was purified and dried by the standard procedure.[21]

Reaction Procedure. Typically, $[CpFe(CO)_2]_2$ (1.0×10^{-3} M) and $(BNA)_2$ (1.0×10^{-3} M) were added to an NMR tube which contained deaerated CD_3CN solution (0.60 cm^3) under an atmospheric pressure of argon and the solution was irradiated with a Xe lamp (Ushio Model V1-501C) through a UV cut-off filter (Toshiba UV-31) transmitting $\lambda > 300$ nm at 298 K for 30 min. The reaction products of $[CpFe(CO)_2]_2$ and $[Cp^*Fe(CO)_2]_2$ with $(BNA)_2$ were identified by the ^1H NMR spectra by comparing with those of authentic samples. The ^1H NMR measurements were performed using a JNM-GSX-400 (400 MHz) NMR spectrometer. ^1H NMR (CD_3CN): $[CpFe(CO)_2]^-$: δ (Me_4Si, ppm) 4.16 (s, 5H); BNA^+: δ 5.76 (s, 2H), 7.49 (m, 5H), 8.11 (t, 1H, J = 6.8 Hz), 8.80 (m 2H,), 9.16 (s, 1H).

Quantum Yield Determinations. A standard actinometer (potassium ferrioxalate)[22] was used for the quantum yield determination of the photoreduction of $[CpFe(CO)_2]_2$ by $(BNA)_2$. Square quartz cuvettes (10 mm i.d.) which contained a deaerated MeCN solution (3.0 cm^3) of $(BNA)_2$ (5.6×10^{-4} M) together with $[CpFe(CO)_2]_2$ at various concentrations were irradiated with monochromatized light of λ = 350 nm from a Shimadzu RF-5000 fluorescence spectrophotometer. Under the conditions of actinometry experiments, the

actinometer and $(BNA)_2$ absorbed essentially all the incident light of λ = 350 nm. The light intensity of monochromatized light of λ = 350 nm was determined as 2.32×10^{-9} einstein s^{-1} with the slit width of 20 nm. The photochemical reaction was monitored using a Hewlett Packard 8452A diode-array spectrophotometer. The quantum yields were determined from an increase in absorbance due to the cyclopentadienyliron dicarbonyl anion, $[CpFe(CO)_2]^-$. In order to avoid the contribution of light absorption of the products, only the initial rates were determined for determination of the quantum yields.

Cyclic Voltammetry. Cyclic voltammetry measurements were performed with a homemade potentiostat[23] and a wave-form generator, PAR model 175. The fast scan cyclic voltammograms were recorded with a Nicolet 3091 digital oscilloscope. The one-compartment electrochemical cell was of air tight design with high-vacuum glass stopcock fitted with either Teflon or Kalretz (Du Pont) O-rings in order to prevent contamination by grease. The connections to the high-vacuum line and to the Schlenck containing the solvent were obtained by spherical joints also fitted with Kalretz O-rings. The working electrode was a home-made platinum disk microelectrode of 10 μm radius.[24] The counter electrode consisted of a platinum spiral, and the quasi-reference electrode was a silver spiral. The quasi-reference electrode drift was negligible for the time required by a single experiment. Both the counter and the reference electrode were separated from the working electrode by ~0.5 cm. Potentials were measured with ferrocene standard and are always referred to SCE. $E_{1/2}$ values correspond to $(E_{pc} + E_{pa})/2$ from CV curves. Ferrocene was also used as an internal standard for checking the electrochemical reversibility of a redox couple.

Fluorescence Quenching. Fluorescence measurements were carried out on a Shimadzu RF-5000 spectrofluorophotometer. The solution was deoxygenated by argon purging for 10 min prior to the measurements. The fluorescence decay of $(BNA)_2$ was measured using a Horiba NAES-1100 time-resolved spectrofluorophotometer.

Laser Flash Photolysis. The measurements of transient absorption spectra of $^3[(BNA)_2]^*$ in the presence of $[CpFe(CO)_2]_2$ were performed according to the following procedures. The $(BNA)_2$ solution (1.0×10^{-3} M) was excited by a Nd:YAG laser (Quanta-Ray, GCR-130, 6 ns fwhm) at 350 nm with the power of 7 mJ. A pulsed Xenon flash lamp (Tokyo Instruments, XF80-60, 15 J, 60 ms fwhm) was used for the probe beam, which was detected with a Si-PIN photodiode (Hamamatsu G5125-10) after passing through the photochemical quartz vessel (10 mm x 10 mm) and a monochromator. The output from Si-PIN photodiode was recorded with a digitizing oscilloscope (HP 54510B, 300 MHz). Since

the solution of $(BNA)_2$ in acetonitrile disappeared by each laser shot (350 nm; 7 mJ) in the presence of $[CpFe(CO)_2]_2$, the transient spectra were recorded using fresh solutions in each laser excitation. All experiments were performed at 298 K. The solution was deoxygenated by argon purging for 10 min prior to the measurements.

ESR Measurements. ESR spectra of the photolyzed MeCN solution of $[CpFe(CO)_2]_2$ (5.0×10^{-4} M) and $(BNA)_2$ (5.0×10^{-4} M) were taken on a JEOL JES-RE1XE and were recorded under nonsaturating microwave power conditions. A sample solution was irradiated by using a high pressure mercury lamp (USH–1005D) focusing at the sample cell in the ESR cavity. The magnitude of modulation was chosen to optimize the resolution and signal-to-noise (S/N) ratio of the observed spectra. The *g* values were calibrated using a Mn^{2+} marker.

Theoretical Calculations. Density functional calculations were performed on a COMPAQ DS20E computer using the Amsterdam Density Functional (ADF) program version 1999.02 developed by Baerends et al.[25] The electronic configurations of the molecular systems were described by an uncontracted triple-ζ Slater-type orbital basis set (ADF basis set IV) with a single polarization function used for each atom. Core orbitals were frozen through 1s (C, O) and 3p (Fe). The calculations were performed using the local exchange-correlation potential by Vosko et al.[26] and the nonlocal gradient corrections by Becke[27] and Perdew[28] during the geometry optimizations. First-order scalar relativistic correlations were added to the total energy. Final geometries and energetics were optimized by using the algorithm of Versluis and Ziegler[29] provided in the ADF package and were considered converged when the changes in bond lengths between subsequent iterations fell below 0.01 Å.

Results and Discussion

Photoreduction of $[CpFe(CO)_2]_2$ Irradiation of an acetonitrile (MeCN) solution containing $(BNA)_2$ (7.0×10^{-5} M, λ_{max} = 350 nm) and $[CpFe(CO)_2]_2$ (7.0×10^{-5} M) with UV-visible light (λ = 350 nm) results in the disappearance of absorbance due to $[CpFe(CO)_2]_2$ and $(BNA)_2$ accompanied by the appearance of a new broad absorption band at ca. λ = 450 nm with clean isosbestic points as shown in Figure 1. The oxidation and reduction products of $(BNA)_2$ and $[CpFe(CO)_2]_2$ were identified as BNA^+ and $[CpFe(CO)_2]^-$ by the ^1H NMR spectra of the product solution, respectively (see

Experimental Section). Thus, the stoichiometry of the photochemical reaction was given by eq 1, where $[CpFe(CO)_2]_2$ is known to exist predominantly as a *cis* isomer in the two-carbonyl bridged form.[30-32] When $[CpFe(CO)_2]_2$ was replaced by pentamethylcyclopentadienyliron dicarbonyl dimer, $[Cp^*Fe(CO)_2]_2$ ($Cp^* = \eta^5$–C_5Me_5), the photoreduction of $[Cp^*Fe(CO)_2]_2$ by $(BNA)_2$ hardly occurred.

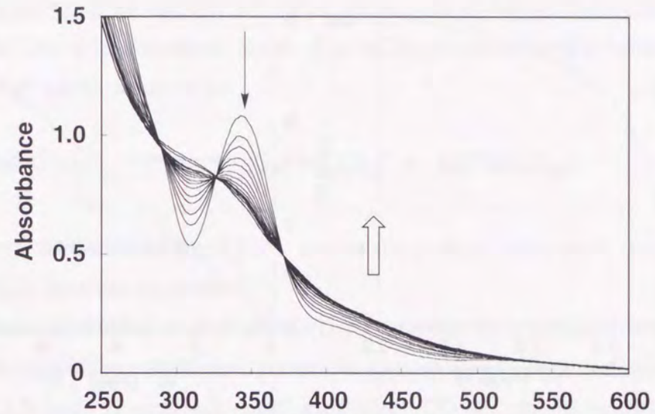

Figure 1. Electronic absorption spectra observed in the photochemical reaction of $[CpFe(CO)_2]_2$ (7.0×10^{-5} M) with $(BNA)_2$ (7.0×10^{-5} M) in deaerated MeCN at 298 K.

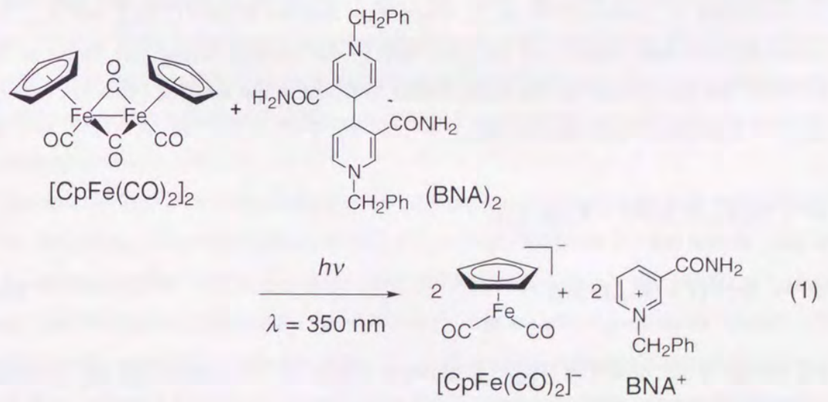

(1)

The irradiation with the light of λ_{max} of $(BNA)_2$ is essential for the selective formation of $[CpFe(CO)_2]^-$ without loss of CO. The quantum yield of the photo generation of $[CpFe(CO)_2]^-$ was determined from an increase in absorbance due to $[CpFe(CO)_2]^-$ under irradiation of the light at $\lambda = 350$ nm. The quantum yield (Φ) increased with an increase in the $[CpFe(CO)_2]_2$ concentration to approach a limiting value

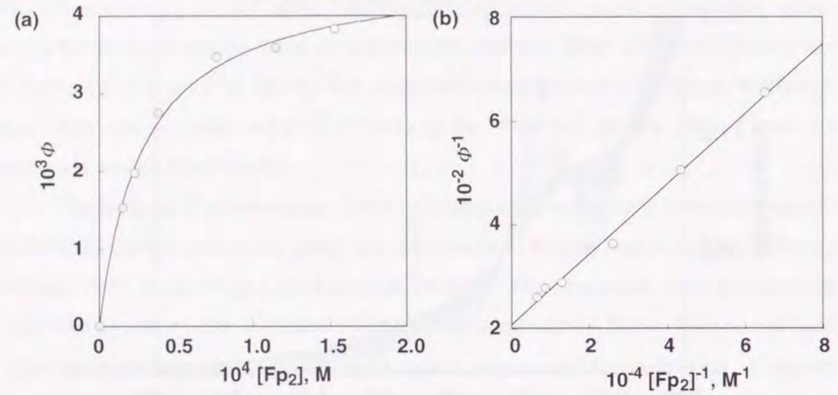

Figure 2. (a) Dependence of the quantum yield (Φ) on $[Fp_2]$ for the photoreduction of $[CpFe(CO)_2]_2$ (Fp_2) by $(BNA)_2$ (5.6×10^{-5} M) in deaerated MeCN at 298 K. (b) Plot of Φ^{-1} vs $[Fp_2]^{-1}$.

(Φ_∞), as shown in Figure 2a. Such a saturated dependence of Φ on the $[CpFe(CO)_2]_2$ concentration is expressed by eq 2, where Fp_2 denotes $[CpFe(CO)_2]_2$ and K_{obs} is the quenching constant which can be converted to the corresponding rate constant (k_{obs}) provided that the lifetime of the excited state involved in the reaction (τ) is known: $k_{obs} = K_{obs}\tau^{-1}$. Equation 2 is rewritten as eq 3,

$$\Phi = \Phi_\infty K_{obs}[Fp_2]/(1 + K_{obs}[Fp_2]) \qquad (2)$$

$$\Phi^{-1} = \Phi_\infty^{-1}[1 + (K_{obs}[Fp_2])^{-1}] \qquad (3)$$

and the linear plot of Φ^{-1} vs $[Fp_2]^{-1}$ is shown in Figure 2b. From the slope and intercept are obtained the Φ_∞ and K_{obs} values as 4.8×10^{-3} and 3.3×10^4 M^{-1}.

energy as 3.36 eV. Since the one-electron oxidation potential (E^0_{ox}) of $(BNA)_2$ is 0.26 V (*vs* SCE),[18] the E^0_{ox} value of the singlet excited state $[^1(BNA)_2{}^*]$ is determined as –3.1 V by subtracting the excitation energy from the E^0_{ox} value of the ground state. On the other hand, a fast-scan cyclic voltammetry was used to determine the one-electron reduction potential (E^0_{red}) of $[CpFe(CO)_2]_2$ in MeCN at 298 K. Slow-scan voltammograms of $[CpFe(CO)_2]_2$ at temperatures above 248 K have been reported to show an irreversible reduction wave due to the instability of an initially produced dimer radical anion $[CpFe(CO)_2]_2^{\bullet-}$ which dissociates into a mononuclear anion, $[CpFe(CO)_2]^-$, and a further reducible radical, $[CpFe(CO)_2]^\bullet$ (eq 4), resulting in

$$[CpFe(CO)_2]_2^{\bullet-} \longrightarrow [CpFe(CO)_2]^\bullet + [CpFe(CO)_2]^- \qquad (4)$$

the net two-electron reduction.[9,33,34] As the temperature is lowered, the reduction of $[CpFe(CO)_2]_2$ becomes reversible.[34]

Electrochemical Oxidation of $[CpFe(CO)_2]^-$. At moderate scan rates ($v < 10^2$ V s^{-1}) the steady state limit of the voltammetric pattern obtained upon continuous cycling between –0.42 V and –2.1 V *vs* SCE on a bulk solution of $[CpFe(CO)_2]^-$ exhibits two major waves as reported previously.[34,35] One, wave I_a, is anodic and features the one-electron oxidation of $[CpFe(CO)_2]^-$ at *ca.* –0.75 V *vs* SCE.[33,34] The other, wave II_c, of approximately equal current intensity, is observed around *ca.* –1.75 V *vs* SCE and features the reduction of the $[CpFe(CO)_2]_2$ dimer as evidenced by comparison with an authentic sample. This pattern confirms that the radical $[CpFe(CO)_2]^\bullet$ formed upon the one-electron oxidation of $[CpFe(CO)_2]^-$ at wave I_a undergoes a fast dimerization to afford $[CpFe(CO)_2]_2$ that is then reduced through an overall two-electron reduction at wave II_c to regenerate the parent anion, thus giving rise to the impression of the occurrence of a reversible couple with a large peak-to-peak separation (*ca.* 1 V).

Besides the facts that both peak potentials experience displacements with the scan rate (*ca.* –20 mV *per* log *v* for wave I_a, and *ca.* –30 mV *per* log *v* for wave II_c) and that the peak of wave I_a depends on the concentration of $[CpFe(CO)_2]^\bullet$ (*ca.* –20 mV *per* log *C*), a further evidence that the system I_a/II_c is not a canonical reversible couple is given by the growth of a reversible anodic wave, II_a, coupled to wave II_c, as soon as the scan rate is increased above a few 10^2 V s^{-1}. Above a few kV s^{-1}, wave II_a has a peak current intensity comparable to that

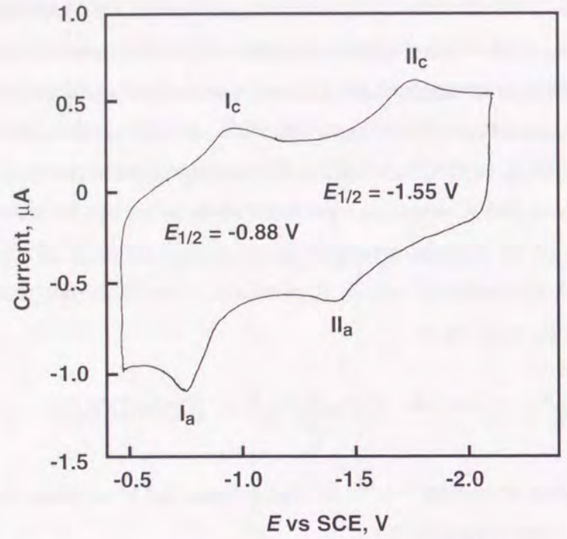

Figure 3. Cyclic voltammogram for the oxidation of the monomer anion $[CpFe(CO)_2]^-$ (3.1 x 10^{-3} M) in deaerated MeCN containing Bu_4NBF_4 with Pt electrode at 298 K; sweep rate 3280 V s^{-1}.

of wave II_c, showing that a full reversible behavior is achieved for the redox couple $[CpFe(CO)_2]_2/[CpFe(CO)_2]_2^{\bullet-}$ as shown in Figure 3. This allows the determination of the rate constant k_c = 5 x 10^2 s^{-1}, of the Fe–Fe bond cleavage in $[CpFe(CO)_2]_2^{\bullet-}$, as well as of the standard reduction potential of $[CpFe(CO)_2]_2$ at $E_{1/2}$ = –1.55 V *vs* SCE.

When the scan rate approaches the kV s^{-1} range, a second cathodic wave (I_c) develops, being apparently the anodic counterpart of wave I_a. The growth of this wave upon increasing the scan rate is concomitant with a comparable decay of the system of waves II_c/II_a, showing that the species reduced at wave I_c is an intermediate on the way to $[CpFe(CO)_2]_2$. At v = 3 kV s^{-1} (Figure 3), the peak current intensity of wave I_c is approximately equal to those of waves II_c and II_a. This establishes that the intermediate reduced at wave I_c has a half-life-time of *ca.* 140 μs. Such a voltammetric behavior would suggest that this intermediate is the $[CpFe(CO)_2]^{\bullet}$ radical formed upon the one-electron oxidation of $[CpFe(CO)_2]^-$ at wave I_a. However, this interpretation must be ruled out because this radical is reported to dimerize with a rate constant of 3.2 x 10^9 M^{-1} s^{-1},[13] so that intercepting its fast dimerization under the

millimolar conditions used here would require scan rates *ca.* 100 times larger than that used in Figure 3.[35] Moreover, would the $[CpFe(CO)_2]^{\bullet}$ radical be detected under the conditions of Figure 3, its ESR spectrum should be observable under irradiation of a mixture of $(BNA)_2$ and $[CpFe(CO)_2]_2$ (*vide infra*) with an intensity being approximately 20% that of $[CpFe(CO)_2]_2^{\bullet-}$ based on their relative life-times. Such ESR signal is not observed (*vide infra*) which points out to a much larger reaction rate for $[CpFe(CO)_2]^{\bullet}$, in agreement with a previous report.[13] Henceforth, under the conditions used in Figure 3, the $[CpFe(CO)_2]^{\bullet}$ radical must undergo a quantitative dimerization and none can be reduced at wave I_c. This evidences that the species detected at wave I_c is an intermediate on the way to $[CpFe(CO)_2]_2$ in which the Fe-Fe bond is already made.

In fact, $[CpFe(CO)_2]_2$ is known to predominantly exist under the stable two-carbonyl bridged form, but also under a less stable unbridged form.[30-32] The unbridged form having a significantly weaker Fe-Fe bond than the bridged form, it is reasonable for such species to be reducible at a much lesser negative potential than its more stable $[CpFe(CO)_2]_2$ isomer (note that the peak potential separation between waves I_c and II_c is *ca.* 0.8 V). Furthermore, its one-electron reduction at wave I_c should produce a more unstable anion-radical than $[CpFe(CO)_2]_2^{\bullet-}$ that is detected at wave II_a, so that its reduction should regenerate its parent anion $[CpFe(CO)_2]^-$ faster than that of the more stable $[CpFe(CO)_2]_2$ isomer. In other words, although it resulted impossible for us to characterize further this species, it seems highly probable that this species detected by its reduction at wave I_c is the unbridged dimer, and that the 140 μs half-life-time corresponds to the bridging rate constant (5 x 10^3 s^{-1}) of the two carbonyl ligands as shown in Scheme 1.

Upon reducing voltammetrically an authentic sample of the stable $[CpFe(CO)_2]_2$ isomer, the existence of the equilibrium between the unbridged and bridged isomers in Scheme 1[30-32] should lead to a CE sequence as soon as the electrode potential reaches wave I_c. Therefore, $[CpFe(CO)_2]_2$ could be reduced *via* the continuous displacement of the equilibrium (Scheme 1) to the side of the unbridged isomer owing to the consumption of the unbridged isomer at wave I_c, unless the backward rate constant is too small.[36] We did not observe any evidence of such a behavior even for the smallest scan rates used in this study (50 mV s^{-1}). Therefore, the backward rate constant of equilibrium (Scheme 1) has to be much less than 1 s^{-1}. Henceforth the equilibrium constant of CO bridging has to be much larger than 5 x 10^3 (*viz.*, ΔG^0 < -5.0 kcal mol^{-1}). Within this outline, the $E_{1/2}$ = –0.88 V *vs* SCE deduced from the half-sum of the peak potentials of waves I_a and I_c does not

Scheme 1

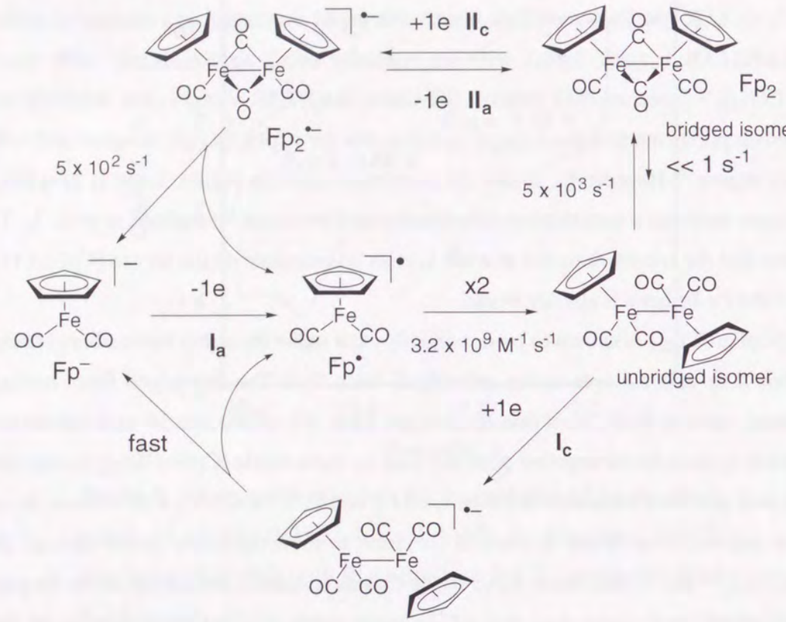

correspond at all to the standard oxidation potential of $[CpFe(CO)_2]^\bullet$ but to a kinetic potential corresponding to the *pseudo*-reversible sequence in Scheme 1.

The thermodynamic stabilities of the bridged and unbridged isomers of $[CpFe(CO)_2]_2$ were evaluated by the Amsterdam Density Functional (ADF) calculations (see Experimental Section).[25-29] The final geometries and energetics were obtained by optimizing the total molecular energy with respect to all structural variables as shown in Figure 4. Consistent with the above estimation on the ΔG^0 value (< –5.0 kcal mol^{-1}), we find that the bridged isomer is more stable than the unbridged trans-isomer by 12.3 kcal mol^{-1}. The unbridged *cis*-isomer is less stable than the unbridged trans-isomer by 13.7 kcal mol^{-1}. The LUMO (lowest unoccupied molecular orbital) of unbridged isomer consists of the Fe-Fe σ antibonding orbital whereas the LUMO of bridged isomer involves the Fe-CO d-π^* bonding orbital. This may be the reason for the facile cleavage of the Fe-Fe bond of the unbridged isomer upon the one-electron reduction (Scheme 1).

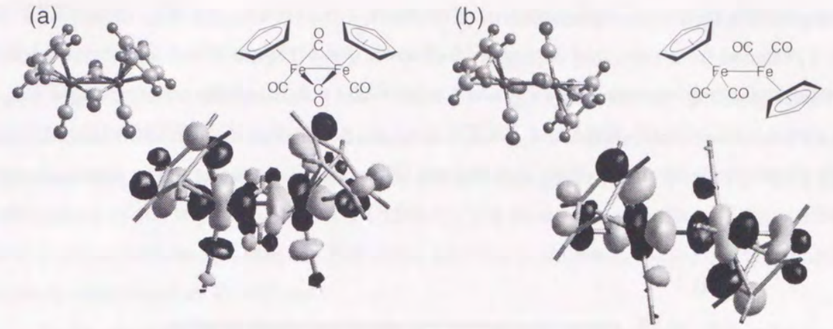

Figure 4. Ball and stick diagrams of the optimized structures of (a) the bridged and (b) unbridged isomers of $[CpFe(CO)_2]_2$ and the LUMO orbitals.

Mechanism of Photoreduction of $[CpFe(CO)_2]_2$ by $(BNA)_2$. Judging from the one-electron redox potentials of $^1(BNA)_2^*$ (E^0_{ox} = –3.10 V) and $[CpFe(CO)_2]_2$ (E^0_{red} = –1.55 V), the photoinduced electron transfer from $^1(BNA)_2^*$ to $[CpFe(CO)_2]_2$ is highly exergonic, since the free energy change of electron transfer (ΔG^0_{et}) is –1.55 eV.

The fluorescence decay of $^1(BNA)_2^*$ obeys first-order kinetics as shown in Figure 5. The fluorescence lifetime was determined as 7.4 ns. If the singlet excited state $^1(BNA)_2^*$

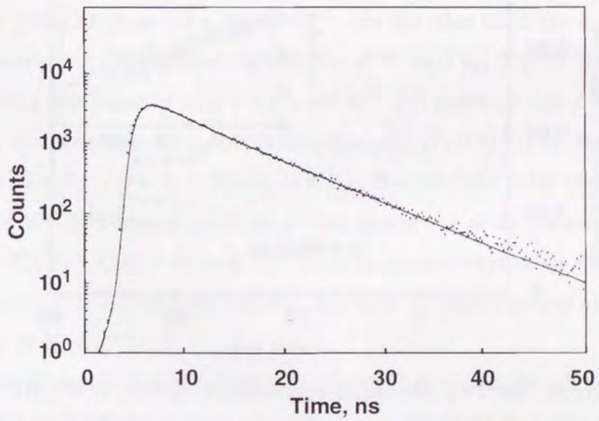

Figure 5. Fluorescence decay of $(BNA)_2$ (1.0 x 10^{-4} M) at λ = 390 nm in deaerated MeCN at 298 K.

is responsible for the photoreduction of $[CpFe(CO)_2]_2$ by $(BNA)_2$,the K_{obs} value (3.3×10^4 M^{-1}) obtained from saturated dependence of Φ on $[Fp_2]$ (Figure 2) would be converted to the corresponding rate constant ($k_{obs} = 4.5 \times 10^{12}$ M^{-1} s^{-1}) using the relation, $k_{obs} = K_{obs}\tau^{-1}$ and $\tau = 7.4$ ns. The estimated k_{obs} value is much larger than the diffusion-limited value (2.0×10^{10} M^{-1} s^{-1}).[37] This indicates that the excited state involved in the photoreduction of

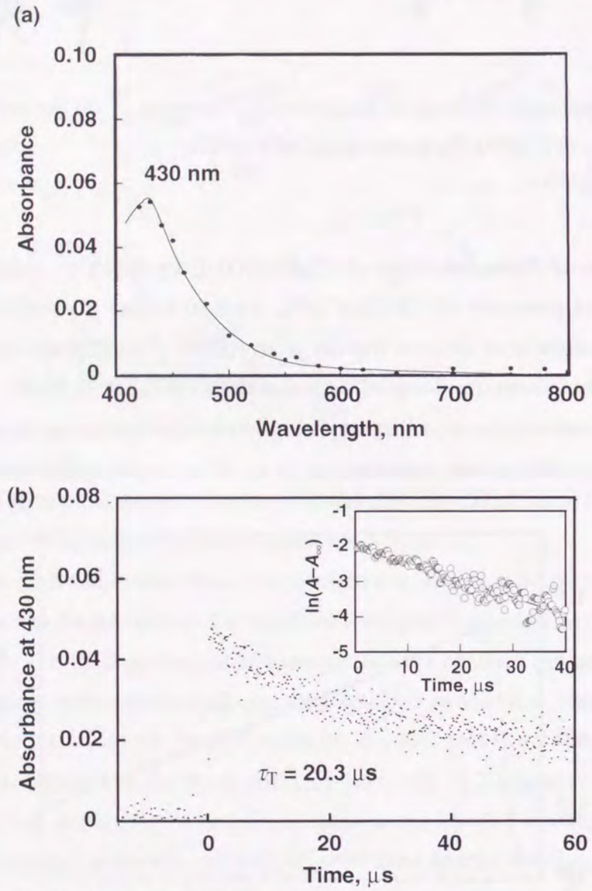

Figure 6. (a) T–T absorption spectrum of $(BNA)_2$ (1.0×10^{-3} M) obtained by the laser flash photolysis in deaerated MeCN at 298 K. (b) Kinetic trace for the T–T absorption at 430 nm in deaerated MeCN. Inset: first-order plot.

$[CpFe(CO)_2]_2$ by $(BNA)_2$ should have a much longer lifetime than the singlet excited state and therefore it may be the triplet excited state of $(BNA)_2$.

The existence of the triplet excited state of $(BNA)_2$ is shown by the laser flash photolysis of an MeCN solution of $(BNA)_2$ with 355 nm laser light. The result is shown in Figure 6a where a new absorption band at 430 nm which is attributed to the triplet-triplet (T-T) absorption of the triplet excites state $[^3(BNA)_2^*]$ is observed upon the laser excitation. The T-T absorption decays obeying first-order kinetics as shown in Figure 6b. The triplet lifetime is determined as $\tau_T = 20$ ms.

In the presence of $[CpFe(CO)_2]_2$, the T-T absorption observed at 0.25 μs after laser excitation ($\lambda_{max} = 430$ nm) is changed to a new transient absorption band at 2.5 μs ($\lambda_{max} = 470$ nm), which may be attributed to $[CpFe(CO)_2]_2^{\bullet-}$ produced by photoinduced electron transfer from $^3(BNA)_2^*$ to $[CpFe(CO)_2]_2$ as shown in Figure 7a. On the other hand, the oxidized product of $(BNA)_2$ $[(BNA)_2^{\bullet+}]$ is known to be converted to $BNA^\bullet$ and BNA^+ via facile C–C bond cleavage.[18,19] Since the transient absorption spectrum of $NAD^\bullet$ was reported to appear at $\lambda_{max} = 500$ nm,[38] the absorption spectrum of $BNA^\bullet$ may be overlapped with that of $[CpFe(CO)_2]_2^{\bullet-}$ at 470 nm. An increase in absorbance due to $[CpFe(CO)_2]_2^{\bullet-}$ at 470 nm obeys pseudo-first-order kinetics as shown in Figure 6b and the pseudo-first-order rate constant increases linearly with increasing the $[CpFe(CO)_2]_2$ concentration. From the slope of a linear correlation of the pseudo-first-order rate constant vs the $[CpFe(CO)_2]_2$ concentration is obtained the rate constant (k_{et}) of photoinduced electron transfer from $^3(BNA)_2^*$ to $[CpFe(CO)_2]_2$ as 1.8×10^9 M^{-1} s^{-1}. On the other hand, the K_{obs} value (3.3×10^4 M^{-1}) obtained from the saturated dependence of Φ on $[Fp_2]$ (Figure 2) is converted to the corresponding rate constant ($k_{obs} = 1.6 \times 10^9$ M^{-1} s^{-1}) provided that the triplet excited state $^3(BNA)_2^*$ is responsible for the photoreduction of $[CpFe(CO)_2]_2$ by $(BNA)_2$, using the relation, $k_{obs} = K_{obs}\tau_T^{-1}$. and $\tau_T = 20$ ms. The k_{obs} thus obtained value agrees with the k_{et} value (1.8×10^9 M^{-1} s^{-1}) determined directly from appearance of the transient absorption at 470 nm due to $[CpFe(CO)_2]_2^{\bullet-}$ (Figure 7a). Such an agreement strongly indicates that the photoreduction of $[CpFe(CO)_2]_2$ by $(BNA)_2$ proceeds via photoinduced electron transfer from $^3(BNA)_2^*$ to $[CpFe(CO)_2]_2$.

The Fe–Fe bond of $[CpFe(CO)_2]_2^{\bullet-}$ generated in photoinduced electron transfer from $^3(BNA)_2^*$ to $[CpFe(CO)_2]_2$ is cleaved to give $[CpFe(CO)_2]^\bullet$ and $[CpFe(CO)_2]^-$ (Scheme 1).[33,34] However, the cleavage rate is relatively slow as estimated by the electrochemical measurements (Scheme 1).[33,34]

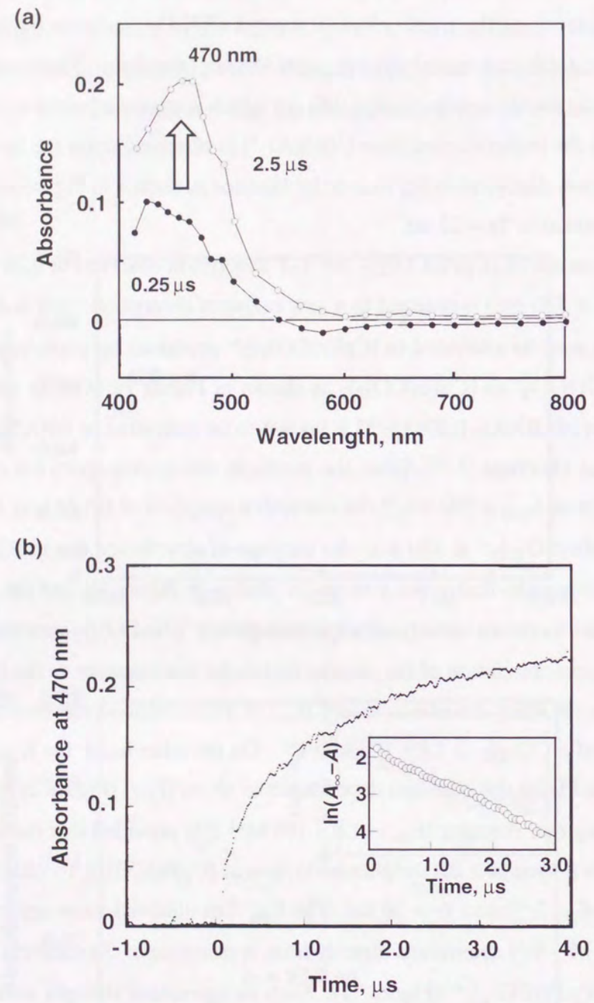

Figure 7. (a) Transient absorption spectra observed in the photoreduction of $[CpFe(CO)_2]_2$ (3.0 x 10^{-4} M) by $(BNA)_2$ (1.0 x 10^{-3} M) after laser excitation in deaerated MeCN at 298 K. (b) Kinetic trace for formation of $[CpFe(CO)_2]_2^{\bullet-}$. Inset: first-order plot.

In such a case $[CpFe(CO)_2]_2^{\bullet-}$ may be stable enough to be detected by ESR at a low temperature. In fact, a broad isotropic ESR signal (g = 2.0073) is detected under photo irradiation of an MeCN solution of $(BNA)_2$ (5.0 x 10^{-4} M) and $[CpFe(CO)_2]_2$ (5.0 x 10^{-4} M) with a high pressure mercury lamp at 243 K as shown in Figure 8. When the temperature is lowered to 173 K, the isotropic signal is changed to the anisotropic signal in a frozen medium with g_1 = 2.0554, g_2 = 2.0031, and g_3 = 1.9635. The averaged value (2.0073) agrees with the isotropic value in solution. The ESR spectrum with g value (2.0073) which is much larger than the free spin value may be attributed to $[CpFe(CO)_2]_2^{\bullet-}$. No organic radicals such as $BNA^{\bullet}$ was detected probably because of the fast dimerization.[19,39] In such a case it is unlikely that $[CpFe(CO)_2]^{\bullet}$ is detected by ESR, since dimerization of $[CpFe(CO)_2]^{\bullet}$ is known to be as rapid as that of $BNA^{\bullet}$.[13,19]

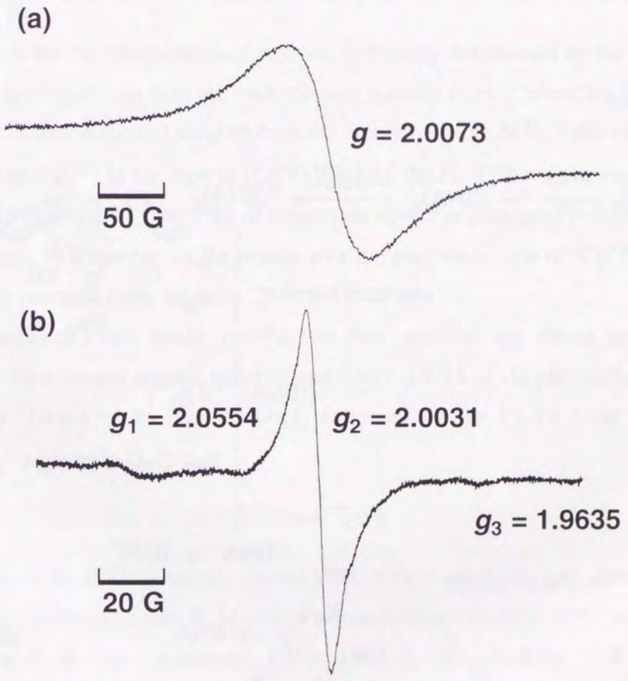

Figure 8. ESR spectra of $[CpFe(CO)_2]_2^{\bullet-}$ observed under irradiation of a deaerated MeCN solution containing $(BNA)_2$ (5.0 x 10^{-4} M) and $[CpFe(CO)_2]_2$ (5.0 x 10^{-4} M) (a) at 243 K and (b) at 173 K (frozen).

Based on the above results, the reaction mechanism of the photoreduction of $[CpFe(CO)_2]_2$ by $(BNA)_2$ is summarized as shown in Scheme 2. The triplet excited state $^3(BNA)_2^*$ generated by the intersystem crossing upon photo excitation of $(BNA)_2$ is quenched by electron transfer to $[CpFe(CO)_2]_2$ to give the radical ion pair in competition with the decay to the ground state.[40] The C–C bond of $(BNA)_2^{\bullet+}$ is readily cleaved to produce $BNA^\bullet$ and BNA^+. In the case of the photoinduced electron transfer from $(BNA)_2$ to C_{70}, the C–C bond cleavage of $(BNA)_2^{\bullet+}$ is reported to be much faster than the back electron transfer from $C_{70}^{\bullet-}$ to $(BNA)_2^{\bullet+}$, leading to formation of the products with 100 % quantum efficiency.[41] In the present case as well, the photoinduced electron transfer from $^3(BNA)_2^*$ to $[CpFe(CO)_2]_2$ results in formation of $BNA^\bullet$, BNA^+ and $[CpFe(CO)_2]_2^{\bullet-}$. Since the E^0_{red} value of BNA^+ (–1.08 V vs SCE)[39] is less negative than the E^0_{ox} value of $[CpFe(CO)_2]_2^{\bullet-}$ (–1.55 V), back electron transfer from $[CpFe(CO)_2]_2^{\bullet-}$ to BNA^+ (ΔG^0_{et} = 0.47 eV) may occur

Scheme 2

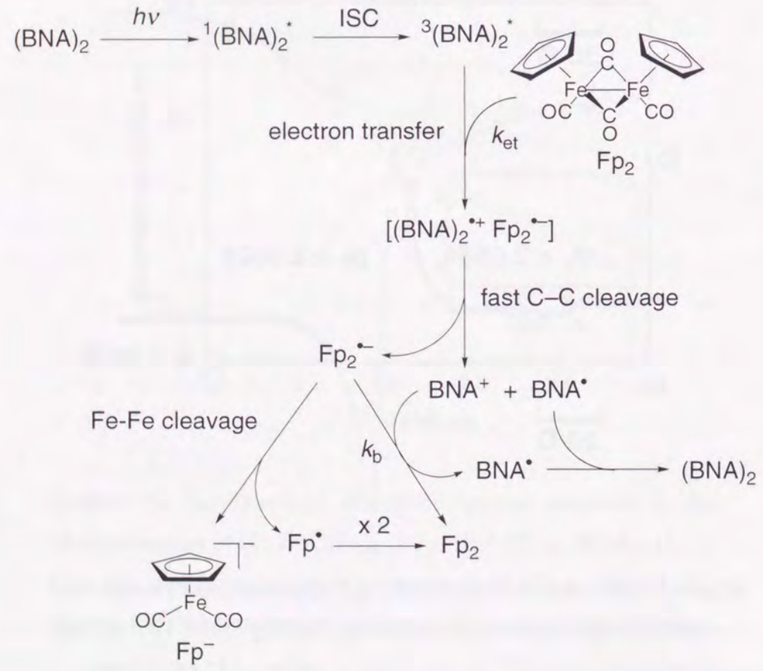

to regenerate $[CpFe(CO)_2]_2$, accompanied by formation of $BNA^\bullet$ which dimerized to reproduce $(BNA)_2$. In competition with such a back electron transfer process (k_b), the Fe–Fe bond cleavage (k_c) occurs to give $[CpFe(CO)_2]^-$ and $[CpFe(CO)_2]^\bullet$.[42] The electron transfer from $BNA^\bullet$ to $[CpFe(CO)_2]^\bullet$ gives BNA^+ and $[CpFe(CO)_2]^-$. Thus, the net reaction is two-electron reduction of $[CpFe(CO)_2]_2$ by $(BNA)_2$ to yield two equiv of $[CpFe(CO)_2]^-$ and BNA^+ (Scheme 2).

By applying the steady-state approximation to the reactive intermediates in Scheme 2, the dependence of quantum yields on the substrate concentration $[Fp_2]$ is derived as shown in eq 5, which agrees with the experimental observation in eq 2.

$$\Phi = [k_c/(k_c + k_b)]k_{et}\tau_T[Fp_2]/(1 + k_{et}\tau_T[Fp_2]) \quad (5)$$

The efficiency for the photochemical reaction is thereby determined by the Fe–Fe bond cleavage rate in competition with the back electron transfer from $[CpFe(CO)_2]_2^{\bullet-}$ to BNA^+, which may be diffusion-limited judging from the highly negative ΔG^0_{et} value of the electron transfer (*vide supra*).[43] In the case of $[Cp^*Fe(CO)_2]_2$, the Fe–Fe bond cleavage rate in the radical anion is known to be two-order of magnitude slower as compared to the cleavage rate of $[CpFe(CO)_2]_2$.[34] This may be the reason why the photoreduction of $[Cp^*Fe(CO)_2]_2$ by $(BNA)_2$ hardly occurred (*vide supra*).

In conclusion, this study provides a new method for photo generation of $[CpFe(CO)_2]^-$ by a unique organic two-electron donor $[(BNA)_2]$ via photoinduced electron transfer from $^3(BNA)_2^*$ to $[CpFe(CO)_2]_2$ followed by the Fe–Fe bond cleavage in $[CpFe(CO)_2]_2^{\bullet-}$.

References

(1) (a) Ellis, J. E. *J. Organomet. Chem.* **1975**, *86*, 1. (b) Ellis, J. E. *Comprehensive Organic Synthesis,*; Trost, B. M., Ed.; Pergamon Press: Oxford, 1991; Vol. 4.

(2) (a) King, R. B. *Adv. Organomet. Chem.* **1964**, *2*, 157. (b) King, R. B. *Acc. Chem. Res.* **1970**, *3*, 417.

(3) (a) Nitay, M.; Priester, W.; Rosenblum, M. *J. Am. Chem. Soc.* **1978**, *100*, 3620. (b) Rosenblum, M. *Acc. Chem. Res.* **1974**, *7*, 122. (c) Rosenblum, M. *J. Organomet. Chem.* **1986**, *300*, 191. (d) Davis, R.; Khazaal, N. M. S.; Maistry, V. *J. Chem. Soc.*,

Chem. Commun. **1986**, 1387.

(4) King, R. B. *Organometallic Synthesis*, Vol. 1; Academic Press: New York; 1965.

(5) Ellis, J. E.; Flom, E. A. *J. Organomet. Chem.* **1975**, *99*, 263.

(6) (a) Piper, T. S.; Wilkinson, G. *J. Inorg. Nucl. Chem.* **1956**, *3*, 104. (b) Fischer, E. O.; Böttcher, R. Z. *Naturforsch., Teil B* **1955**, *10*, 600. (c) Reger, D. L.; Fauth, D. J.; Dukes, M. D. *Synth. Reac. Inorg. Met.-Org. Chem.* **1977**, *7*, 151.

(7) Gladysz, J. A.; Williams, G. M.; Tam, W.; Johnson, D. L.; Parker, D. W.; Selover, J. C. *Inorg. Chem.* **1979**, *18*, 553.

(8) (a) Connelly, N. G.; Geiger, W. E. *Adv. Organomet. Chem.* **1984**, *23*, 1. (b) Ferguson, J. A.; Meyer, T. J. *Inorg. Chem.* **1971**, *10*, 1025. (c) Johnson, E. C.; Meyer, T. J.; Winterton, N. *Inorg. Chem.* **1971**, *10*, 1673. (d) Pugh, J. R.; Meyer, T. J. *J. Am. Chem. Soc.* **1988**, *110*, 8245.

(9) (a) Dessy, R. E.; Weissman, P. M.; Pohl, R. L. *J. Am. Chem. Soc.* **1966**, *88*, 5117. (b) Legzdins, P.; Wassink, B. *Organometallics* **1984**, *3*, 1811. (c) Miholová, D.; Vlcek, A. A. *Inorg. Chim. Acta* **1980**, *41*, 119. (d) Morán, M.; Cuadrado, I.; Losada, J. *J. Organomet. Chem.* **1987**, *320*, 317.

(10) (a) Meyer, T. J. *Prog. Inorg. Chem.* **1975**, *19*, 1. (b) Bullock, J. P.; Palazotto, M. C.; Mann, K. R. *Inorg. Chem.* **1991**, *30*, 1284.

(11) Pugh, J. R.; Meyer, T. J. *J. Am. Chem. Soc.* **1992**, *114*, 3784.

(12) Wrighton, M. *Chem. Rev.* **1974**, *74*, 401.

(13) (a) Meyer, T. J.; Caspar, J. V. *Chem. Rev.* **1985**, *85*, 187. (b) Caspar, J. V.; Meyer, T. J. *J. Am. Chem. Soc.* **1980**, *102*, 7794.

(14) Geofroy, G. L.; Wrighton, M. S. *Organometallic Photochemistry*; Academic Press: New York, 1979.

(15) (a) Abrahamson, H. B.; Palazzotto, M. C.; Reichel, C. L.; Wrighton, M. S. *J. Am. Chem. Soc.* **1979**, *101*, 4123. (b) Blaha, J. P.; Bursten, B. E.; Dewan, J. C.; Frankel, R. B.; Randolph, C. L.; Wilson, B. A.; Wrighton, M. S. *J. Am. Chem. Soc.* **1985**, *107*, 4561. (c) Hooker, R. H.; Mahmoud, K. A.; Rest, A. J. *J. Chem. Soc., Chem. Commun.* **1983**, 1022.

(16) (a) Bursten, B. E.; McKee, S. D.; Platz, M. *J. Am. Chem. Soc.* **1989**, *111*, 3428. (b) Zhang, S.; Brown, T. L. *J. Am. Chem. Soc.* **1993**, *115*, 1779. (c) Kvietok, F. A.; Bursten, B. E. *J. Am. Chem. Soc.* **1994**, *116*, 9807. (d) Tyler, D. R.; Schmidt, M. A.; Gray, H. B. *J. Am. Chem. Soc.* **1979**, *101*, 2753.

(17) (a) George, M. W.; Dougherty, T. P.; Heilweil, E. J. *J. Phys. Chem.* **1996**, *100*, 201. (b) Dixon, A. J.; George, M. W.; Hughes, C.; Poliakoff, M.; Turner, J. J. *J. Am. Chem. Soc.* **1992**, *114*, 1719. (c) Dixon, A. J.; Healy, M. A.; Poliakoff, M.; Turner, J. J. *J. Chem. Soc., Chem. Commun.* **1986**, 994.

(18) Patz, M.; Kuwahara, Y.; Suenobu, T.; Fukuzumi, S. *Chem. Lett.* **1997**, 567.

(19) Fukuzumi, S.; Suenobu, T.; Patz, M.; Hirasaka, T.; Itoh, S.; Fujitsuka, M.; Ito, O. *J. Am. Chem. Soc.* **1998**, *120*, 8060.

(20) Wallenfels, K.; Gellrich, M. *Chem. Ber.* **1959**, *92*, 1406.

(21) Perrin, D. D.; Armarego, W. L. F. *Purification of Laboratory Chemicals*; Butterworth-Heinemann: Oxford, 1998.

(22) Hatchard, C. G.; Parker, C. A. *Proc. R. Soc. London, Ser. A* **1956**, *235*, 518.

(23) Amatore, C.; Lefrou, C.; Pflüger, F. *J. Electroanal. Chem.* **1989**, *270*, 43.

(24) Amatore, C.; Thouin, L.; Bento, M.F. *J. Electroanal. Chem.* **1999**, *463*, 45.

(25) (a) Baerends, E. J.; Ellis, D. E.; Ros, P. *Chem. Phys.* **1973**, *2*, 41. (b) te Velde, B.; Baerends, E. J. *J. Comput. Phys.* **1992**, *99*, 84.

(26) Vosko, S. H.; Wilk, L.; Nusair, M. *Can. J. Phys.* **1980**, *58*, 1200.

(27) Becke, A. *Phys. Rev. A* **1988**, *38*, 3098.

(28) (a) Perdew, J. P. *Phys. Rev. B* **1986**, *33*, 8822. (b) Perdew, J. P. *Phys. Rev. B* **1986**, *34*, 7406.

(29) Versluis, L.; Ziegler, T. *J. Chem. Phys.* **1988**, *88*, 322.

(30) Hepp, A. F.; Blaha, J. P.; Lewis, C.; Wrighton, M. S. *Organometallics* **1984**, *3*, 174.

(31) Bullitt, J. G.; Cotton, F. A.; Marks, T. J. *J. Am. Chem. Soc.* **1970**, *92*, 2155.

(32) Adams, R. D.; Cotton, F. A. *J. Am. Chem. Soc.* **1973**, *95*, 6589.

(33) Davies, S. G.; Simpson, S. J.; Parker, V. D. *J. Chem. Soc., Chem. Commun.* **1984**, 352.

(34) Dalton, E. F.; Ching, S.; Murray, R. W. *Inorg. Chem.* **1991**, *30*, 2642.

(35) Amatore, C.; Jutand, A.; Pflüger, F. *J. Electroanal. Chem.* **1987**, *218*, 361.

(36) Bard, A.J.; Faulkner, L.R. *Electrochemical Methods*; J. Wiley & Sons: New York, 1980.

(37) Rehn, A.; Weller, A. *Isr. J. Chem.* **1970**, *8*, 259.

(38) Czochralska, B.; Lindqvist, L. *Chem. Phys. Lett.* **1983**, *101*, 297. (b) Lindqvist, L.; Czochralska, B.; Grigorov, I. *Chem. Phys. Lett.* **1985**, *119*, 494.

(39) Fukuzumi, S.; Koumitsu, S.; Hironaka, K.; Tanaka, T. *J. Am. Chem. Soc.* **1987**, *109*,

305.

(40) Under our experimental conditions, the irradiation at 350 nm results in mostly formation of $^3(BNA)_2^*$ and the photo cleavage of Fe-CO bond of $[CpFe(CO)_2]_2$ is negligible based on the stoichiometry of the photochemical reaction (see Experimental Section).

(41) Fukuzumi, S.; Suenobu, T.; Hirasaka, T.; Sakurada, N.; Arakawa, R.; Fujitsuka, M.; Ito; O. *J. Phys. Chem. A* **1999**,*103*, 5935.

(42) Acetonitrile used as the solvent for the photochemical reaction via photoinduced electron transfer may be coordinated to Fe in coordinately unsaturated intermediates in Scheme 2.

(43) The photoreduction of $[CpFe(CO)_2]_2$ by $(BNA)_2$ may also proceed via photoinduced electron transfer from $^3(BNA)_2^*$ to the unbridged trans-isomer, which exists as a much less stable form, leading to the facile Fe–Fe bond cleavage in the dimer radical anion. If this is the major pathway, the rate constant ($k_{obs} = K_{obs}\tau_T^{-1}$) derived from the dependence of F on $[Fp_2]$ (eq 2) would be much smaller than the rate constant of photoinduced electron transfer determined directly from appearance of the transient absorption at 470 nm due to $[CpFe(CO)_2]_2^{\bullet-}$ (Figure 7b). The agreement between the k_{obs} and k_{et} values obtained in this study indicates that a reaction pathway via a cleavage precursor such as an unbridged isomer of $[CpFe(CO)_2]_2$ is not a major pathway in the photoreduction of $[CpFe(CO)_2]_2$ by $(BNA)_2$.

Chapter 5

Catalysis of Metal Ions of Electron Transfer

Section 5. 1

Quantitative Evaluation of Lewis Acidity of Metal Ions Derived from the *g*-Values of ESR Spectra of Superoxide-Metal Ion Complexes in Relation with the Promoting Effects in Electron Transfer Reactions

Abstract: The g-values of ESR spectra of superoxide-metal ion complexes ($O_2^{\bullet-}$–M^{n+}, n = 1, 2, 3) are determined in acetonitrile at 143 K. The binding energies (ΔE) of metal ions with $O_2^{\bullet-}$ have been evaluated from deviation of the g_{zz}-values from the free spin value. The ΔE values are well correlated with the catalytic reactivities of metal ions in electron transfer from cobalt(II) tetraphenylporphyrin to O_2 and p-benzoquinone, which does not occur in the absence of metal ions under otherwise the same experimental conditions. The ΔE values can thereby be used as the first quantitative measure for Lewis acidity of metal ions in relation with the catalytic reactivities in electron transfer reactions.

Introduction

Metal ions acting as Lewis acids has played a pivotal role in promoting various reactions of synthetic value because of the high reactivities and selectivities achieved under the mild reaction conditions.[1,2] The Lewis acid-promoted reactions are believed to proceed through the coordination of a Lewis acid to a lone pair of heteroatoms, such as oxygen of carbonyl compounds and a nitrogen atom of imines.[1,2] The coordination of a Lewis acid to π-electrons of C–C multiple bonds has also been reported to be effective for the regio- and chemoselective reduction of aldehydes with an alkynyl group.[3] Metal ions and the salts acting as Lewis acids can also promote free radical reactions[4,5] and electron transfer reactions.[6,7] The promoting effects of metal ions are certainly related to the Lewis acidity of metal ion salts. Charges and ion radii are important factors to determine the Lewis acidity of metal ions. To the best of our knowledge, however, there has so far been no *quantitative* experimental measure to determine the Lewis acidity of a wide variety of metal ions in

relation with the promoting effects, although limited number of formation constants for metal ion complexes with substrates are known.

We report herein that the g_{zz}-values of ESR spectra of superoxide-metal ion complexes are highly sensitive to the Lewis acidity of a variety of metal ions and that the binding energies readily derived from the g_{zz}-values provide the first quantitative experimental measure of Lewis acidity of a wide variety of metal ions, which are shown to be directly correlated with the promoting effects in electron transfer reactions.

Experimental Section

Materials. Cobalt(II) tetraphenylporphyrin, (TPP)Co, was prepared as described in the literature.[8] *p*-Benzoquinone was purchased from Tokyo Kasei Organic Chemicals, and purified by the standard methods.[9] The dimeric 1-benzyl-1,4-dihydronicotinamide [$(BNA)_2$] was prepared according to the literature.[10] Scandium triflate [$Sc(OTf)_3$] was purchased from Pacific Metals Co., Ltd. (Taiheiyo Kinzoku). Lanthanum triflate [$La(OTf)_3$] was obtained from Aldrich as hexahydrate form. Yttrium triflate [$Y(OTf)_3$], europium triflate [$Eu(OTf)_3$], ytterbium triflate [$Yb(OTf)_3$] and lutetium triflate [$Lu(OTf)_3$] were prepared as follows.[11] A deionized aqueous solution was mixed (1:1 v/v) with trifluoromethanesulfonic acid (> 99.5 %, 10.6 mL) obtained from Central Glass, Co., Ltd., Japan. The trifluoromethanesulfonic acid solution was slowly added to a flask which contained the corresponding metal oxide (> 99.9 %, 30 mmol). The mixture was refluxed at 100 °C for 3 days. After centrifugation of the reaction mixture, the solution containing metal triflate was separated and water was removed by vacuum evaporation. Yttrium oxide, europium oxide and ytterbium triflate were supplied from Shin Etsu Chemical, Co., Ltd., Japan. Lutetium oxide supplied from Nichia Corporation, Japan. Metal triflates were dried under vacuum evacuation at 403 K for 40 h prior to use. Magnesium perchlorate [$Mg(ClO_4)_2$] and sodium perchlorate ($NaClO_4$) were obtained from Wako Pure Chemical Ind. Ltd., Japan. Calcium perchlorate [$Ca(ClO_4)_2$], strontium perchlorate [$Sr(ClO_4)_2$], barium perchlorate [$Ba(ClO_4)_2$] and lithium perchlorate ($LiClO_4$) were obtained from Nacalai Tesque, Japan. Acetonitrile (MeCN) used as solvent was purified and dried by the standard procedure.[9]

ESR Measurements. A quartz ESR tube (4.5-mm i.d.) containing an oxygen-saturated MeCN solution of $(BNA)_2$ (1.0×10^{-4} M) and a metal ion (1.0×10^{-3} M) was irradiated in the cavity of the ESR spectrometer with the focused light of a 1000-W high-pressure Hg lamp through an aqueous filter. The ESR spectra of $O_2^{\bullet-}$–M^{n+} in frozen MeCN were measured at 143 K with a JEOL X-band spectrometer (JES-RE1XE) using an attached VT (Variable Temperature) apparatus under nonsaturating microwave power conditions. The *g* values were calibrated precisely with a Mn^{2+} marker which was used as a reference.

Spectral and Kinetic Measurements. Kinetic measurements for electron transfer from (TPP)Co to oxygen and *p*-benzoquinone were carried out using a Hewlett-Packard 8453 photodiode array spectrophotometer or a Shimadzu UV-3100PC spectrophotometer at 298 K. The rates of the electron transfer were followed by spectrally monitoring an increase or decrease in absorbance due to $[(TPP)Co]^+$ or (TPP)Co. The rate constants of electron transfer (k_{et}) were determined by the pseudo-first order plots for the electron transfer reactions in the presence of a large excess oxygen and metal ions. It was confirmed that the pseudo-first order rate constant was proportional to the oxygen (or *p*-benzoquinone) and metal ion concentrations. The pseudo-first-order rate constants were determined by a least-squares curve fit using a Macintosh microcomputer. The pseudo-first-order plots were linear for three or more half-lives with the correlation coefficient $\rho > 0.999$. The k_{et} values in Table 1 were determined within an experimental error of ±5%.

Theoretical Calculations. Density functional calculations were performed on a COMPAQ DS20E computer using the spin-restricted B3LYP functional for the open shell $O_2^{\bullet-}$-M^{n+}.[11] B3LYP geometries for $O_2^{\bullet-}$-M^{n+} were determined using the 6-311++G(3d,3p) basis and the Gaussian 98 program.[12] The $\langle S^2 \rangle$ value was determined to range from 0.755 to 0.762 for $O_2^{\bullet-}$ and $O_2^{\bullet-}$-M^{n+} ($M^{n+} = Li^+$, Mg^{2+} and Sc^{3+}), indicating a good representation of the doublet state.

Results and Discussion

Superoxide ion is produced by the photoinduced reduction of O_2 by the dimeric 1-benzyl-1,4-dihydronicotinamide [$(BNA)_2$] in acetonitrile (MeCN),[13] which can act as a unique two electron donor,[14] as shown in (eq. 1). When an oxygen-saturated MeCN solution containing $(BNA)_2$ (1.0×10^{-4} M) was irradiated with a high pressure mercury lamp, $O_2^{\bullet-}$ formed photochemically is detected by the ESR spectrum in frozen MeCN at 143 K. The ESR spectrum shows a typical anisotropic signal with $g_{//} = 2.090$ and $g_{\perp} = 2.005$.[15] The ESR spectra of $O_2^{\bullet-}$ produced in the presence of a variety of closed shell metal ions were

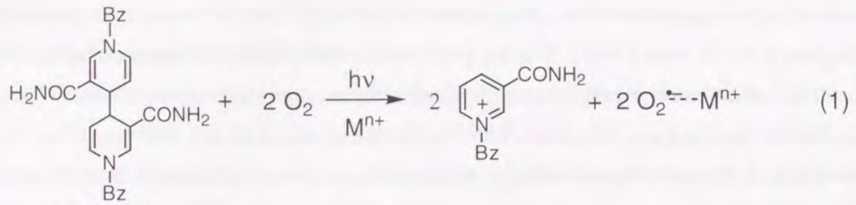

also measured at 143 K and the g_{zz}-values are listed in Table 1.[16] The anisotropic ESR signals are changed significantly in the presence of each metal ion as compared to that in its absence. In particular, the g_{zz}-values of $O_2^{\bullet-}$ in the presence of metal ions become significantly smaller than the value of $O_2^{\bullet-}$ due to the complexation of metal ions with $O_2^{\bullet-}$ ($O_2^{\bullet-}$–M^{n+}, n = 1–3). Figure 1 shows typical examples of ESR spectra of M^{2+}–$O_2^{\bullet-}$ complexes (M^{2+} = Mg^{2+}, Ca^{2+}, Sr^{2+} and Ba^{2+}) measured in frozen MeCN at 143 K. The g_{zz}-values of a series of metal ion-$O_2^{\bullet-}$ complexes are listed in Table 1.

The g-tensor in particular the g_{zz}-value gives valuable information concerning the binding strength of $O_2^{\bullet-}$-M^{n+}. The deviation of the g_{zz}-value from the free spin value (g_e = 2.0023) is caused by the spin-orbit interaction as given by eq. 2.[17]

$$g_{zz} = g_e + 2\sqrt{\frac{\lambda^2}{\lambda^2 + \Delta E^2}} \qquad (2)$$

where λ is the spin-orbit coupling constant of oxygen which is known as 0.014 eV,[18] and ΔE is the energy splitting of π_g levels due to the complex formation between $O_2^{\bullet-}$ and M^{n+}. Under the conditions that $\Delta E >> \lambda$, eq. 2 is reduced to a simple relation, $g_{zz} = g_e + 2\lambda/\Delta E$. Thus, the ΔE values are readily determined from the deviation of the g_{zz}-values from the g_e-value as listed in Table 1.[19] It should be noted that the g_{zz}-values can be determined quite accurately within experimental errors ± 0.0001. The ΔE value increases generally with in order: monovalent cations (M^+) < divalent cations (M^{2+}) < trivalent cations (M^{3+}) except for Li^+ which has the smallest ion radius.[20] The ΔE value also increases with decreasing the ion radius when the oxidation state of the metal ion is the same (Table 1). Thus, the ΔE value of a monovalent cation (Li^+) becomes larger than those of divalent cations (Ba^{2+} and Sr^{2+}) whose radii are significantly larger than that of Li^+ (Table 1).[21] Scandium ion which has the smallest ion radius among the trivalent metal cations gives the largest ΔE value, and this indicates that

the binding energy between Sc^{3+} and $O_2^{\bullet-}$ is the strongest. In the case of $O_2^{\bullet-}$-Sc^{3+}, an "end-on" coordination form of $^{\bullet}O$-O^--Sc^{3+} is indicated by the hyperfine splitting of two different ^{17}O atoms (I = 5/2) in which the electron spin is more localized at the terminal oxygen (60%).[8] This is confirmed by the DFT (density function theory) calculation using the spin-restricted B3LYP functional and the 6-311++G(3d,3p) basis set for the open shell $O_2^{\bullet-}$-Sc^{3+}, which gives more localized spin density at the terminal oxygen (65%) (see Experimental section).[22] The structures of $O_2^{\bullet-}$ and $O_2^{\bullet-}$-M^{n+} (M^{n+} = Li^+, Mg^{2+} and Sc^{3+} were also calculated. The O-O distance decreases in order: $O_2^{\bullet-}$ (1.343 Å) > $O_2^{\bullet-}$-Li^+ (1.309 Å) > $O_2^{\bullet-}$-Mg^{2+} (1.297 Å) > $O_2^{\bullet-}$-Sc^{3+} (1.211 Å) as the ΔE vlaue increases (Table 1).

Metal ions such as Mg^{2+} has been reported to promote electron transfer from (TPP)Co (TPP^{2-} = dianion of tetraphenylporphyrin) to *p*-benzoquinone, although no reaction between (TPP)Co and *p*-benzoquinone occurs in the absence of metal ions in MeCN.[7e] Such promoting effects of metal ions in electron transfer reduction of substrates have been ascribed to the binding of metal ions to the radical anions produced in the electron transfer reactions.[6] Thus, in order to assess a relation between the ΔE value and promoting effects of metal ions in electron transfer reduction of O_2, the rates of electron transfer from (TPP)Co to O_2 are determined in the presence of a series of metal ions (M^{n+}, n = 1–3) by the UV–vis spectral change for the decay of (TPP)Co (λ_{max} = 411 nm) and the formation of $[(TPP)Co]^+$ (λ_{max} = 434 nm) in MeCN at 298 K.

No electron transfer from (TPP)Co (E^0_{ox} = 0.35 V *vs* SCE in MeCN)[23] to O_2 (E^0_{red} = –0.86 V *vs* SCE in MeCN)[24] has occurred in MeCN at 298 K. In the presence of M^{n+}, however, an efficient electron transfer from (TPP)Co to O_2 occurs to yield $[(TPP)Co]^+$ eq. 3 as shown in Figure 2. The electron transfer rates obeyed second–order

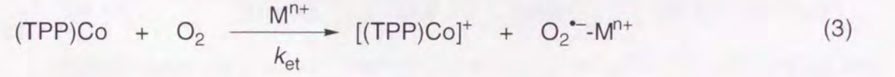

kinetics, showing a first–order dependence on the concentration of each reactant [O_2 and (TPP)Co] (Figure 3a). The observed second–order rate constant (k_{obs}) for the M^{n+}-promoted electron transfer increases linearly with increasing the metal ion concentration (Figure 3b). The M^{n+}-promoted electron transfer rate constants (k_{et}) determined from the slope of the linear plot of k_{obs} vs [M^{n+}] are also listed in Table 1.

Table 1. g_{zz}-Values of ESR Spectra of $O_2^{\bullet-}$–M^{n+}, Rate Constants (k_{et}) for M^{n+}-Promoted Electron Transfer from (TPP)Co to O_2 and *p*–Benzoquinone (Q) and Ionic Radii (r) of M^{n+}

				k_{et} / $M^{-2}\,s^{-1}$	
M^{n+}	r / Å[a]	g_{zz}	ΔE, eV	O_2	Q
free	——	2.0900	0.32	[b]	[b]
Li^{+} [c]	0.92	2.0546	0.53	3.6×10^{-1}	1.6×10^{-1}
Na^{+} [c]	1.18	2.0841	0.34	[b]	[b]
Mg^{2+} [c]	0.89	2.0451	0.65	1.3×10	3.3
Ca^{2+} [c]	1.12	2.0499	0.58	1.1	7.0×10^{-1}
Sr^{2+} [c]	1.26	2.0558	0.52	1.0×10^{-1}	1.6×10^{-1}
Ba^{2+} [c]	1.42	2.0587	0.49	5.1×10^{-2}	3.0×10^{-2}
Sc^{3+} [d]	0.81	2.0304	1.00	1.9×10^{6}	2.7×10^{5}
Y^{3+} [d]	1.02	2.0349	0.85	1.2×10^{4}	2.7×10^{4}
La^{3+} [d]	1.16	2.0365	0.82	3.0×10^{3}	1.9×10^{3}
Eu^{3+} [d]	1.25	2.0362	0.82	7.0×10^{2}	1.1×10^{3}
Yb^{3+} [d]	1.14	2.0357	0.83	8.2×10^{2}	1.2×10^{3}
Lu^{3+} [d]	0.98	2.0358	0.83	1.1×10^{3}	8.2×10^{2}

a) Effective ionic radii (coordination number = 8).[21] (b) No reaction or too slow to be determined accurately. (c) ClO_4^- salt. (d) $CF_3OSO_3^-$ salt.

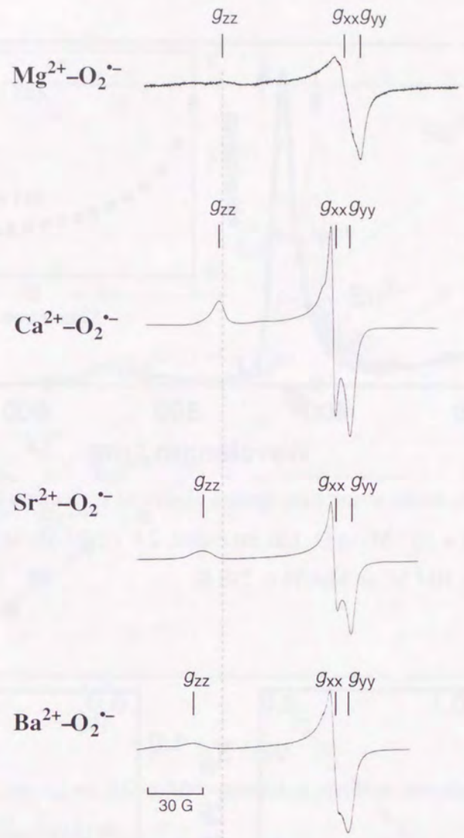

Figure 1. ESR spectra of M^{2+}–$O_2^{\bullet-}$ complexes (M^{2+} = Mg^{2+}, Ca^{2+}, Sr^{2+} and Ba^{2+}) in frozen MeCN at 143 K.

There is a *striking linear correlation* between log k_{et} and ΔE of $O_2^{\bullet-}$–M^{n+} derived from the g_{zz}-values as shown in Figure 4. The remarkable correlation spans a range of almost 10^7 in the rate constant. The slope of the linear correlation between logk_{et} and ΔE is obtained as 14.0 which is close to the value of $1/2.3kT$ (=16.9, where k is the Boltzmann constant and T = 298 K).[25] This means that the variation of ΔE is well reflected in the difference in the activation free energy for the M^{n+}-promoted electron transfer from (TPP)Co to O_2. The stronger the binding of M^{n+} with $O_2^{\bullet-}$, the larger will be the promoting effects of M^{n+}.

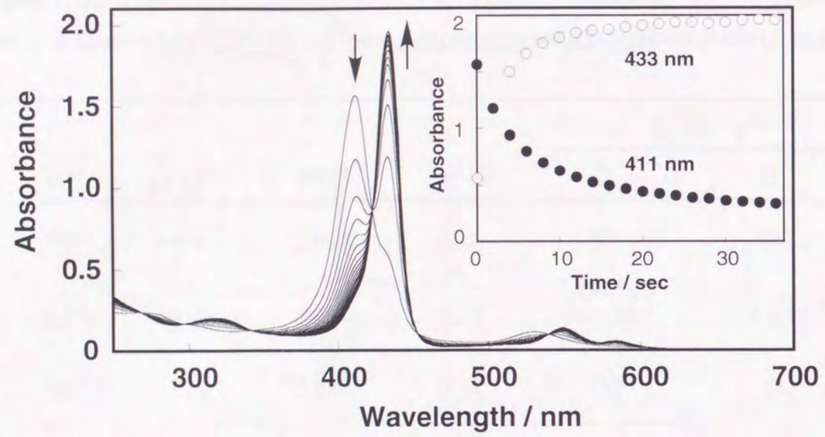

Figure 2. Electronic absorption spectra observed in electron transfer from (TPP)Co (1.0×10^{-5} M) to O_2 (air saturated, 2.6×10^{-3} M) in the presence of Sc^{3+} (1.7×10^{-5} M) in MeCN at 298 K.

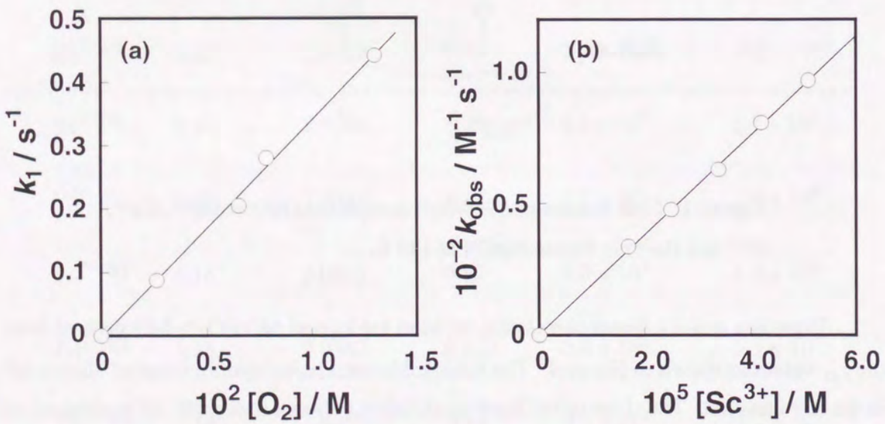

Figure 3. (a) Plot of pseudo-first order rate constants (k_1) vs [O_2] in the presence of Sc^{3+} (1.7×10^{-5} M) in MeCN at 298 K. (b) Plot of k_{obs} vs [Sc^{3+}] in MeCN at 298 K.

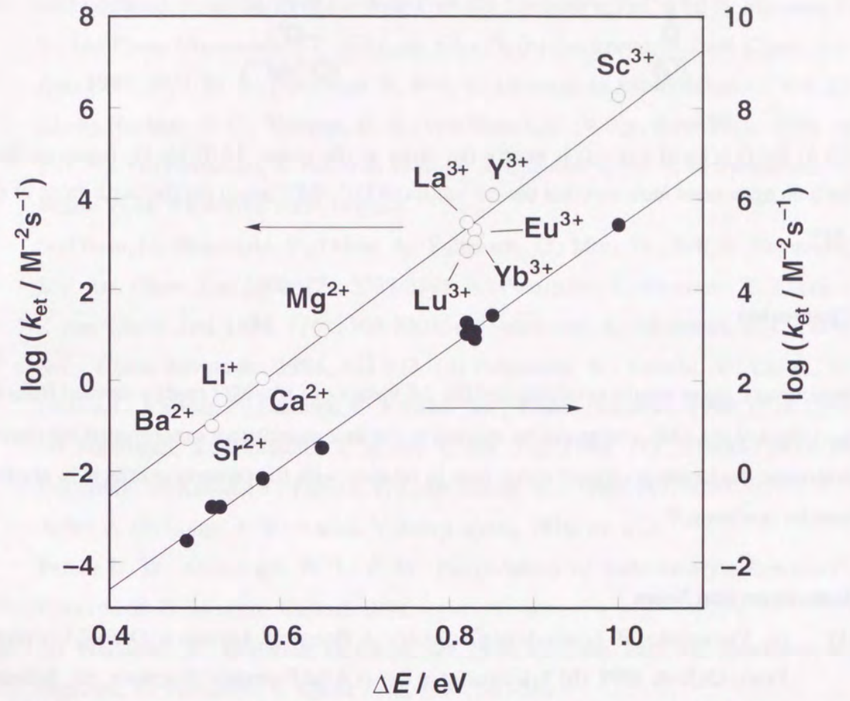

Figure 4. Plots of log k_{et} vs ΔE in M^{n+}-promoted electron transfer from (TPP)Co to O_2 (○) and *p*-benzoquinone(●).

Thus, ΔE can be regarded as good measure of the binding energies in the $O_2^{\bullet-}$–M^{n+} complexes.

The applicability of ΔE to predict the reactivities in M^{n+}-promoted electron transfer reactions is also examined in M^{n+}-promoted electron transfer from (TPP)Co to *p*-benzoquinone (Q) (eq. 4). It should be noted that no electron transfer occurred from (TPP)Co to Q (E^0_{red} = –0.51 V vs SCE) in the absence of M^{n+}. The M^{n+}-promoted electron transfer rate constants (k_{et}) determined from the slopes of the linear plots of k_{obs} vs [M^{n+}] for Q are also listed in Table 1. There is also an excellent linear correlation between log k_{et} and ΔE as shown in Figure 4 (closed circles). More importantly the slope

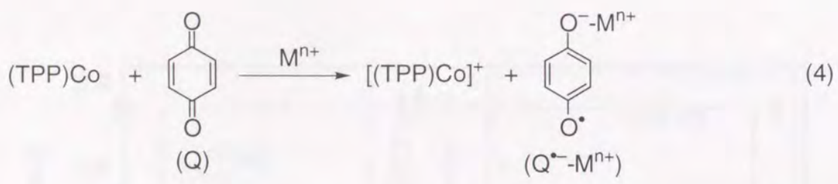

(4)

(13.3) for Q (closed circles) is nearly the same as the slope (14.0) for O_2 (open circles). Such an agreement indicates that the ΔE values of $O_2^{\bullet-}$–M^{n+} are in parallel with those of $Q^{\bullet-}$–M^{n+}.

Conclusion

In summary, these results establish that the ΔE values of $O_2^{\bullet-}$–M^{n+} readily derived from the g_{zz}-values of the ESR spectra can be utilized as the first quantitative experimental measure to determine the Lewis acidity of metal ions in relation with the promoting effects in electron transfer reactions.[26]

References and Notes

(1) (a) Yamamoto, H. *Lewis Acid Chemistry: A Practical Approach*, Oxford University Press, Oxford, 1999. (b) *Selectivities in Lewis Acid Promoted Reactions*, ed.: Schinzer, D., Kluwer Academic Publishers, Dordrecht, The Netherlands, 1989. (c) Santelli, M.; Pons, J.-M. *Lewis Acids and Selectivity in Organic Synthesis*, CRC Press, Boca Raton, FL, 1995. (d) Reetz, M. T. *Angew. Chem., Int. Ed. Engl.* **1984**, *23*, 556-569.

(2) (a) Singh, P. *Chem. Rev.* **1997**, *97*, 721-737. (b) Mahrwald, R. *Chem. Rev.* **1999**, *99*, 1095-1120.

(3) Asao, N.; Asano, T.; Ohishi, T.; Yamamoto, Y. *J. Am. Chem. Soc.* **2000**, *122*, 4817-4818.

(4) (a) Renaud, P.; Gerster, M. *Angew. Chem., Int. Ed. Engl.*, **1998**, *37*, 2562-2579. (b) Guindon, Y.; Guerin, B.; Rancourt, J.; Chabot, C.; Mackintosh, N.; Ogilvie, W. W. *Pure Appl. Chem.* **1996**, *68*, 89-96.

(5) (a) Mero, C. L.; Porter, N. A. *J. Am. Chem. Soc.* **1999**, *121*, 5155-5160. (b) Sibi, M. P.; Ji, J.; Sausker, J. B.; Jasperse, C. P. *J. Am. Chem. Soc.* **1999**, *121*, 7517-7526. (c) Sibi, M. P.; Ji, J. *Angew. Chem., Int. Ed. Engl.*, **1997**, *36*, 274-276. (d) Yamamoto, Y.; Onuki, S.; Yumoto, M.; Asao, N. *J. Am. Chem. Soc.* **1994**, *116*, 421-422. (e) Wu, J. H.; Radinov, R.; Porter, N. A. *J. Am. Chem. Soc.* **1995**, *117*, 11029-11030.

(6) (a) Fukuzumi, S. *Advances in Electron Transfer Chemistry*, *Vol. 2*, ed by Mariano, P. S., JAI Press, Greenwich, CT, 1992, pp. 67-175. (b) Fukuzumi, S. *Bull. Chem. Soc. Jpn.* **1997**, *70*, 1-28. (c) Fukuzumi, S.; Itoh, S. *Advances in Photochemistry*, *Vol. 25*, eds by Neckers, D. C.; Volman, D. H.; von Bünau, G., Wiley, New York, 1998, pp 107-172. (d) Fukuzumi, S. *Electron Transfer in Chemistry*, *Vol. 5*, ed by Balzani, V. Wiley-VCH, Weinheim, 2000, in press.

(7) (a) Ohtsu, H.; Shimazaki, Y.; Odani, A.; Yamauchi, O.; Mori, W.; Itoh, S.; Fukuzumi, S. *J. Am. Chem. Soc.* **2000**, *122*, 5733-5741. (b) Fukuzumi, S.; Okamoto, T.; Otera, J. *J. Am. Chem. Soc.* **1994**, *116*, 5503-5504. (c) Fukuzumi, S.; Okamoto, T. *J. Chem. Soc., Chem. Commun.*, **1994**, 521-522. (d) Fukuzumi, S.; Tokuda, Y.; Chiba, Y.; Gereci, L.; Carloni, P.; Damiani, E. *J. Chem. Soc., Chem. Commun.*, **1993**, 1575-1577. (e) Fukuzumi, S.; Okamoto, T. *J. Am. Chem. Soc.* **1993**, *115*, 11600-11601. (f) Fukuzumi, S.; Kuroda, S.; Tanaka, T. *J. Am. Chem. Soc.* **1985**, *107*, 3020-3027.

(8) Adler, A. D.; Longo, F. R.; Váradi, V. *Inorg. Synth.* **1976**, *16*, 213.

(9) Perrin D. D.; Armarego, W. L. F. In "*Purification of Laboratory Chemicals*", Butterworth-Heinemann: Oxford, 1988.

(10) (a) Wallenfels, K.; Gellerich, M. *Chem. Ber.* **1959**, *92*, 1406. Patz, M.; Kuwahara, Y.; Suenobu, T.; Fukuzumi, S. *Chem. Lett.*, **1997**, 567-568.

(11) (a) Forsberg, J. H.; Spaziano, V. T.; Balasubramanian, T. M.; Liu, G. K.; Kinsley, S. A.; Duckworth, C. A.; Poteruca, J. J.; Brown, P. S.; Miller, J. L. *J. Org. Chem.* **1987**, *52*, 1017-1021. (b) Kobayashi, S.; Hachiya, I. *J. Org. Chem.* **1994**, *59*, 3590-3596.

(12) Frisch, M. J.; Trucks, G. W.; Schlegel, H. B.; Scuseria, G. E.; Robb, M. A.; Cheeseman, J. R.; Zakrzewski, V. G.; Montgomery, J. A., Jr.; Stratmann, R. E.; Burant, J. C.; Dapprich, S.; Millam, J. M.; Daniels, A. D.; Kudin, K. N.; Strain, M. C.; Farkas, O.; Tomasi, J.; Barone, V.; Cossi, M.; Cammi, R.; Mennucci, B.; Pomelli, C.; Adamo, C.; Clifford, S.; Ochterski, J.; Petersson, G. A.; Ayala, P. Y.; Cui, Q.; Morokuma, K.; Malick, D. K.; Rabuck, A. D.; Raghavachari, K.; Foresman, J. B.; Cioslowski, J.; Ortiz, J. V.; Baboul, A. G.; Stefanov, B. B.; Liu, G.; Liashenko, A.; Piskorz, P.; Komaromi, I.; Gomperts, R.; Martin, R. L.; Fox, D. J.; Keith, T.; Al-Laham, M. A.; Peng, C. Y.; Nanayakkara, A.; Gonzalez, C.; Challacombe, M.; Gill, P. M. W.; Johnson, B.; Chen, W.; Wong, M. W.; Andres, J. L.; Gonzalez, C.; Head-

Gordon, M.; Replogle, E. S.; Pople, J. A. *Gaussian 98 (Revision A.7)* Gaussian, Inc.; Pittsburgh PA, 1998.

(13) Fukuzumi, S.; Patz, M.; Suenobu, T.; Kuwahara, Y.; Itoh, S. *J. Am. Chem. Soc.* **1999**, *121*, 1605-1606.

(14) (a) Fukuzumi, S.; Suenobu, T.; Patz, M.; Hirasaka, T.; Itoh, S.; Fujitsuka, M.; Ito, O. *J. Am. Chem. Soc.* **1998**, *120*, 8060-8068. (b) Patz, M.; Kuwahara, Y.; Suenobu, T.; Fukuzumi, S. *Chem. Lett.*, **1997**, 567-568.

(15) Bagchi, R. N.; Bond, A. M.; Scholz, F.; Stösser, R. *J. Am. Chem. Soc.* **1989**, *111*, 8270-8271.

(16) Since open shell metal ion complexes with $O_2^{\bullet-}$ are ESR silent, determination of ΔE values are limited to closed shell metal ions.

(17) (a) Känzig, W.; Cohen, M. H. *Phys. Rev. Lett.* **1959**, *3*, 509-510. (b) Zeller, H. R.; Kanzig, W. *Helv. Phys. Acta* **1967**, *40*, 845.

(18) Kasai, P. H. *J. Chem. Phys.* **1965**, *43*, 3322-3327.

(19) The ΔE values can also be derived from g_{xx}- and g_{yy}-values.(12) However, the g_{zz}-values are used to determine the ΔE values since they are the most sensitive to the ΔE values.

(20) The same trend has been reported for $O_2^{\bullet-}$ adsorbed on the surface of various metal oxides; see: (a) Lunsford, J. H. *Catal. Rev.* **1973**, *8*, 135-157. (b) Che, M. *Chem. Rev.* **1997**, *97*, 305-331.

(21) Shannon, R. D. *Acta Cryst.* **1976**, *A32*, 751.

(22) Becke, A. D. *J. Chem. Phys.* **1993**, *98*, 5648-5652.

(23) Fukuzumi, S.; Mochizuki, S.; Tanaka, T. *Inorg. Chem.* **1989**, *28*, 2459-2465.

(24) Sawyer, D. T.; Calderwood, T. S.; Yamaguchi, K.; Angelis, C. T. *Inorg. Chem.* **1983**, *22*, 2577-2583.

(25) The value is obtained from $1/2.3kT = (1.602 \times 10^{-19}\ \text{J})/[2.3(1.381 \times 10^{-23}\ \text{J K}^{-1})(298\ \text{K})] = 16.9$.

(26) The ΔE values may also be applied to predict the reactivities of metal ions in a variety of metal ion-promoted reactions, although more general applicability of the ΔE values has yet to be examined.

Section 5. 2

Exohedral Coordination of Fullerene Dianions to Metal Ions and the Accelerating Effects in Disproportionation of Fullerene Radical Anions

Abstract: Metal ions such as Mg^{2+}, Ca^{2+}, Sr^{2+} and Ba^{2+} are found to accelerate the disproportionation of $C_{60}^{\bullet-}$ and $C_{70}^{\bullet-}$. The accelerating effects of metal ions are well correlated with the metal ion-promoted electron transfer from (TPP)Co (TPP^{2-} = tetraphenylporphyrin dianion) to *p*-benzoquinone (Q). This indicates that the electron transfer disproportionation of $C_{60}^{\bullet-}$ and $C_{70}^{\bullet-}$ is accelerated by the exohedral coordination of C_{60}^{2-} and C_{70}^{2-} to metal ions. Metal ions can also accelerate electron transfer from $C_{60}^{\bullet-}$ to phenacyl bromide.

Introduction

Fullerenes are unique compounds containing a large number of π-electrons. In the reduction of C_{60}, the first electron is added to a triply degenerate t_{1u} unoccupied molecular orbital and the stepwise addition of up to six electrons to C_{60} has been achieved.[1,2] $C_{60}^{\bullet-}$, once formed, is stable and virtually no disproportionation of $C_{60}^{\bullet-}$ occurs, since electron transfer between two $C_{60}^{\bullet-}$ molecules to produce C_{60} and C_{60}^{2-} is endergonic by 0.45 eV.[1,2] However, the disproportionation equilibrium could be shifted if metal ions can bind with C_{60}^{2-}. Although strong binding of metal ions with fullerene anions has been no report on the external interaction between metal ions well-established in endohedral metallofullerenes,[3] there has and fullerene anions to form exohedral metallofullerenes.[4] Metal ions acting as Lewis acids are known to be coordinated by a lone pair of heteroatoms such as an oxygen of carbonyl compounds and a nitrogen atom of immines to enhance the electrophilicity of these substrates.[5] This is one of the most fundamental and important concepts in organic chemistry.[5] There are also a number of examples for electron transfer reactions which are accelerated significantly by the presence of metal ions.[6,7]. A number of redox reactions which would otherwise be unlikely to occur have been made to proceed efficiently by the presence of metal ions.[6,7] As is the case of Lewis acid-promoted organic synthesis, the metal

ions acting as Lewis acids to accelerate electron transfer reactions have so far been limited to those which can bind with oxygen of the radical anions of carbonyl compounds.[6,7,8]

We report herein that an efficient disproportionation of $C_{60}^{\bullet-}$ and $C_{70}^{\bullet-}$ proceeds in the presence of various metal ions, *i.e.*, Mg^{2+}, Ca^{2+}, Sr^{2+} and Ba^{2+} via the exohedral coordination of the dianions to metal ions. The accelerating effects of metal ions are compared to those in the metal ion-promoted electron transfer from (TPP)Co (TPP^{2-} = tetraphenylporphyrin dianion) to *p*-benzoquinone (Q). This is the first report that the external coordination of fullerene dianions to metal ions acting as Lewis acids results in an enhanced electron acceptor ability of the monoanions. The fullerene monoaions, which have no interaction with acidic metal ions unless further reduced to the dianions, can be used as unique electron donors in metal ion-promoted electron transfer reactions under acidic conditions in competition with the metal ion-promoted dispoportionation.

Results and Discussion

$C_{60}^{\bullet-}$ was prepared by the photochemical reduction of C_{60} with 1,1'-dibenzyl-1,1',4,4'-tetrahydro-4,4'-dinicoti-namide [$(BNA)_2$] in deaerated benzonitrile (PhCN).[9] No disproportionation of $C_{60}^{\bullet-}$ occurs in PhCN. However, the addition of $Ca(ClO_4)_2$ to a PhCN solution of $C_{60}^{\bullet-}$ results in disproportionation of $C_{60}^{\bullet-}$ (eq 1) as shown in Figure 1.

$$C_{60}^{\bullet-} + C_{60}^{\bullet-} \xrightarrow{Ca^{2+}} C_{60} + C_{60}^{2-}\text{-}Ca^{2+} \qquad (1)$$

After the reaction, the spcetrum is identical of that of a 1:1 mixture of C_{60} and 1,2-$C_{60}H_2$ by comparing the spectrum with that of authentic sample.[9,10,11] Thus, the final reduced product of $C_{60}^{\bullet-}$ is 1,2-$C_{60}H_2$ which may be produced by the hydration of C_{60}^{2-}-Ca^{2+}.

The disproportionation rate was measured by monitoring the decrease in $C_{60}^{\bullet-}$ absorbance at λ_{max} = 1080 nm (ε_{max} = 12000 M^{-1} cm^{-1}). The rate obeys second-order kinetics (inset of Figure 1). The observed second-order rate constant (k_{obs}) determined from

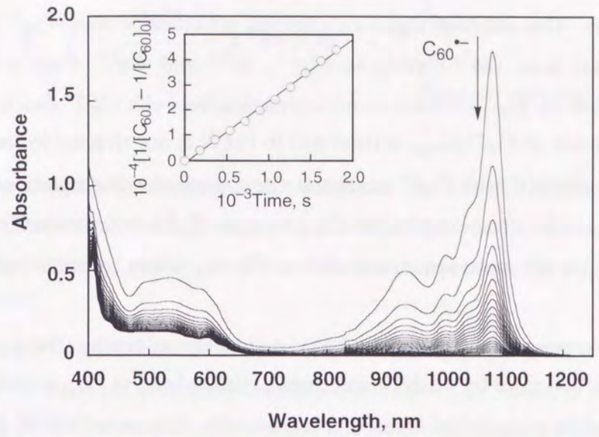

Figure 1. Vis-NIR spectra observed in the disproportionation reaction of $C_{60}^{\bullet-}$ (1.4×10^{-4} M) in the presence of $Ca(ClO_4)_2$ (1.8×10^{-3} M) in deaerated PhCN at 298 K. Inset: second-order plot.

Table 1 Rate constants (k_M) of metal ion (M^{2+})-promoted disproportionation of $C_{60}^{\bullet-}$ and $C_{70}^{\bullet-}$, and electron transfer from (TPP)Co to *p*-Benzoquinone (Q) in MeCN at 298 K.

		k_M / M^{-2} s^{-1}		
M^{2+} [a]	r / Å [b]	$C_{60}^{\bullet-}$	$C_{70}^{\bullet-}$	Q
Mg^{2+}	0.89	3.7×10^{4}	1.1×10^{6}	3.3
Ca^{2+}	1.12	9.5×10^{3}	7.1×10^{4}	7.0×10^{-1}
Sr^{2+}	1.26	1.0×10^{3}	1.6×10^{4}	1.6×10^{-1}
Ba^{2+}	1.42	3.4×10^{2}	6.3×10^{3}	3.0×10^{-2}

[a] Perchlorate salt. [b] Ionic radius (r) taken from ref. 12.

the slope of the second-order plot increases linearly with increasing $Ca(ClO_4)_2$ concentration (0 - 1.8 x 10^{-3} M). This indicates that a 1:1 complex is formed between C_{60}^{2-} and Ca^{2+} (eq 1). Other metal ions (M^{2+}) such as Mg^{2+}, Sr^{2+} and Ba^{2+} also accelerate the disproportionation of $C_{60}^{\bullet-}$. There is no interaction between $C_{60}^{\bullet-}$ and M^{2+} since the absorption maximum of $C_{60}^{\bullet-}$ (λ_{max} = 1080 nm) in PhCN is not affected by the presence of M^{2+}. The binding of M^{2+} with C_{60}^{2-} makes the electron transfer disproportionation of $C_{60}^{\bullet-}$ irreversible (eq 1). The metal ion-promoted rate constant (k_M) was determined from the slope of the plot of k_{obs} vs the metal ion concentration. The k_M values of metal ions are listed in Table 1.

$C_{70}^{\bullet-}$ was also prepared by the photochemical reduction of C_{70} by $(BNA)_2$ in deaerated PhCN and is characterized by the NIR spectrum having a band at λ_{max} = 1374 nm.[12] The $C_{70}^{\bullet-}$ generated in the photochemical reaction is also stable in deaerated PhCN, but decays via a disproportionation reaction (eq 2) in the presence of metal ions (M^{2+}). The k_M values were determined as listed in Table 1.

$$C_{70}^{\bullet-} + C_{70}^{\bullet-} \xrightarrow{M^{2+}} C_{70} + C_{70}^{2-}\text{-}M^{2+} \qquad (2)$$

The k_M value for the metal ion-promoted disproportionation of $C_{70}^{\bullet-}$ is larger than the corresponding value of $C_{60}^{\bullet-}$ (Table 1). This indicates that the binding of $C_{70}^{\bullet-}$ with a metal ion is stronger than that of $C_{60}^{\bullet-}$ because of the more localized negative charge in $C_{70}^{\bullet-}$ as compared to $C_{60}^{\bullet-}$. Such a difference between $C_{70}^{\bullet-}$ and $C_{60}^{\bullet-}$ may result from the loss of symmetry, *i.e.*, upon going from I_h symmetry in C_{60} to D_{5h} symmetry in C_{70}. The symmetry change results in an increase in the number of different types of carbon atoms from just one in C_{60} to five in C_{70} and an associated change in the number of chemically different C–C bonds from two in C_{60} to eight in C_{70}.[13]

The absence of an interaction between $C_{60}^{\bullet-}$ and Mg^{2+} was also confirmed by cyclic voltammograms of C_{60} in deaerated PhCN in the presence and absence of Mg^{2+}, which. shows the same $C_{60}/C_{60}^{\bullet-}$ half wave potential in the absence and presence of Mg^{2+}. However, the anodic peak for the oxidation of C_{60}^{2-} disappears in the presence of Mg^{2+}. indicating that there is an interaction between C_{60}^{2-} and Mg^{2+}.

Mg^{2+} has been reported to promote electron transfer from (TPP)Co (TPP^{2-} = dianion of tetraphenylporphyrin) to *p*-benzoquinone (Q) (eq 2) although no reaction between

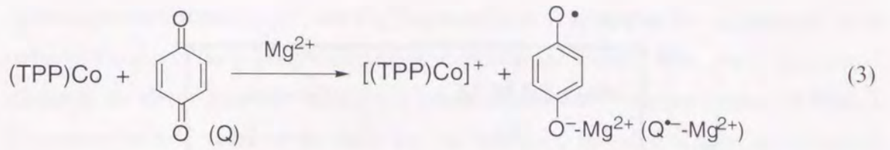

(3)

(TPP)Co and *p*-benzoquinone occurs in the absence of Mg^{2+} in acetonitrile (MeCN).[14] Such accelerating effects of metal ions on electron transfer reduction of substrates has been well-ascribed to the binding of metal ions to the radical anions produced in the electron transfer reactions.[3,4,14,15]

The rates of electron transfer from (TPP)Co to Q in the presence of metal ions employed for the metal ion-promoted disproportionation of $C_{60}^{\bullet-}$ and $C_{70}^{\bullet-}$ were determined by measuring the increase in absorbance due to $[(TPP)Co]^+$ (λ_{max} = 434 nm) and obeyed pseudo-first-order kinetics under experimental conditions where the Q concentration is

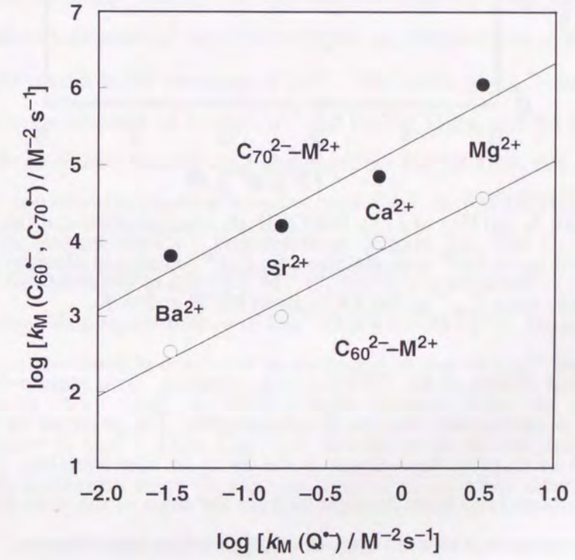

Figure 2. Comparison of the log k_M values for the metal ion-promoted disproportionation of $C_{60}^{\bullet-}$ (○) and $C_{70}^{\bullet-}$ (●) with those for the metal ion-promoted electron transfer from (TPP)Co to Q.

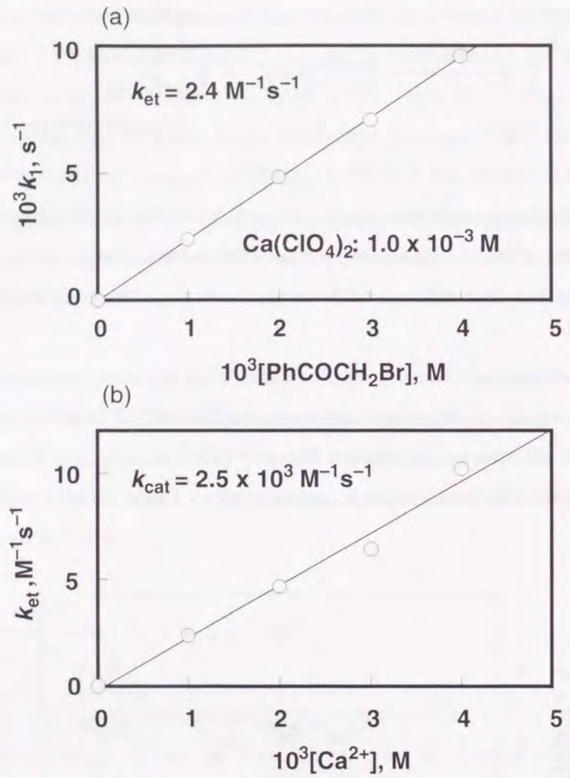

Figure 3. (a) Plot of k_1 vs $PhCOCH_2Br$ concentration and (b) plot of k_{et} vs Ca^{2+} concentration for Ca^{2+} -catalyzed electron transfer from $C_{60}^{\bullet-}$ to $PhCOCH_2Br$ in PhCN at 298 K.

greater than 10-fold excess of the (TPP)Co concentration. The pseudo-first-order rate constants increase proportionally with the Q concentration. The observed second-order rate constant exhibited a first-order dependence on the metal ion concentration. The metal ion-promoted rate constants (k_M) were determined from the slope of the plots of the observed second-order rate constants of electron transfer *vs* the metal ion concentration.

The log $k_M$values for the metal ion-promoted disproportionation of $C_{60}^{\bullet-}$ and $C_{70}^{\bullet-}$ are compared with values for the metal ion-promoted electron transfer from (TPP)Co to Q (Figure 2), and show good linear correlations between them. Such linear correlations indicate that the electron transfer disproportionation of $C_{60}^{\bullet-}$ and $C_{70}^{\bullet-}$ is accelerated by the

exohedral coordination of C_{60}^{2-} and C_{70}^{2-} to metal ions as is the case for coordination of the carbonyl oxygen of the *p*-benzosemiquinone radical anion to metal ions, which is known to accelerate the electron transfer reduction of *p*-benzoquinone.[15, 16] As summarized in Table 1, the smaller the ionic radius of the metal ion, the stronger is its Lewis acidity, the stronger is the binding of the metal ion with the reduced species, and the more enhanced is the accelerating effects of the metal ion on the electron transfer reaction.

Since there is no interaction between $C_{60}^{\bullet-}$ and metal ions (*vide infra*), $C_{60}^{\bullet-}$ can act as a unique electron donor for metal ion-catalyzed electron transfer reduction of acceptors, provided that the metal ion-catalyzed electron transfer reduction is faster than the metal ion-catalyzed electron transfer disproportionation of $C_{60}^{\bullet-}$. Phenacyl bromide ($PhCOCH_2Br$) is known to be reduced to acetophenone by the acid-promoted electron transfer form 1,1'-dimethylferrocene to $PhCOCH_2Br$.[17] In general, anionic electron donors cannot be used for such acid-promoted electron transfer reactions because of the facile protonation of the anions. However, $C_{60}^{\bullet-}$ can be used as a unique anionic electron donor in the presence of an acidic metal ion for the metal-ion promoted electron transfer reduction of $PhCOCH_2Br$. Although there is no reaction between $C_{60}^{\bullet-}$ and $PhCOCH_2Br$, an efficient electron transfer from $C_{60}^{\bullet-}$ to $PhCOCH_2Br$ occurs in the presence of Ca^{2+}. The decay of $C_{60}^{\bullet-}$ obeys pseudo-first-order kinetics in the presence of excess Ca^{2+} and $PhCOCH_2Br$, and the pseudo-first-order rate constant (k_1) increases linearly with increasing the $PhCOCH_2Br$ concentration (Figure 3a). The rate constant for electron transfer from $C_{60}^{\bullet-}$ to $PhCOCH_2Br$ (k_{et}) increases linearly with increasing the Ca^{2+} concentration (Figure 3b). The Ca^{2+}-promoted rate constants (k_M) is determined as 2.5 x 10^3 M^{-2} s^{-1}, which is comparable with the k_M value of the Ca^{2+}-promoted disproportionation of $C_{60}^{\bullet-}$ (9.5 x 10^3 M^{-2} s^{-1}). When the much larger $PhCOCH_2Br$ concentration is employed as compared to that of $C_{60}^{\bullet-}$, the Ca^{2+}-promoted electron transfer from $C_{60}^{\bullet-}$ to $PhCOCH_2Br$ prevails over the Ca^{2+}-promoted disproportionation of $C_{60}^{\bullet-}$. Thus, $C_{60}^{\bullet-}$ can be used as an anionic electron donor even under the acidic conditions when the electron transfer reduction of substrates is promoted significantly.

References and Notes

(1) Hirsh, A. *The Chemistry of Fullerenes*, Thieme Medical Publishers, Inc., New York, 1994.

(2) Echegoyen, L.; Diederich F.; Echegoyen, L. E. *Fullenes: Chemistry, Physics and Technology*, Eds. Kadish K. M.; Ruoff, R. S. Wiley, New York, 2000, pp. 1-51.

(3) (a) Shinohara, H. *Fullerenes: Chemistry, Physics and Technology*, Eds. Kadish K. M.; Ruoff, R. S.: Wiley, New York, 2000, pp. 357-393. (b) Nagase, S.; Kobayashi, K.; Akasaka T. Wakahara, T. in *Fullerenes: Chemistry, Physics and Technology*, Eds. Kadish K. M.; Ruoff, R. S.: Wiley, New York, 2000, pp. 395-436.

(4) Although there has been controversy over whether or not the metal atom is really trapped inside the fullerene cage in the early studies on metallofullerenes, the endohedral nature of metallofullerenes is now well-established.[3]

(5) (a)Yamamoto, H. *Lewis Acid Chemistry: A Practical Approach*, Oxford University Press, Oxford, 1999. (b) Santelli M.; Pons, J.-M. *Lewis Acids and Selectivity in Organic Synthesis*, CRC Press, Boca Raton, FL, 1995. (c) Reetz, M. T. *Angew. Chem., Int. Ed. Engl.* **1984**, *23*, 556.

(6) Fukuzumi, S. *Advances in Electron Transfer Chemistry*, Ed. by Mariano, P. S. JAI Press, Greenwich, CT, 1992, Vol. 2, pp. 67-175. (b) Fukuzumi, S. *Bull. Chem. Soc. Jpn.* **1997**, *70*, 1; (c) Fukuzumi S.; Itoh, S. *Advances in Photochemistry*, Eds. by Neckers, D. C.; Volman, D. H.; von Bünau, G. Wiley, New York, 1998, Vol. 25, pp. 107-172.

(7) Fukuzumi, S. *Electron Transfer in Chemistry*, Ed. Balzani, V. Wiley-VCH, Weinheim, 2001, Vol. 5, in press.

(8) The regio- and chemoselective reactions controlled by the coordination of Lewis acids to π-electrons of alkynes together with an oxygen of aldehydes have recently been reported; see: Asao, N.; Asano, T.; Ohishi, T.; Yamamoto, Y. *J. Am. Chem. Soc.* **2000**, *122*, 4817.

(9) Fukuzumi, S.; Suenobu, T.; Patz, M.; Hirasaka, T.; Itoh, S.; Fujitsuka M.; Ito, O. *J. Am. Chem. Soc.* **1998**, *120*, 8060.

(10) The diagonistic absorption bands due to 1,2-$C_{60}H_2$ (lmax = 434 and 714 nm) can be seen clearly in the enlarged spectrum of Figure 1.

(11) (a) Henderson C. C.;Cahill, P. A. *Science* **1993**, *259*, 1885. (b) Becker, L.; Evans, T. P.; Bada, J. L. *J. Org. Chem.* **1993**, *58*, 7630.

(12) Shannon, R. D. *Acta Cryst.* **1976**, *A32*, 751.

(13) Fukuzumi, S. Suenobu, T.; Hirasaka, T.; Sakurada, N.; Arakawa, R.; Fujitsuka M.; Ito, O. *J. Phys. Chem. A* **1999**, *102*, 5935.

(14) Hedberg, K.; Hedberg, L.; Bühl, M.; Bethune, D. S.; Brown C. A.; Johnson, R. D. *J. Am. Chem. Soc.* **1997**, *119*, 5314.

(15) Fukuzumi S.; Okamoto, T. *J. Am. Chem. Soc.* **1993**, *115*, 11600.

(16) Fukuzumi, S.; Patz, M.; Suenobu, T.; Kuwahara Y.; Itoh, S. *J. Am. Chem. Soc.* **1999**, *121*, 1605.

(17) The direct detection of the C_{60}^{2-}–La^{3+} complex formed in the disproportionation of $C_{60}^{\bullet-}$ in the presence of La^{3+} in PhCN by using electrospray ionization mass spectroscopy (ESI-MS) was unsuccessful due to the instability of the complex.

(18) Fukuzumi, S.; Mochizuki, S.; Tanaka, T. *J. Am. Chem. Soc.* **1989**, *111*, 1497.

Concluding Remarks

This thesis has reported the thermal and photoinduced electron transfer reactions involving cleavage of various types of chemical bonds, i.e., carbon–hydrogen, metal–carbon, metal-oxygen and metal–metal bonds. The actual role of the EDA complces in electron transfer reactions between electron donors and acceptors has also been clarified by demonstrating the negative temperature dependence of the rate of electron–proton–electron transfer system. The catalysis of metal ions in electron transfer reactions has also been systematically studied and evaluated quantitatively. The results and finding in this work are summarized as follows.

1. The observed negative temperature dependence of the rate of hydride transfer from $AcrH_2$ to DDQ gave an unequivocal evidence for the role of the observed CT complex as an actual intermediate in the hydride transfer reaction. The magnitude of the observed rate constant for the reactions of AcrHR with a hydride acceptor varies significantly depending on the type of substituent R in AcrHR at C-9 position and spans a range of 10^7. The overall reactivity is determined by the three consecutive steps, *i.e.*, the CT complex formation, the electron transfer and the proton transfer steps, since the electron transfer in the final step is much faster than the previous proton transfer step. Thus, this study has provided first comprehensive and confirmative understanding of the mechanism of sequential electron-proton-electron transfer via CT complexes.
2. A charge shift type of photoinduced electron transfer reactions from various electron donors to the singlet excited state of 10-decylacridinium ion ($DeAcrH^+$) in a nonpolar solvent are found to be as efficient as those of 10-methylacridinium ion and $DeAcrH^+$ in a polar solvent. 100 % selective oxygenation of *p*-xylene to *p*-tolualdehyde has been archived via photoinduced electron transfer from *p*-xylene to the singlet excited state of 10-methyl-9-phenylacridinium ion under visible light irradiation.
3. The $\Delta H^{\neq}$ values for the Co–C bond cleavage of coenzyme B_{12} model complexes can be easily decreased by formation of the higher oxidation state, Co(IV), the stronger donor ability of the σ–bonded R, the steric pressure of the substituent as well as the axial coordination of a strong base (L) complex, but that an decrease in the $\Delta H^{\neq}$ value is compensated by the concomitant decrease in the $\Delta S^{\neq}$ value. This indicates that the Co–C bond weakening in terms of enthalpy is readily achieved by the deformation of the flexible $(DH)_2$ ligand but that it is accompanied by a decrease in the probability to have the optimized conformation for the Co–C bond cleavage, resulting in a compensating decrease in the entropy term. Thus, the protein–coenzyme interaction may play an important role in fixing the optimized conformation for the Co–C bond cleavage of coenzyme B_{12} and thereby preventing a decease in the $\Delta S^{\neq}$ value in order to enhance the Co–C bond cleavage.

Photolysis of a benzonitrile solution of $(DH)_2Co^{III}(R)(L)$ in the presence of C_{60} by using visible light results in alkylation of C_{60} to yield R_2C_{60} via photocleavage of cobalt–carbon bond of $(DH)_2Co^{III}(R)(L)$.

The photoinduced electron transfer from organosilanes and organostannanes to $AcrH^{+*}$ and $X\text{-}QuH^{+*}$ provides a unique reaction pathway for regioselective addition of organosilanes and organostannanes, which is reversed in the corresponding thermal nucleophilic addition reactions with $AcrH^+$ and $X\text{-}QuH^+$.

The nucleophilic reactivities of ketene silyl acetals vary significantly depending on the steric demand at the reaction center, but they are well correlated with the electron transfer reactivities when the steric demand at the reaction center for the C–C bond formation remains constant.

4 Irradiation of the absorption band of an NAD (nicotinamide adenine dinucleotide) dimer analogue, 1-benzyl-1,4-dihydronicotinamide dimer, $(BNA)_2$, in acetonitrile containing cyclopentadienyliron dicarbonyl dimer, $[CpFe(CO)_2]_2$, results in generation of cyclopentadienyliron dicarbonyl anion, $[CpFe(CO)_2]^-$. This reaction is convenient method for generation of $[CpFe(CO)_2]^-$ photochemical reduction of $[CpFe(CO)_2]_2$.

5 The ΔE values of $O_2^{\bullet-}$–M^{n+} readily derived from the g_{zz}-values of the ESR spectra can be utilized as the first quantitative experimental measure to determine the Lewis acidity of metal ions in relation with the promoting effects in electron transfer reactions.

Metal ions are found to accelerate the disproportionation of $C_{60}^{\bullet-}$ and $C_{70}^{\bullet-}$. This indicates that the electron transfer disproportionation of $C_{60}^{\bullet-}$ and $C_{70}^{\bullet-}$ is accelerated by the exohedral coordination of C_{60}^{2-} and C_{70}^{2-} to metal ions.

List of Publications

The content of thesis is composed of the following papers.

Publications

(1) Hydride Transfer from 9-Substituted 10-Methyl-9,10-dihydroacridines to Hydride Acceptors via Charge-Transfer Complexes and Sequential Electron-Proton-Electron Transfer. A Negative Temperature Dependence of the Rates
Fukuzumi, S.; Ohkubo, K.; Tokuda, Y.; Suenobu, T.
J. Am. Chem. Soc. **2000**, *122*, 4286-4294.

(2) 100% Selective Oxygenation of *p*-Xylene to *p*-Tolualdehyde via Photoinduced Electron Transfer
Ohkubo, K.; Fukuzumi, S.
Org. Lett. **2000**, *2*, 3647-3650.

(3) Photoalkylation of C_{60} by Alkylcobalt(III) Complexes.
Ohkubo, K.; Fukuzumi, S.
Inorg. React. Mech. **2000**, *2*, 147-153.

(4) Quantitative Evaluation of Lewis Acidity of Metal Ions Derived from the g-Values of ESR Spectra of Superoxide-Metal Ion Complexes in Relation with the Promoting Effects in Electron Transfer Reactions.
Fukuzumi, S.; Ohkubo, K.
Chem. Eur. J. **2000**, *6*, 4532-4535.

(5) Comparison between Electron Transfer and Nucleophilic Reactivities of Ketene Silyl Acetals with Cationic Electrophiles.
Fukuzumi, S.; Ohkubo, K.; Otera, J.
J. Org. Chem. **2001**, *66*, in press.

(6) Regioreversed Thermal and Photochemical Reduction of 10-Methylacridinium and 1-Methylquinolinium Ions by Organosilanes and Oraganostannanes.
Fukuzumi, S. Fujita, M.; Noura, S.; Ohkubo, K.; Suenobu, T.; Araki, Y.; Ito, O.
J. Phys. Chem. A **2001**, *115*, in press.

(7) Photochemical Generation of Cyclopentadienyliron Dicarbonyl Anion by an NAD Dimer Analogue.
Fukuzumi, S.; Ohkubo, K.; Fujitsuka, M.; Ito, O.; Teichmann, M. C.; Maisonhaute, E.; Amatore, C.
Inorg. Chem. in press.

(8) Activation Parameters for Cobalt–Carbon Bond Cleavage of Organocobalt(III, IV) Complexes with Dimethylglyoxime and Porphyrin Ligands
Ohkubo, K.; Fukuzumi, S.
J. Am. Chem. Soc. in contribution.

(9) A Charge Shift Type of Photoinduced Electron Transfer Reactions of 10-Alkylacridinium Ion Controlled by Solvent Polarity.
Fukuzumi, S.; Ohkubo, K.; Suenobu, T.; Kato, K.; Fujitsuka, M.; Ito, O.
J. Am. Chem. Soc. submitted.

(10) Exohedral Coordination of Fullerene Dianions to Metal Ions and the Accelerating Effects in Disproportionation of Fullerene Radical Anions
Fukuzumi, S.; Ohkubo, K.; Shao, J.; Kadish, K. M.
Org. Lett. submitted.

Patent

光電子移動を利用するアルキルベンゼンの選択的部分酸素化触媒系の開発
福住　俊一・大久保　敬・末延　知義
特願2000-309122

Proceedings

(1) Electron Transfer Disproportionation of C_{60} Radical Anion Catalyzed by Metal Ions
Fukuzumi, S.; Ohkubo, K.; Suenobu, T.; Ito, O.; Fujitsuka, M.; Kadish, K. M.
Fullerenes 2000: Electrochemistry and Photochemistry; Fukuzumi, S.; D'Souza, F.; Guldi, D. M., Eds.; The Electrochemical Society, Inc.: Pennington, NJ, 2000; Vol. 8, pp 68-78.

(2) $O_2^{\bullet-}$ Generation in C_{60}^- Photosensitized Oxidation of NADH and Analogue by Oxygen.
Nakanishi, I.; Yamakoshi, Y.; Ohkubo, K.; Fujita, S.; Fujitsuka, M.; Ito, O.; Fukuzumi, S., Miyata, N.

Fullerenes 2000: Electrochemistry and Photochemistry; Fukuzumi, S.; D'Souza, F.; Guldi, D. M., Eds.; The Electrochemical Society, Inc.: Pennington, NJ, 2000; Vol. 8, pp 242-255.

Supplementary Publications

(1) Signal Transduction in the Transcriptional Activator CooA Containing a Heme-Based CO Sensor: Isolation of a Dominant Positive Mutant Which is Active as the Transcriptional Activator even in the Absence of CO.
Aono, S.; Matsuo, T. Shimono, T.; Ohkubo, K.; Takasaki, H.; Nakajima, H.
Biochem. Biophys. Res. Commun. **1997**, *240*, 783-786.

(2) A Carbon Monoxide Dependent Transcriptional Regulator which contains b-Type Heme as a Carbon Monoxide Sensor.
Aono, S.; Ohkubo, K.; Matsuo, T.; Okada, M.; Nakajima, H.
J. Inorg. Biochem., **1997**, *67*, 362.

(3) Heme Environmental Structure of CooA Is Modulated by the Target DNA Binding. Evidence from Resonance Raman Spectroscopy and CO Rebinding Kinetics.
Uchida, T.; Takahashi, S.; Ishimori, K, Morishima, I.; Ohkubo, K.; Nakajima, H.; Aono, S.
J. Biol. Chem. **1998**, *273*, 19988-19992.

(4) Redox-Controlled Ligand Exchange of the Heme in the CO-Sensing Transcriptional Activator CooA.
Aono, S.; Ohkubo, K.; Nakajima, H.
J. Biol. Chem. **1998**, *273*, 25757-25764.

(5) CO Sensing and Regulation of Gene Expression by the Transcriptional Activator CooA.
Aono, S.; Honma, Y.; Ohkubo, K.; Tawara, T.; Kamiya, T.; Nakajima, H.
J. Inorg. Biochem. **2000**, *82*, 51-56.

Acknowledgment

The author would like to express his gratitude to Professor Shunichi Fukuzumi for his kind guidance, invaluable suggestions, and encouragement throughout this study.

The author desires to express his sincere thanks to Dr. Tomoyoshi Suenobu, Dr. Shinobu Itoh and Dr. Hiroshi Imahori for their useful suggestions and continuous encouragement throughout this study.

The author is deeply grateful to Professor Karl M. Kadish (University of Houston), Professor Christian Amatore (Ecole Normale Supérieure) and Professor Osamu Ito (Tohoku University) for their kind guidance and helpful comments.

Thanks also go to the author's co-workers and all the member of the laboratory of Physical Chemistry for Life Science at Department of Material and Life Science, Graduated School of Engineering, Osaka University for their help, valuable suggestions, and friendships.

Finally, the author acknowledges continuous encouragement and assistance given by his father, Mr. Osamu Ohkubo, his mother, Mrs. Mieko Ohkubo, and his brother, Mr. Go Ohkubo.

Kei O

Kei Ohkubo
Department of Material and Life Science
Graduate School of Engineering
Osaka University
CREST, JAPAN Science and
Technology Corporation

Osaka, Japan

January, 2001